The PDZ adaptor protein, NHERF1, organizes and regulates protein complexes at the cell membrane

by

David S. Wheeler

Bachelor of Arts, Johns Hopkins University, 2005

Submitted to the Graduate Faculty of

University of Pittsburgh School of Medicine in partial fulfillment

of the requirements of the degree of

Doctor of Philosophy

University of Pittsburgh

2010

UNIVERSITY OF PITTSBURGH

SCHOOL OF MEDICINE

This thesis was presented

by

David S. Wheeler

It was defended on

November 18, 2010

And approved by

Donald DeFranco, Chairperson

Professor, Department of Pharmacology and Chemical Biology

Peter A. Friedman

Professor, Department of Pharmacology and Chemical Biology

Jean-Pierre Vilardaga

Assistant Professor, Department of Pharmacology and Chemical Biology

Linton M. Traub

Associate Professor, Department of Cell Biology and Physiology

Guillermo Romero, Dissertation Advisor

Associate Professor, Department of Pharmacology and Chemical Biology

The PDZ adaptor protein, NHERF1, organizes and regulates protein complexes at the cell membrane

David S. Wheeler, PhD

University of Pittsburgh, 2010

G-protein coupled receptors (GPCRs) are the largest family of transmembrane proteins, constituting 2% of the human genome. They mediate signaling from a diverse set of ligands, ranging from photons to large peptides. Their intracellular signaling cascades are complex and highly malleable depending on cellular context. Yet, GPCR signaling *in vivo* is highly specific. Cells maintain this tight control over GPCR signaling through the expression of adaptor proteins. These adaptors regulate GPCR function and activation on many levels - they localize receptors to specific subcellular domains, assemble functional signaling complexes, alter the specificity of G-proteins coupling to the receptor, or regulate receptor traffic to and from the plasma membrane. By balancing the expression of these adaptor proteins, cells control where, when and how long GPCRs signal.

Na^+/H^+ Exchanger Regulatory Factor 1 (NHERF1), also known as Ezrin binding phosphoprotein 50kDa (EBP50), is the prototypical PDZ adaptor protein. Expression of NHERF1 clusters parathyroid hormone type 1 receptor (PTH1R) and frizzled (Fzd) along actin stress fibers in non-polarized cells at the apical actin cap in polarized cells. In addition to proper localization, interaction with NHERF1 has several signaling manifestations. For PTH1R, interaction with NHERF1 can cause either a G-protein

switch or can scaffold a PTH1R-PKA-calcium channel signaling complex. For Fzd, interaction with NHERF1 blocks Wnt-induced β-catenin activation. NHERF1 knockout mice exhibit PTH-resistant phosphate excretion and enhanced PTH-induced vitamin D synthesis, as well as increased mammary duct density secondary to heightened Wnt-Fzd signaling. NHERF1 is a prime example of how PDZ adaptor proteins regulate GPCR localization and diversify GPCR signaling in physiologically significant ways.

Guillermo Romero

TABLE OF CONENTS

LIST OF FIGURES

PREFACE

Some luck lies in not getting what you thought you wanted but getting what you have, which once you have got it you may be smart enough to see is what you would have wanted had you known. -Garrison Keillor

He who does not tire, tires adversity. – Martin Tupper

Some of the world's greatest feats were accomplished by people not smart enough to know they were impossible. -Doug Larson

Mas sabe el diablo por viejo que por diablo.
(The devil knows more because he's old than because he's the devil.)

Brick walls are there for a reason. The brick walls are not there to keep us out. The brick walls are there to show how badly we want something. Because the brick walls are there to stop the people who don’t want something badly enough. They are there to keep out the other people. - Randy Pausch

He who would learn to fly one day must first learn to stand and walk and run and climb and dance; one cannot fly into flying. - Friedrich Nietzsche

I. REGULATION OF GPCRS BY PDZ PROTEINS

G-protein coupled receptors (GPCRs) are the largest family of transmembrane proteins, constituting 2% of the human genome [1, 2]. They mediate signaling from a diverse set of ligands, ranging from photons to large peptides. Their intracellular signaling cascades are complex and highly malleable depending on cellular context. Yet, GPCR signaling *in vivo* is highly specific. One way that cells maintain this tight control over GPCR signaling is through the expression of adaptor proteins. These adaptors regulate GPCR function and activation on many levels - they localize receptors to specific subcellular domains, assemble functional signaling complexes, alter the specificity of G-proteins coupling to the receptor, or regulate receptor traffic to and from the plasma membrane. By balancing the expression of these adaptor proteins, cells control where, when, and how long GPCRs signal.

Most adaptor proteins interact with their targets via well-conserved modular protein-protein domains (e.g. SH3, PTB, PDZ). The most abundant of these domains are PDZ domains, named for the first three proteins in which they were discovered (PSD-95, Discs-large and ZO-1). These 80-90 amino-acid long domains fold into a globular structure composed of six β-sheets and 2 α-helices [3]. Although internal PDZ ligands have been described (e.g. the –K-T-x-x-x-W- motif in Frizzled receptors [4]), the majority are located at the C-terminus of the target protein. The PDZ ligand docks in a groove between the second β-sheet (βB) and the second α-helix (αB), with the terminal

hydrophobic amino acid of the ligand occupying a hydrophobic cavity at the top of the groove (Figure 1) [5, 6]. Class I PDZ domains interact with proteins terminating in the consensus sequence $–x^{-3}$-S/T^{-2}-x^{-1}-L/V/M^{0} (where x represents any amino acid, numbers represent position from C-terminus) [7]. Class II domains prefer a hydrophobic amino acid in position -2 [7]. Structural comparison of class I and class II PDZ domains demonstrates this ligand preference results from the presence of a histidine in class I (which favors serine or threonine) or hydrophobic pocket in class II (which favors a hydrophobic amino acid) at the distal end of αB. Based on the particular amino acid sequence, a PDZ domain of either class may favor specific ligands based on residues located at the -3, -4 and -5 position [7, 8]. For example, the PDZ domains of Na/H Exchanger Regulator Factor 1 (NHERF1) contain an arginine that can electrostatically interact with a glutamate or aspartate at the -3 position (Figure 1) [5, 6]. While preferring targets with Glu/Asp at the -3 position, NHERF1 is still able to interact with targets that have a different amino acid at -3 (i.e. Npt2a which terminates in –A-T-R-L-) [9].

In addition to GPCRs, PDZ adaptor proteins interact with a wide range of proteins including transporters, ion channels, receptor tyrosine kinases and enzymes. Regardless of the partner, the most universal function of PDZ adaptor proteins is to localize their targets to the correct domain at the plasma membrane. In polarized epithelial cells, different PDZ proteins can be found along the apical, junctional, lateral and basal membrane domains with their partners likewise distributed. For example, the human somatostatin receptor 3 is targeted to epithelial tight junctions by multiple PDZ domains of MUPP1 [10]. The receptor tyrosine kinase Her2 and the potassium channel Kir2.3 are both maintained at the basolateral membrane by binding the PDZ proteins ERBIN and Lin-7/CASK, respectively [11, 12]. A subset of PDZ proteins (42 of 141 found in the human genome) contain multiple PDZ domains. The presence of multiple domains

allows these proteins not only to direct sub-cellular localization, but also to scaffold protein complexes. In neurons, the multi-PDZ protein PSD-95 is responsible for clustering several receptors (NMDA [13], β1-adredergic [14]) and ion channels (Shaker K+ channel [15]) at the synapse.

The Na/H Exchanger Regulatory Factor family of PDZ adaptor proteins consists of four family members, NHERF1-4, which contain 2 or 4 tandem PDZ domains (Figure 2A). Initially arising in invertebrates, they remain highly conserved throughout all higher order organisms (Figure 2B). NHERF1, also known as ezrin-binding phosphoprotein 50kDa (EBP50), was the first of the family to be discovered and is the prototypical PDZ adaptor protein. NHERF1 contains two tandem class I PDZ domains and a C-terminal moesin-ezrin-radixin-moesin (MERM) binding domain (Figure 2a). The first known function of NHERF1 was as a co-factor essential for cAMP/PKA-induced inhibition of Na/H exchanger isoform 3 (NHE3) [16], but numerous other functions have been identified over the past decade. NHERF1 is expressed by all polarized epithelial cells and by a small subset of non-polarized mesenchymal cells (i.e., osteoblasts and macrophages) (Figure 3). NHERF1 localizes to the apical membrane of polarized cells and is found along actin fibers neighboring the plasma membrane in non-polarized cells. Numerous GPCRs (PTH1R, β2-AR, k-opioid), transporters (CFTR, NHE3, EAAT1), receptor tyrosine kinases (PDGFR, EGFR), and enzymes (PLC, nNOS) interact with NHERF1 (reviewed in [9]), although the physiologic consequences of many of the interactions are not well characterized. In the most well-studied cases, NHERF1 functions by targeting proteins to the apical membrane and scaffolding protein-protein complexes. For example, the apical localization of CFTR and inward rectifier K+ channel ROMK depends on interactions between their PDZ ligands and NHERF1 or 2. At the

apical membrane, NHERF coordinates a ternary complex containing ROMK and CFTR that alters the functional properties of the ion channels [17]. Furthermore, recent studies show that NHERF1 can interact with itself and other members of the NHERF family *in vitro*, but *in vivo* evidence supporting this phenomenon is lacking [18, 19].

One extensively studied binding partner for NHERF1 is the parathyroid hormone type 1 receptor (PTH1R). This family B GPCR is the main regulator of calcium and phosphate homeostasis (reviewed in [20]). Decreases in serum calcium trigger the release of parathyroid hormone (PTH) into the circulation. PTH activates PTH1R, expressed in bone and kidney, stimulating bone breakdown and calcium reabsorption from the urine. Renal PTH1R activation also upregulates transcription of the enzyme 1α-OHase, which increases production of 1,25 $(OH)_2$ vitamin D. Active vitamin D acts on the intestine to increase calcium absorption. These three processes increase serum calcium, which provides negative feedback on PTH secretion. The distribution and signaling of PTH1R is highly variable and depends on both the sub-cellular microenvironment and cell type. In the distal convoluted tubule (DCT) of the kidney, PTH1R localizes to the basolateral membrane and mainly signals through $G\alpha_s$ and adenylyl cyclase to produce cAMP. In the proximal convoluted tubule (PCT) of the kidney, PTH1R is expressed on both the apical and basolateral surfaces and signals though both cAMP and intracellular calcium transients [21-23]. In osteoblasts, the main cellular target in bone, PTH1R activation generates both cAMP and prolonged intracellular calcium bursts [24]. A major breakthrough in our understanding of the cell-specific behaviors of PTH1R was the discovery that PTH1R binds NHERF1 [23, 25]. Expression of NHERF1 causes PTH1R signaling to “switch” from exclusively cAMP to cAMP and phospholipase C (PLC)-dependent calcium flux [23, 25]. Since NHERF1 is

expressed in osteoblasts and PCT cells, but not in DCT cells, this may explain the variability in PTH1R signaling [26]. The quintessential proof that NHERF1 was critical for PTH1R function was that a NHERF1 knock-out mouse exhibited a constellation of phenotypes consistent with PTH1R dysfunction (disturbed mineral ion homeostasis, altered vitamin D level, and improper bone morphology) [27].

II. NHERF1 AND PTH1R: A CASE STUDY

A. DIFFUSION, DYNAMICS AND DISTRIBUTION

NHERF1 contains two PDZ domains and a C-terminal MERM domain that interact with the cytoskeleton. Therefore, it was logically assumed that NHERF1 functions by tethering its targets to the actin cytoskeleton. Prior work using co-immunoprecipitation and GST-pulldowns showed that NHERF1 interacts with MERM [28, 29] proteins and with PTH1R, [23, 25] but ability to assemble the ternary complex was only inferred. If NHERF1 tethers PTH1R to the actin cytoskeleton, then expression of NHERF1 should decrease the receptor's mobility on the plasma membrane. Furthermore, this decrease in mobility should depend on the integrity of PDZ – PDZ ligand interaction and the actin cytoskeleton. In several non-polarized cell lines, NHERF1 expression significantly decreased the diffusion coefficient of the PTH1R (Figure 4, column 2) [30, 31]. Depolymerization of the actin cytoskeleton with latrunculin A increases, but does not completely restore, the mobility of the receptor, suggesting that PTH1R still interacts with NHERF1 but is no longer tethered to the cytoskeleton (Figure 4, column 4). NHERF1 failed to decrease the diffusion coefficient of PTH1R M593A (Figure 4, column 2), a receptor construct containing a non-functional PDZ ligand [31, 32]. This proves that the interaction between NHERF1 and PTH1R is mediated by the receptor's PDZ ligand. Addition of PTH increases the average diffusion coefficient of the receptor in a time-dependent manner [31]. This demonstrates that ligand-induced

activation of PTH1R causes the dissociation of NHERF1 and disruption of the ternary complex.

The ability of NHERF1 to tether PTH1R to the actin cytoskeleton can be qualitatively observed by imaging surface PTH1R with total internal reflection (TIRF) microscopy. In the absence of NHERF1, PTH1R is diffusely spread across the entire membrane (Figure 5A). Expression of NHERF1 clusters the receptor along actin stress fibers (Figure 5B). These bundles are not seen when PTH1R M593A is coexpressed with NHERF1 (Figure 5C) or when cells are pre-treated with latrunculin A [30, 31]. Interestingly, the receptors confined to the “bundle” regions diffuse significantly faster than receptors in the bulk membrane [31]. Furthermore, receptor motion is not isotropic, but movement along the bundles occurs four times faster than movement across the bundles [31]. This suggests that tethered PTH1R is being moved along the bundles by actin treadmilling. Although further evidence would be needed to support such a hypothesis, this is a novel mechanism for the regulation of GPCR dynamics.

Although most studies investigating interaction between NHERF1 and PTH1R have been conducted in non-polarized cells, the majority of cells that express both proteins are polarized epithelial cells. In the kidney, PTH1R is expressed on both apical and basolateral membranes of NHERF1-expressing cells, but only on the basolateral membrane of cells lacking NHERF1. This suggests that NHERF1 has a role in the apical localization of PTH1R. The majority (~60%) of endogenous PTH1R is apically localized in MDCK cells expressing endogenous levels of NHERF1 (Figure 6A). Not surprisingly, 70% of ectopically expressed PTH1R-GFP also localizes to the apical membrane (Figure 7). Only 20% of PTH1R M593A GFP is found on the apical surface, indicating that the PDZ binding domain of PTH1R is critical for apical localization (data not shown).

Finally, knockdown of NHERF1 using shRNA causes a redistribution of PTH1R-GFP to the basolateral membrane (Figure 7). In the absence of NHERF1, the receptor density is constant, indicating random distribution of the receptor (Figure 6B). These data strongly support a model where PTH1R is sorted randomly to the apical or basolateral membrane. Interaction with NHERF1 at the apical membrane stabilizes PTH1R at the membrane and inhibits constitutive internalization.

B. SIGNALING THROUGHOUT THE SCAFFOLD

The initial characterization of the NHERF "signaling switch" in non-polarized cells showed that expression of NHERF2 decreases PTH-induced cAMP generation and triggers a PTH-dependent calcium transient. Further studies established that NHERF1 expression causes this signaling switch by increasing the affinity of PTH1R for G_i [33]. Activation of $G\alpha_i$ results in inhibition of adenylyl cyclase, while the release of $G\beta\gamma$ subunits activates PLCβ resulting in a calcium transient [23]. However, unanswered questions still remained, including whether NHERF1 causes PTH1R to signal differently from apical and basolateral membranes within the same cell and if the NHERF1 "signaling switch" is the same in all cell types.

In the proximal convoluted tubule, NHERF1 localizes to the apical membrane, whereas PTH1R is expressed on both apical and basolateral surfaces [21-23, 34]. Therefore, NHERF1 should "switch" apical PTH1R signaling from cAMP generation to formation of a calcium transient. Consistent with this hypothesis, addition of PTH to the apical membrane of polarized MDCK cells stimulates both cAMP and a calcium

transient, whereas addition to the basolateral membrane only stimulates cAMP (Figure 8A, 9A). At saturating concentrations of PTH the total amount of cAMP generated is higher for the apical membrane (Figure 8A). However, normalization to receptor density reveals that basolateral receptors generate four fold more cAMP per receptor. Furthermore, the EC_{50} for PTH-induced cAMP is significantly higher for the apical membrane than the basolateral membrane (approximately 30nM for apical vs. 4nM for basolateral). This difference in EC_{50} is thought to be a consequence of the interaction between PTH1R and NHERF1 and is discussed in detail below. Consistent with observations made in non-polarized cells, the calcium transient is sensitive to both pertussis toxin and gallein, implicating the $G\beta\gamma$ subunits of G_i (Figure 9B). Addition of PTH to the apical membrane of NHERF1 knockout cells results in minimal cAMP generation and no measurable calcium transients (Figure 9C). However, addition of PTH to basolateral surface stimulates a robust 6-fold increase in cAMP. In the absence of NHERF1, the EC_{50} for cAMP generation and average cAMP generated per receptor are comparable for both the apical and basolateral membranes (Figure 8B). Clearly, NHERF1 expression is the major determinant in the polarized distribution and signaling of PTH1R.

PTH increases intracellular calcium in a number of NHERF1-expressing osteoblastic cell lines (UMR-106, ROS cells stably expressing NHERF1), as well as in primary rat and human osteoblasts [35-39]. Unlike cells of renal origin, PTH-induced calcium transients in bone are relatively long (200 sec in ROS vs. 20-50 sec in MDCK or OK) and are insensitive to pertussis toxin [30, 40, 41]. Furthermore, in renal cells NHERF1 expression decreases PTH-induced cAMP generation, whereas in bone NHERF1 expression increases cAMP [30]. Clearly, NHERF1 regulates PTH1R signaling differently in these cell types. In bone, activation of aggregated PTH1R creates high

local concentrations of cAMP, which activates PKA in a spatially restricted manor. Activated PKA phosphorylates neighboring L-type calcium channels, increasing channel activity and producing a prolonged calcium transient (Figure 10) [42]. Consistent with this, PTH-induced calcium transients are blocked by chelation of extracellular calcium or L-type calcium channel inhibitors [30]. Two isoforms of the L-type calcium channel (1C and 1D) terminate in PDZ ligands (-Y-V-S-S-L and –C-I-T-T-L respectively), so it is possible that in osteoblasts NHERF1 nucleates a signaling complex containing both PTH1R and L-type calcium channels.

In both polarized and non-polarized cells, NHERF1 augments PTH1R signaling by creating new protein complexes at the plasma membrane. On the apical membrane of polarized cells, NHERF1 brings together PTH1R and G_i causing a PTH-induced PLC-mediated calcium burst (Figure 11). In osteoblasts, NHERF1 clusters PTH1R together with L-type calcium channels causing a prolonged calcium transient (Figure 10). In addition to the role of NHERF1 in PTH1R localization, it also induces differential signaling at opposite sides of the membrane within the same cell and can produce distinct effects on PTH second messenger systems in different cell types.

C. THE PCT PARADOX

NHERF1 knockout mice exhibit a complex phenotype linked to PTH1R function in the proximal convoluted tubule. Although serum PTH levels are normal, these mice exhibit PTH-insensitive renal phosphate wasting and elevated levels of 1,25 $(OH)_2$ vitamin D [27, 43]. This phenotype is paradoxical because it requires PTH1R signaling to be both inhibited and enhanced, respectively, in the same cell. PTH-insensitive

phosphate reabsorption suggests that PTH signaling is defective, yet high levels of vitamin D imply enhanced PTH1R activation. The key to understanding this phenotype is NHERF1's ability to regulate both the distribution and signaling of the PTH1R. Under normal conditions, NHERF1 targets the majority of PTH1R to the apical surface. Activation of this apical pool of PTH1R generates a small amount cAMP and PLC-dependent calcium transients, which inhibits phosphate reabsorption but does not induce expression of 1α-OHase (Figure 12). Activation of the PTH1R on the basolateral membrane induces expression of 1α-OHase but has minimal effect on phosphate uptake (Figure 12). The loss of NHERF1 causes a redistribution of PTH1R from the apical to basolateral membrane. The depleted pool of apical receptors is unable to produce a calcium burst in response to PTH and thus cannot regulate phosphate reabsorption (Figure 11). The increase in receptor density on the basolateral surface causes enhanced PTH signaling, elevated transcription of 1α-OHase and increased levels of 1,25 $(OH)_2$ vitamin D (Figure 13). Because NHERF1 expression is critical for the proper distribution and signaling of polarized PTH1R, it is fitting that NHERF1 knockout mice exhibit a phenotype reflecting dysfunction in both apical and basolateral signaling.

III. NHERF1 AND FRIZZLED: NOVEL PARTNERS

A. TETHERING THE TAILS

Frizzled receptors (Fzds) are a family of seven-transmembrane proteins that bind to Wnt and activate numerous signaling cascades (reviewed in [44]). They have a characteristically short intracellular tail that encodes both an internal PDZ ligand and, in some isoforms, a terminal PDZ ligand. Fzds 1, 2, 4 and 7 all terminate in the sequence E-T-x-V, which is predicted to have high affinity for class I PDZ domains (Figure 14) [7, 45]. All four of these Fzd receptors interact with PSD-95 in a yeast-2-hybrid assay [46]. In mammalian cells, Fzds 4 and 7 interact with the PDZ adaptor protein MAGI-3 [47], and Fzd 7 functionally binds syntenin [48].

As with PTH1R, NHERF1-Fzd interactions were demonstrated using multiple methods. NHERF1 co-immunoprecipitated with Fzd 4 but not with Fzd 4 containing a mutated PDZ ligand (Fzd 4 V573A) [49]. Similarly, NHERF1 expression decreased the diffusion coefficient of Fzd 4-GFP but had no effect on the mobility of Fzd 4 V573A-GFP. When expressed in NHERF1-containing cells, Fzd 4 clustered along phalloidin-positive fibers while Fzd 4 V573A remained uniformly distributed regardless of the presence of NHERF1 (Figure 15 A,B). Interestingly, Fzd 4 bound only to the second PDZ domain of NHERF1; transfection of a NHERF1 construct with a scrambled PDZ2 domain failed to influence the dynamics or distribution of Fzd 4 [49]. These results indicate that NHERF1 interacts with the C-terminus of Fzd 4 and tethers the receptor to the actin cytoskeleton.

Given the great similarity of the intracellular tails of Fzds 1, 2, 4, and 7 and the functional data below, it is reasonable to speculate that NHERF1 interacts with all four Fzds.

B. DUELING PDZ DOMAINS

The internal Dvl binding motif (K-T-x-x-x-W) interacts with the PDZ domain of disheveled (Dvl) and is necessary for signal transduction [4]. This internal PDZ ligand is separated from the terminal PDZ ligand by as few as 12 amino acids. Therefore, it is likely that binding of one PDZ protein will preclude binding of a second PDZ protein to the neighboring PDZ ligand. Fluorescently-tagged Dvl2 adopts a membrane-like distribution when expressed with Fzd 4. Co-expression of NHERF1 displaced Dvl2 from the membrane to the cytosol (Figure 16A). This suggests that NHERF1 and Dvl compete for the C-termini of Fzd receptors and under basal conditions there is higher affinity for NHERF1. The addition of Wnt induces the dissociation of NHERF1 allowing Dvl to be recruited to the membrane (Figure 16B).

Both canonical (i.e. β-catenin activation) and non-canonical (i.e. activation of small GTPases Rac and Rho) Wnt signaling appear to be mediated by different domains of the Dvl protein (reviewed in [50, 51]). If NHERF1 antagonizes Dvl-Fzd binding, then expression of NHERF1 should alter some aspects of Wnt signaling. Expression of NHERF1 profoundly inhibited Wnt-induced β-catenin affinity for Fzd 2, 4 and 7 (Figure 17A). As expected, it had no effect on Wnt signaling through Fzd 3, as Fzd 3 does not terminate in a PDZ ligand (Figure 17A) [49]. Inhibition of Wnt signaling was entirely mediated by interaction between the PDZ ligand of Fzd and PDZ2 of NHERF1 because

mutation in either of those domains blocked the effect (Figure 17B,C). In the human breast cancer cell line MCF7, shRNA knockdown of NHERF1 dramatically increased β-catenin signaling (Figure 17E). This increase in signaling is accompanied by a significant elevation in cyclin-D1 expression (a β-catenin response gene) and cellular proliferation (Figure 17F,G). This result has been confirmed *in vivo* by a proteomic study showing elevated levels of cytosolic β-catenin and increased expression of β-catenin responsive genes at the brush border of NHERF1 -/- mice [52]. Although previous reports show PDZ adaptor proteins can regulate non-canonical Wnt signaling [48], NHERF1 is currently the only PDZ protein known to regulate canonical Wnt signaling.

C. DISTORTED DUCT DENSITY

Expression of NHERF1 regulates cellular proliferation and migration (reviewed in [29]). Loss of NHERF1 increases cellular proliferation and invasion in multiple human breast cancer cells lines [49, 53-55]. This growth suppressive / tumor suppressive role for NHERF1 is consistent with the observation that NHERF1 is a key regulator of canonical Wnt signaling. *In vivo*, abnormal Wnt signaling manifests itself as a hyperproliferation of mammary ducts [56]. Consistent with this, the duct density of the mammary glands of virgin 10-week old NHERF1 knockout mice was four times greater than that of wild type littermates (Figure 18A). Almost 25% of the NHERF1 null mammary epithelium stained positive for the proliferation marker BrdU compared to 5% in wild type controls(Figure 18B). Immunofluorescence confirmed increased levels and increased nuclear localization of β-catenin in the ductal epithelium of NHERF1-null mice (Figure 18C). Interestingly, heterozygous mice also exhibited increased duct density

implying that both copies of NHERF1 are needed for complete regulation of Wnt signaling. This is especially significant because over 50% of human breast cancers exhibit loss of heterozygosity at the NHERF1 locus (17Q25.1) [53]. Thus, even a 50% decrease of NHERF1 expression can contribute to deregulated Wnt signaling and hyperproliferation.

Tamoxifen, an ERα antagonist, is a standard treatment for ER(+) breast malignancies. A subset of tamoxifen-treated patients develops highly aggressive recurrent tumors that are resistant to hormone therapy. Although clinically difficult to treat, a recent study shows these recurrent tumors are inhibited by low-dose estrogen treatment [57]. This paradoxical phenomenon may result from altered NHERF1/Wnt dynamics. NHERF1 expression is known to be estrogen-dependent and is inhibited by chronic tamoxifen treatment [58]. Reduced expression of NHERF1 would enhance Wnt signaling, increasing tumor proliferation and invasion (Figure 20A). Low-dose estrogen stimulates NHERF1 expression, dampening Wnt signaling. Consistent with this scheme, MCF7 cells made resistant to tamoxifen by chronic exposure (MCF7 LY2) express 75% less NHERF1 than the parental cell line (Figure 20B). As expected, these cells demonstrate enhanced Wnt-induced β-catenin activation and proliferation (Figure 20C). Ectopic expression of NHERF1 blunts the enhanced Wnt response, returning it to levels found in parental line (unpublished observation). If NHERF1 expression could be increased pharmacologically in the absence of estrogen, we propose that heightened Wnt responses would not occur and these hormone-resistant tumors would fail to form.

IV. DISCUSSION

A universal model of the biological roles of PDZ adaptor proteins must include three basic aspects of their cellular functions. First, PDZ adaptors direct delivery of their targets to specific subcellular regions. This requires the adaptor proteins to contain at least two domains – one (the PDZ domain) to interact with the target and another to determine the subcellular location (i.e. the MERM binding domain of NHERF1). Second, PDZ adaptors assemble and organize protein complexes in a dynamic manner. This dynamic scaffolding requires low affinity interactions that can be rapidly established or broken in response to extracellular cues. Finally, PDZ adaptors regulate downstream signaling by altering receptor-ligand affinity, modifying the second messenger cascade, or changing downstream effectors. The following discussion will elaborate on specific aspects of this model using the interactions of NHERF1 as an example.

A. DIRECTED DISTRIBUTION

In both non-polarized and polarized cells, NHERF1 clusters its targets to actin-rich domains. In non-polarized cells, NHERF1 co-localizes with phalloidin-positive actin fibers [31]. The distribution of NHERF1 in polarized cells is more complex. Although phalloidin-positive actin structures are found on the apical, lateral and basal surfaces, NHERF1 expression is limited to the apical surface (Figure 21). NHERF1 lacking the C-terminal MERM domain is homogeneously expressed in the cytoplasm, suggesting that

interaction with MERM proteins is critical for polarized localization (data not shown). Thus, I hypothesize that this confined distribution of NHERF1 is the result of its interactions with MERM proteins, because these proteins are also restricted to the apical surface. Consistent with this, staining of both mouse and human polarized epithelium shows that ezrin is primarily located at the apical membrane (data not shown). The reason for the apical localization of ezrin and other MERM proteins is unknown. One potential explanation is a disparity in phosphorylation states. Ezrin's binding to the actin cytoskeleton is driven by PKA-dependent phosphorylation [59, 60]. Therefore, the apical distribution of ezrin may reflect enhanced PKA activity at the apical membrane, which may be due to increased apical signaling, higher PKA levels at the apical surface, or to a lack of inactivating phosphodiesterases at the apical end of the cell. Although the mechanism is not clear, it is likely that the apical distribution of actin-binding proteins causes the same apical localization of NHERF1.

Although NHERF1 is the main adapter protein that targets PTH1R to actin fibers, it is not the only adapter protein capable of doing so. In fact, in CHO cells lacking NHERF1 approximately 30% of PTH1R clusters in bundles that run parallel to actin fibers (Figure 5A) [31]. Mutation of the PTH1R's PDZ ligand further reduces this clustering, suggesting that a second PDZ adaptor protein may be involved (Figure 5C). A prime candidate for this second PDZ protein is NHERF2, which interacts with PTH1R and binds the actin cytoskeleton [25, 61, 62]. Other adaptor proteins such as Dvl, ezrin, Tctex-1, and 4.1G could also target PTH1R along actin fibers as they bind both PTH1R and the actin cytoskeleton [63-67]. Given that all of these PTH1R partners bind downstream of residue 470, their contribution to PTH1R targeting could be experimentally tested using a PTH1R construct truncated at residue 470 (470Stop [63]). Finally, the potential for PTH1R to heterodimerize with other actin-directed membrane

proteins cannot be excluded. Previous work suggested that PTH1R heterodimerizes with the TGFβ receptor, which terminates in a class II PDZ ligand (-G-I-K-M) [68]. Therefore, it is possible that low affinity heterodimerization with other membrane proteins that themselves terminate in a PDZ ligand could recruit a fraction of PTH1R to the actin cytoskeleton.

In polarized cells, some PTH1R is still retained on the apical membrane following NHERF1 knockdown (Figure 6A, 7A). A similar fraction of PTH1R M593A localizes to the apical membrane implying that this apical pool is not the result of interaction with PDZ proteins (unpublished observation). Previous work suggested that in the absence of NHERF1 these receptors are held at the apical surface by direct interaction with ezrin [67]. My work suggests that these apical receptors are not actively targeted but randomly distributed. When unable to bind to NHERF1 (due to either NHERF1 knockdown or mutations in the PDZ ligand), approximately 28% of PTH1R resides on the apical surface. Importantly, the apical membrane constitutes 25% of the total membrane surface of MDCK cells [69]. The similarity between these two numbers suggests that in the absence of NHERF1, PTH1R uniformly coats both the apical and basolateral membranes. This model does not explain the *in vivo* distribution of PTH1R in the distal convoluted tubule (DCT). In DCT cells, which do not express NHERF1, PTH1R is restricted to the basolateral membrane, and not uniformly distributed. One possible explanation is that DCT cells express basolaterally targeted PDZ proteins that can interact with PTH1R and polarize its distribution to the basolateral membrane.

Although not experimentally shown, it is likely that NHERF1 targets Frizzled receptors to the apical membrane. NHERF1's ability to maintain proper apical distribution of Fzd receptors may be necessary for proper Wnt-Fzd signaling. In

Drosophila, both Frizzled receptor isoforms (fz and fz2 as designated in *Drosophila*) exist in polarized distributions and signal via different pathways (reviewed in [70]). Fz is apically localized and activates non-canonical/planar cell polarity (PCP) Wnt signaling, whereas fz2 is distributed along both the apical and basolateral membranes and mediates canonical Wnt signaling [71]. Interaction between the C-terminal tail of each receptor and polarized adaptor proteins (as of yet unidentified) mediates this polarized distribution. *Drosophila* express a NHERF1 analog (SIP-1), but its ability to interact with the fz receptors has not been tested [72]. Switching the distribution profiles of the two fz receptors (by switching the C-terminal portions of their tails) mildly inhibits PCP signaling but profoundly reduces canonical Wnt signaling [71]. Further investigation demonstrated that the decrease in canonical Wnt signaling was due to a redistribution of Dvl from the basolateral to apical surface [71]. Although Fzd distribution has not been linked to Wnt signaling in mammalian cells, these studies in *Drosophila* do raise the possibility that Fzd receptors may signal differently depending on which membrane they reside. Fzds on the apical membrane may preferentially signal through non-canonical pathways, while Fzds on the basolateral surface may preferentially activate β-catenin. Expression of NHERF1 should then favor non-canonical signaling and reduce canonical signaling. Consistent with this model, the NHERF1-/- mice exhibit phenotypes of enhanced β-catenin activation (increased mammary proliferation) and impaired non-canonical signaling (misalignment of ependymal cilia). The tissue specificity of these phenotypes probably results from the unique tissue-specific expression pattern of Wnts, Fzds and PDZ adaptor proteins.

B. DYNAMIC SCAFFOLDING

The second major function of PDZ adaptor proteins is to scaffold protein complexes. While perceived as static structures, the protein complexes are highly dynamic and rapidly reorganize in response to ligand binding or changes in the local environment. At its core, dynamic scaffolding relies on competition between adaptor proteins for low affinity binding sites in close proximity.

PDZ domains interact with their target via the four C-terminal amino acids, the so-called PDZ ligand. While a single PDZ domain is able to interact with PDZ ligands of difference sequences, it is likely that different PDZ ligand sequences have different binding affinities. These small differences in affinity could produce a PDZ domain bias. For example, full length NHERF1 binds both the PDZ ligand of PTH1R (E-T-V-M) and the PDZ ligand of Fzd 4 (E-T-V-V). The conservative substitution of methionine with valine should not dramatically alter the binding affinity. Yet, the PDZ ligand of PTH1R preferentially associates with PDZ1 of NHERF1 [73], but the PDZ ligand of Fzd 4 interacts almost exclusively with PDZ2 [49]. The subtle difference in affinities afforded by the methionine to valine substitution is enough to direct the PDZ ligand of Fzd 4 to the second PDZ domain of NHERF1. In a cell that expresses a diverse set of PDZ ligands, these subtle differences in affinity may dictate which PDZ ligands interact with which PDZ domains. Experimentally, these subtle biases may be overlooked due to the fact that overexpression of a protein shifts the equilibrium to favor binding of the overexpressed protein. This may explain why PDZ proteins, like NHERF1, have

numerous binding partners *in vitro* yet a very select number of functionally relevant binding partners *in vivo*.

PDZ domains bind PDZ ligands with affinities around 100 nM [7, 74-76]. Prior kinetic studies demonstrate that this binding occurs without rate-limiting conformational changes [77], allowing us to estimate the half life of the complex to be on the order of seconds. These low affinity, short half-life interactions allow the complex to be highly dynamic. Addition of PTH rapidly induces the dissociation of NHERF1 from PTH1R [31]. Uncoupling from NHERF1 allows PTH1R to complex with a second adaptor protein, β-arrestin. Competition between adaptor proteins arises when the binding sites are in close proximity. For example, the short C-terminal tail of Fzd 4 contains binding sites for both NHERF1 and Dvl separated by only twenty residues. The proximity of these binding sites makes it unlikely that both proteins occupy the receptor simultaneously. At rest, the majority of Fzd 4 is bound to NHERF1 and Dvl is diffusely distributed in the cytosol (Figure 16A). Binding of Wnt induces the rapid dissociation of NHERF1 from Fzd 4, which opens the Dvl binding site. Dvl is recruited to the C-terminus of Fzd 4 where it both transduces signals and internalizes the receptor (Figure 16B,C). This shift in binding partner can be observed by measuring Dvl recruitment to the membrane following the addition of Wnt. Within 6-8 half lives (~180 to 250 seconds) Fzd's PDZ ligand dissociates from NHERF1 and binds Dvl, causing an increase in Dvl at the membrane (Figure 16B).

C. REGULATION OF GPCR SIGNALING

In addition to targeting and scaffolding, adaptor proteins also directly regulate GPCR signal transduction. By interacting with PTH1R, NHERF1 can alter the sensitivity for the ligand, alter which G-proteins couple to the receptor and change which effectors are activated by the second messenger.

I^{125}-PTH binding experiments in CHO cells clearly demonstrate that PTH1R has decreased affinity for PTH when bound to NHERF1 (2.4 nM in control cells vs. 12.8 nM in NHERF1 expressing cells, Figure 22). This difference in K_d is also observed when comparing PTH1R on the apical and basolateral membranes of polarized MDCK cells (Figure 6A). The simplest explanation of this behavior is based on thermodynamic considerations. The complex of receptor, NHERF1 and PTH can be modeled as simultaneous binding of multiple ligands (NHERF1 and PTH). In a multi-ligand system, negative cooperativity occurs when the binding of one ligand decreases the affinity for the second. Because binding of PTH to the receptor induces the dissociation of NHERF1 (i.e. lowers the affinity of PTH1R for NHERF1) [31], PTH and NHERF1 exhibit negative cooperativity. The converse must also be true; binding of NHERF1 to PTH1R must decrease its affinity for PTH. However, this simple thermodynamic model must be viewed with caution, as it assumes that the system is in equilibrium, a condition that might not be found in a live cell. Furthermore, there is abundant evidence of covalent modifications of both PTH1R and NHERF1 after the addition of PTH (i.e., phosphorylation [29, 78-80] and ubiquitination [81]). Thus, the magnitude of this cooperative effect may be small and masked by other biological processes. Finally, PTH-induced recruitment of additional intracellular partners of PTH1R, such as β-

arrestin, must be taken into account. My data show that expression of NHERF1 delays recruitment of β-arrestin to the receptor [31, 82], demonstrating that NHERF1 and β-arrestin binding are not independent phenomena. Nevertheless, regardless of the exact mechanism, my experiments show that, at least in some cells, NHERF1 decreases the affinity of PTH1R for PTH. Under experimental conditions using saturating concentrations of PTH this decrease may be trivial, but *in vivo,* where circulating PTH concentrations range from 1-7 pM, this small decrease may have important consequences [83].

In addition to regulating ligand affinity, NHERF1 also regulates which G-proteins couple with PTH1R. In their initial description of this "signaling switch", Mahon and colleagues demonstrated that expression of NHERF1 caused PTH signaling to switch from exclusively cAMP to cAMP and calcium. The PTH-induced NHERF1-dependent calcium transients were sensitive to both Pertussis toxin and pharmacologic phospholipase C inhibition, suggesting the involvement of $G\alpha_i$ [23]. GTP-γ-S binding experiments from our laboratory confirmed that NHERF1 expression causes PTH to activate G-proteins other than $G\alpha_s$ [63]. Interestingly, expression of NHERF1 increases the amount of PTH-induced activation of $G\alpha_q$, not $G\alpha_i$, as hypothesized by Mahon and colleagues [23]. My work with MDCK cells supports a model where NHERF1 increases coupling of PTH1R and Pertussis toxin-sensitive $G\alpha_i$. One possible explanation for these discordant results is that the NHERF1-induced G-protein switch is cell-type specific. In proximal tubule-like MDCK and OK cells NHERF1 couples PTH1R and $G\alpha_i$, but in less differentiated HEK293 cells, NHERF1 couples PTH1R to $G\alpha_q$. In bone cells (UMR and ROS expressing NHERF1) this signaling switch does not occur [30].

Although the exact mechanism of the NHERF1-mediated G-protein switch is unknown, several models have been proposed. One possible mechanism is that G_i is enriched at the apical membrane [84, 85]. NHERF1 recruits PTH1R to the apical membrane, where it is exposed to high concentrations of G_i. When activated by PTH, a small subset of PTH1R would couple to $G_i\alpha\beta\gamma$ and produce a calcium transient. Consistent with this model, disruption of the apical targeting of PTH1R by depolymerizing the actin cytoskeleton with cytochalasin D inhibits PTH-induced calcium transients [23]. Coupling only a small percentage of receptor to G_i is also consistent with the observation that apical PTH stimulates a large amount of cAMP in polarized MDCK cells (Figure 8A). Furthermore, immunohistochemistry has shown that at least two isoforms ($G\alpha_i1$ and $G\alpha_i2$) localize to the apical membrane of renal tubular cells [86]. A second potential mechanism is that NHERF1 directly recruits G_q to the receptor. The second PDZ domain of NHERF1 binds PLCβ, which in turn interacts with G_q [67, 87]. Activated receptor couples to this vicinal G_q and produces a calcium transient. This model is supported by the observation that PLCβ strongly co-localizes with PTH1R and that NHERF1 expression increases PTH-induced GTP-γ-S binding to G_q. However, it does not explain why the calcium transients are Pertussis toxin-sensitive, as G_q is unaffected by Pertussis toxin treatment. These two models are not mutually exclusive and may occur to distinct degrees in different cell types. Experimentally, these two models can be differentiated based on the requirement for either the second PDZ domain or MERM binding domain. NHERF1 lacking the C-terminal MERM binding domain (NHERF1 ΔERM) should delocalize the receptor from the actin cytoskeleton but still allow PLCβ and G_q recruitment. NHERF1 containing a mutated PDZ2 domain (NHERF1 S2) would still properly localize the receptor but would be unable to scaffold the receptor-PLCβ-G_q complex. If the main function of NHERF1 is to localize PTH1R to

G-protein rich domains (i.e. model 1) then NHERF1 S2 should function identically to wild type while NHERF1 and ΔERM should abolish PTH-induced calcium transients. If NHERF1 is serving as a scaffold, then a NHERF1 ΔERM construct that contains both PDZ domains should permit PTH-induced calcium signaling while expression of NHERF1 S2 should not.

As mentioned above, the G-protein switch does not occur in cell lines derived from bone. This is likely due to differences in protein expression. While NHERF1 still localizes PTH1R to actin fibers, osteoblastic cells may not express the correct adapter protein or G-protein isoform to enrich these areas with G_i. Even if the cells express the correct G-protein / adapter protein pair, the expression may not be high enough to force coupling of a significant amount of PTH1R. In addition to not being able to create G_i-rich subcellular regions, bone cells may express different NHERF1 interaction proteins that prevent G_q recruitment. While all three PLCβ isoforms interact with NHERF1 *in vitro*, only PLCβ1 and 3 interact *in vivo* [23]. If bone cells predominantly express PLCβ2, then NHERF1 would be unable to scaffold the PTH1R-NHERF1-PLCβ1-G_q complex. Assuming bone cells express the correct PLCβ isoform, they may also express other NHERF1 binding proteins that compete for the second PDZ domain. As noted earlier, two isoforms of the L-type calcium channel (1D and 1C) terminate in PDZ ligands predicted to interact with NHERF1. It is possible that in bone cells NHERF1 clusters PTH1R and L-type calcium channels instead of scaffolding PTH1R with PLCβ and G_q. This would be consistent with our data that NHERF1 does not cause a G-protein switch in ROS cells but promotes PTH-induced activation of L-type calcium channels [30].

The final way that NHERF1 alters PTH1R signaling is by altering which effectors are activated by second messenger signaling. Addition of 100 nM PTH to the apical or basolateral membrane stimulates almost identical cAMP responses (Figure 8A). However, only basolateral cAMP appears to induce transcription of the 1α-OHase gene (Figure 12B). This suggests that cAMP generated on the apical membrane activates different effectors than cAMP generated from the basolateral surface. Specifically, basolateral cAMP activates the transcription factor CREB which enters the nucleus and increases transcription of 1α-OHase. While controversial, generation of apical cAMP appears to be more important for internalizing the sodium phosphate transporter and regulating phosphate uptake (reviewed in [88]). Therefore, by determining the localization of the receptor, NHERF1 can influence what downstream effectors will be activated by the second messenger cascade.

D. PUZZLING PHENOTYPES FOR MOUSE AND MAN

In addition to the phenotypes already described, NHERF1-/- mice also exhibit a 30% decrease in bone density and a 40% decrease in bone mineral content [27]. The majority of NHERF1-/- mice have evidence of bone fractures by X-ray [27]. Histologically, these mice exhibit irregular trabecular bone with large amount of unmineralized osteoid (unpublished observation). This pathology is very similar to that seen in the human disease rickets. Osteoblasts build bone by depositing collagen matrix (osteoid) that is then coated by calcium hydroxyapatite crystals ($Ca_{10}(PO_4)_6OH_2$). This calcium-phosphate lattice gives bones their rigidity and tensile strength. Rickets (also known as osteomalacia when it occurs in adults) is characterized by the inability to

deposit calcium and phosphate onto osteoid. Patients with rickets present with bowed legs, craniotabes (soft skull bones), and multiple bone fractures. The most common cause of rickets is nutritional vitamin D deficiency. Low levels of vitamin D prevent proper calcium absorption by the small intestine resulting in low serum calcium (hypocalcemia) and secondary elevation of PTH (secondary hyperparathyroidism). Calcium is not deposited onto osteoid causing weak bone. This pathophysiology is not consistent with the NHERF1-/- phenotype because the knockout mouse exhibits elevated levels of vitamin D (Figure 13B) and normal serum calcium values [27]. A second, rarer form of rickets, hypophosphatemic rickets, is caused by excessive phosphate wasting. The inability to retain phosphate leads to low serum phosphate levels and defective bone mineralization despite high levels of circulating vitamin D. Hereditary rickets with hypercalciuria (HHRH) is a genetic form of hypophosphatemic rickets caused by mutations in Npt2a (SLC34A3) [89]. HHRH patients present with low levels of serum phosphate (hypophosphatemia), increased excretion of phosphate (hyperphosphaturia) and calcium (hypercalciuria), normal PTH and elevated vitamin D levels. This presentation is consistent with the NHERF1-/- mice that exhibit decreased serum phosphate levels, increased urine phosphate levels, normal PTH levels and elevated vitamin D levels [27, 43]. Superficially, phosphate wasting due to loss of NHERF1 seems to explain the bone phenotype in NHERF1-/- mice. However, knockout of Npt2a, the alleged target of NHERF1 in the kidney, produces a more severe phosphate wasting but no rachitic phenotype [90, 91]. This suggests that phosphate wasting may not be the cause of the NHERF1-/- bone phenotype. To experimentally test this, NHERF1-/- mice should be supplemented with phosphate. If phosphate supplementation normalizes both the hypophosphatemia and bone phenotypes, then a causative relationship is correct. If supplementation does not correct the bone phenotype

that is strong evidence that the bone and kidney phenotypes of the NHERF1-/- mouse are independent.

If the bone phenotype is independent of mineral ion disturbances, then what is the molecular mechanism? One clue may be that the marrow cavity of NHERF1-/- mice is filled with adipose tissue. Progenitor cells in the marrow cavity proliferate and differentiate into either osteoblasts or adipocytes in response to paracrine and endocrine signals. *In vitro* and *in vivo,* transient PTH administration increases both proliferation and differentiation of osteoblasts [92-96]. These effects are thought to be mediated by changes in gene expression secondary to phosphorylation and activation of transcription factors AP-1, CREB and Runx2 (Figure 10). Consistent with this hypothesis, knockout of c-fos (a member of the AP-1 transcription factor family) and mutation of PKA-phosphorylation sites on CREB and Runx2 inhibit PTH-induced osteoblastogenesis and bone formation [97-100]. Based on our studies in an osteosarcoma cell line, NHERF1 knockout progenitor cells should not be able to generate a calcium transient in response to PTH [30]. Therefore, in the absence of NHERF1, PTH-induced PKC activation of AP-1 would be impaired. Furthermore, PTH stimulates less cAMP in the absence of NHERF1 [30]. Decreased cAMP will result in less PKA activation and decreased activation of CREB and Runx2. All together, the loss of NHERF1 should significantly diminish PTH-induced gene expression. In the absence of pro-osteoblast signals, progenitor cells differentiate into adipocytes by default. Canonical Wnt signaling also contributes to the differentiation of osteoprogenitors and pre-osteoblasts to osteoblasts (reviewed in [101]). However, the majority of this signaling is mediated by Fzd 6 (which does not terminate in a PDZ ligand) and thus would be insensitive to NHERF1 [102].

NHERF1 interacts with Fzd receptors and inhibits Wnt-induced β-catenin activation (Figure 19). One would expect the NHERF1-/- mouse to have deregulated Wnt signaling, resulting in developmental defects and neoplasia. However, the NHERF1 knockout develops normally and does not develop spontaneous neoplasia within the first two years of life. How can we reconcile these two facts? Although we speculate that NHERF1 interacts with eight of the ten Fzd receptors due to the presence of canonical C-terminal PDZ ligands in their sequences, we have only experimentally proven this interaction for Fzd 1, 2, 4 and 7. Furthermore, we have proven that Fzd 3 does not interact with NHERF1. Therefore, it is possible that the majority of Wnt signaling is transduced by Fzds that do not interact with NHERF1. An alternative hypothesis would be that there are other PDZ proteins that can also regulate canonical Wnt signaling. Previous work demonstrates that several other PDZ proteins are capable of interacting with Fzd receptors. For example, MAGI-3, which has a similar expression pattern to NHERF1, binds Fzd 4 (and presumably other Fzds) with its second PDZ domain [47, 103]. Interestingly, while other PDZ adaptor proteins have been found to interact with the Fzd receptor, they only appear to regulate non-canonical signaling. NHERF1 appears to be unique in its ability to regulate canonical signaling. However, future studies may reveal this is not the case.

The promoter of NHERF1 contains several estrogen response elements [58, 104]. Consistent with this, NHERF1 expression is estrogen-dependent in a variety of tissues including mammary, colonic, biliary, and endometrial epithelia [58, 105-107]. Conversely, estrogen does not increase NHERF1 expression in renal proximal convoluted tubule or pituitary GH3 cells [108, 109]. These results indicate that regulation of NHERF1 by estrogen is cell-type specific. This cell-type specific signaling does not appear to be mediated by differential expression of estrogen receptor isoforms, as

several observations suggest that both ERα and ERβ can stimulate NHERF1 expression [54, 105, 106, 110, 111]. Estrogen regulates NHERF1 expression in both the uterus, which predominantly expresses ERα, and the colon, which mainly utilizes ERβ [105, 106, 110]. Estrogen up-regulated NHERF1 expression in human osteosarcoma cells stably expressing either ERα or ERβ [111]. Finally, NHERF1 is expressed at high levels in breast cancer cells that express either ERα or ERβ alone [54]. Assuming that both ER isoforms are capable of interacting with the ERE in NHERF1's promoter, it may be differential expression of ER co-activators or co-repressors that mediate the cell-specific effects.

Not surprisingly, tamoxifen and other anti-estrogens can decrease NHERF1 expression. As described above, treatment of MCF7 cells with tamoxifen results in decreased NHERF1 expression (Figure 20B). This also occurs *in vivo*; tumors recurring after tamoxifen treatment express less NHERF1 than the parental tumor (Figure 23). However, it is still unclear whether this tamoxifen-induced decrease in NHERF1 has functional or clinical relevance. Based on our *in vitro* studies, decreases in NHERF1 expression should enhance Wnt signaling and induce a more aggressive tumor phenotype. While some tumors do become more aggressive following tamoxifen treatment, they comprise only a small minority [112, 113]. Clearly, there are other factors that determine if tamoxifen-induced NHERF1 suppression will correlate with poor treatment outcome. One such factor may be the initial level of NHERF1 expression. A recent proteomic study of tamoxifen-sensitive and tamoxifen-resistant tumors found that NHERF1 expression was approximately 2.5-fold higher in tamoxifen-sensitive tumors [114]. This increased NHERF1 expression was independent of estrogen receptor levels and thus assumed to be partially mediated by estrogen-independent pathways. If a

tumor has high NHERF1 levels, tamoxifen treatment may not decrease NHERF1 sufficiently to increase Wnt signaling. The tumor would be unable to respond to estrogen (due to tamoxifen) or Wnt (due to sufficient levels of NHERF1) and would remain in remission. In tumors with low initial levels of NHERF1, tamoxifen would decrease NHERF1 below a critical threshold, where Wnt signaling would be enhanced and the treatment would fail. Significantly, this model suggests that a pharmacological agent able to induce NHERF1 expression should significantly enhance tamoxifen treatment and decrease the occurrence of tamoxifen-resistant tumors.

V. IMPLICATION FOR DISEASE

Given the central role of PDZ-PDZ ligand interactions in proper cell function, it is not surprising that their disruption causes disease. Disruption of the multiple-PDZ containing protein harmonin (either by frameshift mutation [115], insertion [116], or point mutation within PDZ1[117]) results in Usher syndrome, a severe sensory disorder resulting in hearing loss and retinal degeneration. Similarly, frameshift [118, 119] and point mutations [120] in the PDZ protein periaxin causes Charcot-Marie-Tooth disease, an inherited neuropathy. Polymorphisms in the NHERF family of PDZ proteins contribute to the development of metabolic and mineral ion disorders. A single nucleotide polymorphism (SNP) in NHERF3 (PDZK1_i33968 C > T) is associated with elevated plasma triglycerides, abdominal obesity and metabolic syndrome [121]. In the related family member NHERF1, two polymorphisms (c.328C > T, c.458 G > A) and one mutation (c.673G > A) have been linked to nephrolithiasis and bone demineralization [122]. Still other mutations (c.516 A > G, c.537 C > T, c.902 A > T) have been found in breast cancer cells but not in normal controls [53]. The majority of these mutations are in the second PDZ domain, implying that PDZ2 is particularly important for proper NHERF1 function. This is unexpected given that the majority of proteins interact with NHERF1 through the first PDZ domain. As we understand more about how PDZ proteins regulate cellular signaling their role in disease is sure to expand.

The emerging recognition of the role of PDZ proteins in disease makes them attractive targets for drug development. The first attempt at modulating PDZ-PDZ ligand

interactions came in the form of blocking peptides. The Glu2 subunit of AMPA receptors interacts with the PDZ proteins PICK1 and GRIP. Expression of a 10-amino acid peptide corresponding to the C-terminus of Glu2 blocked interaction between Glu2 and its PDZ partners, resulting in decreased surface expression and inhibition of long term depression (LTD) [123]. Despite the effectiveness of blocking peptides, they are of limited therapeutic use due to poor membrane permeability and rapid degradation. Although more difficult to create, small molecular inhibitors offer the best chance of being medically useful. Given the structural diversity and specificity of the binding pocket of PDZ domains, it should be possible to engineer class- and domain-specific inhibitors. Using indole-based chemistry, small-molecule antagonists have been developed for PDZ domains in MAGI3 [124, 125], Dvl [126] and NHERF1 [127]. When evaluated with purified PDZ domains and ligands, these molecules inhibited interactions with IC_{50}s in the mid-micromolar range [127]. Recently, a second generation inhibitor for the PDZ domain of Dvl has been identified that blocks Wnt signaling both *in vitro* and *in vivo* at nanomolar concentrations [128]. With continued research, PDZ domain inhibitors will increase in number, diversity, specificity, and potency and will likely provide novel treatments for rare and common diseases.

It is clear that there is still much to learn about the cell biology, physiology, pathology and pharmacology of PDZ adaptor proteins. The next steps in PDZ biology will be to fully characterize the ligand profile for all known PDZ proteins and decipher the role of these interactions *in vitro* and *in vivo*. With this knowledge, we will be able to understand better how mutations and dysregulation of PDZ proteins contribute to disease. Finally, discovery of specific PDZ protein inhibitors has the potential to make a profound impact in treating numerous metabolic and neoplastic disorders.

PUBLICATIONS

The following publications provide the basis of the work described in this thesis.

Wheeler D and Sneddon WB. *Mutation of Phenylalanine-34 of Parathyroid Hormone Disrupts NHERF1 Regulation of PTH Type I Receptor Signaling.* Endocrine. 2006 Dec;30(3):343-52.

Wheeler D, Sneddon WB, Wang B, Friedman PA, Romero G. *Dynamics and Traffic of the Parathyroid Hormone Receptor: Regulation by NHERF-1 and the Cytoskeleton.* JBC. 2007 Aug 24;282(34):25076-87.

Wheeler D, Garrido JL, Bisello A, Kim YK, Friedman PA, Romero G. *Regulation of PTH1R dynamics, traffic and signaling by the Na+/H+ exchanger regulatory factor-1 (NHERF-1) in rat osteosarcoma ROS 17/28 cells.* Mol Endocrinol. 2008 May;22(5):1163-70. Epub 2008 Jan 17.

Wheeler D, Barrick SR, Brufsky A, Friedman PA and Romero G. *Direct interaction between NHERF1 and Frizzled regulates β-catenin signaling and inhibits cancer proliferation*. Oncogene. 2010 Aug 30. [Epub ahead of print]

Wheeler D, Barrick SR, Igwe B, Romero G, Friedman PA. *NHERF1 determines the localization and signaling of Parathyroid hormone type 1 receptor (PTH1R) in polarized epithelium*. (in preparation)

The following publications were completed during graduate studies but are not included in this thesis.

Zhang X*, **Wheeler D***, Tang Y, Guo L, Shapiro RA, Ribar TJ, Means AR, Billiar TR, Angus DC, Rosengart MR. *Calcium/calmodulin-dependent protein kinase (CaMK) IV mediates nucleocytoplasmic shutting and release of HMGB1 during LPS stimulation of macrophages*. J Immunol. 2008 Oct 1;181(7):5015-23. (*These authors contributed equally)

Garrido JL*, **Wheeler D***, Leiva-Vega L, Friedman PA, Romero G. *The role of Phospholipase D in Parathyroid Hormone Receptor signaling and trafficking.* Mol Endocrinol. 2009 Dec;23(12):2048-59. Epub 2009 Oct 16. (*These authors contributed equally)

Romero G, Sneddon WB, Yang Y, **Wheeler D**, Blair HC, Friedman PA. *Parathyroid hormone receptor directly interacts with dishevelled to regulate β-catenin signaling and osteoclastogenesis.* 2009. J Biol Chem. 2010 May 7;285(19):14756-63. Epub 2010 Mar

Feinstein TN, Wehbi VL, Ardura J, **Wheeler DS**, Ferrandon S, Gardella TF, Vilardaga JP. *Retromer terminates the generation of cAMP by internalized parathyroiod hormone receptors*. (in revisions for Nat Chem Biol.)

FIGURE LEGENDS

Figure 1: Structural model of PDZ – PDZ ligand interaction. A model of the PTH1R PDZ ligand (ball and stick, CPK colored) docked in PDZ1 of NHERF1 (ribbon diagram, navy blue). Terminal Met593 occupies a hydrophobic pocket at the head of the groove. His72 (yellow) and Arg40 (red) salt bridge with Thr591 and Glu590 providing specificity for the consensus sequence-E-S/T-x-V/L/M.

Figure 2: Structure and phylogeny of NHERF family of PDZ proteins.

Figure 3: Tissue distribution of NHERF1. Hemi-section of a mouse stained for NHERF1 (A). NHERF1 is expressed in the proximal convoluted tubules of the kidney (B) the ependyma of the brain (C) and osteoblasts in bone (D).

Figure 4: NHERF1 decreases the lateral mobility of PTH1R. CHO-N10 cells were transfected with PTH1R-eGFP or PTH1R M593A-eGFP and NHERF1 expression was induced with tetracycline for 24 hours. The diffusion coefficient of the fluorescent receptor was measured using image cross-correlation spectroscopy as described in [31].

Figure 5. Distribution of PTH1R in non-polarized cells. CHO-N10 cells expressing the indicated constructs were imaged using TIRF microscopy. The percentage of receptor was measured as described in [31] and is indicated above the scale bar. Scale bar represents 5 μm.

Figure 6. Distribution of endogenous PTH1R in wild type and shNHERF1 polarized MDCK cells. (**A**) Wild type and shNHERF1 MDCK cells were grown to confluency on transwell filters. Cells were considered to be polarized when the transepithelial resistance was greater than 2,000 Ohms. Receptor numbers were calculated from radioligand binding experiments as previously described [30]. (**B**) Receptor density was calculated by dividing the receptor number by the membrane surface area as reported by [69].

Figure 7. Distribution of PTH1R-eGFP in wild type and shNHERF1 polarized MDCK cells. (**A**) Sub-confluent wild type or shNHERF1 MDCK cells were transfected with PTH1R-eGFP and grown to confluency on transwell filters. Upon polarization of the MDCK cells, the filters were fixed, removed from the transwells, stained for E-cadherin, mounted on slides and imaged with confocal microscopy. A 15-20 image Z-stack was obtained for each cell. (**B**) The basolateral membrane was defined by presence of E-cadherin staining (images not shown). The intensity of PTH1R on the apical and basolateral membranes was measured using ImageJ. The percentage of apical and basolateral PTH1R was calculated by dividing the individual intensities by the total sum.

Figure 8. PTH-induced cAMP generation at the apical and basolateral membrane. (**A**) Various concentrations of PTH were added to the apical or basolateral membrane of polarized MDCK cells. cAMP was measured as previously described [30]. (**B**) NHERF1 knockdown MDCK cells showed decreased apical and increased basolateral cAMP response.

Figure 9. Expression of NHERF1 causes apical PTH1R to couple to $G\alpha_i$ and stimulate a calcium transient. (**A**) PTH-induces a rapid calcium transient when added to the apical membrane of polarized wild type MDCK cells. This calcium transient is not observed when PTH is added to the basolateral surface. (**B**) PTH-induced calcium transients are inhibited by pre-treatment with Pertussis toxin or gallein. (**C**) Knockdown of NHERF1 prevents apical PTH1R from generating calcium transients.

Figure 10. Model describing how NHERF1 directs PTH1R signaling in osteoblasts. NHERF1 binds the PDZ ligand of PTH1R and clusters it along actin fibers. Aggregated PTH1R produces high concentrations of cAMP, which activate PKA. PKA phosphorylates L-type calcium channels enhancing their activity and producing a calcium transient. This calcium transient activates PKC. PKA and PKC phosphorylate transcription factors (AP-1, CREB, and Runx2) that increase expression of genes necessary for proliferation and osteoblastic differentiation.

Figure 11. NHERF1 regulates the distribution and signaling of PTH1R in polarized cells.

Figure 12. Apical PTH1R regulates phosphate uptake, while basolateral PTH1R regulates 1α-OHase expression. (**A**) Polarized MDCK cells were treated with vehicle, 100 nM apical PTH or 100 nM basolateral PTH for 4 hours. Radioactive phosphate uptake in Na-replete or Na-free buffer was measured by liquid scintillation. Na-dependent phosphate uptake was calculated by subtracting Na-free phosphate uptake from phosphate uptake in Na-replete buffer. (**B**) Polarized MDCK cells were treated with vehicle, 100 nM PTH on the apical surface, 100 nM PTH on the basolateral surface or

100 nM PTH on both surfaces for 8 hours. 1α-OHase expression was quantified with qPCR using GAPDH as an endogenous control.

Figure 13. NHERF1-/- mice have increased expression of 1α-OHase and increased concentrations of $1,25(OH)_2$ vitamin D. (**A**) 1α-OHase and VDR mRNA levels were measured in whole kidney lysates using qPCR (* $p < 0.05$, Students' t-test). (**B**) Serum $1,25(OH)_2$ vitamin D concentrations of NHERF1+/+ and NHERF1-/- littermates (* $p < 0.05$, Students' t-test).

Figure 14. Multiple sequence alignment of the terminal amino-acids of Fzd receptors.

Figure 15. NHERF1 modulates the distribution and dynamics of Fzd 4. (**A, B**) CHO-N10 cells were transfected with Fzd 4-eGFP or Fzd 4 V573A-eGFP and stained with phalloidin-Alexa 546. Scale bar represents 5 μm. (**C, D**) Lateral mobility of Fzd 4 in control and NHERF1 expressing cells was measured by FRAP. (* $p < 0.05$, Students' t-test)

Figure 16. NHERF1 inhibits Fzd-Dvl coupling. (**A**) In control CHO-N10 cells Dvl2-mRFP localizes to the plasma membrane. Expression of NHERF1 displaces Dvl2 from the membrane to the cytosol. (**B**) CHO-N10 cells expressing Fzd 4-eGFP and Dvl2-mRFP were rapidly imaged using TIRF microscopy. All intensities were normalized to Fzd 4-eGFP to account for receptor internalization. Addition of Wnt5a is indicated by an arrow. (**C**) NHERF1 expression decreases the amount of Dvl2 that co-immunoprecipitates with Fzd 4. The amount of Dvl-Fzd complex after Wnt5a treatment was not affected by NHERF1 expression.

Figure 17. Enhanced Wnt signaling occurs in the absence of NHERF1. (**A**) CHO-N10 cells were co-transfected with the indicated Fzd receptors and either TOP or FOP luciferase reporter plasmid. NHERF1 expression blunted Wnt-induced luciferase expression via Fzd 2, 4 and 7 but had no effect on Wnt signaling through Fzd3 (** $p < 0.01$, * $p < 0.05$, Two-way ANOVA with Bonferroni post-hoc tests). (**B**) Mutational ablation of the Fzd 4 PDZ ligand (Fzd 4 V573A) rescues Wnt signaling from NHERF1 inhibition. This mutation has no effect on Wnt signaling in the absence of NHERF1. (**C**) Wnt-induced β-catenin activation was blocked by wild type NHERF1 and NHERF1 containing a mutated PDZ1 domain (S1). This inhibition was not generated by NHERF1 containing a mutated PDZ2 domain (S2) or with both PDZ domains mutated (S1S2) (*** $p < 0.001$, One-way ANOVA with Tukey post-hoc tests). (**D**) Transfection of MCF7 cells with NHERF1-targeted shRNA reduced expression by 95%. (**E**) NHERF1 knockdown enhanced Wnt-induced β-catenin activation in MCF7 cells (* $p < 0.05$, ** $p < 0.01$, Two-way ANOVA with Bonferroni post-hoc tests). (**F**) Following 8 hours of treatment with Wnt, NHERF1 knockdown cells shown increased levels of cyclin-D1. (*** $p < 0.001$, Two-way ANOVA with Bonferroni post-hoc tests). (**G**) Wnt-induced proliferation was measured using a 24 hour radiolabeled-thymidine incorporation assay. MCF7 cells lacking NHERF1 showed marked proliferative responses to both Wnt3a and Wnt5a compared to scrambled controls (** $p < 0.01$, *** $p < 0.001$, Two-way ANOVA with Bonferroni post-hoc tests). Adapted from [49].

Figure 18. Mammary glands of NHERF1-/- mice exhibit elevated duct density, increased proliferation and heightened β-catenin activation. (**A**) The fourth and fifth mammary glands from virgin NHERF1+/+ and NHERF1-/- mice were removed and histologically

prepared. Ductal density was quantified from at least 10 high-power fields from three different animals (* $p<0.05$, Students' t-test). (**B**) Breasts from NHERF1+/+ and NHERF1-/- mice injected with BrdU were removed, embedded in paraffin and sectioned. BrdU incorporation was visualized by immunofluorescence. Percentage of BrdU(+) cells was quantified from three independent animals (* $p<0.05$, Students' t-test). (**C**) Individual ducts from NHERF1+/+ and NHERF1-/- mice stained with DAPI, anti-β-catenin and NHERF1. Scale bar 20 μm.

Figure 19. Model for NHERF1 regulation of distribution and signaling of Fzd receptors. PDZ2 of NHERF1 interacts with the C-terminal PDZ ligand of Fzd receptors, tethering them to the actin cytoskeleton. Addition of Wnt induces the dissociation of NHERF1, allowing Dvl to be recruited and activated. In the absence of NHERF1, Fzd-Dvl precoupling causes enhanced Wnt signaling and hyperproliferation.

Figure 20. Tamoxifen treatment reduces NHERF1 expression and enhances Wnt signaling. (**A**) Schema for the regulation of NHERF1 expression and Wnt signaling by tamoxifen. (**B**) NHERF1 expression was measured by qPCR in MCF7 cells and MCF7 cells chronically treated with tamoxifen (MCF7 LY2). (**C**) Wnt-induced β-catenin in MCF7 and MCF7 LY2 cells was measured using the TOP/FOP luciferase reporter assay.

Figure 21. NHERF1 localizes to the apical membrane in polarized MDCK cells.

Figure 22. NHERF1 expression right-shifts ^{125}I-PTH binding curves in CHO-N10 cells.

Figure 23. Decreased NHERF1 expression and increased β-catenin staining are observed in breast tumors that recur following tamoxifen treatment.

FIGURES

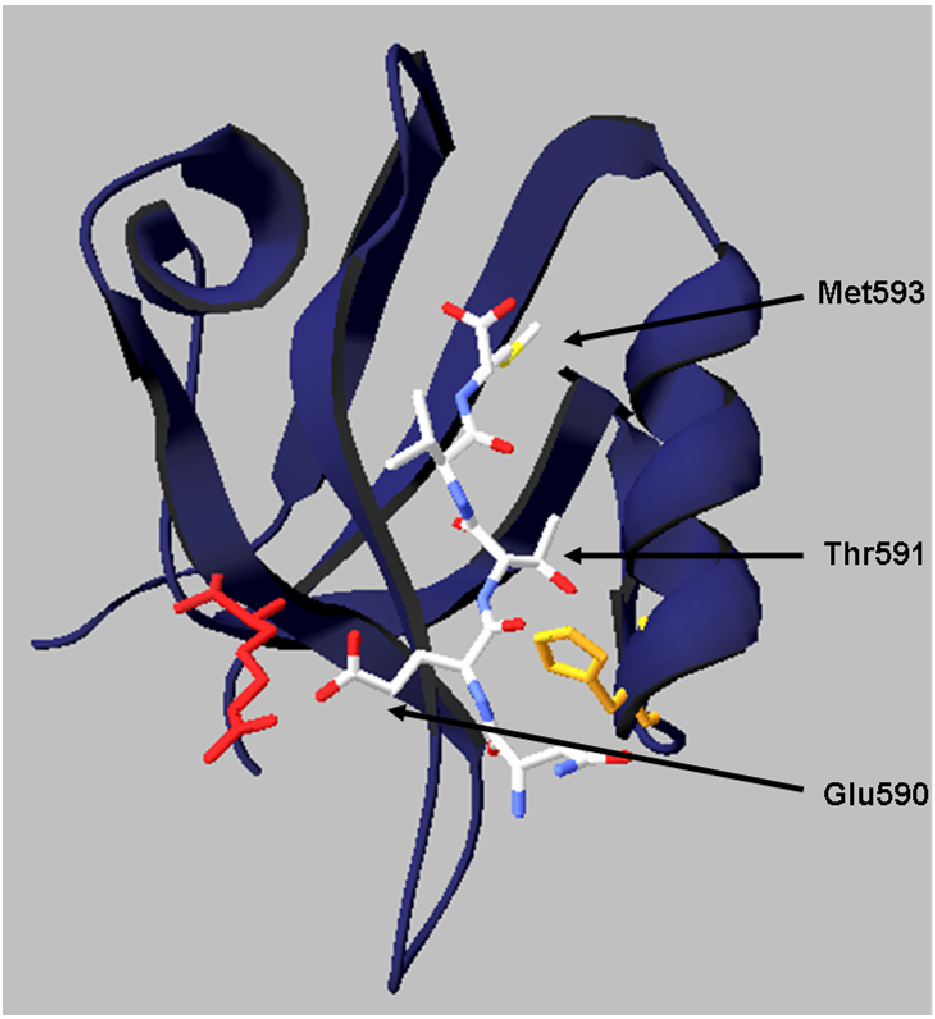

Figure 1

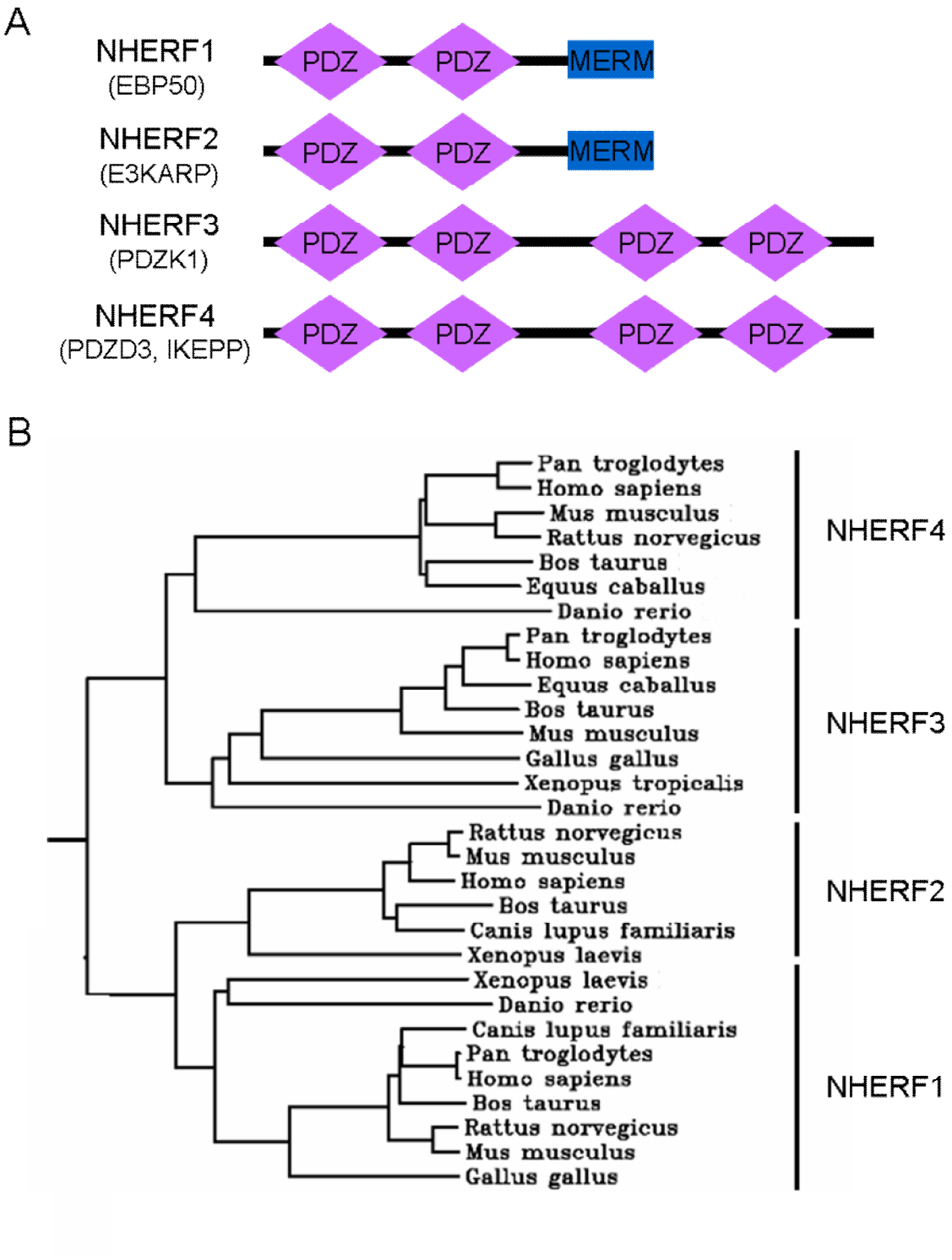
A
NHERF1
(EBP50)
PDZ
PDZ
MERM
NHERF2
(E3KARP)
PDZ
PDZ
MERM
NHERF3
(PDZK1)
PDZ
PDZ
PDZ
PDZ
NHERF4
(PDZD3, IKEPP)
PDZ
PDZ
PDZ
PDZ
B
Pan troglodytes
Homo sapiens
Mus musculus
Rattus norvegicus
Bos taurus
Equus caballus
Danio rerio
NHERF4
Pan troglodytes
Homo sapiens
Equus caballus
Bos taurus
Mus musculus
Gallus gallus
Xenopus tropicalis
Danio rerio
NHERF3
Rattus norvegicus
Mus musculus
Homo sapiens
Bos taurus
Canis lupus familiaris
Xenopus laevis
NHERF2
Xenopus laevis
Danio rerio
Canis lupus familiaris
Pan troglodytes
Homo sapiens
Bos taurus
Rattus norvegicus
Mus musculus
Gallus gallus
NHERF1

Figure 2

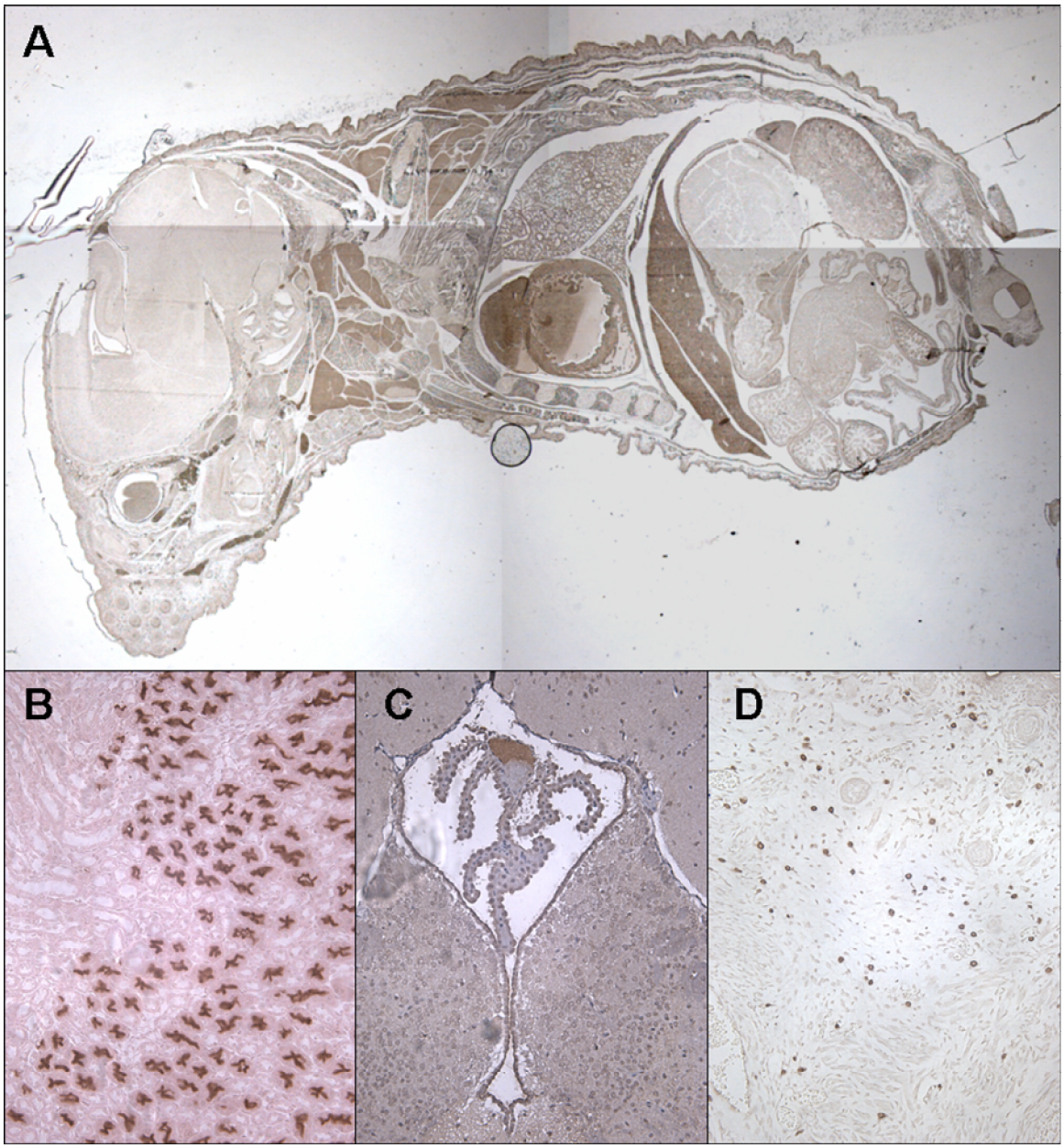

Figure 3

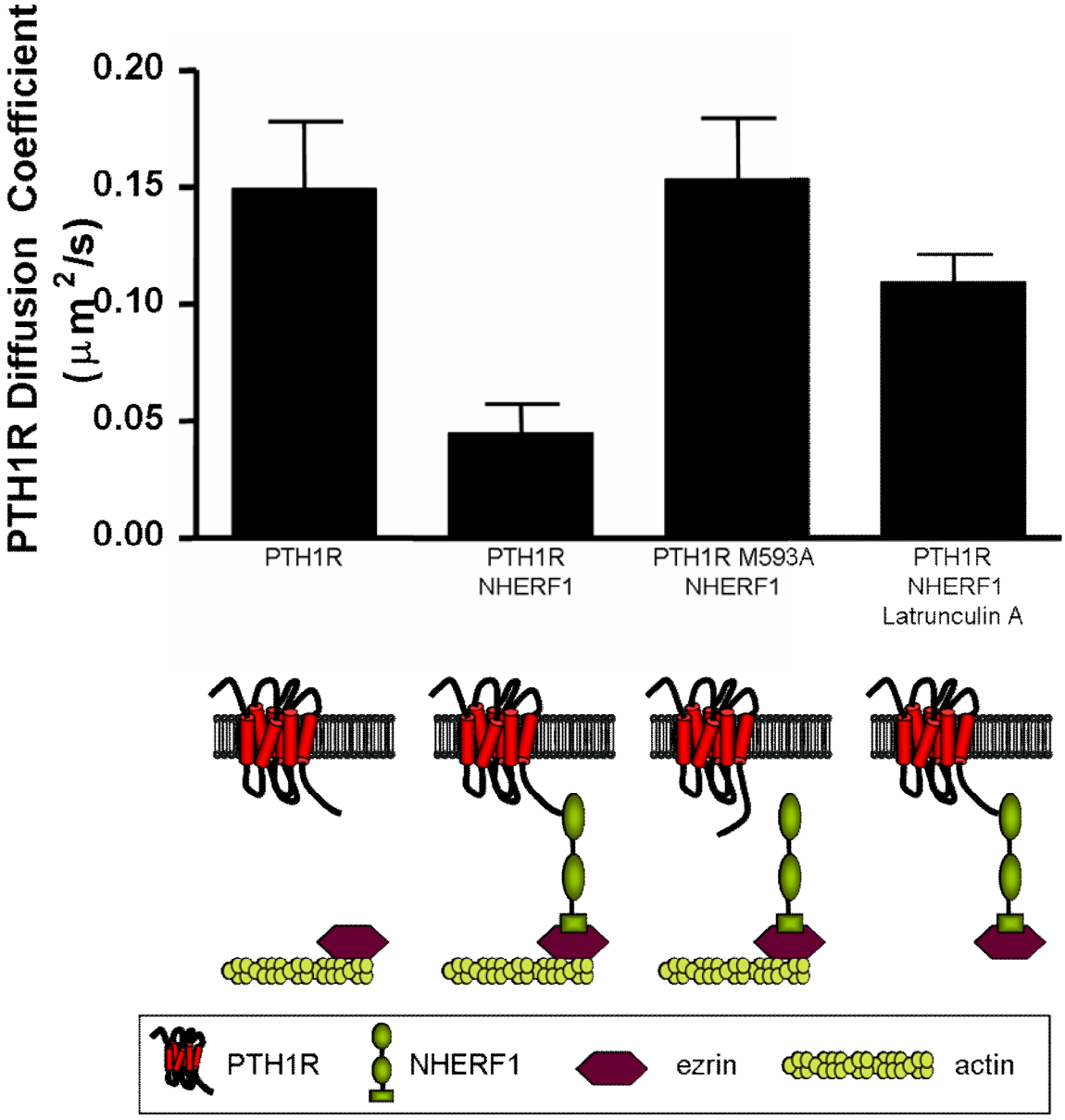
PTH1R Diffusion Coefficient
(μm²/s)
0.20
0.15
0.10
0.05
0.00
PTH1R
PTH1R NHERF1
PTH1R M593A NHERF1
PTH1R NHERF1 Latrunculin A
PTH1R
NHERF1
ezrin
actin

Figure 4

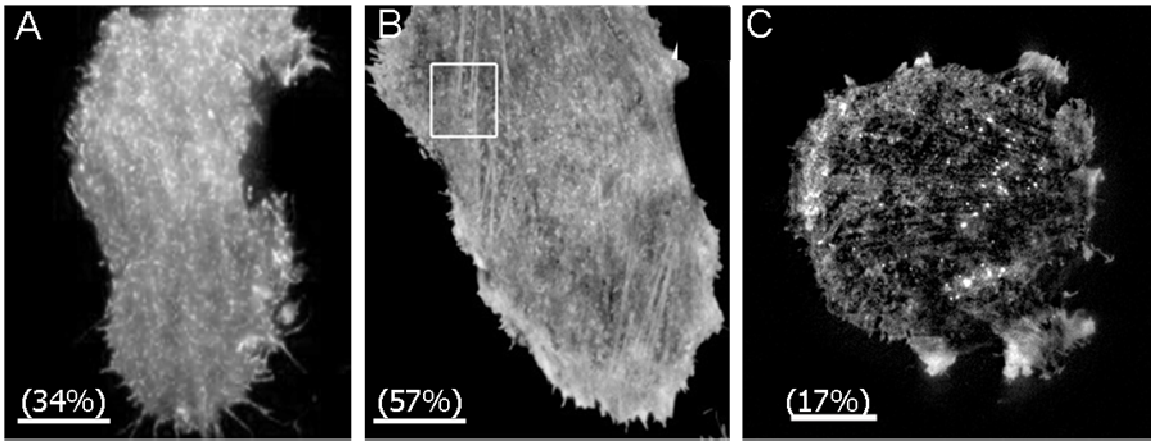
A
(34%)
PTH1R-eGFP
B
(57%)
PTH1R-eGFP
NHERF1
C
(17%)
PTH1R M593A -eGFP
NHERF1

Figure 5

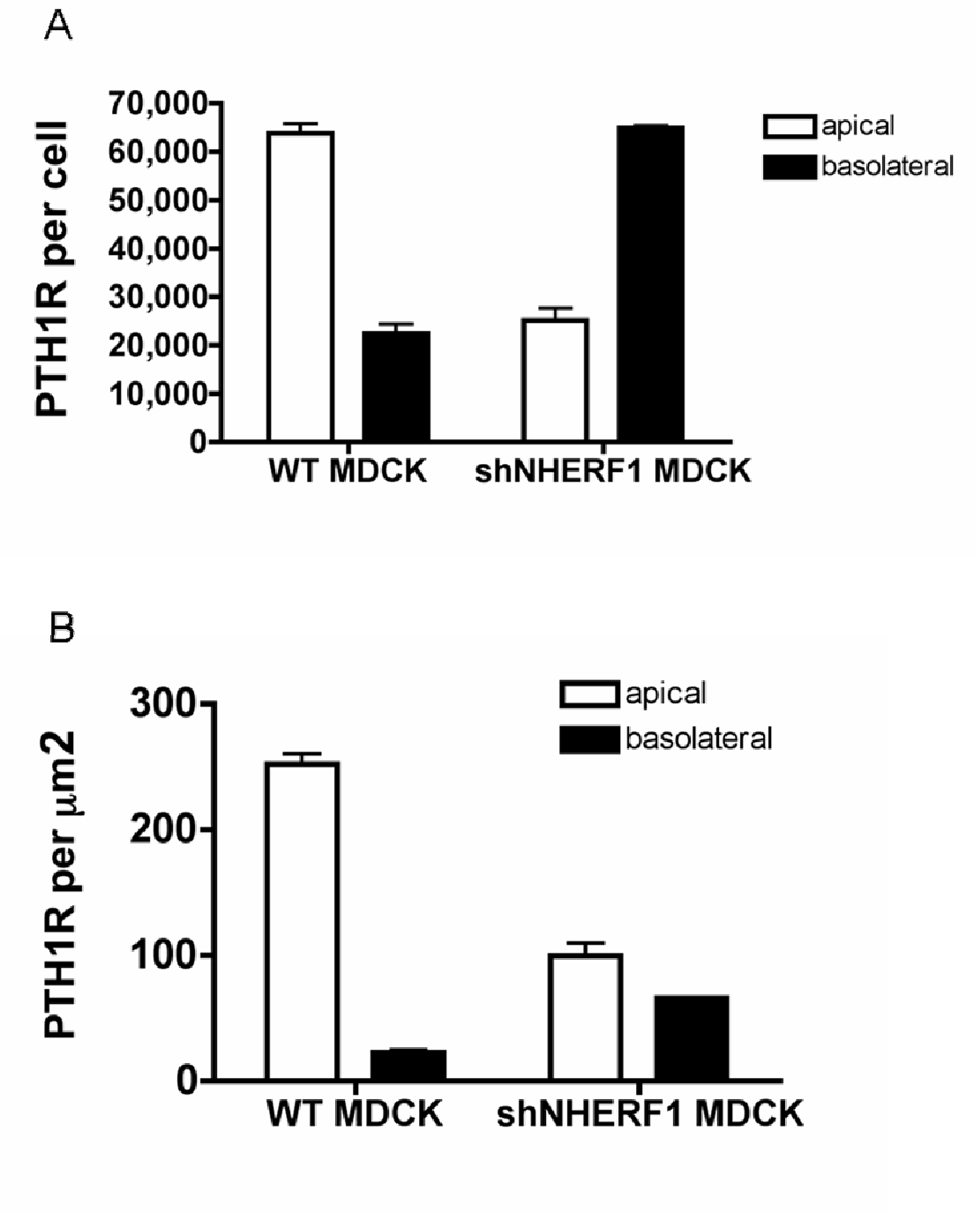
A
PTH1R per cell
70,000
60,000
50,000
40,000
30,000
20,000
10,000
0
apical
basolateral
WT MDCK
shNHERF1 MDCK
B
PTH1R per μm2
300
200
100
0
apical
basolateral
WT MDCK
shNHERF1 MDCK

Figure 6

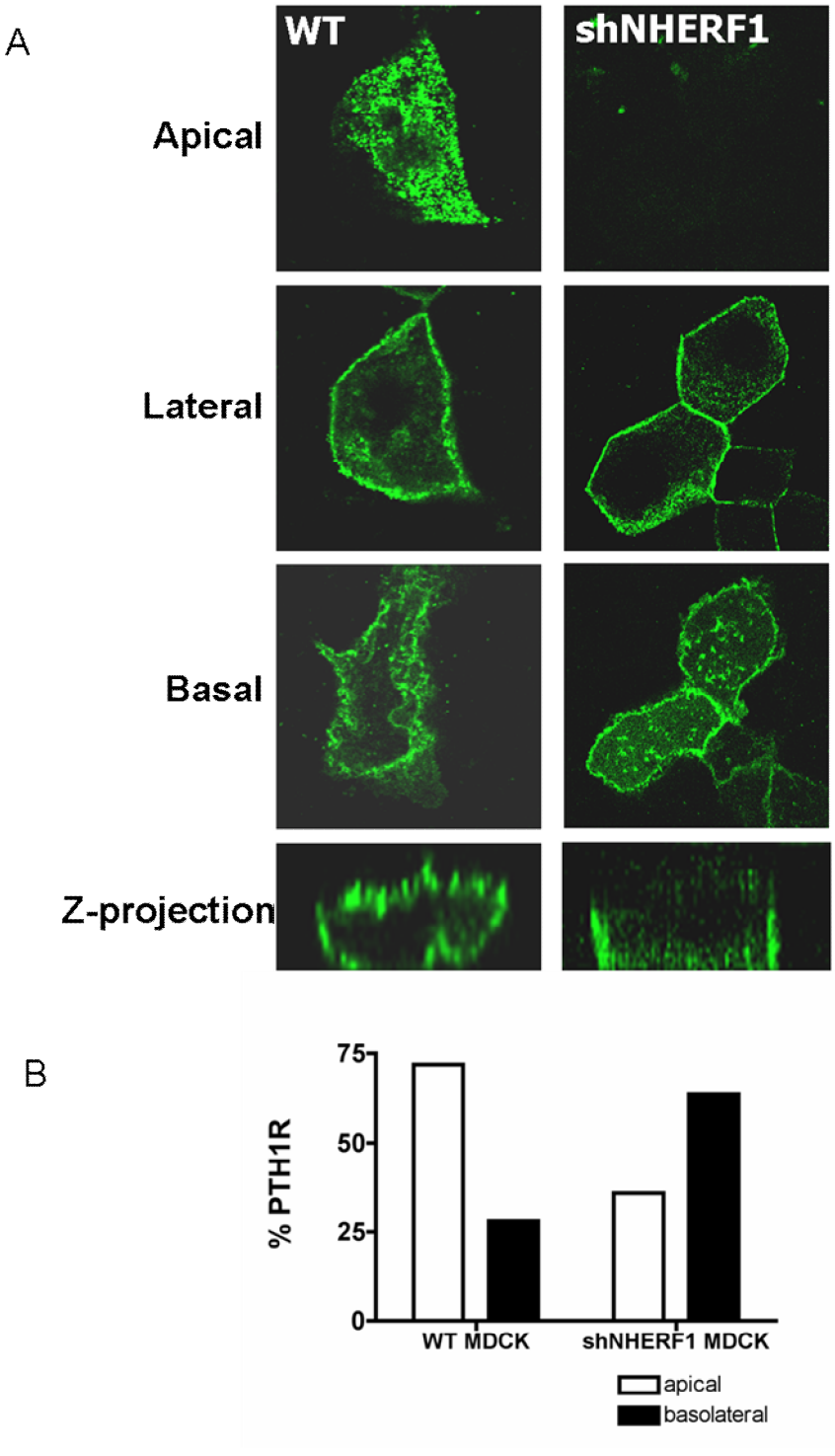
A
WT
shNHERF1
Apical
Lateral
Basal
Z-projection
B
% PTH1R
75
50
25
0
WT MDCK
shNHERF1 MDCK
apical
basolateral

Figure 7

A

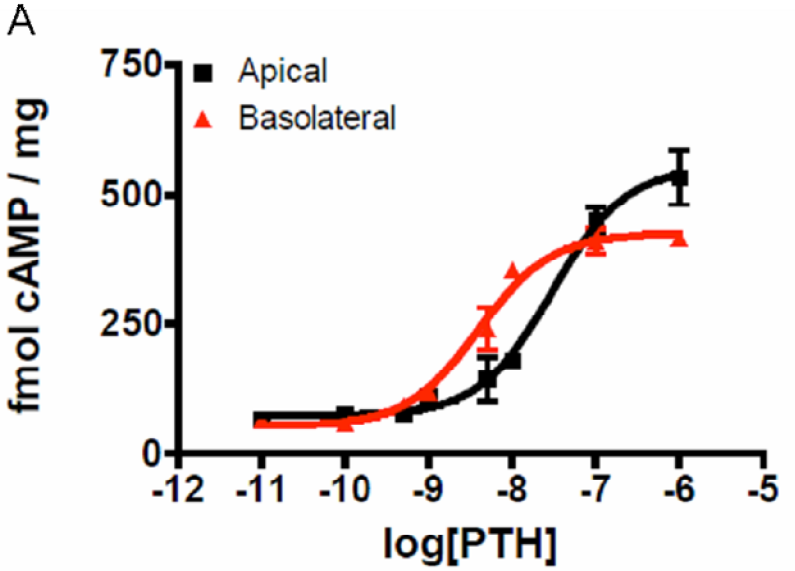

	Apical	Basolateral
BOTTOM	73.80	52.49
TOP	552.0	425.6
LOGEC50	-7.525	-8.405
EC50	2.985e-008	3.934e-009

B

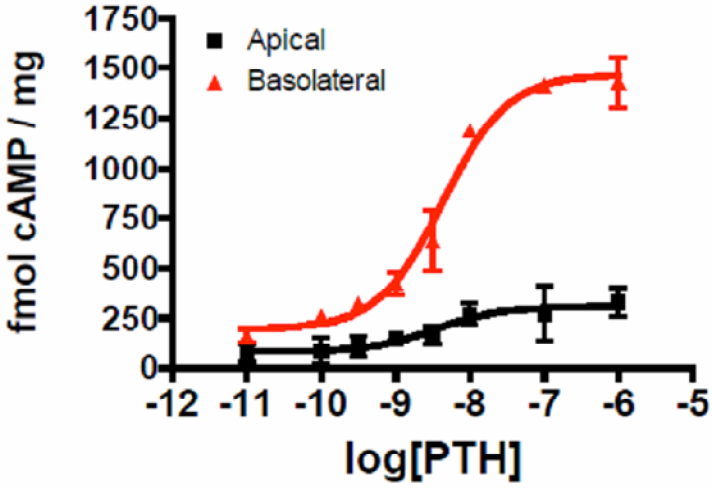

	Apical	Basolateral
BOTTOM	81.22	195.3
TOP	308.1	1469
LOGEC50	-8.465	-8.364
EC50	3.426e-009	4.329e-009

Figure 8

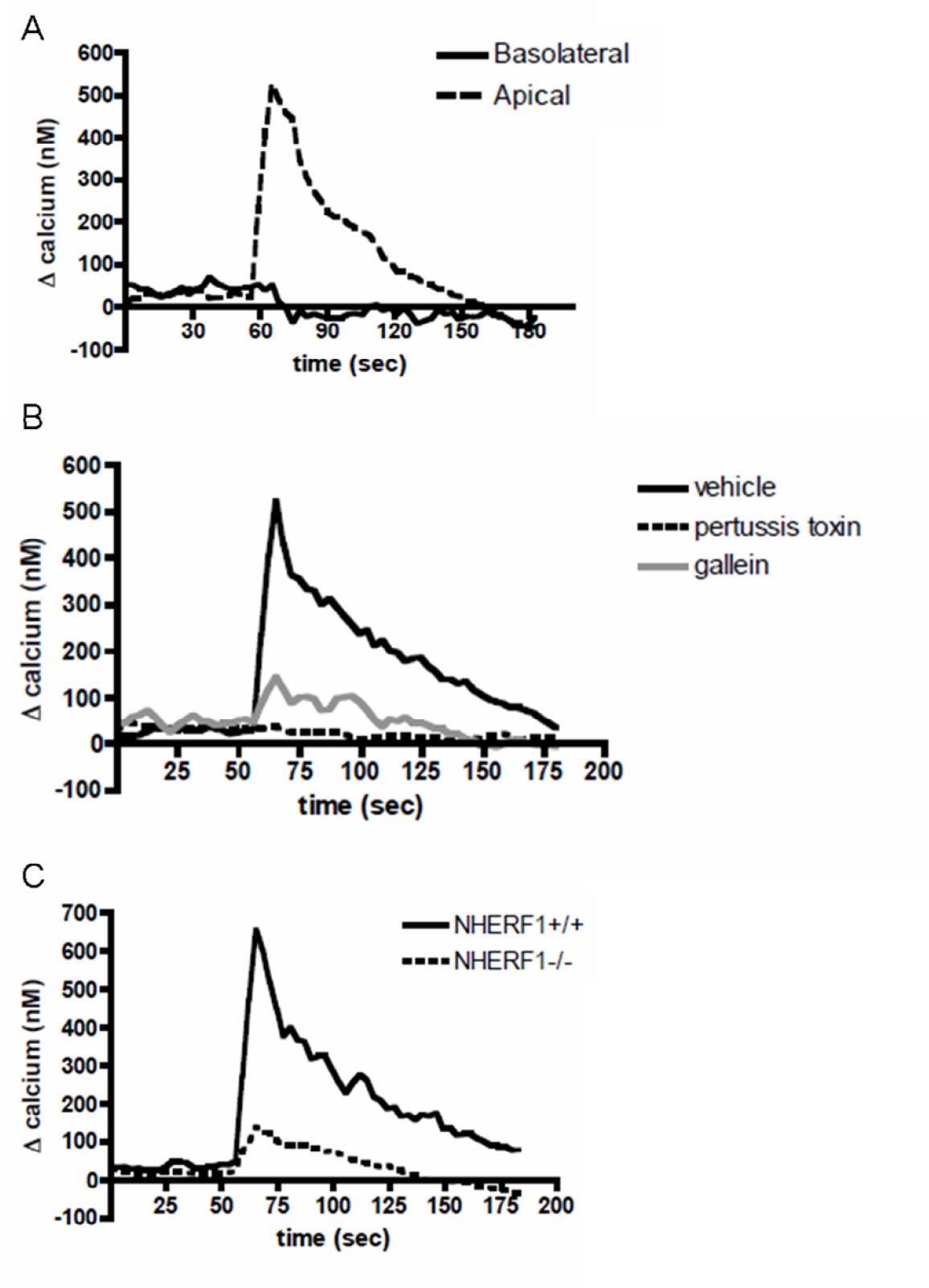
A
Basolateral
Apical
Δ calcium (nM)
600
500
400
300
200
100
0
-100
30
60
90
120
150
180
time (sec)
B
vehicle
pertussis toxin
gallein
Δ calcium (nM)
600
500
400
300
200
100
0
-100
25
50
75
100
125
150
175
200
time (sec)
C
NHERF1+/+
NHERF1-/-
Δ calcium (nM)
700
600
500
400
300
200
100
0
-100
25
50
75
100
125
150
175
200
time (sec)

Figure 9

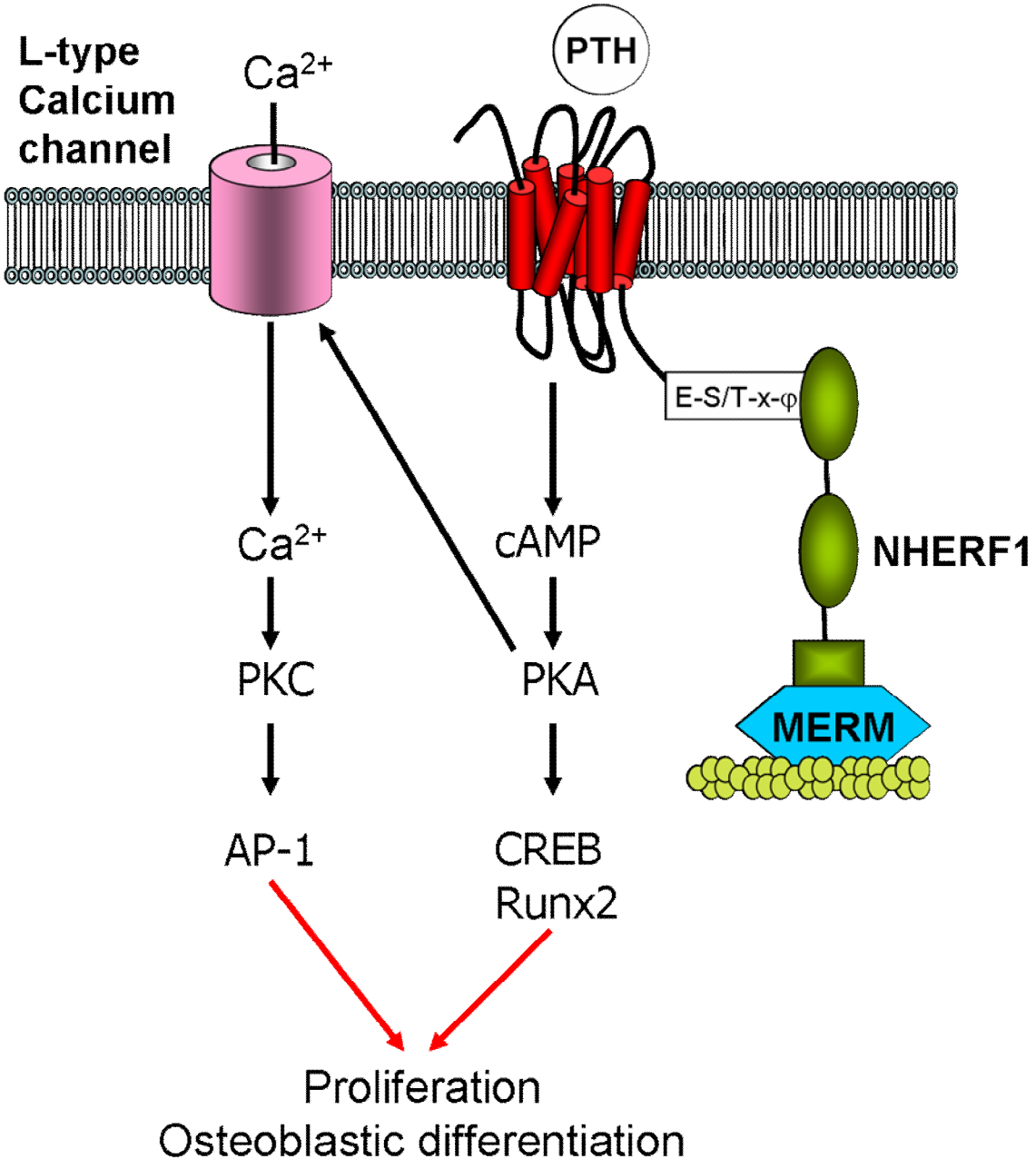
L-type
Calcium
channel
Ca2+
PTH
E-S/T-x-φ
NHERF1
MERM
Ca2+
cAMP
PKC
PKA
AP-1
CREB
Runx2
Proliferation
Osteoblastic differentiation

Figure 10

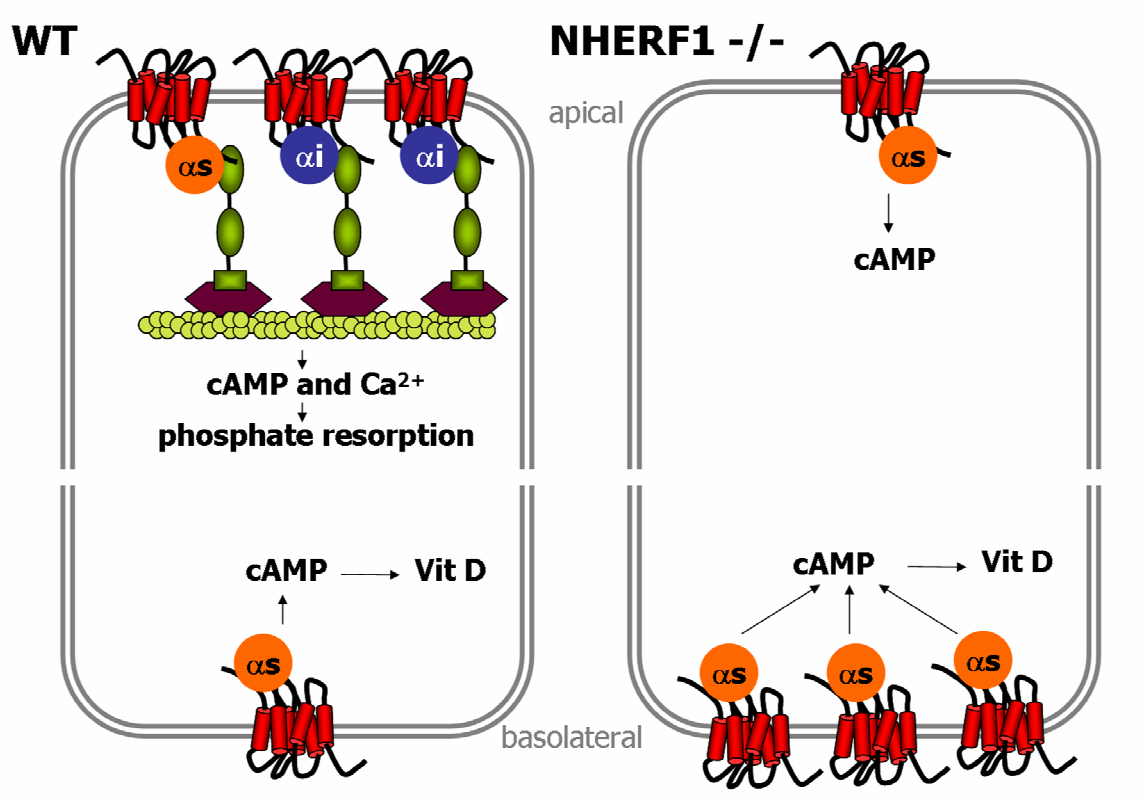
WT
NHERF1 -/-
apical
αs
αi
αi
cAMP and Ca2+
phosphate resorption
cAMP
Vit D
αs
basolateral
αs
cAMP
Vit D
αs
αs
αs

Figure 11

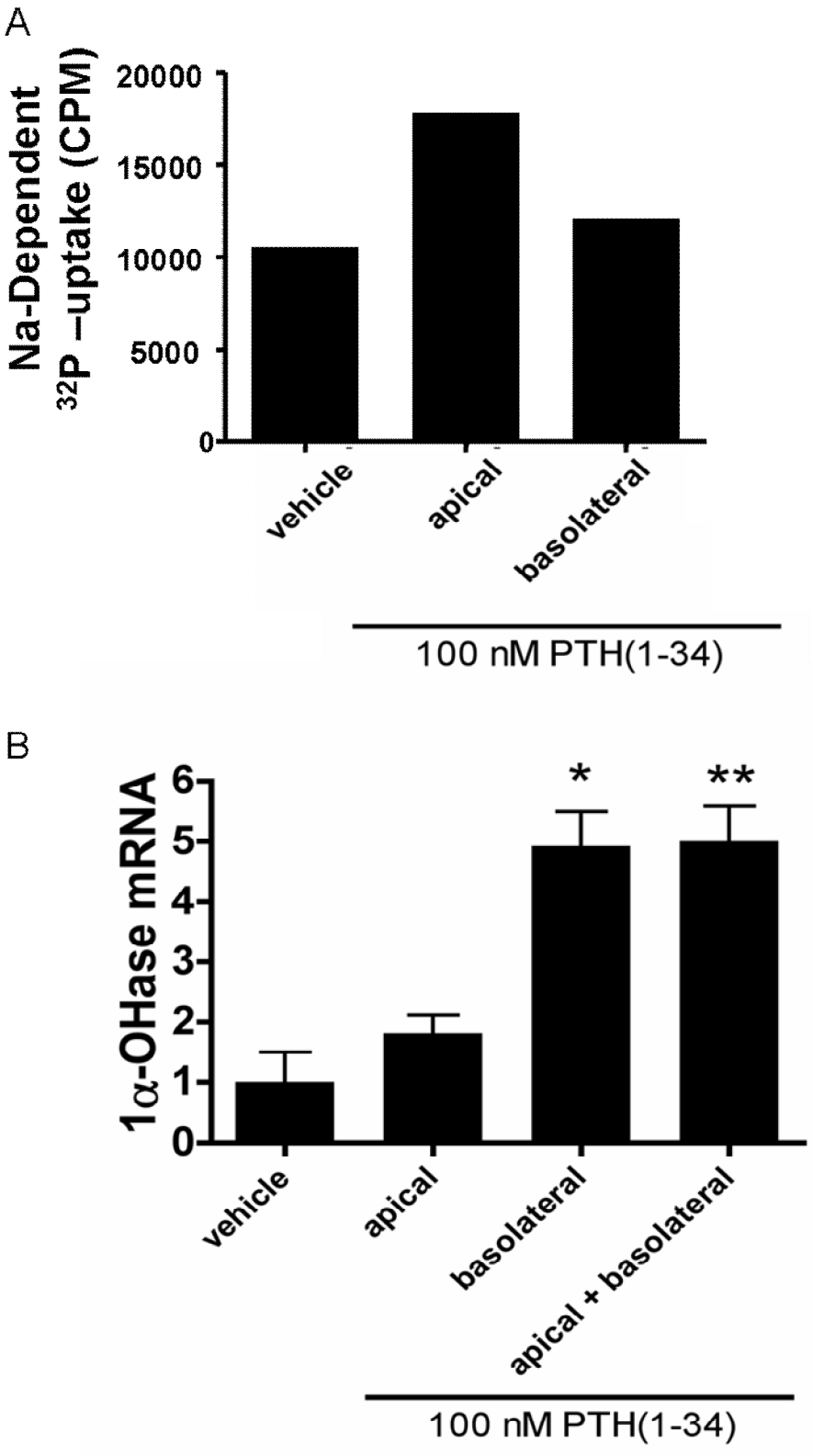
A
Na-Dependent
32P –uptake (CPM)
20000
15000
10000
5000
0
vehicle
apical
basolateral
100 nM PTH(1-34)
B
1α-OHase mRNA
6
5
4
3
2
1
0
*
**
vehicle
apical
basolateral
apical + basolateral
100 nM PTH(1-34)

Figure 12

A

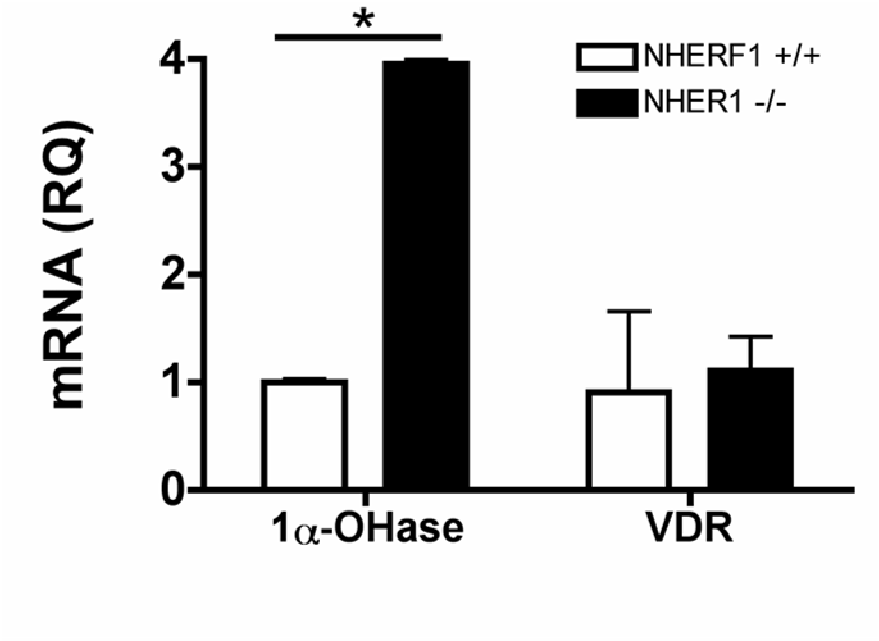
*
NHERF1 +/+
NHER1 -/-
mRNA (RQ)
4
3
2
1
0
1α-OHase
VDR

B

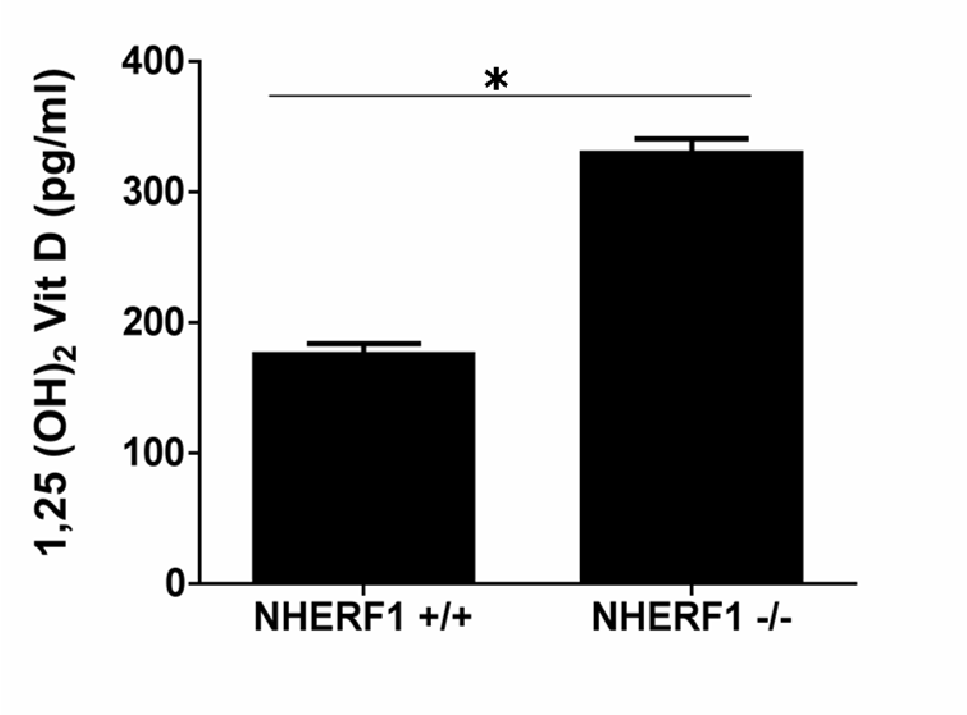
*
1,25 (OH)2 Vit D (pg/ml)
400
300
200
100
0
NHERF1 +/+
NHERF1 -/-

Figure 13

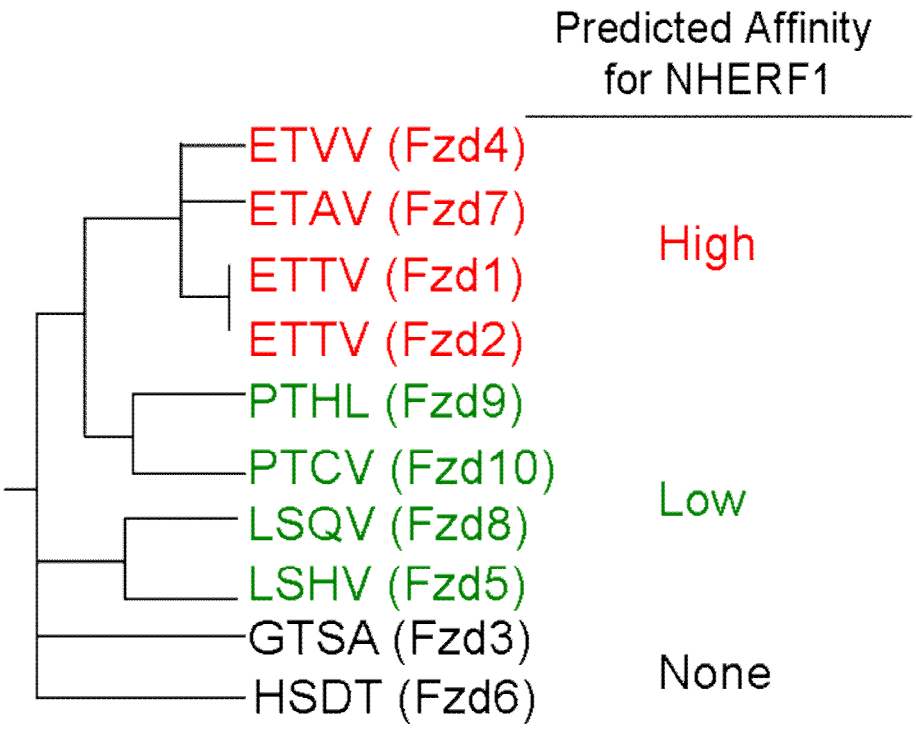
Predicted Affinity
for NHERF1
ETVV (Fzd4)
ETAV (Fzd7)
ETTV (Fzd1)
ETTV (Fzd2)
PTHL (Fzd9)
PTCV (Fzd10)
LSQV (Fzd8)
LSHV (Fzd5)
GTSA (Fzd3)
HSDT (Fzd6)
High
Low
None

Figure 14

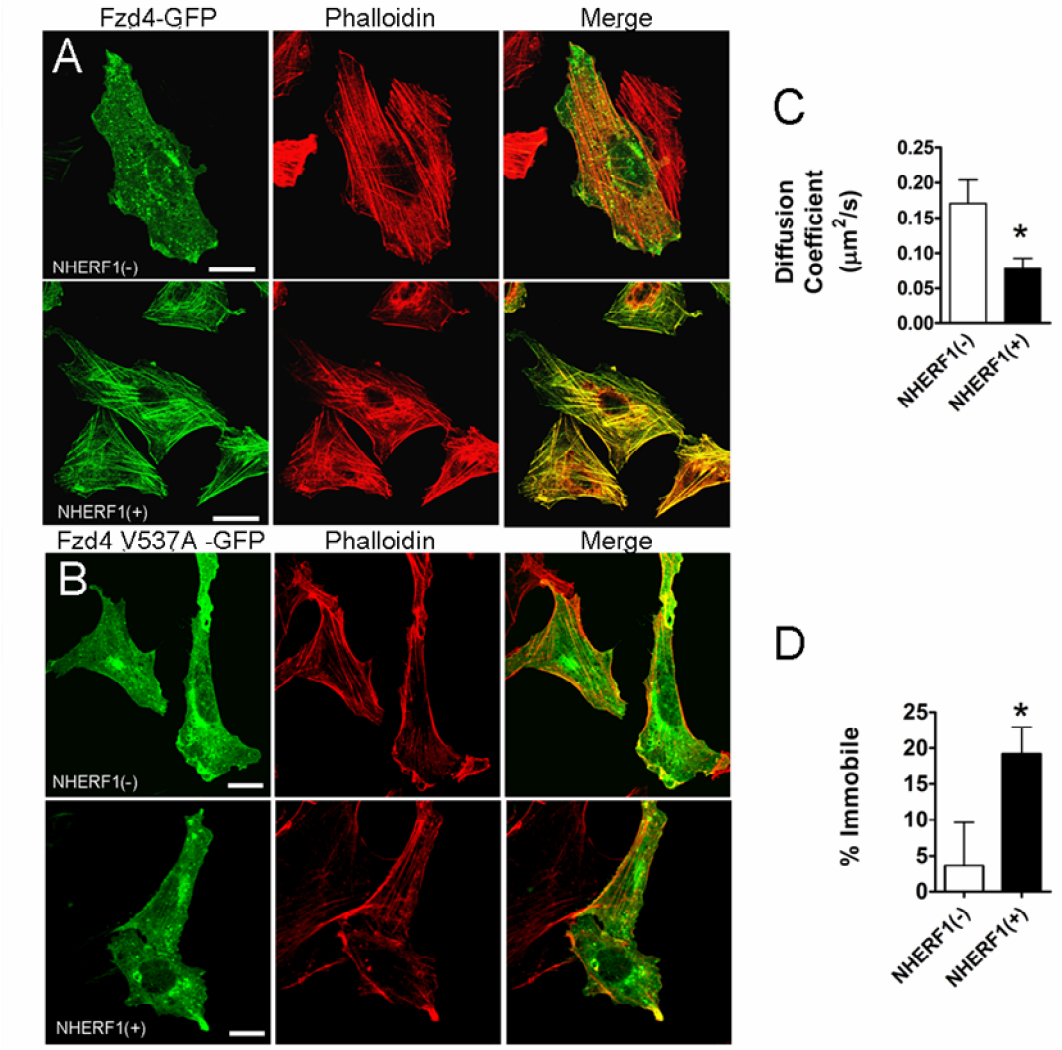
Fzd4-GFP
Phalloidin
Merge
A
NHERF1(-)
NHERF1(+)
Fzd4 V537A -GFP
Phalloidin
Merge
B
NHERF1(-)
NHERF1(+)
C
Diffusion Coefficient (μm²/s)
0.25
0.20
0.15
0.10
0.05
0.00
*
NHERF1(-)
NHERF1(+)
D
% Immobile
25
20
15
10
5
0
*
NHERF1(-)
NHERF1(+)

Figure 15

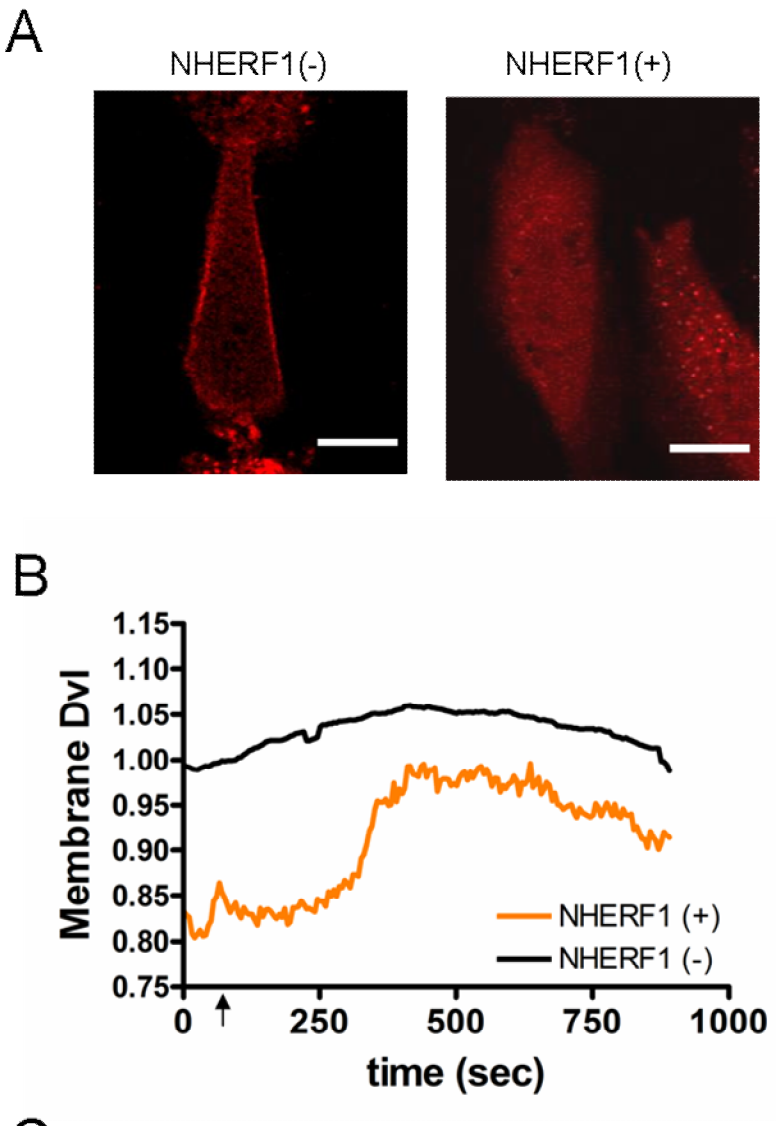
A
NHERF1(-)
NHERF1(+)
B
Membrane Dvl
1.15
1.10
1.05
1.00
0.95
0.90
0.85
0.80
0.75
0
250
500
750
1000
time (sec)
NHERF1 (+)
NHERF1 (-)
C
IP: HA-Fzd4
IB: myc-Dvl2
IP: HA-Fzd4
IB: HA-Fzd4
NHERF1
+
-
+
-
Control
Wnt5a

Figure 16

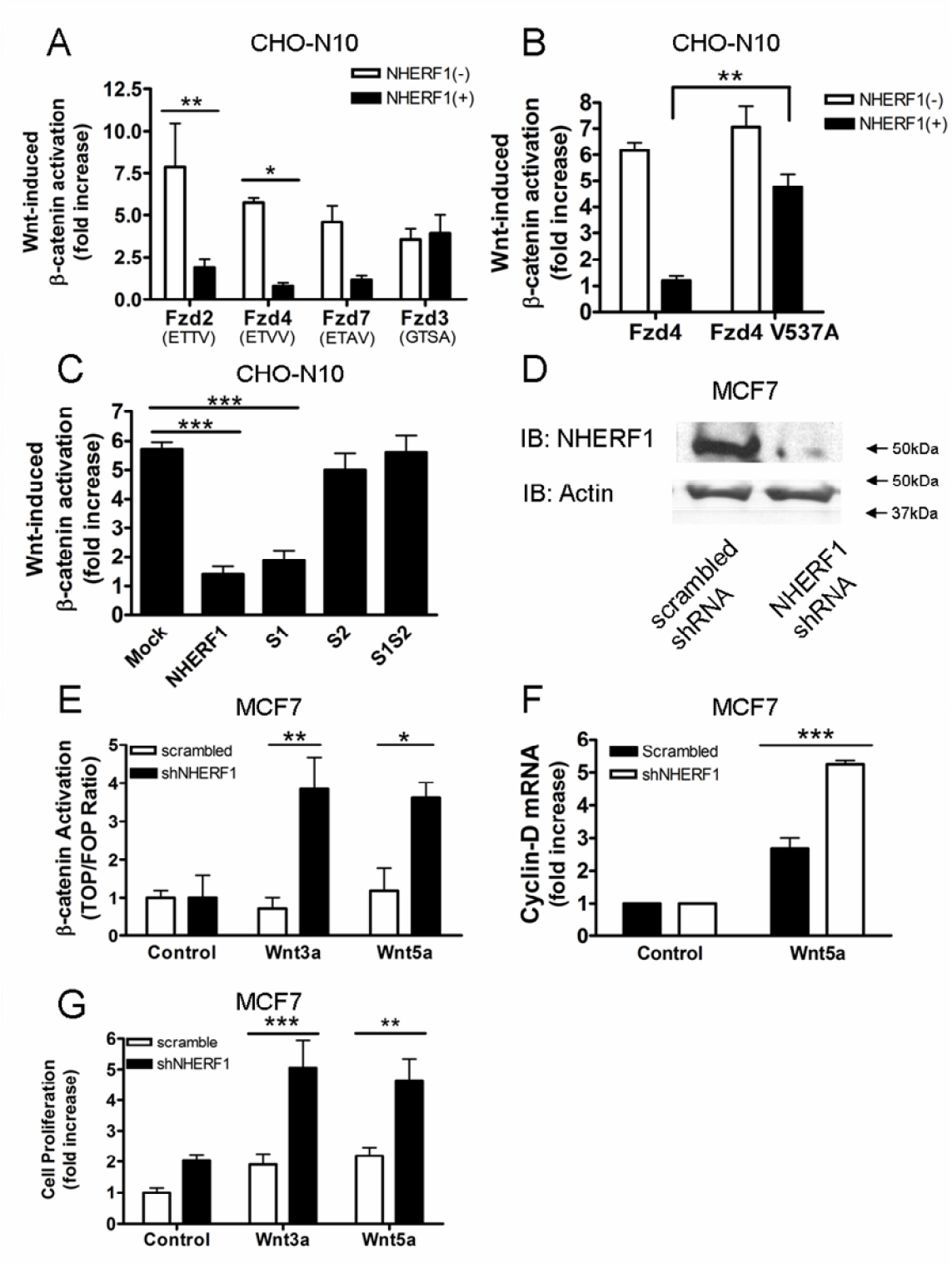
A
CHO-N10
NHERF1(-)
NHERF1(+)
Wnt-induced β-catenin activation (fold increase)
12.5
10.0
7.5
5.0
2.5
0.0
**
*
Fzd2 (ETTV)
Fzd4 (ETVV)
Fzd7 (ETAV)
Fzd3 (GTSA)
B
CHO-N10
**
NHERF1(-)
NHERF1(+)
Wnt-induced β-catenin activation (fold increase)
Fzd4
Fzd4 V537A
C
CHO-N10
***
***
Wnt-induced β-catenin activation (fold increase)
Mock
NHERF1
S1
S2
S1S2
D
MCF7
IB: NHERF1
IB: Actin
50kDa
50kDa
37kDa
scrambled shRNA
NHERF1 shRNA
E
MCF7
scrambled
shNHERF1
β-catenin Activation (TOP/FOP Ratio)
**
*
Control
Wnt3a
Wnt5a
F
MCF7
Scrambled
shNHERF1
Cyclin-D mRNA (fold increase)
***
Control
Wnt5a
G
MCF7
scramble
shNHERF1
Cell Proliferation (fold increase)
***
**
Control
Wnt3a
Wnt5a

Figure 17

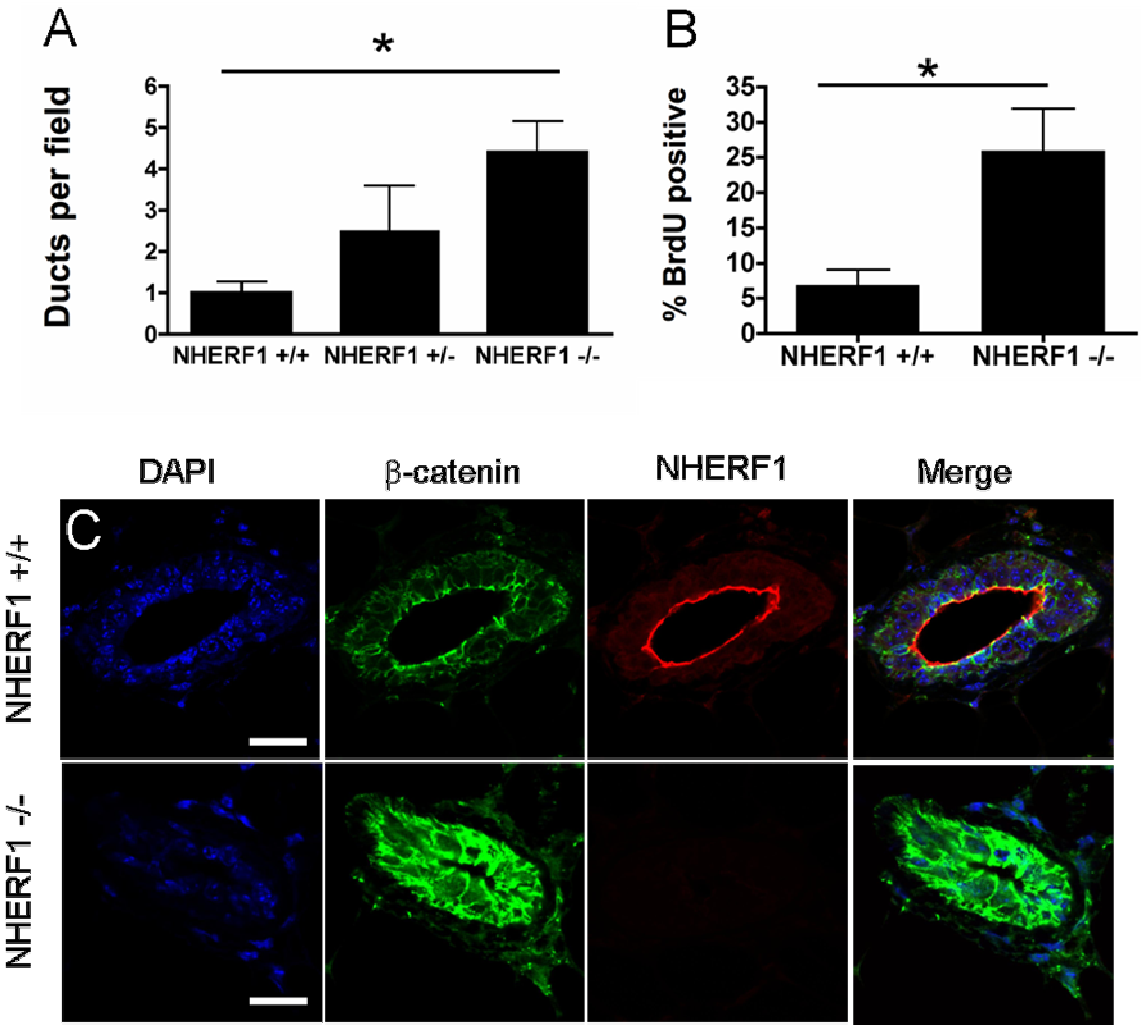
A
Ducts per field
*
0
1
2
3
4
5
6
NHERF1 +/+
NHERF1 +/-
NHERF1 -/-
B
% BrdU positive
*
0
5
10
15
20
25
30
35
NHERF1 +/+
NHERF1 -/-
DAPI
β-catenin
NHERF1
Merge
C
NHERF1 +/+
NHERF1 -/-

Figure 18

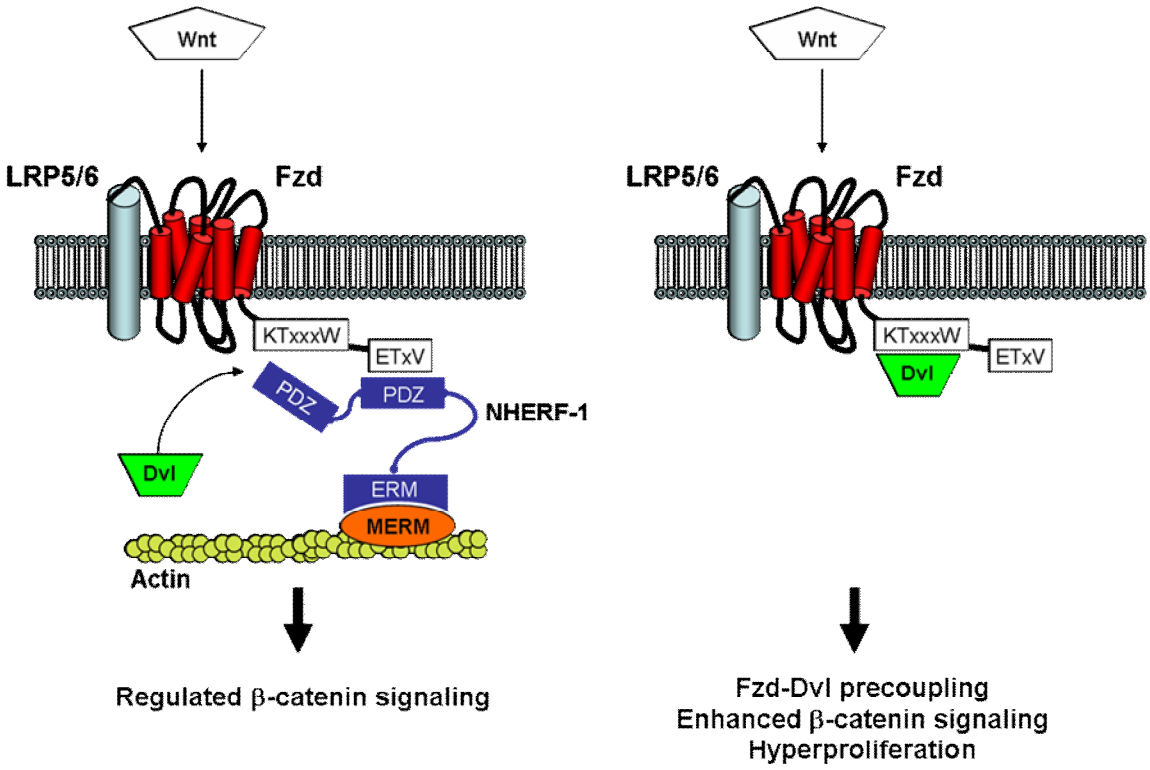
Wnt
LRP5/6
Fzd
KTxxxW
ETxV
PDZ
PDZ
NHERF-1
Dvl
ERM
MERM
Actin
Regulated β-catenin signaling
Wnt
LRP5/6
Fzd
KTxxxW
Dvl
ETxV
Fzd-Dvl precoupling
Enhanced β-catenin signaling
Hyperproliferation

Figure 19

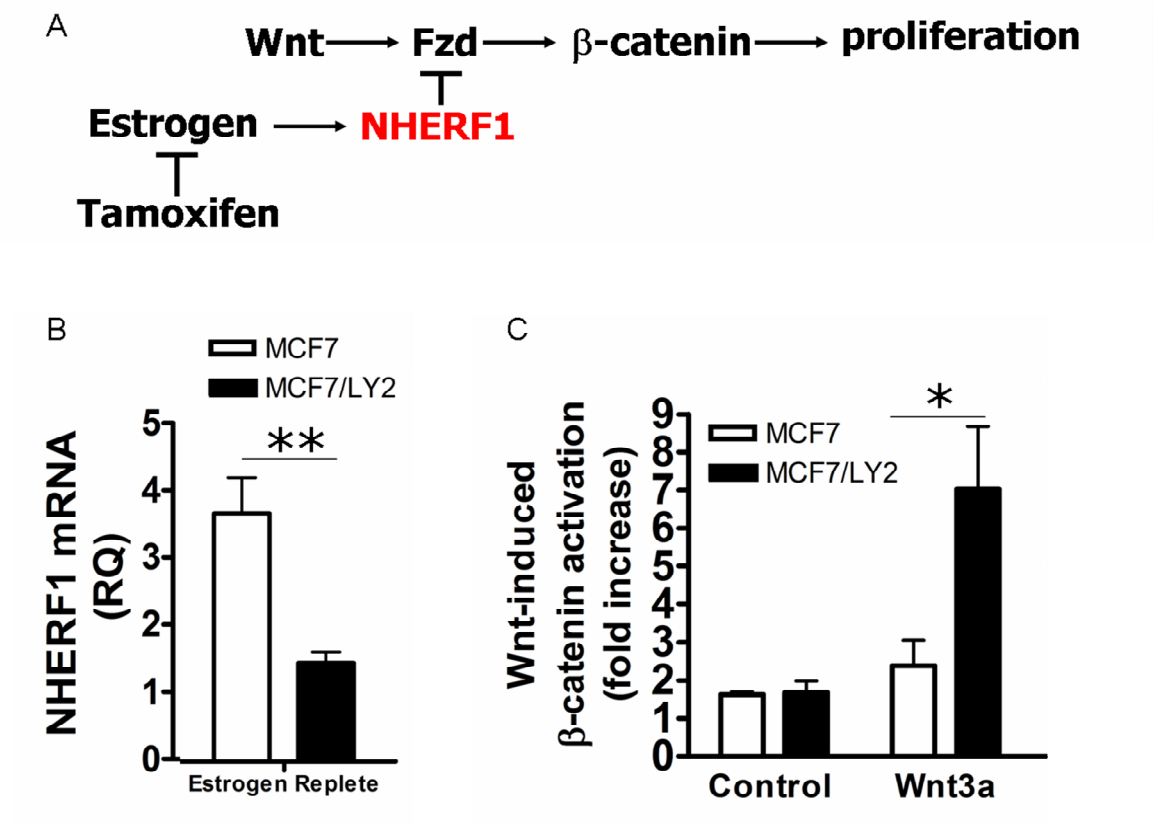
A
Wnt
Fzd
β-catenin
proliferation
Estrogen
NHERF1
Tamoxifen
B
MCF7
MCF7/LY2
NHERF1 mRNA (RQ)
**
Estrogen Replete
C
Wnt-induced β-catenin activation (fold increase)
MCF7
MCF7/LY2
*
Control
Wnt3a

Figure 20

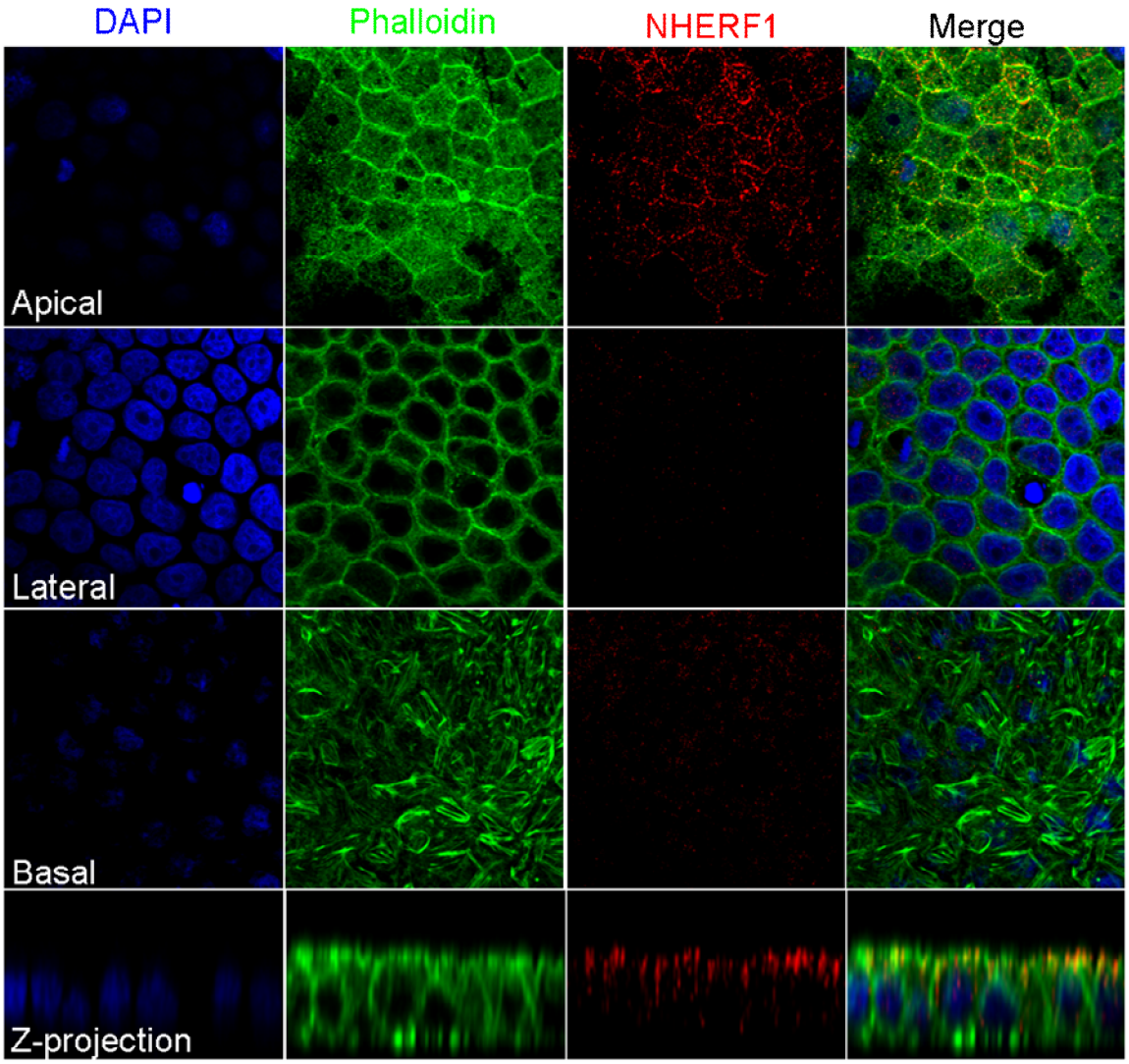
DAPI
Phalloidin
NHERF1
Merge
Apical
Lateral
Basal
Z-projection

Figure 21

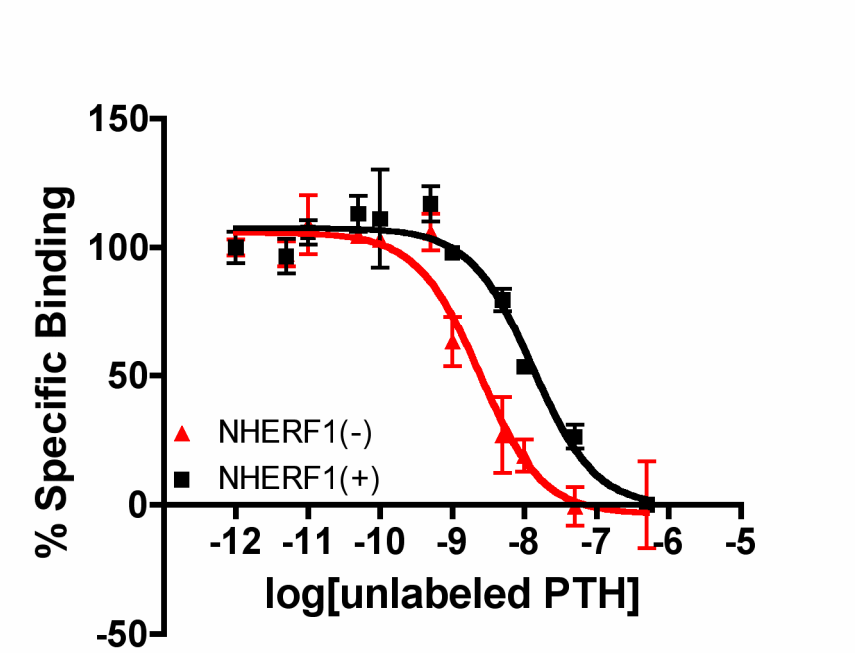
150
100
50
0
-50
% Specific Binding
NHERF1(-)
NHERF1(+)
-12
-11
-10
-9
-8
-7
-6
-5
log[unlabeled PTH]

Figure 22

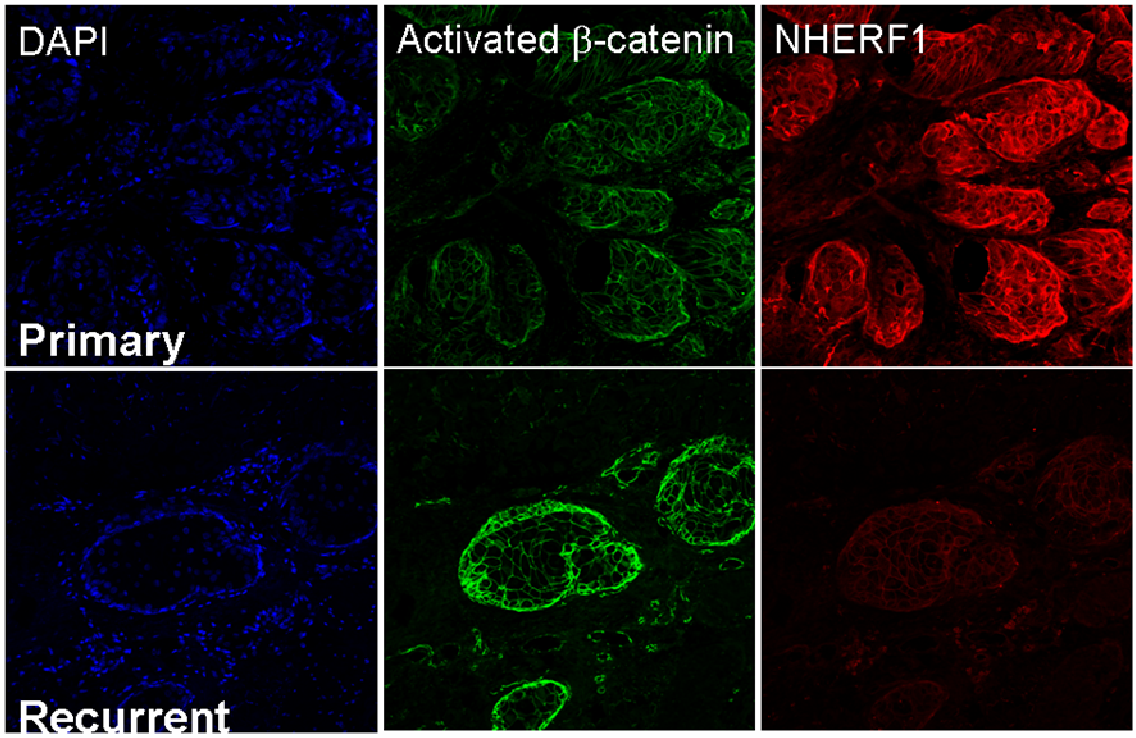

Figure 23

REFERENCES

1. Lander, E.S., et al., *Initial sequencing and analysis of the human genome.* Nature, 2001. **409**(6822): p. 860-921.
2. Takeda, S., et al., *Identification of G protein-coupled receptor genes from the human genome sequence.* FEBS Lett, 2002. **520**(1-3): p. 97-101.
3. Fanning, A.S. and J.M. Anderson, *PDZ domains: fundamental building blocks in the organization of protein complexes at the plasma membrane.* J Clin Invest, 1999. **103**(6): p. 767-72.
4. Umbhauer, M., et al., *The C-terminal cytoplasmic Lys-thr-X-X-X-Trp motif in frizzled receptors mediates Wnt/beta-catenin signalling.* EMBO J, 2000. **19**(18): p. 4944-54.
5. Karthikeyan, S., et al., *Crystal structure of the PDZ1 domain of human Na(+)/H(+) exchanger regulatory factor provides insights into the mechanism of carboxyl-terminal leucine recognition by class I PDZ domains.* J Mol Biol, 2001. **308**(5): p. 963-73.
6. Karthikeyan, S., T. Leung, and J.A. Ladias, *Structural basis of the Na+/H+ exchanger regulatory factor PDZ1 interaction with the carboxyl-terminal region of the cystic fibrosis transmembrane conductance regulator.* J Biol Chem, 2001. **276**(23): p. 19683-6.
7. Songyang, Z., et al., *Recognition of unique carboxyl-terminal motifs by distinct PDZ domains.* Science, 1997. **275**(5296): p. 73-7.
8. Hock, B., et al., *PDZ-domain-mediated interaction of the Eph-related receptor tyrosine kinase EphB3 and the ras-binding protein AF6 depends on the kinase activity of the receptor.* Proc Natl Acad Sci U S A, 1998. **95**(17): p. 9779-84.
9. Shenolikar, S., et al., *Regulation of ion transport by the NHERF family of PDZ proteins.* Physiology (Bethesda), 2004. **19**: p. 362-9.
10. Liew, C.W., et al., *Interaction of the human somatostatin receptor 3 with the multiple PDZ domain protein MUPP1 enables somatostatin to control permeability of epithelial tight junctions.* FEBS Lett, 2009. **583**(1): p. 49-54.
11. Borg, J.P., et al., *ERBIN: a basolateral PDZ protein that interacts with the mammalian ERBB2/HER2 receptor.* Nat Cell Biol, 2000. **2**(7): p. 407-14.
12. Olsen, O., et al., *Basolateral membrane expression of the Kir 2.3 channel is coordinated by PDZ interaction with Lin-7/CASK complex.* Am J Physiol Cell Physiol, 2002. **282**(1): p. C183-95.
13. Bassand, P., et al., *Differential interaction of the tSXV motifs of the NR1 and NR2A NMDA receptor subunits with PSD-95 and SAP97.* Eur J Neurosci, 1999. **11**(6): p. 2031-43.
14. Hu, L.A., et al., *beta 1-adrenergic receptor association with PSD-95. Inhibition of receptor internalization and facilitation of beta 1-adrenergic receptor interaction with N-methyl-D-aspartate receptors.* J Biol Chem, 2000. **275**(49): p. 38659-66.
15. Tejedor, F.J., et al., *Essential role for dlg in synaptic clustering of Shaker K+ channels in vivo.* J Neurosci, 1997. **17**(1): p. 152-9.
16. Yun, C.H., et al., *cAMP-mediated inhibition of the epithelial brush border Na+/H+ exchanger, NHE3, requires an associated regulatory protein.* Proc Natl Acad Sci U S A, 1997. **94**(7): p. 3010-5.

17. Yoo, D., et al., *Assembly and trafficking of a multiprotein ROMK (Kir 1.1) channel complex by PDZ interactions.* J Biol Chem, 2004. **279**(8): p. 6863-73.
18. Morales, F.C., et al., *NHERF1/EBP50 head-to-tail intramolecular interaction masks association with PDZ domain ligands.* Mol Cell Biol, 2007. **27**(7): p. 2527-37.
19. Maudsley, S., et al., *Platelet-derived growth factor receptor association with Na(+)/H(+) exchanger regulatory factor potentiates receptor activity.* Mol Cell Biol, 2000. **20**(22): p. 8352-63.
20. Mannstadt, M., H. Juppner, and T.J. Gardella, *Receptors for PTH and PTHrP: their biological importance and functional properties.* Am J Physiol, 1999. **277**(5 Pt 2): p. F665-75.
21. Ba, J., D. Brown, and P.A. Friedman, *Calcium-sensing receptor regulation of PTH-inhibitable proximal tubule phosphate transport.* Am J Physiol Renal Physiol, 2003. **285**(6): p. F1233-43.
22. Traebert, M., et al., *Luminal and contraluminal action of 1-34 and 3-34 PTH peptides on renal type IIa Na-P(i) cotransporter.* Am J Physiol Renal Physiol, 2000. **278**(5): p. F792-8.
23. Mahon, M.J. and G.V. Segre, *Stimulation by parathyroid hormone of a NHERF-1-assembled complex consisting of the parathyroid hormone I receptor, phospholipase Cbeta, and actin increases intracellular calcium in opossum kidney cells.* J Biol Chem, 2004. **279**(22): p. 23550-8.
24. Abou-Samra, A.B., et al., *Expression cloning of a common receptor for parathyroid hormone and parathyroid hormone-related peptide from rat osteoblast-like cells: a single receptor stimulates intracellular accumulation of both cAMP and inositol trisphosphates and increases intracellular free calcium.* Proc Natl Acad Sci U S A, 1992. **89**(7): p. 2732-6.
25. Mahon, M.J., et al., *Na(+)/H(+) exchanger regulatory factor 2 directs parathyroid hormone 1 receptor signalling.* Nature, 2002. **417**(6891): p. 858-61.
26. Wade, J.B., et al., *Differential renal distribution of NHERF isoforms and their colocalization with NHE3, ezrin, and ROMK.* Am J Physiol Cell Physiol, 2001. **280**(1): p. C192-8.
27. Shenolikar, S., et al., *Targeted disruption of the mouse NHERF-1 gene promotes internalization of proximal tubule sodium-phosphate cotransporter type IIa and renal phosphate wasting.* Proc Natl Acad Sci U S A, 2002. **99**(17): p. 11470-5.
28. Shenolikar, S. and E.J. Weinman, *NHERF: targeting and trafficking membrane proteins.* Am J Physiol Renal Physiol, 2001. **280**(3): p. F389-95.
29. Voltz, J.W., E.J. Weinman, and S. Shenolikar, *Expanding the role of NHERF, a PDZ-domain containing protein adapter, to growth regulation.* Oncogene, 2001. **20**(44): p. 6309-14.
30. Wheeler, D., et al., *Regulation of parathyroid hormone type 1 receptor dynamics, traffic, and signaling by the Na+/H+ exchanger regulatory factor-1 in rat osteosarcoma ROS 17/2.8 cells.* Mol Endocrinol, 2008. **22**(5): p. 1163-70.
31. Wheeler, D., et al., *NHERF-1 and the cytoskeleton regulate the traffic and membrane dynamics of G protein-coupled receptors.* J Biol Chem, 2007. **282**(34): p. 25076-87.
32. Sneddon, W.B., et al., *Activation-independent parathyroid hormone receptor internalization is regulated by NHERF1 (EBP50).* J Biol Chem, 2003. **278**(44): p. 43787-96.
33. Wang, B., et al., *Na/H exchanger regulatory factors control parathyroid hormone receptor signaling by facilitating differential activation of G(alpha) protein subunits.* J Biol Chem, 2010. **285**(35): p. 26976-86.

34. Weinman, E.J., et al., *The role of NHERF-1 in the regulation of renal proximal tubule sodium-hydrogen exchanger 3 and sodium-dependent phosphate cotransporter 2a.* J Physiol, 2005. **567**(Pt 1): p. 27-32.
35. Donahue, H.J., et al., *Differential effects of parathyroid hormone and its analogues on cytosolic calcium ion and cAMP levels in cultured rat osteoblast-like cells.* J Biol Chem, 1988. **263**(27): p. 13522-7.
36. Lowik, C.W., et al., *A two-receptor model for the action of parathyroid hormone on osteoblasts: a role for intracellular free calcium and cAMP.* Cell Calcium, 1985. **6**(4): p. 311-26.
37. Reid, I.R., et al., *Parathyroid hormone acutely elevates intracellular calcium in osteoblastlike cells.* Am J Physiol, 1987. **253**(1 Pt 1): p. E45-51.
38. Yamaguchi, D.T., et al., *Parathyroid hormone-activated calcium channels in an osteoblast-like clonal osteosarcoma cell line. cAMP-dependent and cAMP-independent calcium channels.* J Biol Chem, 1987. **262**(16): p. 7711-8.
39. Yamaguchi, D.T., C.R. Kleeman, and S. Muallem, *Protein kinase C-activated calcium channel in the osteoblast-like clonal osteosarcoma cell line UMR-106.* J Biol Chem, 1987. **262**(31): p. 14967-73.
40. Dunlay, R. and K. Hruska, *PTH receptor coupling to phospholipase C is an alternate pathway of signal transduction in bone and kidney.* Am J Physiol, 1990. **258**(2 Pt 2): p. F223-31.
41. Civitelli, R., et al., *PTH elevates inositol polyphosphates and diacylglycerol in a rat osteoblast-like cell line.* Am J Physiol, 1988. **255**(5 Pt 1): p. E660-7.
42. Kamp, T.J. and J.W. Hell, *Regulation of cardiac L-type calcium channels by protein kinase A and protein kinase C.* Circ Res, 2000. **87**(12): p. 1095-102.
43. Weinman, E.J., et al., *Longitudinal study of urinary excretion of phosphate, calcium, and uric acid in mutant NHERF-1 null mice.* Am J Physiol Renal Physiol, 2006. **290**(4): p. F838-43.
44. Logan, C.Y. and R. Nusse, *The Wnt signaling pathway in development and disease.* Annu Rev Cell Dev Biol, 2004. **20**: p. 781-810.
45. Weinman, E.J., et al., *The association of NHERF adaptor proteins with g protein-coupled receptors and receptor tyrosine kinases.* Annu Rev Physiol, 2006. **68**: p. 491-505.
46. Hering, H. and M. Sheng, *Direct interaction of Frizzled-1, -2, -4, and -7 with PDZ domains of PSD-95.* FEBS Lett, 2002. **521**(1-3): p. 185-9.
47. Yao, R., Y. Natsume, and T. Noda, *MAGI-3 is involved in the regulation of the JNK signaling pathway as a scaffold protein for frizzled and Ltap.* Oncogene, 2004. **23**(36): p. 6023-30.
48. Luyten, A., et al., *The postsynaptic density 95/disc-large/zona occludens protein syntenin directly interacts with frizzled 7 and supports noncanonical Wnt signaling.* Mol Biol Cell, 2008. **19**(4): p. 1594-604.
49. Wheeler, D.S., et al., *Direct interaction between NHERF1 and Frizzled regulates beta-catenin signaling.* Oncogene, 2010.
50. Vincan, E., *Frizzled/WNT signalling: the insidious promoter of tumour growth and progression.* Front Biosci, 2004. **9**: p. 1023-34.
51. Boutros, M. and M. Mlodzik, *Dishevelled: at the crossroads of divergent intracellular signaling pathways.* Mech Dev, 1999. **83**(1-2): p. 27-37.
52. Donowitz, M., et al., *Alterations in the Proteome of the NHERF1 Knockout Mouse Jejunal Brush Border Membrane Vesicles.* Physiol Genomics, 2010.
53. Dai, J.L., et al., *NHERF (Na+/H+ exchanger regulatory factor) gene mutations in human breast cancer.* Oncogene, 2004. **23**(53): p. 8681-7.

54. Pan, Y., L. Wang, and J.L. Dai, *Suppression of breast cancer cell growth by Na+/H+ exchanger regulatory factor 1 (NHERF1).* Breast Cancer Res, 2006. **8**(6): p. R63.
55. Kreimann, E.L., et al., *Cortical stabilization of beta-catenin contributes to NHERF1/EBP50 tumor suppressor function.* Oncogene, 2007. **26**(36): p. 5290-9.
56. Li, Y., W.P. Hively, and H.E. Varmus, *Use of MMTV-Wnt-1 transgenic mice for studying the genetic basis of breast cancer.* Oncogene, 2000. **19**(8): p. 1002-9.
57. Ellis, M.J., et al., *Lower-dose vs high-dose oral estradiol therapy of hormone receptor-positive, aromatase inhibitor-resistant advanced breast cancer: a phase 2 randomized study.* JAMA, 2009. **302**(7): p. 774-80.
58. Ediger, T.R., et al., *Estrogen receptor regulation of the Na+/H+ exchange regulatory factor.* Endocrinology, 1999. **140**(7): p. 2976-82.
59. Chen, J., J.A. Cohn, and L.J. Mandel, *Dephosphorylation of ezrin as an early event in renal microvillar breakdown and anoxic injury.* Proc Natl Acad Sci U S A, 1995. **92**(16): p. 7495-9.
60. Dransfield, D.T., et al., *Ezrin is a cyclic AMP-dependent protein kinase anchoring protein.* EMBO J, 1997. **16**(1): p. 35-43.
61. Padanyi, R., et al., *Apical scaffolding protein NHERF2 modulates the localization of alternatively spliced plasma membrane Ca2+ pump 2B variants in polarized epithelial cells.* J Biol Chem, 2010. **285**(41): p. 31704-12.
62. Cha, B., et al., *NHE3 mobility in brush borders increases upon NHERF2-dependent stimulation by lyophosphatidic acid.* J Cell Sci, 2010. **123**(Pt 14): p. 2434-43.
63. Romero, G., et al., *Parathyroid hormone receptor directly interacts with dishevelled to regulate beta-Catenin signaling and osteoclastogenesis.* J Biol Chem, 2010. **285**(19): p. 14756-63.
64. Sugai, M., et al., *PTH/PTH-related protein receptor interacts directly with Tctex-1 through its COOH terminus.* Biochem Biophys Res Commun, 2003. **311**(1): p. 24-31.
65. Chuang, J.Z., et al., *The dynein light chain Tctex-1 has a dynein-independent role in actin remodeling during neurite outgrowth.* Dev Cell, 2005. **9**(1): p. 75-86.
66. Saito, M., et al., *Increase in cell-surface localization of parathyroid hormone receptor by cytoskeletal protein 4.1G.* Biochem J, 2005. **392**(Pt 1): p. 75-81.
67. Mahon, M.J., *The parathyroid hormone 1 receptor directly binds to the FERM domain of ezrin, an interaction that supports apical receptor localization and signaling in LLC-PK1 cells.* Mol Endocrinol, 2009. **23**(10): p. 1691-701.
68. Qiu, T., et al., *TGF-beta type II receptor phosphorylates PTH receptor to integrate bone remodelling signalling.* Nat Cell Biol, 2010. **12**(3): p. 224-34.
69. von Bonsdorff, C.H., S.D. Fuller, and K. Simons, *Apical and basolateral endocytosis in Madin-Darby canine kidney (MDCK) cells grown on nitrocellulose filters.* EMBO J, 1985. **4**(11): p. 2781-92.
70. Bejsovec, A., *Wnt pathway activation: new relations and locations.* Cell, 2005. **120**(1): p. 11-4.
71. Wu, J., T.J. Klein, and M. Mlodzik, *Subcellular localization of frizzled receptors, mediated by their cytoplasmic tails, regulates signaling pathway specificity.* PLoS Biol, 2004. **2**(7): p. E158.
72. Hughes, S.C., E. Formstecher, and R.G. Fehon, *Sip1, the Drosophila orthologue of EBP50/NHERF1, functions with the sterile 20 family kinase Slik to regulate Moesin activity.* J Cell Sci, 2010. **123**(Pt 7): p. 1099-107.
73. Wang, B., et al., *NHERF1 regulates parathyroid hormone receptor membrane retention without affecting recycling.* J Biol Chem, 2007. **282**(50): p. 36214-22.

74. Li, J., D.J. Callaway, and Z. Bu, *Ezrin induces long-range interdomain allostery in the scaffolding protein NHERF1.* J Mol Biol, 2009. **392**(1): p. 166-80.
75. Li, J., et al., *Ezrin controls the macromolecular complexes formed between an adapter protein Na+/H+ exchanger regulatory factor and the cystic fibrosis transmembrane conductance regulator.* J Biol Chem, 2005. **280**(45): p. 37634-43.
76. Skelton, N.J., et al., *Origins of PDZ domain ligand specificity. Structure determination and mutagenesis of the Erbin PDZ domain.* J Biol Chem, 2003. **278**(9): p. 7645-54.
77. Gianni, S., et al., *The kinetics of PDZ domain-ligand interactions and implications for the binding mechanism.* J Biol Chem, 2005. **280**(41): p. 34805-12.
78. Tawfeek, H.A., F. Qian, and A.B. Abou-Samra, *Phosphorylation of the receptor for PTH and PTHrP is required for internalization and regulates receptor signaling.* Mol Endocrinol, 2002. **16**(1): p. 1-13.
79. Weinman, E.J., et al., *Cooperativity between the phosphorylation of Thr95 and Ser77 of NHERF-1 in the hormonal regulation of renal phosphate transport.* J Biol Chem, 2010. **285**(33): p. 25134-8.
80. Weinman, E.J., et al., *Parathyroid hormone inhibits renal phosphate transport by phosphorylation of serine 77 of sodium-hydrogen exchanger regulatory factor-1.* J Clin Invest, 2007. **117**(11): p. 3412-20.
81. Magyar, C., et al., *PTH (7-34) downregulates PTH1 receptor by a ubiquitin-sensitive pathway.* J Bone Miner Res, 2004. **19**: p. 174-75.
82. Wheeler, D. and W.B. Sneddon, *Mutation of phenylalanine-34 of parathyroid hormone disrupts NHERF1 regulation of PTH type I receptor signaling.* Endocrine, 2006. **30**(3): p. 343-52.
83. Juppner, H. and G. Fuleihan, *Parathyroid hormone assays and their clinical use.* UpToDate, 2010.
84. Brunskill, N., et al., *Localization and polar distribution of several G-protein subunits along nephron segments.* Kidney Int, 1991. **40**(6): p. 997-1006.
85. Halpern, M., L.S. Shapiro, and C. Jia, *Differential localization of G proteins in the opossum vomeronasal system.* Brain Res, 1995. **677**(1): p. 157-61.
86. Berglund, L., et al., *A genecentric Human Protein Atlas for expression profiles based on antibodies.* Mol Cell Proteomics, 2008. **7**(10): p. 2019-27.
87. Singer, A.U., et al., *A unique fold of phospholipase C-beta mediates dimerization and interaction with G alpha q.* Nat Struct Biol, 2002. **9**(1): p. 32-6.
88. Forster, I.C., et al., *Proximal tubular handling of phosphate: A molecular perspective.* Kidney Int, 2006. **70**(9): p. 1548-59.
89. Bergwitz, C., et al., *SLC34A3 mutations in patients with hereditary hypophosphatemic rickets with hypercalciuria predict a key role for the sodium-phosphate cotransporter NaPi-IIc in maintaining phosphate homeostasis.* Am J Hum Genet, 2006. **78**(2): p. 179-92.
90. Beck, L., et al., *Targeted inactivation of Npt2 in mice leads to severe renal phosphate wasting, hypercalciuria, and skeletal abnormalities.* Proc Natl Acad Sci U S A, 1998. **95**(9): p. 5372-7.
91. Miedlich, S.U., et al., *The receptor-dependent actions of 1,25-dihydroxyvitamin D are required for normal growth plate maturation in NPt2a knockout mice.* Endocrinology, 2010. **151**(10): p. 4607-12.
92. Datta, N.S., et al., *Cyclin D1 as a target for the proliferative effects of PTH and PTHrP in early osteoblastic cells.* J Bone Miner Res, 2007. **22**(7): p. 951-64.

93. MacDonald, B.R., J.A. Gallagher, and R.G. Russell, *Parathyroid hormone stimulates the proliferation of cells derived from human bone.* Endocrinology, 1986. **118**(6): p. 2445-9.
94. Canalis, E., et al., *Insulin-like growth factor I mediates selective anabolic effects of parathyroid hormone in bone cultures.* J Clin Invest, 1989. **83**(1): p. 60-5.
95. Nishida, S., et al., *Increased bone formation by intermittent parathyroid hormone administration is due to the stimulation of proliferation and differentiation of osteoprogenitor cells in bone marrow.* Bone, 1994. **15**(6): p. 717-23.
96. Pettway, G.J., et al., *Parathyroid hormone mediates bone growth through the regulation of osteoblast proliferation and differentiation.* Bone, 2008. **42**(4): p. 806-18.
97. Datta, N.S., et al., *PTHrP signaling targets cyclin D1 and induces osteoblastic cell growth arrest.* J Bone Miner Res, 2005. **20**(6): p. 1051-64.
98. Demiralp, B., et al., *Anabolic actions of parathyroid hormone during bone growth are dependent on c-fos.* Endocrinology, 2002. **143**(10): p. 4038-47.
99. Pearman, A.T., et al., *Parathyroid hormone induces c-fos promoter activity in osteoblastic cells through phosphorylated cAMP response element (CRE)-binding protein binding to the major CRE.* J Biol Chem, 1996. **271**(41): p. 25715-21.
100. Gonzalez, G.A. and M.R. Montminy, *Cyclic AMP stimulates somatostatin gene transcription by phosphorylation of CREB at serine 133.* Cell, 1989. **59**(4): p. 675-80.
101. Westendorf, J.J., R.A. Kahler, and T.M. Schroeder, *Wnt signaling in osteoblasts and bone diseases.* Gene, 2004. **341**: p. 19-39.
102. Kato, M., et al., *Cbfa1-independent decrease in osteoblast proliferation, osteopenia, and persistent embryonic eye vascularization in mice deficient in Lrp5, a Wnt coreceptor.* J Cell Biol, 2002. **157**(2): p. 303-14.
103. Laura, R.P., et al., *MAGI-1: a widely expressed, alternatively spliced tight junction protein.* Exp Cell Res, 2002. **275**(2): p. 155-70.
104. Katzenellenbogen, B.S., et al., *Molecular mechanisms of estrogen action: selective ligands and receptor pharmacology.* J Steroid Biochem Mol Biol, 2000. **74**(5): p. 279-85.
105. Cuello-Carrion, F.D., et al., *Estrogens regulate the expression of NHERF1 in normal colon during the reproductive cycle of Wistar rats.* Histochem Cell Biol, 2010.
106. Stemmer-Rachamimov, A.O., et al., *NHE-RF, a merlin-interacting protein, is primarily expressed in luminal epithelia, proliferative endometrium, and estrogen receptor-positive breast carcinomas.* Am J Pathol, 2001. **158**(1): p. 57-62.
107. Fouassier, L., et al., *Ezrin-radixin-moesin-binding phosphoprotein (EBP50), an estrogen-inducible scaffold protein, contributes to biliary epithelial cell proliferation.* Am J Pathol, 2009. **174**(3): p. 869-80.
108. Faroqui, S., et al., *Estrogen downregulates the proximal tubule type IIa sodium phosphate cotransporter causing phosphate wasting and hypophosphatemia.* Kidney Int, 2008. **73**(10): p. 1141-50.
109. Smith, P.M., et al., *Tissue-specific regulation by estrogen of ezrin and ezrin/radixin/moesin-binding protein 50.* Endocrine, 2003. **22**(2): p. 119-26.
110. Papaxoinis, K., et al., *Subsite-specific differences of estrogen receptor beta expression in the normal colonic epithelium: implications for carcinogenesis and colorectal cancer epidemiology.* Eur J Gastroenterol Hepatol, 2010. **22**(5): p. 614-9.

111. Stossi, F., et al., *Transcriptional profiling of estrogen-regulated gene expression via estrogen receptor (ER) alpha or ERbeta in human osteosarcoma cells: distinct and common target genes for these receptors.* Endocrinology, 2004. **145**(7): p. 3473-86.
112. *Effects of chemotherapy and hormonal therapy for early breast cancer on recurrence and 15-year survival: an overview of the randomised trials.* Lancet, 2005. **365**(9472): p. 1687-717.
113. Smith, C.L., Z. Nawaz, and B.W. O'Malley, *Coactivator and corepressor regulation of the agonist/antagonist activity of the mixed antiestrogen, 4-hydroxytamoxifen.* Mol Endocrinol, 1997. **11**(6): p. 657-66.
114. Umar, A., et al., *Identification of a putative protein profile associated with tamoxifen therapy resistance in breast cancer.* Mol Cell Proteomics, 2009. **8**(6): p. 1278-94.
115. Verpy, E., et al., *A defect in harmonin, a PDZ domain-containing protein expressed in the inner ear sensory hair cells, underlies Usher syndrome type 1C.* Nat Genet, 2000. **26**(1): p. 51-5.
116. Chen, J.M., et al., *Meta-analysis of gross insertions causing human genetic disease: novel mutational mechanisms and the role of replication slippage.* Hum Mutat, 2005. **25**(2): p. 207-21.
117. Blaydon, D.C., et al., *The contribution of USH1C mutations to syndromic and non-syndromic deafness in the UK.* Clin Genet, 2003. **63**(4): p. 303-7.
118. Boerkoel, C.F., et al., *Periaxin mutations cause recessive Dejerine-Sottas neuropathy.* Am J Hum Genet, 2001. **68**(2): p. 325-33.
119. Guilbot, A., et al., *A mutation in periaxin is responsible for CMT4F, an autosomal recessive form of Charcot-Marie-Tooth disease.* Hum Mol Genet, 2001. **10**(4): p. 415-21.
120. Kijima, K., et al., *Periaxin mutation causes early-onset but slow-progressive Charcot-Marie-Tooth disease.* J Hum Genet, 2004. **49**(7): p. 376-9.
121. Junyent, M., et al., *The effects of ABCG5/G8 polymorphisms on plasma HDL cholesterol concentrations depend on smoking habit in the Boston Puerto Rican Health Study.* J Lipid Res, 2009. **50**(3): p. 565-73.
122. Karim, Z., et al., *NHERF1 mutations and responsiveness of renal parathyroid hormone.* N Engl J Med, 2008. **359**(11): p. 1128-35.
123. Daw, M.I., et al., *PDZ proteins interacting with C-terminal GluR2/3 are involved in a PKC-dependent regulation of AMPA receptors at hippocampal synapses.* Neuron, 2000. **28**(3): p. 873-86.
124. Fujii, N., et al., *Rational design of a nonpeptide general chemical scaffold for reversible inhibition of PDZ domain interactions.* Bioorg Med Chem Lett, 2007. **17**(2): p. 549-52.
125. Fujii, N., et al., *A selective irreversible inhibitor targeting a PDZ protein interaction domain.* J Am Chem Soc, 2003. **125**(40): p. 12074-5.
126. Fujii, N., et al., *Design of a selective chemical probe for class I PDZ domains.* Bioorg Med Chem Lett, 2007. **17**(2): p. 546-8.
127. Mayasundari, A., et al., *Rational design of the first small-molecule antagonists of NHERF1/EBP50 PDZ domains.* Bioorg Med Chem Lett, 2008. **18**(3): p. 942-5.
128. Grandy, D., et al., *Discovery and characterization of a small molecule inhibitor of the PDZ domain of dishevelled.* J Biol Chem, 2009. **284**(24): p. 16256-63.

APPENDIX

The following appendix contains a copy of publications completed during graduate training.

Endocrine, *vol. 30, no. 3, 343–352, December 2006* 0969–711X/06/30:343–352/$30.00
ENDO (Online) ISSN 1559-0100

Mutation of Phenylalanine-34 of Parathyroid Hormone Disrupts NHERF1 Regulation of PTH Type I Receptor Signaling

David Wheeler and W. Bruce Sneddon

Department of Pharmacology, University of Pittsburgh School of Medicine, Pittsburgh, PA 15261

Internalization of the PTH type I receptor (PTH1R) is regulated in a cell- and ligand-specific manner. We previously demonstrated that the sodium/proton exchanger regulatory factor type 1 (NHERF1; EBP50) is pivotal in determining the range of peptides that internalize the PTH1R. Antagonist PTH fragments can internalize the PTH1R in some kidney and bone cell models. PTH(7-34), which binds to, but does not activate, the PTH1R, internalizes the PTH1R in kidney distal tubule (DT) cells, where NHERF1 is not expressed. The effect of antagonist PTHrP peptides has not, to this point, been assessed. PTH1R internalization was measured by real-time confocal fluorescence microscopy of DT cells stably expressing 10^5 EGFP-tagged PTH1R/cell *(1)*. PTHrP(7-34) internalized the PTH1R in a manner indistinguishable from PTH(7-34). Introduction of NHERF1 into DT cells, however, blocked PTH(7-34)–, but not PTHrP(7-34)–, induced PTH1R internalization. To delineate the sequences within PTHrP that determine whether PTH1R internalization is affected by NHERF1, chimeric PTH/PTHrP fragments were tested for their ability to induce PTH1R internalization. PTH(7-21)/PTHrP (22-34), PTH(7-32)/PTHrP(33-34), and PTH(7-33)/PTHrP(34) at 1 μ*M* each internalized the PTH1R 50–70% in a NHERF1-independent manner. When the C terminus of PTHrP was replaced with homologous amino acids from PTH, NHERF1 inhibited PTH1R internalization. It was determined that simply mutating F34 to A in PTH induced PTH1R internalization in a NHERF1-independent manner. None of the chimeric peptides activated the PTH1R but all effectively competed for 1 n*M* PTH(1-34) in cyclic AMP assays. In addition, all chimeric peptides competed for radiolabeled PTH(1-34) in binding assays in DT cells. PTH(1-34) and PTHrP(7-34), but not PTH(7-34), efficiently recruited β-arrestin1 to plasma membrane PTH1Rs. We, therefore, conclude that PTH(1-34) and PTHrP(7-34) induce a conformational change in the PTH1R that promotes arrestin binding and dissociates NHERF1 from PTH1R internalization.

Key Words: Hormones and receptors; PTH/PTHrP; signaling.

Introduction

Parathyroid hormone (PTH) is an 84-amino-acid peptide hormone that is secreted by the parathyroid glands in response to low serum calcium levels. PTH binds to and activates the PTH/PTHrP receptor, also known as the type I PTH receptor (PTH1R). The first 34 amino acids of PTH are sufficient to bind with high affinity and activate the PTH1R. Positions 1–6 are important for adenylyl cyclase stimulation by the PTH1R, the first two positions being required for full activity *(2–5)*. Positions 1 and 29–32 are critical for stimulation of phosphoinositide turnover and activation of protein kinase C *(6,7)*. Sequences distal to position 15 are thought to be important for binding of PTH to the N terminal extracellular ligand-binding domain of the PTH1R. The PTH-related protein (PTHrP) is synthesized and released by many normal and malignant cell types. It acts typically in an autocrine or paracrine fashion, in contrast to the endocrine actions of PTH. In bone development, PTHrP plays a pivotal role as a growth factor in bone development, delaying chrondrocyte differentiation and promoting bone growth *(8)*. PTHrP is a 141-amino-acid hormone that has high sequence identity to PTH at its N terminus, sharing 8 of 13 amino acids. PTHrP also binds to and activates the PTH1R. The first 34 amino acids of PTHrP, like PTH, can fully activate the PTH1R. There are, however, differences in the interactions between PTH and PTHrP with the PTH1R, even in regions of high identity between these two peptides *(4)*.

The PTH1R belongs to Class B (also called Class II) of the seven-transmembrane family of guanine nucleotide binding protein (G protein)–coupled receptors (GPCRs) *(9)*. Receptors in this family bear some structural similarity and exhibit a defining characteristic in that they activate both adenylyl cyclase and phospholipase C (PLC) *(10–12)*. The responses of the PTH1R to agonists are regulated by

Received November 16, 2006; Revised December 11, 2006; Accepted December 21, 2006.

Author to whom all correspondence and reprint requests should be addressed: W. Bruce Sneddon, PhD, University of Pittsburgh School of Medicine, Department of Pharmacology, E-1103 Biomedical Science Tower, Pittsburgh, PA. E-mail: wbs2@pitt.edu

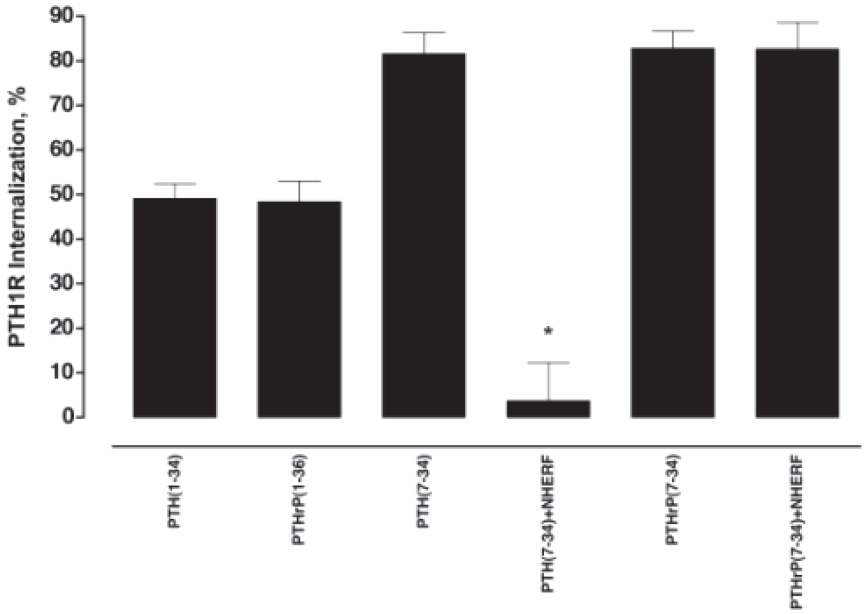

Fig. 1. PTH(7-34) and PTHrP(7-34) both induce PTH1R endocytosis. The effect of 10^{-6} *M* of the indicated peptides on PTH1R internalization in kidney distal tubule cells expressing 100,000 PTH1R/EGFP per cell (D1 cells). Receptor endocytosis was measured by real-time quantitative confocal microscopy in D1 cells that had been transfected with empty pcDNA3 vector or NHERF1. The extent of PTH1R internalization after a 15 min peptide exposure is presented. Results are the means ± SEM of triplicate determinations in three independent experiments. $*p < 0.01$ for PTH(7-34) in the presence of NHERF1 vs the absence of NHERF1 as determined by a one-way ANOVA with a post-hoc Bonferroni test for statistical significance.

multiple mechanisms. Upon activation, downstream second messengers can feed back and attempt to shut off the signal from the PTH1R. Typically, G protein–coupled receptor kinase 2 (GRK2) phosphorylates the agonist-activated receptor *(13,14)*. This promotes arrestin recruitment *(15–17)* and uncoupling of the receptor from its cognate G proteins, G_s and G_q. Following this desensitization, the PTH1R is endocytosed into intracellular compartments after which it can be recycled back to the plasma membrane (resensitization) *(18)*, or targeted for degradation, leading to receptor downregulation *(19,20)*. We have demonstrated that both the synthetic PTH(7-34) and the secreted form of the peptide PTH(7-84), which bind to but do not activate the PTH1R, internalize the PTH1R very efficiently in kidney distal tubule cells and rat osteosarcoma ROS 17/2.8 cells *(1)*. In contrast, neither PTH(7-34) nor PTH(7-84) internalizes the PTH1R in kidney proximal tubule cells or the human SaOS-2 osteosarcoma cell line. The cell-specific effects of PTH(7-34) on PTH1R internalization depend of the expression of NHERF1 *(1)*. NHERF1 is expressed in kidney proximal tubule cells and SaOS cells but is absent in kidney distal tubule and ROS17/2.8 cells *(1)*. Expression of NHERF1 inhibits PTH(7-34) induces PTH1R internalization in kidney distal tubule cells *(1)*. In contrast, expression of a dominant negative NHERF1 promotes PTH(7-34)-induced PTH1R internalization in proximal tubule cells where NHERF1 is expressed at high levels. The synthetic peptide PTHrP(7-34), like PTH(7-34), is a PTH1R antagonist. To this point, it has not been compared with PTH for its ability to induce PTH1R endocytosis.

Results

In previous studies, we demonstrated that PTH(7-34) internalizes the PTH1R and that this internalization is regulated by NHERF1. Because PTH and PTHrP both bind to and activate the PTH1R, we sought to determine if PTHrP-stimulated PTH1R internalization was similarly regulated. PTH(1-34) and PTHrP(1-36), both PTH1R agonists, share 8 of 13 N terminal amino acids. PTH(7-34) and PTHrP(7-34), by comparison, share four amino acids between positions 7 and 13. We, therefore, inquired whether these sequence disparities translated into differentially regulated PTH1R internalization. PTH(1-34) and PTHrP(1-36) at 1 μ*M* each internalized the PTH1R 50% after 15 min (Fig. 1) in mouse kidney distal tubule cells that stably express 10^5 PTH1R/cell (D1 cells). These cells do not express NHERF1 *(1)*. Expression of NHERF1 does not inhibit PTH1R internalization by these agonists *(1)* (data not shown). PTH(7-34) and PTHrP(7-34) at 1 μ*M* internalized the PTH1R 80% after 15 min in D1 cells (Fig. 1). PTH(7-34)–induced PTH1R internalization was blocked by expression of NHERF1 (Fig. 1) *(1)*, PTHrP(7 34)–stimulated PTH1R internalization was not inhibited by NHERF1 (Fig. 1).

In order to determine the sequences within PTHrP that promote PTH1R internalization by a NHERF1-independent mechanism, a series of chimeric PTH/PTHrP peptides were

Table 1
PTH and PTHrP(7-34) and Chimeric Peptides were Designed to Identify Sequences Within PTH That Confer NHERF1-Sensitivity to PTH1R Internalization

PTH(7-34)	**L**M**H**N	L**GK**HLNSME**R**	VEW**L**RKKLQD	V**H**NF
PTHrP(7-34)	**L**L**H**D	K**GK**SIQDLR**R**	RFF**L**HHLIAE	I**H**TA
PTH(7-21)PTHrP(22-34)	**L**M**H**N	L**GK**HLNSME**R**	VFF**L**HHLIAE	I**H**TA
PTHrP(7-21)PTH(22-34)	**L**L**H**D	K**GK**SIQDLR**R**	REW**L**RKKLQD	V**H**NF
PTH(7-32)PTHrP(33-34)	**L**M**H**N	L**GK**HLNSME**R**	VEW**L**RKKLQD	V**H**TA
PTHrP(7-32)PTH(33-34)	**L**L**H**D	K**GK**SIQDLR**R**	RFF**L**HHLIAE	I**H**NF
PTH(7-33)PTHrP(34)	**L**M**H**N	L**GK**HLNSME**R**	VEW**L**RKKLQD	V**H**NA
PTHrP(7-33)PTH(34)	**L**L**H**D	K**GK**SIQDLR**R**	RFF**L**HHLIAE	I**H**TF

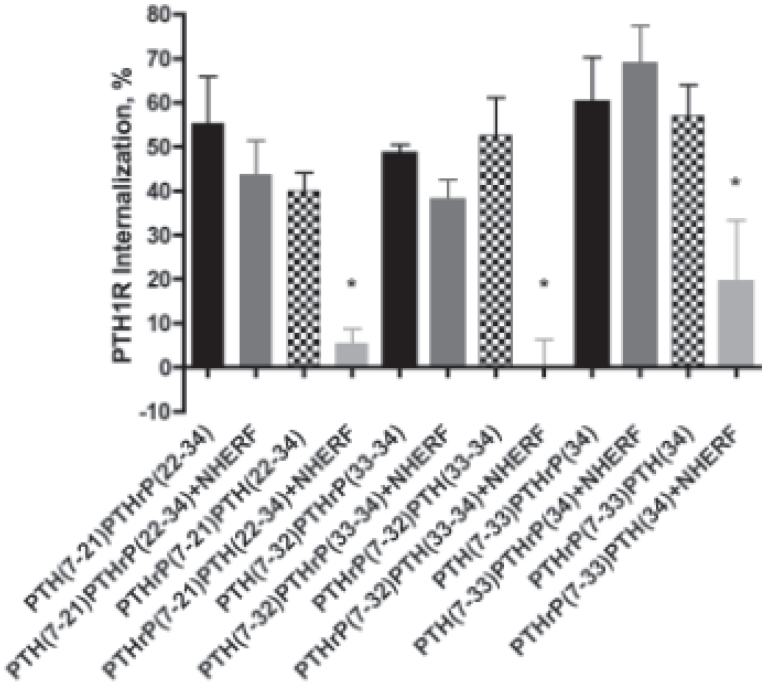

Fig. 2. NHERF1 inhibition of PTH1R internalization is dependent on sequences in the C terminus of PTH(7-34). The effect of 10^{-6} *M* of the indicated peptides on PTH1R internalization in D1 cells. Receptor endocytosis was measured as outlined in Fig. 1. The extent of PTH1R internalization after a 15 min peptide exposure is presented. Results are the means ± SEM of triplicate determinations in four independent experiments. *$p < 0.01$ in the presence of NHERF1 vs the absence of NHERF1 as determined by a one-way ANOVA with a post-hoc Bonferroni test for statistical significance.

designed (Table 1). Previous work of Gardella indicated, that the C terminus of PTH is incompatible with the N terminus of PTHrP with respect to receptor binding *(28)*. Positions 5, 19, and 21 were found to be critical to maintaining binding activity of chimeric peptides. We, therefore, decided that the dividing point for initial chimeric peptides would be at position 21. PTH(7-21)PTHrP(22-34) internalized the PTH1R 55% after 15 min in D1 cells (Fig. 2). This is somewhat less than PTH(7-34) and may reflect a reduced efficiency of the chimeric peptides to induce a conformational change in the PTH1R that promotes receptor internalization. Expression of NHERF1 had a minimal effect on PTH(7-21)PTHrP(22-34)–stimulated PTH1R endocytosis. The reverse chimera, PTHrP(7-21)PTH(22-34), internalized the PTH1R 40% after 15 min (Fig. 2) and expression of NHERF1 completely blocked this effect. These data suggest that replacement of PTH sequences between positions 22 and 34 with homologous amino acids from PTHrP dissociate NHERF1 and PTH1R internalization.

PTH(8-34) and PTH(9-34) internalized the PTH1R 45% and 40%, respectively, and this endocytosis was blocked by expression of NHERF1 (Fig. 3). In contrast, neither PTH (10-34) nor PTH(7-31) internalized the PTH1R in D1 cells (Fig. 3). This indicated that positions 7-9 and 32-34 might be important for promoting PTH1R internalization by PTH. We have also demonstrated that PTH(7-34)–induced PTH1R internalization is PKC dependent *(22)*. Positions 29–32 are critical for activation of PKC by PTH (*6,7*). Taken together, this suggested that positions 32–34 of PTH might be important amino acids for PTH1R endocytosis. Both PTH and

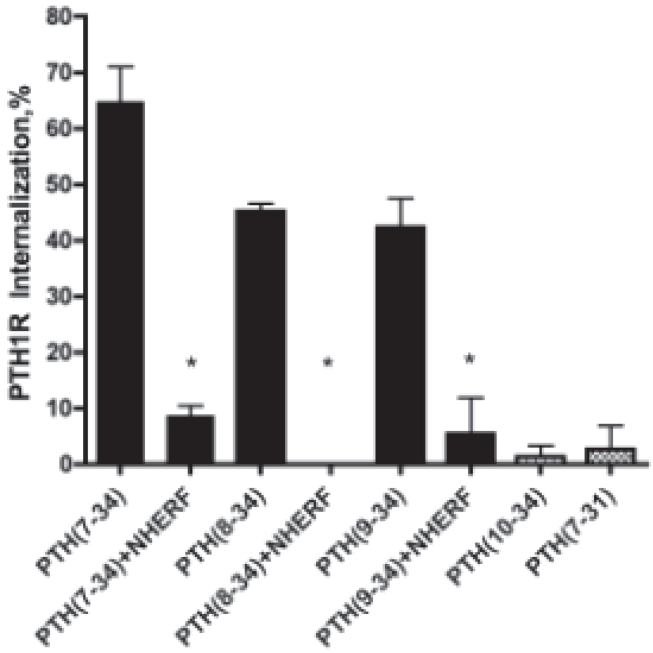

Fig. 3. Induction of PTH1R internalization requires positions 7–9 and 32–34 of PTH(7-34). The effect of 10^{-6} *M* of the indicated peptides on PTH1R internalization in D1 cells is presented. Receptor endocytosis was measured by real-time quantitative confocal microscopy in D1 cells that had been transfected with empty pcDNA3 vector or NHERF1. The extent of PTH1R internalization after a 15 min peptide exposure is presented. Results are the means ± SEM of triplicate determinations in four independent experiments. *$p < 0.01$ in the presence of NHERF1 vs the absence of NHERF1 as determined by a one-way ANOVA with a post-hoc Bonferroni test for statistical significance.

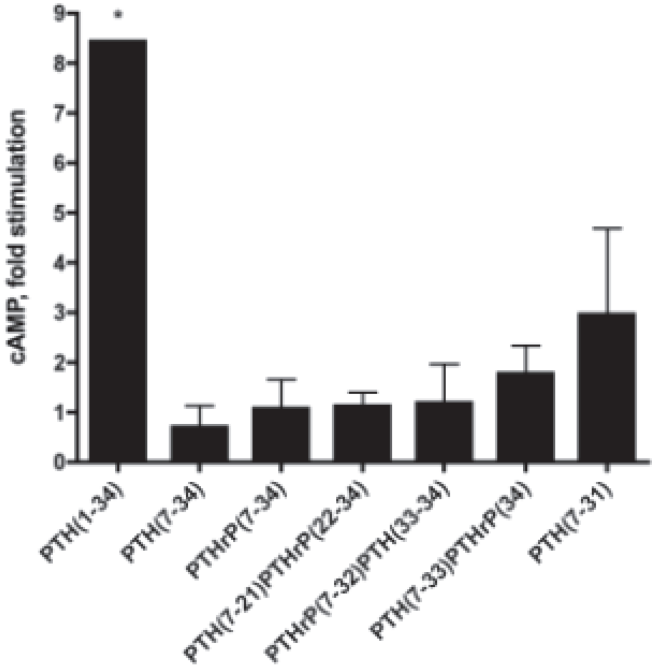

Fig. 4. Stimulation of adenylyl cyclase by chimeric PTH/PTHrP peptide fragments. D1 cells were exposed to 10^{-6} *M* of the indicated peptide for 15 min at 37°C and cAMP accumulation was measured. Data are the mean ± SEM normalized to unstimulated controls ($n = 3$). *$p < 0.01$ vs control.

PTHrP share a histidine at position 32. Therefore, chimeric PTH/PTHrP peptides were designed where positions 33 and 34 were substituted. PTH(7-32)PTHrP(33-34) internalized the PTH1R 50% in D1 cells and this process, as with PTHrP (7-34), was not inhibited by NHERF1 expression (Fig. 2). PTHrP(7-32)PTH(33-34) internalized the PTH1R 53% and, like PTH(7-34), this action was completely inhibited by NHERF1 expression (Fig. 2). These data clearly demonstrate that mutation of N33 and F34 in PTH promotes NHERF1-insensitive PTH1R internalization by PTH(7-34).

PTH and PTHrP have the amino acids NF and TA in positions 33–34, respectively. Asparagine and threonine are polar amino acids that constitute a relatively conservative substitution at position 33. In contrast, phenylalanine 34 of PTH has a large aromatic sidechain and is very different in size from alanine 34 of PTHrP. We, therefore, focused our attention on position 34. PTH(7-33)PTHrP(34) internalized the PTH1R in a NHERF-insensitive manner, whereas PTHrP(7-33)PTH(34) stimulated PTH1R internalization with the same magnitude but in a NHERF-sensitive manner (Fig. 2). A single mutation of F34 in PTH therefore alters the pathway of PTH1R trafficking by PTH(7-34).

Peptide concentrations of 1 μ*M* were employed for all of the chimeric PTH/PTHrP PTH1R internalization experiments. All of the peptides induced PTH1R internalization at this concentration and we wanted to test their respective antagonist properties in D1 cells. Therefore, we determined the ability of each of these peptides to stimulate cyclic AMP formation on their own in D1 cells and to inhibit cyclic AMP formation by 1 n*M* PTH(1-34). As shown in Fig. 4, only PTH(1-34) stimulated cyclic AMP formation in D1 cells (8.3-fold of control). Neither PTH(7-34), PTH(7-31), nor any of the chimeric PTH/PTHrP peptides tested affected cyclic AMP. In contrast, all of the peptides tested, with one exception, inhibited cyclic AMP formation by 1 n*M* PTH(1-34) with EC_{50}s in the 200–2000 n*M* range and these values were not affected by NHERF1 expression (Table 2). The notable exception to this was PTHrP(7-21)PTH(22-34), which inhibited PTH(1-34)–stimulated cyclic AMP formation with an EC_{50} of 0.2 n*M* in D1 cells. Expression of NHERF1 in D1 cells shifted the EC_{50} for this peptide to 200 n*M*.

We also performed binding studies using [^{125}I]PTH(1-34) as a tracer in D1 cells in the presence and absence of NHERF1 (Table 3). Both PTH(7-34) and PTHrP(7-34) inhibited radiolabeled PTHrP binding with IC_{50} values of 50 n*M*. Most of the chimeric peptides inhibited tracer binding with similar affinity. There were exceptions to this, however. Similar to its ability to inhibit cyclic AMP formation by PTH(1-34), PTHrP(7-21)PTH(22-34) robustly inhibited tracer binding in D1 cells with an IC_{50} of 3 p*M*. To our knowl-

Table 2
EC_{50} Values ± SEM for Inhibition by Chimeric PTH/PTHrP Peptides of 1 n*M* PTH(1-34)–Stimulated Cyclic AMP Formation in D1 Cells[a]

Peptide	EC_{50} (−NHERF), n*M*	EC_{50} (+NHERF), n*M*
PTH(7-21)PTHrP(22-34)	500 ± 10	700 ± 15
PTHrP(7-21)PTH(22-34)	0.2 ± 0.05	200 ± 10
PTH(7-32)PTHrP(33-34)	800 ± 10	1300 ± 10
PTHrP(7-32)PTH(33-34)	200 ± 5	300 ± 10
PTH(7-33)PTHrP(34)	200 ± 15	200 ± 10
PTHrP(7-33)PTH(34)	2000 ± 10	1500 ± 15

[a]Data represent $n = 3$ performed in triplicate.

Table 3
IC_{50} Values ± SEM for Inhibition of Radiolabeled PTH(1-34) Binding in D1 Cells[a]

Peptide	IC_{50} (-NHERF), n*M*	IC_{50} (+NHERF), n*M*
PTH(7-34)	50 ± 5	300 ± 10
PTHrP(7-34)	50 ± 5	20 ± 0.5
PTH(7-21)PTHrP(22-34)	50 ± 0.5	5 ± 0.5
PTHrP(7-21)PTH(22-34)	0.005 ± 0.001	0.4 ± 0.05
PTH(7-32)PTHrP(33-34)	4 ± 0.05	0.2 ± 0.05
PTHrP(7-32)PTH(33-34)	90 ± 5	400 ± 15
PTH(7-33)PTHrP(34)	6 ± 0.5	60 ± 15
PTHrP(7-33)PTH(34)	300 ± 15	40 ± 5

[a]Data represent $n = 3$ performed in triplicate.

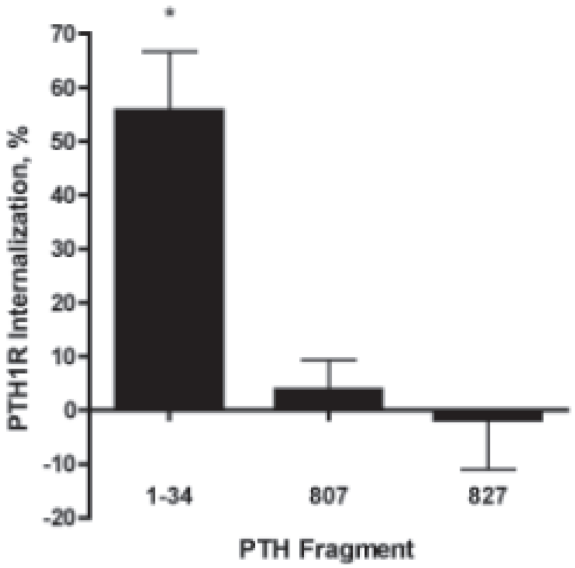

Fig. 5. J domain antagonists do not internalize the PTH1R . The effect of 10^{-6} *M* of the indicated peptides on PTH1R internalization in D1 cells. Receptor endocytosis was measured by real-time quantitative confocal microscopy in D1 cells that had been transfected with empty pcDNA3 vector or NHERF1. The extent of PTH1R internalization after a 15 min peptide exposure is presented. Results are the means ± SEM of triplicate determinations in three independent experiments. *$p < 0.01$ vs control as determined by a one-way ANOVA with a post-hoc Bonferroni test for statistical significance.

edge, this is the highest affinity PTH1R ligand described to date. This is a very exciting finding and is the focus of ongoing investigations in our laboratory. The presence of NHERF1 shifted the IC_{50} for this peptide to 400 p*M*. PTH (7-32)PTHrP(33-34) and PTH(7-33)PTHrP(34) also inhibited tracer binding with greater affinity than PTH(7-34), with IC_{50}s of 4 n*M* and 6 n*M*, respectively. The data indicate that all of the chimeric PTH/PTHrP peptides tested in the PTH1R internalization should be bound to the PTH1R at maximal levels at a concentration of 1 μ*M* and NHERF1 expression has a modest effect on the binding.

Based on photoaffinity crosslinking studies, PTH1R antagonists such as PTH(7-34) are thought to primarily interact with the extracellular N terminus of the PTH1R (the N domain), with minimal contacts to the transmembrane helix bundle and extracellular loops (the J domain) *(2,29, 30)*. Recently, a new class of synthetic PTH1R antagonists was characterized that bind to the J domain *(31)*. We tested two of these peptides for their ability to stimulate PTH1R internalization in D1 cells. Neither peptide 807 ([$Deg^{1,3}$, Bpa^{2},Nle^{8},Q^{10},A^{12},W^{14},Y^{15}]rPTH(1-15)NH2) nor peptide 827 ([$Ac5c^{1}$,Bpa^{2},Aib^{3},Nle^{8},Q^{10},A^{12},W^{14},Y^{15}]rPTH(1-15) NH2) internalized the PTH1R (Fig. 5) as compared with 55% internalization by PTH(1-34). Both peptides were used at 1 μ*M*, well above the IC_{50} for competition with radiolabeled PTH(1-15) of 100 n*M* *(31)*. These data provide a clear distinction between the classical N domain PTH1R antagonists that can internalize the receptor in the absence of NHERF1 and the J domain antagonists that lack this ability.

There are conflicting reports on the importance of receptor phosphorylation in the induction of PTH1R internalization. We previously reported that both PTH(1-34) and (7-34) induce PTH1R phosphorylation *(22)*. We therefore tested PTH(7-34), PTHrP(7-34), and the chimeric peptides for their respective abilities to stimulate PTH1R phosphorylation in D1 cells in the presence or absence of NHERF1 (Fig. 6) using in vivo receptor phosphorylation as described previously *(22)*. All of the peptides induced PTH1R phosphorylation at 1 μ*M*. There may have been a modest inhibitory effect of NHERF1 on PTH1R phosphorylation by PTH(7-32)PTHrP(33,34) and PTHrP(7 32)PTH(33-34). This is not likely related to PTH1R internalization because, despite inducing similar levels of receptor phosphorylation, only PTH(7-32)PTHrP(33,34) is able to internalize the receptor in the presence of NHERF1. While all of the peptides tested reproducibly induced PTH1R phosphorylation, the apparent enhanced ability of PTH(7-21)PTHrP (22-34), PTH(7-32)PTHrP(33,34), and PTHrP(7-32)PTH (33-34) to induce PTH1R was not reproducible.

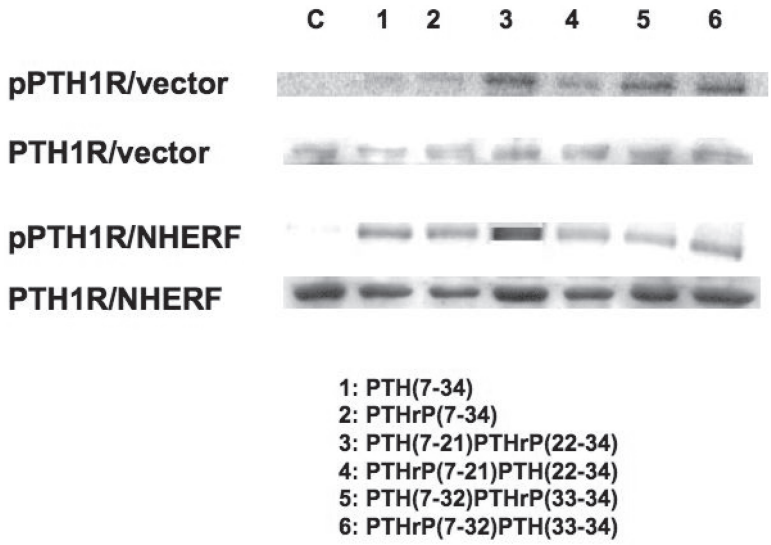

Fig. 6. Chimeric PTH/PTHrP peptides all induce PTH1R phosphorylation. PTH1R phosphorylation was assessed in D1 cells in the presence or absence of NHERF1 as described in Methods. pPTH1R represents the phosphorylated PTH1R. PTH1R represents the level of PTH1R/EGFP as measured by Western blots using a polyclonal anti-EGFP antibody. D1 cells were exposed to 10^{-6} *M* of chimeric peptides 1–6 or vehicle (C) as outlined in Methods. The data were reproduced three times. A representative experiment is presented.

The β-arrestins play a key role in the internalization of GPCRs. We sought to determine if NHERF1 regulates PTH1R mobilization of β-arrestins or arrestin-dependent receptor internalization. We hypothesized that differences therein underlie the ability of some PTH1R ligands to dissociate PTH1R internalization from NHERF1. The binding of β-arrestin1 to PTH1R residing on the plasma membrane of D1 cells was measured using image cross-correlation spectroscopy (ICCS). The fraction of binding was measured in cells with and without NHERF1 (Fig. 7). Binding of arrestin to PTH1R was negligible before the addition of ligand, independent of NHERF1 expression. Addition of PTH(1-34) promoted a dramatic increase in the binding of β-arrestin1 to PTH1R. This increase was modestly but significantly reduced by the expression of NHERF1 ($p = 0.004$). Addition of PTH(7-34) did not induce any increase in β-arrestin-1–bound receptor, independently of the expression of NHERF1. In contrast, 100 n*M* PTHrP(7-34) caused a robust increase in the binding of β-arrestin1 to PTH1R, which was modestly but significantly ($p = 0.04$) decreased by NHERF-1 expression.

Discussion

In our earlier work, we demonstrated that both the synthetic PTH(7-34) and the secreted form of the peptide PTH (7-84), which bind to but do not activate the PTH1R, internalize the PTH1R very efficiently in kidney distal tubule cells and rat osteosarcoma ROS 17/2.8 cells *(1)*. In fact, PTH(7-34) is more efficacious than PTH(1-34) at inducing PTH1R internalization in these cells. The mechanistic details that account for this difference are, at present, unknown. In contrast, neither PTH(7-34) nor PTH(7-84) internalizes the PTH1R in kidney proximal tubule cells or the human

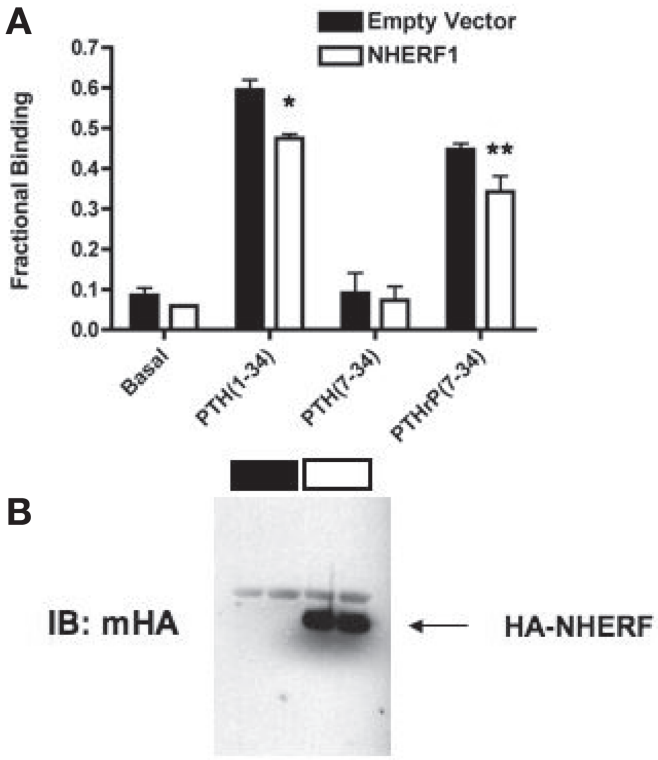

Fig. 7. (**A**) The binding of β-arrestin1 to PTH1R residing on the plasma membrane of D1 cells was measured using image cross-correlation spectroscopy. The fraction of binding was measured in cells with and without NHERF1. The following ligands were used to promote arrestin binding: PTH(1-34) (100 n*M*), PTH(7-34) (100 n*M*), and PTHrP(7-34) (100 n*M*). Data represent mean ± SEM of four independent measurements. *$p < 0.005$, **$p < 0.05$ vs empty vector as determined by a one-way ANOVA with a post-hoc Bonferroni test for statistical significance. (**B**) D1 cells were concurrently transfected as in **A**, lysates prepared, and HA–NHERF1 expression was confirmed in duplicate by immunoblot using a monoclonal anti-HA antibody.

SaOS-2 osteosarcoma cell line. The cell-specific effects of PTH(7-34) on PTH1R internalization depend of the expression of NHERF1 *(1)*. Expression of NHERF1 inhibits PTH(7-34)-induced PTH1R internalization. In this article, we demonstrate that PTHrP(7-34) also internalizes the PTH1R but in a NHERF1-independent manner (Fig. 1). We determined that mutation of phenylalanine 34 of PTH induces PTH1R internalization by a NHERF1-independent mechanism (Fig. 2). Conversely, F34–PTHrP(7-34) (A34 replaced by the homologous amino acid from PTH) fails to alter NHERF1-regulation of PTH1R internalization. Photoaffinity crosslinking studies using photoreactive L-*p*-benzoylphenylalanine (Bpa)–substituted PTH(1-34) and PTHrP(1-34) peptides have identified interactions between the C terminal of the peptide ligands and the extracellular N terminal of the PTH1R. Alanine scanning mutagenesis and crosslinking experiments identified position 23 in the C terminal of PTHrP as having important contacts with the ligand-binding domain of the PTH1R. Bpa^{23}–PTHrP(1-36) binds to threonine-33 and glutamine-37 in the N terminal extracellular domain *(32)*. This interaction is important for binding of the agonist, PTH(1-34), as well as the antagonist, PTH(7-34). Furthermore, Bpa^{27}–PTH(1-34) has been shown to crosslink to leucine-261 in the first extracellular loop *(33)*. The distal portion of PTH(7-34) is critical for induction of receptor internalization. Deletion of positions 32–34 eliminates PTH1R sequestration (Fig. 3) and also results in a reduction of the ability of N-terminally truncated PTH peptides to bind the PTH1R (data not shown). It is tempting to speculate that the large aromatic sidechain of F34 in PTH and the small sidechain of A34 in PTHrP have very different interactions with the ligand binding domain of the PTH1R and that these interactions underlie conformational changes in the PTH1R that could dissociate NHERF1 from the PTH1R.

The interactions of antagonists that bind to the N terminal extracellular domain of the PTH1R are clearly different from antagonists that interact with the transmembrane bundle and the extracellular loops. We demonstrated that the "J domain antagonists," in contrast to the "N domain antagonists" that we are focusing on, are unable to internalize the PTH1R in the presence or absence of NHERF1 (Fig. 5). This is consistent with a role for peptide binding to the N terminus of the PTH1R transducing a signal and altering the receptor conformation that leads to internalization in some cells. The J domain antagonists used in this study were highly modified PTH(1-15) peptides that were optimized for their ability to bind the PTH1R with high affinity *(31)*. In contrast, the native PTH(1-15) sequence only efficiently binds and initiates conformational changes in the receptor in the presence of additional sequences that promote peptide binding to the extracellular N terminus *(34)*.

Receptor phosphorylation plays an important role in the classical mechanism of GPCR internalization. Typically, the agonist-activated receptor is phosphorylated by GRK2 *(13,14)*. This promotes arrestin recruitment (*15–17*) and uncoupling of the receptor from its cognate G proteins, G_s and G_q. Following this desensitization, the PTH1R is endocytosed into intracellular compartments after which it can be recycled back to the plasma membrane (resensitization) *(18)*, or targeted for degradation, leading to receptor downregulation *(19,20)*. The C terminal of the PTH1R contains multiple sites for serine phosphorylation, but there are conflicting data from different cell lines concerning the role that phosphorylation plays in PTH1R internalization. We presented data in this article (Fig. 6) that demonstrate that PTH(7-34), PTHrP(7-34), and chimeric PTH/PTHrP peptides of the same length all induce PTH1R phosphorylation in D1 cells in the presence or absence of NHERF1. These data can be interpreted in a couple of different ways. First, PTH1R phosphorylation by N terminally truncated PTH/PTHrP peptides may be an epiphenomenon that is not related to PTH1R internalization because it occurs even in the presence of NHERF1-induced blockade of receptor endocytosis. Alternatively, antagonist-induced PTH1R phosphorylation may be required for receptor internalization but, in this instance, NHERF1-induced inhibition of PTH1R internalization occurs downstream of PTH1R phosphorylation. This will have to be tested in future studies. PTH1R phosphorylation and internalization has been examined in other cell lines. In LLC–PK1 cells, mutation of seven C-terminal serine residues to alanine markedly reduced agonist induced PTH1R internalization *(35)*. A murine model with a genetic knock-in of this phosphorylation-deficient receptor exhibited exaggerated cAMP and calcemic responses to administered PTH, likely as a result of a reduction in PTH1R desensitization and internalization *(36)*. A similarly substituted, phosphorylation-deficient PTH1R, when expressed at high levels in HEK 293 cells, was internalized normally in response to agonist binding *(24)*. In contrast, a similarly substituted phosphorylation-deficient opossum PTH1R exhibited a 30% reduction in agonist-induced receptor internalization in HEK293 cells *(37)*. This underscores the cell-specific nature of the regulation of PTH1R internalization.

We demonstrated that PTH(7-34) does not recruit β-arrestin1 (Fig. 7) but is, nonetheless, able to robustly internalize the PTH1R *(1)*. This is different from the findings of the Lefkowitz laboratory *(38)*, who determined that PTH(7-34) promoted an interaction between the β-arrestins and the PTH1R in transfected HEK293 cells. The discrepancy likely reflects differences in methodology. The Lefkowitz study examined co-immunoprecipitation of β-arrestins with the PTH1R in whole cell lysates, whereas we were using ICCS to examine only the PTH1R at the plasma membrane. We determined that NHERF1 completely inhibits this β-arrestin–independent PTH1R internalization induced by PTH(7-34). In contrast, both PTH(1-34) and PTHrP(7-34) recruit β-arrestin1 to the PTH1R and receptor internalization is not inhibited by NHERF1. Romero and colleagues,

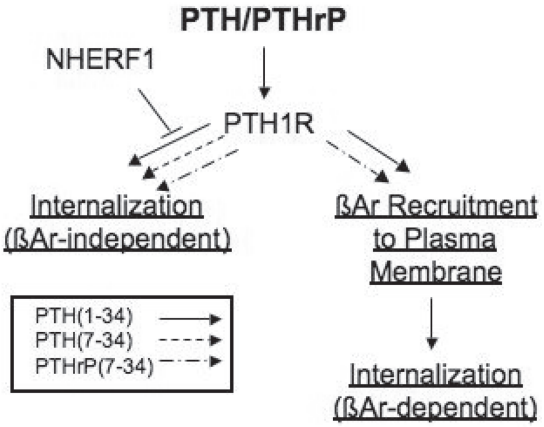

Fig. 8. A working model of NHERF1 regulation of PTH1R internalization. PTH(1-34) and PTHrP(7-34) each recruit β-arrestins to the PTH1R and internalize the PTH1R in a NHERF1-independent manner. PTH(7-34) does not recruit β-arrestins and internalizes the PTH1R in a NHERF1-inhibitable manner. NHERF1 inhibits β-arrestin-independent PTH1R internalization while only modestly affecting β-arrestin binding to the PTH1R.

using total internal reflection and confocal microscopy, have determined that NHERF1 tethers the PTH1R to actin filaments (G. G. Romero, personal communication). This slows down receptor movement in and out of the membrane and facilitates formation of complexes with other cytoskeletal proteins. The PTH1R is concentrated in actin stress fibers in the presence of NHERF. This does not prevent internalization of the PTH1R by ligands that promote β-arrestin recruitment, but it does slow down this process. Tethering by NHERF, however, prevents arrestin-independent internalization of the PTH1R by the antagonist PTH(7-34). In the absence of NHERF1, the PTH1R moves much more freely in the membrane and is more diffusely distributed within the cell and the plasma membrane. We propose that this freedom of movement permits the PTH1R to be internalized without antecedent β-arrestin binding. It is unclear why changing F34 to A in PTH(7-34) promotes PTH1R internalization in the absence of NHERF1. Presumably this alters the receptor conformation induced by ligand binding such that β-arrestins are recruited and NHERF1 is no longer able to tether the PTH1R to actin and it internalizes on binding to A34-PTH(7-34) or PTHrP(7-34). We propose a model in Fig. 8 to summarize these findings. We conclude that NHERF1 blocks arrestin-independent but not arrestin-dependent PTH1R internalization. Furthermore, the differential ability to recruit β-arrestins between PTH(7-34) and PTHrP(7-34) underlies their inability or ability, respectively, to dissociate PTH1R internalization from NHERF1 regulation.

The ability of the synthetic PTHrP(7-34) fragment to induce PTH1R internalization, while not physiological, is informative in terms of how PTH1R levels can be exogenously regulated. Under pathophysiological circumstances such as renal failure, N-terminally truncated PTH peptides are secreted by the parathyroid glands, the most predominant of these being PTH(7-84) *(39)*. Levels of these peptides are elevated and may contribute to PTH resistance by selectively downregulating the PTH1R in specific tissues such as renal distal tubules, where NHERF1 is absent. If a less selective downregulation of the PTH1R is desirable, synthetic peptides could be designed that break the NHERF1-dependence of this process and promote PTH1R internalization in a broader range of cells and tissues. Replacement of F34 in PTH with alanine would likely accomplish this goal. Very little is known about the role of PTH1R conformational changes that occur on binding N-terminally truncated PTH and PTHrP peptides and how this affects arrestin recruitment. It is interesting that the two fragments, PTH(1-34) and PTHrP(7-34), promote very different signaling cascades (the former robustly stimulates cAMP formation, while the latter does not) and yet they both efficiently recruit β-arrestin1 to the PTH1R. Future studies in our laboratory will focus on characterizing PTH1R receptor conformations that promote arrestin binding and how this dissociates the PTH1R from NHERF1.

Methods

Peptides

The chimeric peptides used in the study are described in Table 1. The University of Pittsburgh School of Medicine, Department of Molecular Genetics and Biochemistry Peptide Core Facility synthesized these peptides, and hPTH(7-31), as free acid amides. Each lyophilized peptide was reconstituted in 10 m*M* sodium acetate at a concentration of 100 m*M* and stored at –80°C. In addition, hPTH(8-34), (9-34), and (10-34) were obtained as a gift from Harald Juppner at Massachusetts General Hospital in Boston, MA.

Cell Culture and DNA Transfection

The preparation, subcloning, characterization, and culture conditions of mouse kidney distal tubule cells have been described *(21)*. Cells were grown in a 50:50 mix of DMEM/F12 (10–092-CV; Mediatech, Inc.), which was supplemented with 5% heat-inactivated FCS (Invitrogen) and 1% PS (5 mg penicillin, 5 mg streptomycin/mL; Invitrogen Life Technologies) in a humidified atmosphere of 95% air–5% CO_2 at 37°C. The immortalized mouse DT cells were stably transfected with human (hPTH1R)/enhanced green fluorescent protein (EGFP) as described previously *(22)*. The EGFP moiety lies in frame at the C terminus of the PTH1R. We have previously demonstrated that this does not interfere with PTH1R signaling nor does it impair the interaction between NHERF1 and the PTH1R *(1)*. These D1 cells were maintained in DMEM/F12 supplemented with 5% FCS, 1% PS, and 1% G418 (50 mg/mL solution, Invitrogen). D1 cells express 10^5 receptors/cell as determined

by Scatchard analysis of radioreceptor binding assays using [^{125}I]hPTH(1-34) as the radioligand *(23)*. D1 cells plated on 25 mm glass coverslips, where indicated, were transiently transfected with 1 μg mNHERF1 (a gift from Edward Weinman at the University of Maryland School of Medicine) or empty pcDNA3.1 vector (Invitrogen), using Fugene 6 (Roche Applied Science). Fluorescent PTH1R internalization studies were performed 48 hr post-transfection.

Quantitative, Real-Time Fluorescence Measurement of PTH1R Internalization

PTH1R internalization was examined and quantified in D1 cells as described previously *(1)*. Receptor internalization is measured as a loss of plasma membrane fluorescence after addition of PTH fragments and results are consistent with internalization of radiolabeled PTH(1-34) *(1)*. Control experiments confirm that no photobleaching of EGFP occurs when D1 cells are treated with vehicle.

Cyclic AMP Assays

Ligand-stimulated accumulation of cAMP was determined in the presence of 1 m*M* 3-isobutyl-1-methylxanthine. cAMP was measured chromatographically as previously described *(5)*. Where activation properties of the chimeric PTH/PTHrP peptides were being assessed, cAMP was measured in cells treated for 15 min with 1 μ*M* of the indicated peptide. In competition experiments, cells were incubated with increasing concentrations of chimeric peptide concurrently with 1 n*M* hPTH(1-34). Competition curves were fit and EC_{50} values calculated using a four-point logistic algorithm (Prism, GraphPad Software).

Radioligand Binding

Confluent D1 cells on 24 well plates (100,000–200,000) were incubated on ice for 2 h with 100,000 cpm of high-pressure liquid chromatography–purified [^{125}I][Nle^{8,18}Tyr^{34}] hPTH(1-34)NH2 in 250 μL of Dulbecco's modified Eagle's medium/F-12 medium containing 5% fetal bovine serum, essentially as described *(23,24)*. In brief, cells grown to confluence in 24-well plates were incubated for 2 h on ice to prevent internalization of the radioligand and to achieve equilibrium binding. Under these conditions, the concentration of radioligand was 0.1 n*M*. Where indicated, the radioligand was incubated concurrently with various concentrations of competitor peptides. Following incubation, the cells were washed twice with ice-cold phosphate-buffered saline and collected in 0.5 mL of 0.1 *N* NaOH, and bound [^{125}I]PTH was assessed using a Wallac Wizard 1470 Automatic Gamma Counter. Specific binding competition curves were fit and IC_{50} values calculated using a four-point logistic algorithm (Prism).

In Vivo Receptor Phosphorylation

PTH1R phosphorylation by chimeric PTH/PTHrP peptides in D1 cells was performed exactly as described previously *(22)*. As a control, PTH1R levels were assessed using Western blots as described *(22)* using a rabbit polyclonal anti-GFP antibody (Invitrogen).

Image Cross-Correlation Spectroscopy (ICCS)

These experiments were based on the experimental approach described by Wiseman et al. and Bacia and Schwille *(25,26)*. ICCS involves rapid (approx 60 ms/frame) two-channel scanning of a small section of the plasma membrane of cells containing two different protein-conjugated dyes. Correlations between the fluctuations in the fluorescence intensity of the two channels are used to generate a cross-correlation function, which can then be used to calculate the fractional binding of one of the fluorescent species to the other *(27)*. For these experiments, D1 cells were cultured in Mattek dishes and co-transfected with PTH1R/EGFP and mRed (a monomeric variant of dsRed)–β-arrestin-1. Only cells that expressed comparable amounts of both fluorescent proteins, as determined by confocal microscopy, were used for these studies. All confocal microscopy studies were conducted on an Olympus Fluoview 1000 equipped with a SIM scanner using the photon counting option to ensure accurate quantitation of the fluorescence fluctuations. The 488 nm line of an argon laser and the 543 nm line of a HeNe laser were used to excite eGFP and mRed, respectively. Emission bandpasses were optimized to eliminate bleedthrough using the spectral detection system of the instrument. Images were collected at 50–60 ms intervals. Up to 300 images per experiment were collected. The cells were kept at 37°C using an open perfusion incubator (Harvard Apparatus, Inc). The data collected were exported to ImageJ and analyzed using a plug-in specifically written to calculate image autocorrelation and image cross-correlation. This plug-in was based on code originally developed by Tully (Compix, Inc). The fractional degree of binding of PTH1R to arrestin was calculated from the ratio of the amplitudes of the cross-correlation function and the PTH1R and β-arrestin1 autocorrelation functions, as described by Kim et al. *(27)*.

Statistical Analyses

Where indicated, a one way analysis of variance (ANOVA) was performed, followed by post-hoc Bonferroni analysis using Prism software.

Acknowledgments

This study was supported by the NIH, NIDDK R21DK 068066. The author acknowledges Peter A. Friedman, PhD of the University of Pittsburgh School of Medicine, Pittsburgh, PA, Guillermo G. Romero, PhD of the University of Pittsburgh School of Medicine, Alessandro Bisello, PhD of the University of Pittsburgh School of Medicine, Pittsburgh, PA, and Thomas A Gardella, PhD of Massachusetts General Hospital, Boston, MA, for technical assistance and

helpful discussions before, during, and after the completion of these studies. I also thank Simon Watkins, PhD and the University of Pittsburgh Center for Biologic Imaging, where all of the microscopy studies were performed.

References

1. Sneddon, W. B., Syme, C. A., Bisello, A., et al. (2003). *J. Biol. Chem.* **278,** 43787–43796.
2. Adams, A. E., Bisello, A., Chorev, M., Rosenblatt, M., and Suva, L. J. (1998). *Mol. Endocrinol.* **12,** 1673–1683.
3. Maeda, S., Wu, S. X., Green, J., et al. (1998). *J. Am. Soc. Nephrol.* **9,** 175–181.
4. Behar, V., Bisello, A., Bitan, G., Rosenblatt, M., and Chorev, M. (2000). *J. Biol. Chem.* **275,** 9–17.
5. Bisello, A., Chorev, M., Rosenblatt, M., Monticelli, L., Mierke, D. F., and Ferrari, S. L. (2002). *J. Biol. Chem.* **277,** 38524–38530.
6. Takasu, H., Guo, J., and Bringhurst, F. R. (1999). *J. Bone Mineral Res.* **14,** 11–20.
7. Jouishomme, H., Whitfield, J. F., Gagnon, L., et al. (1994). *J. Bone Mineral Res.* **9,** 943–949.
8. Chung, U. I., Lanske, B., Lee, K., Li, E., and Kronenberg, H. (1998). *Proc. Natl. Acad. Sci. USA* **95,** 13030–13035.
9. Horn, F., Vriend, G., and Cohen, F. E. (2001). *Nucleic Acids Res.* **29,** 346–349.
10. Abou-Samra, A. B., Freeman, M., Juppner, H., Uneno, S., and Segre, G. V. (1990). *J. Biol. Chem.* **265,** 58–62.
11. Bringhurst, F. R., Juppner, H., Guo, J., et al. (1993). *Endocrinology* **132,** 2090–2098.
12. Guo, J., Iida-Klein, A., Huang, X. W., Abou-Samra, A. B., Segre, G. V., and Bringhurst, F. R. (1995). *Endocrinology* **136,** 3884–3891.
13. Dicker, F., Quitterer, U., Winstel, R., Honold, K., and Lohse, M. J. (1999). *Proc. Natl. Acad. Sci. USA* **96,** 5476–5481.
14. Flannery, P. J. and Spurney, R. F. (2001). *Biochem. Pharmacol.* **62,** 1047–1058.
15. Ferrari, S. L., Behar, V., Chorev, M., Rosenblatt, M., and Bisello, A. (1999). *J. Biol. Chem.* **274,** 29968–29975.
16. Tawfeek, H. A. and Abou-Samra, A. B. (1999). *J. Bone Mineral Res.* **14,** S542.
17. Vilardaga, J. P., Frank, M., Krasel, C., Dees, C., Nissenson, R. A., and Lohse, M. J. (2001). *J. Biol. Chem.* **276,** 33435–33443.
18. Chauvin, S., Bencsik, M., Bambino, T., and Nissenson, R. A. (2002). *Mol. Endocrinol.* **16,** 2720–2732.
19. Tian, J., Smogorzewski, M., Kedes, L., and Massry, S. G. (1994). *Am. J. Nephrol.* **14,** 41–46.
20. Ureña, P., Kubrusly, M., Mannstadt, M., et al. (1994). *Kidney Internatl.* **45,** 605–611.
21. Friedman, P. A., Gesek, F. A., Morley, P., Whitfield, J. F., and Willick, G. E. (1999). *Endocrinology* **140,** 301–309.
22. Sneddon, W. B., Magyar, C. E., Willick, G. E., et al. (2004). *Endocrinology* **145,** 2815–2823.
23. Ferrari, S. L. and Bisello, A. (2001). *Mol. Endocrinol.* **15,** 149–163.
24. Malecz, N., Bambino, T., Bencsik, M., and Nissenson, R. A. (1998). *Mol. Endocrinol.* **12,** 1846–1856.
25. Wiseman, P. W., Squier, J. A., Ellisman, M. H., and Wilson, K. R. (2000). *J. Microsc.* **200,** 14–25.
26. Bacia, K. and Schwille, P. (2003). *Methods* **29,** 74–85.
27. Kim, S. A., Heinze, K. G., Bacia, K., Waxham, M. N., and Schwille, P. (2005). *Biophys. J.* **88,** 4319–4336.
28. Gardella, T. J., Luck, M. D., Wilson, A. K., et al. (1995). *J. Biol. Chem.* **270,** 6584–6588.
29. Lee, C., Luck, M. D., Juppner, H., Potts, J. T. Jr., Kronenberg, H. M., and Gardella, T. J. (1995). *Mol. Endocrinol.* **9,** 1269–1278.
30. Carter, P. H., Shimizu, M., Luck, M. D., and Gardella, T. J. (1999). *J. Biol. Chem.* **274,** 31955–31960.
31. Shimizu, N., Dean, T., Tsang, J. C., Khatri, A., Potts, J. T. Jr., and Gardella, T. J. (2005). *J. Biol. Chem.* **280,** 1797–1807.
32. Mannstadt, M., Luck, M. D., Gardella, T. J., and Juppner, H. (1998). *J. Biol. Chem.* **273,** 16890–16896.
33. Greenberg, Z., Bisello, A., Mierke, D. F., Rosenblatt, M., and Chorev, M. (2000). *Biochemistry* **39,** 8142–8152.
34. Bergwitz, C., Gardella, T. J., Flannery, M. R., et al. (1996). *J. Biol. Chem.* **271,** 26469–26472.
35. Qian, F., Leung, A., and Abou-Samra, A. (1998). *Biochemistry* **37,** 6240–6246.
36. Bounoutas, G. S., Tawfeek, H., Frohlich, L. F., Chung, U. I., and Abou-Samra, A. B. (2006). *Endocrinology* **147,** 4674–4679.
37. Vilardaga, J. P., Krasel, C., Chauvin, S., Bambino, T., Lohse, M. J., and Nissenson, R. A. (2002). *J. Biol. Chem.* **277,** 8121–8129.
38. Gesty-Palmer, D., Chen, M., Reiter, E., et al. (2006). *J. Biol. Chem.* **281,** 10856–10864.
39. D'Amour, P., Brossard, J. H., Rousseau, L., et al. (2005). *Kidney Int.* **68,** 998–1007.

THE JOURNAL OF BIOLOGICAL CHEMISTRY VOL. 282, NO. 34, pp. 25076–25087, August 24, 2007

NHERF-1 and the Cytoskeleton Regulate the Traffic and Membrane Dynamics of G Protein-coupled Receptors*

Received for publication, February 21, 2007, and in revised form, May 22, 2007 Published, JBC Papers in Press, June 27, 2007, DOI 10.1074/jbc.M701544200

David Wheeler[‡§], **W. Bruce Sneddon**[‡], **Bin Wang**[‡], **Peter A. Friedman**[‡¶], **and Guillermo Romero**[‡1]

From the [‡]*Department of Pharmacology, the* [§]*Medical Scientist Training Program, and the* [¶]*Department of Medicine, University of Pittsburgh School of Medicine, Pittsburgh, Pennsylvania 15261*

The sodium-hydrogen exchange regulatory factor 1 (NHERF-1/EBP50) interacts with the C terminus of several G protein-coupled receptors (GPCRs). We examined the role of NHERF-1 and the cytoskeleton on the distribution, dynamics, and trafficking of the β_2-adrenergic receptor (β_2AR; a type A receptor), the parathyroid hormone receptor (PTH1R; type B), and the calcium-sensing receptor (CaSR; type C) using fluorescence recovery after photobleaching, total internal reflection fluorescence, and image correlation spectroscopy. β_2AR bundles were observed only in cells that expressed NHERF-1, whereas the PTH1R was localized to bundles that parallel stress fibers independently of NHERF-1. The CaSR was never observed in bundles. NHERF-1 reduced the diffusion of the β_2AR and the PTH1R. The addition of ligand increased the diffusion coefficient and the mobile fraction of the PTH1R. Isoproterenol decreased the immobile fraction but did not affect the diffusion coefficient of the β_2AR. The diffusion of the CaSR was unaffected by NHERF-1 or the addition of calcium. NHERF-1 reduced the rate of ligand-induced internalization of the PTH1R. This phenomenon was accompanied by a reduction of the rate of arrestin binding to PTH1R in ligand-exposed cells. We conclude that some GPCRs, such as the β_2AR, are attached to the cytoskeleton primarily via the binding of NHERF-1. Others, such as the PTH1R, bind the cytoskeleton via several interacting proteins, one of which is NHERF-1. Finally, receptors such as the CaSR do not interact with the cytoskeleton in any significant manner. These interactions, or the lack thereof, govern the dynamics and trafficking of the receptor.

Cell membranes are highly heterogeneous structures consisting of an ensemble of fluctuating microdomains with distinct lipid and protein compositions. These microdomains play important functions in signal transduction processes by increasing the rate and efficiency of coupling of key intermolecular interactions involved in specific signaling processes (1–3). The cytoskeleton has also been implicated in the regulation of signal transduction processes by serving as a substrate for the anchoring of specific proteins (4), regulating traffic (5), and partitioning the cell membrane into microdomains through the formation of effective barriers to the diffusion of lipids and proteins present in the bulk of the plasma membrane (6, 7). However, this general model of the cytoskeleton's role in the regulation of signaling processes depicts a somewhat passive picture. Most studies of the relationships among cytoskeletal structures and signaling processes focused on the effects of extracellular signals on cytoskeletal reorganization rather than on the effects of the cytoskeleton upon signaling pathways. This view has been recently challenged by the discovery of a family of proteins containing N-terminal postsynaptic density protein (PSD95)/*Drosophila* disc large tumor suppressor (DlgA)/Zo-1 protein (PDZ)[2] domains (which interact with a variety of signaling molecules) and a C-terminal Ezrin-Radixin-Moesin (ERM)-binding domain (that enables these proteins to interact with cytoskeletal structures) (8–10). Two of the members of this family, the Na^+/H^+ exchange regulatory factors 1 and 2 (NHERF-1 and -2), interact with and modulate the function of several G protein-coupled receptors (10–13). However, although the data show unequivocally that NHERF-1 and NHERF-2 modulate the function of GPCR, a unified hypothesis to explain the multiple roles of these scaffolding molecules is lacking.

Here, we examined the effects of the expression of NHERF-1/EBP50 in the dynamics of three GPCRs: the β_2-adrenergic receptor (β_2AR), the parathyroid hormone receptor (PTH1R), and the calcium-sensing receptor (CaSR). The β_2AR and the PTH1R are type A and B receptors, respectively, and were chosen because of their well documented interactions with NHERF-1 (10, 12, 14–18). The CaSR is a type C receptor that does not interact with NHERF-1, thus serving as an important control. The data show that the β_2AR and the PTH1R are closely associated to actin stress fibers by a mechanism that is modulated by their interactions with NHERF-1. NHERF-1 expression was not required for the cytoskeletal association of the PTH1R; however, the β_2AR was found in bundles only in cells expressing NHERF-1. The CaSR was not associated with the cytoskeleton independently of NHERF-1 expression. The

* This work was supported by National Institutes of Health Grants DK 54171 and DK 69998 (to P. A. F.). The costs of publication of this article were defrayed in part by the payment of page charges. This article must therefore be hereby marked "*advertisement*" in accordance with 18 U.S.C. Section 1734 solely to indicate this fact.

[1] To whom all correspondence should be addressed: Dept. of Pharmacology, University of Pittsburgh School of Medicine, Pittsburgh, PA 15228. Tel.: 412-648-9408; E-mail: ggr@pitt.edu.

[2] The abbreviations used are: PDZ, postsynaptic density protein (PSD95)/*Drosophila* disc large tumor suppressor (DlgA)/Zo-1 protein; ERM, Ezrin-Radixin-Moesin; β_2AR, β-adrenergic receptor type 2; CaSR, calcium-sensing receptor; FRAP, fluorescence recovery after photobleaching; GPCR, G protein-coupled receptor; ICS, image correlation spectroscopy; ICCS, image cross-correlation spectroscopy; PTH1R, parathyroid hormone receptor type 1; TIRF, total internal fluorescence; TRITC, tetramethylrhodamine isothiocyanate; eGFP, enhanced green fluorescent protein; ANOVA, analysis of variance; CHO, Chinese hamster ovary; wt-PTH1R, wild type PTH1R.

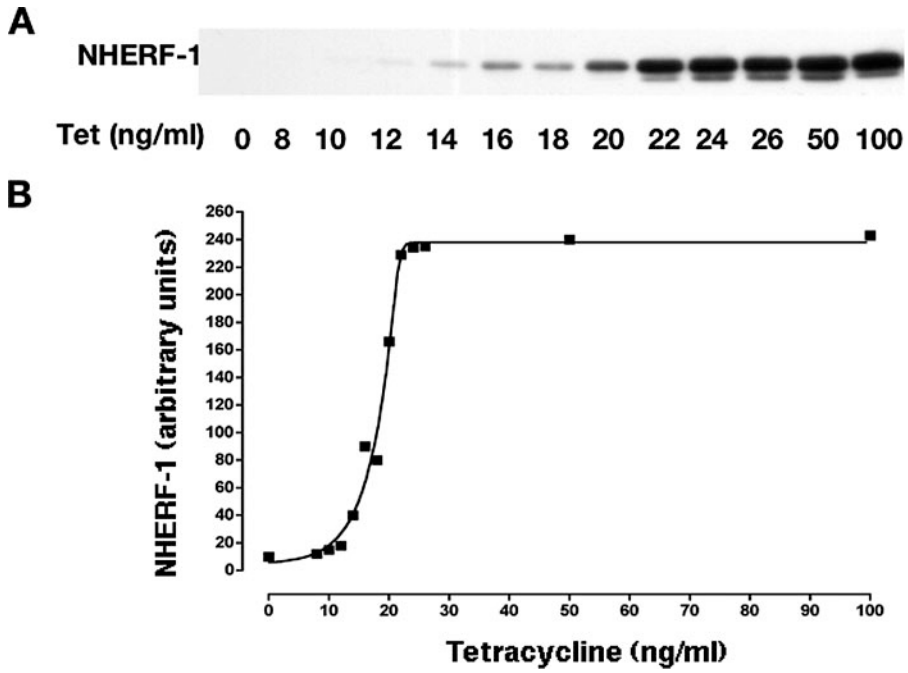

FIGURE 1. **Expression of NHERF-1/EBP50 by CHO-N10 cells.** CHO-N10 cells were cultured as described. NHERF-1 expression was induced by the addition of tetracycline at the indicated doses. NHERF-1 expression was determined 24 h after the addition of tetracycline.

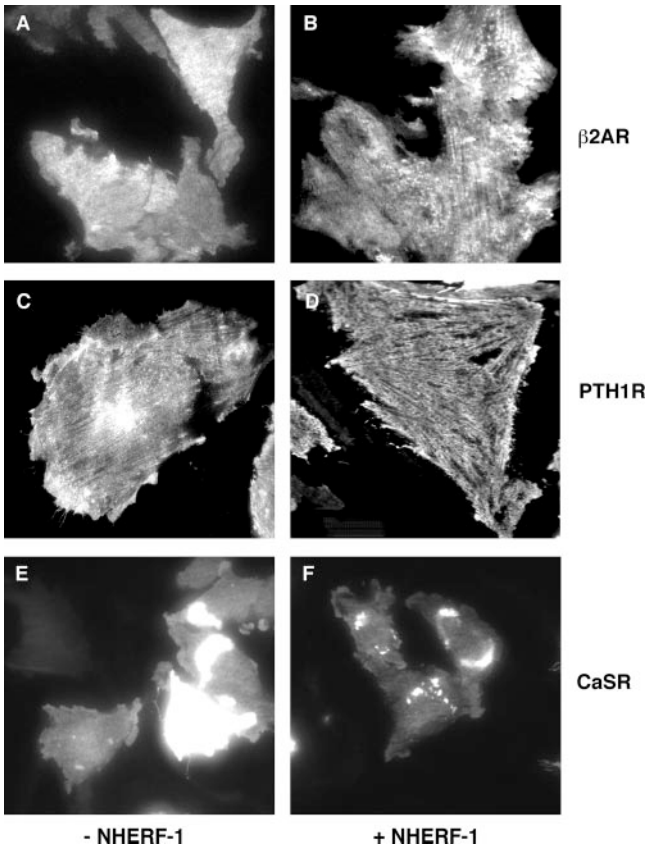

FIGURE 2. **Distribution of β_2AR-eGFP, PTH1R-eGFP, and CaSR-eGFP on the surface of CHO-N10 cells.** CHO-N10 cells were transfected with β_2AR-eGFP (*A* and *B*), PTH1R-eGFP (*C* and *D*), and CaSR-eGFP (*E* and *F*). Where indicated (*NHERF*(+) in *B*, *D*, and *E*), the cells were induced with tetracycline (50 ng/ml; 24 h) prior to transfection. The cells were examined with TIRF microscopy 24 h after transfection with the receptor-GFP chimeras. *Scale bars*, 10 μm.

diffusion of the PTH1R and the β_2AR was strongly influenced by the expression of NHERF-1. Finally, we show that the effects of NHERF-1 on PTH1R traffic are consistent with a novel model in which NHERF-1 interferes with the binding of arrestin to the activated PTH1R.

EXPERIMENTAL PROCEDURES

Materials and Constructs—Anti-NHERF-1 antibody was purchased from Upstate Biotechnology, Inc. Anti-FLAG (M1) was from Sigma, and anti-hemagglutinin (HA11) was purchased from Covance. Anti-rabbit IgG antibody conjugated to TRITC was obtained from Jackson ImmunoResearch. All other materials were purchased from Sigma unless otherwise noted. A pEGFP-N2 plasmid encoding a full-length human PTH1R carboxyl-terminal eGFP fusion protein (PTH1R-eGFP) was kindly provided by C. Silve (INSERM, Paris, France). Similar plasmids coding for the β_2-adrenergic receptor (β_2-AR-eGFP) and the calcium-sensing receptor (CaSR-eGFP) were kindly supplied by Dr. Jeffrey Benovic (Thomas Jefferson University) and Dr. Gerda Breitwieser (Geisinger Medical Center), respectively.

Cell Culture—Chinese hamster ovary N10 cells (CHO-N10) were cultured in Ham's F-12 medium (Mediatech, Inc.) supplemented with 10% fetal bovine serum (Invitrogen) and 1% penicillin/streptomycin solution at 37 °C/5% CO_2. All live cell imaging experiments were done in Mattek dishes in complete medium. Lipofectamine 2000 (Invitrogen) or FuGENE 6 (Roche Applied Science) were used for transient transfections.

Confocal Microscopy—An Olympus Fluoview 1000 confocal microscope equipped with a SIM scanner was used for all experiments unless otherwise indicated. For live cell imaging experiments, the cells were kept at 37 °C using an open perfusion microincubator (Harvard Apparatus Inc.).

Immunocytochemistry—Cells were cultured on glass coverslips, transfected with the desired plasmids, and allowed to grow until 80% confluent. The coverslips were washed in phosphate-buffered saline and fixed for 20 min in 4% paraformaldehyde in phosphate-buffered saline at 4 °C. Cells were permeabilized with 5% nonfat milk, 0.1% Triton X-100 for 1 h at 4 °C and then stained with either phalloidin-TRITC (3 nM) or anti-NHERF-1 antibody (1 μg/ml) overnight at 4 °C. Phalloidin-stained cells were washed four times with phosphate-buffered saline and mounted using gelvatol. Anti-NHERF-1-stained cells were further treated with anti-rabbit IgG conjugated with TRITC (1:1000) in 5% nonfat milk for an additional 2 h at room temperature. The cells were then washed four times with phosphate-buffered saline, mounted with gelvatol, and examined by confocal microscopy.

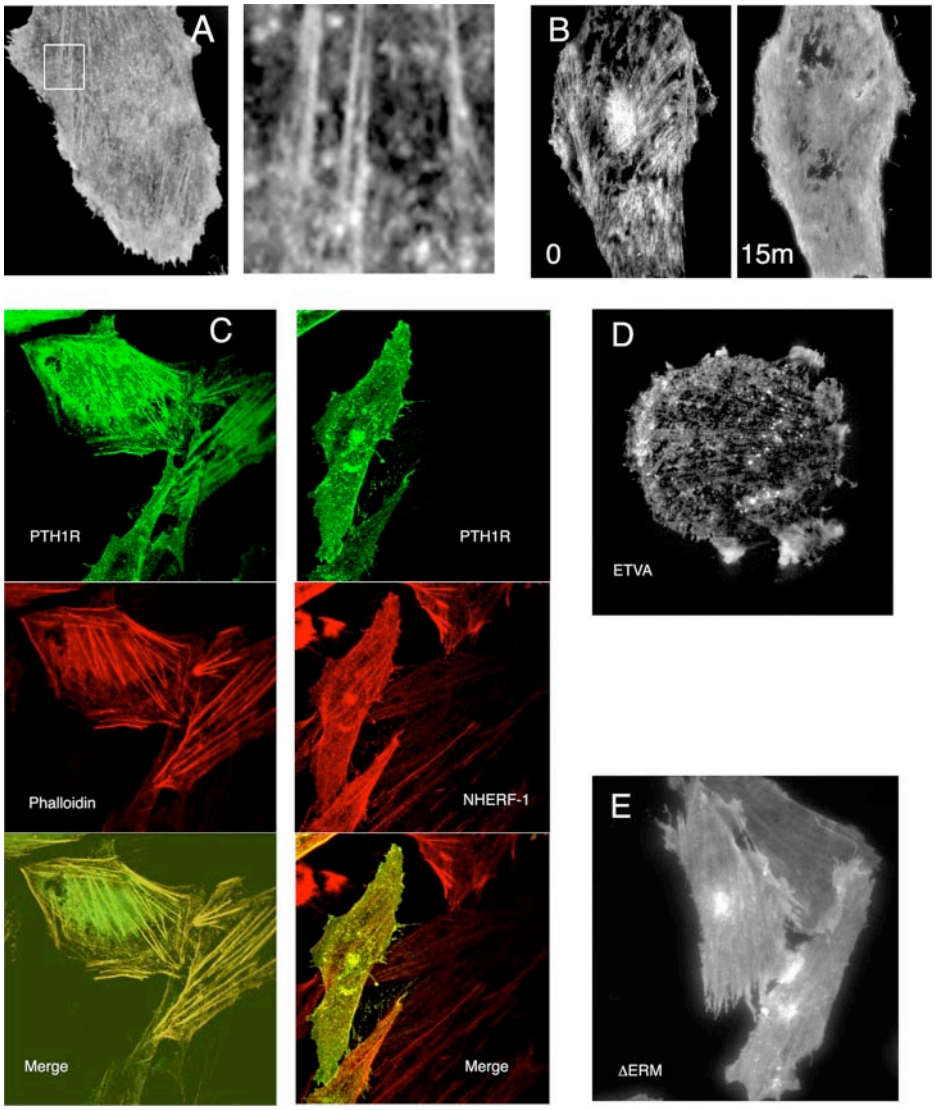

FIGURE 3. **PTH1R distribution on the plasma membrane of CHO-N10 cells.** *A*, TIRF images of the plasma membrane of CHO-N10 cells transfected with PTH1R-eGFP. The cells shown in this image were not induced with tetracycline and therefore did not express NHERF-1. *B*, the addition of latrunculin A (200 ng/ml; 15 min prior to observation) induced the redistribution of the PTH1R from bundles to the bulk membrane. *C*, co-localization of PTH1R (*green*) with F-actin (phalloidin stain; *red*, *left*) and co-localization of PTH1R (*green*) with NHERF-1 (*red*, *right*) in CHO-N10 cells induced with tetracycline. *D*, a mutation of the PDZ domain binding motif of the PTH1R (^{590}ETVM^{593} → ^{590}ETVA^{593}) reduces the interactions of the receptor with cytoskeletal fibers. *E*, overexpression of a truncated NHERF-1 mutant that does not contain the ERM-binding domain significantly reduces the binding of PTH1R to cytoskeleton fibers. *Scale bars*, 10 μm.

Fluorescence Recovery after Photobleaching (FRAP)—All FRAP measurements were done focusing the microscope onto the plasma membrane adjacent to the coverslip. This region of the cell was chosen for two main reasons: 1) it provides a large surface, and 2) many supplemental studies were done using total internal reflection fluorescence (TIRF), a technique that is limited to the observation of the cell membranes adjacent to the coverslip. The plasma membrane was located using a Z-stack scanning procedure (20). Circular regions of interest (between 90 and 200 μm^2) were selected and bleached with a 1-s pulse from a 405-nm laser line using the Fluoview 1000 SIM scanner, whereas recovery data were acquired using the instrument's main scanner and the 488-nm line of an argon gas laser. This short pulse was selected to ensure a Gaussian bleaching spot. To maximize reproducibility of the experimental conditions, all data were acquired in the photon-counting mode of the instrument. Sixty images were then collected at intervals of 1–1.6 s. The images were exported to MetaMorph (Universal Imaging, Inc.), and the average fluorescence intensities of the bleached regions and control regions in other cells or far removed regions of the same cell were obtained. The data were fitted to a single exponential decay and plotted using GraphPad Prism. The diffusion coefficient was calculated using the Stokes-Einstein equation

TABLE 1

Effects of NHERF-1 expression on receptor distribution

CHO-N10 cells expressing the indicated constructs were imaged by TIRF. The distribution of fluorescent receptors was determined using a threshholding procedure to determine "bundle" and "bulk" fluorescence in regions of interest that comprised most of the surface of each examined cell. The percentage of receptors bound to cytoskeletal bundles was measured from the ratio of the integrated fluorescence of identified bundles to the total integrated fluorescence of the regions of interest. At least six independent Mattek plates were examined for each condition. The number *n* denotes the total number of cells examined for each condition. The statistical analyses were done by ANOVA followed by Tukey's multiple comparison tests.

	NHERF-1(−)		NHERF-1(+)	
	Percentage fluorescence in bundles	Fraction of cells with visible bundles	Percentage fluorescence in bundles	Fraction of cells with visible bundles
	%		%	
β_2AR	1.2 ± 0.6 (n = 38)	1/38	19.4 ± 2.7 (n = 27)[a]	21/27
PTH1R	34.4 ± 3.0 (n = 22)	21/22	57.4 ± 2.8 (n = 34)[a,b]	34/34
M593A-PTH1R	17.4 ± 2.9 (n = 16)	12/16	17.69 ± 3.0 (n = 12)	9/12
PTH1R + ΔERM-NHERF-1	14.5 ± 1.3 (n = 15)	8/15	12.1 ± 1.4 (n = 39)	12/39
CaSR	ND[c]	0/22	ND	0/19

[a] Different from NHERF-1(−) cells ($p < 0.001$).
[b] Different from cells expressing M593A-PTH1R or ΔERM-NHERF-1 ($p < 0.001$).
[c] ND, none detected.

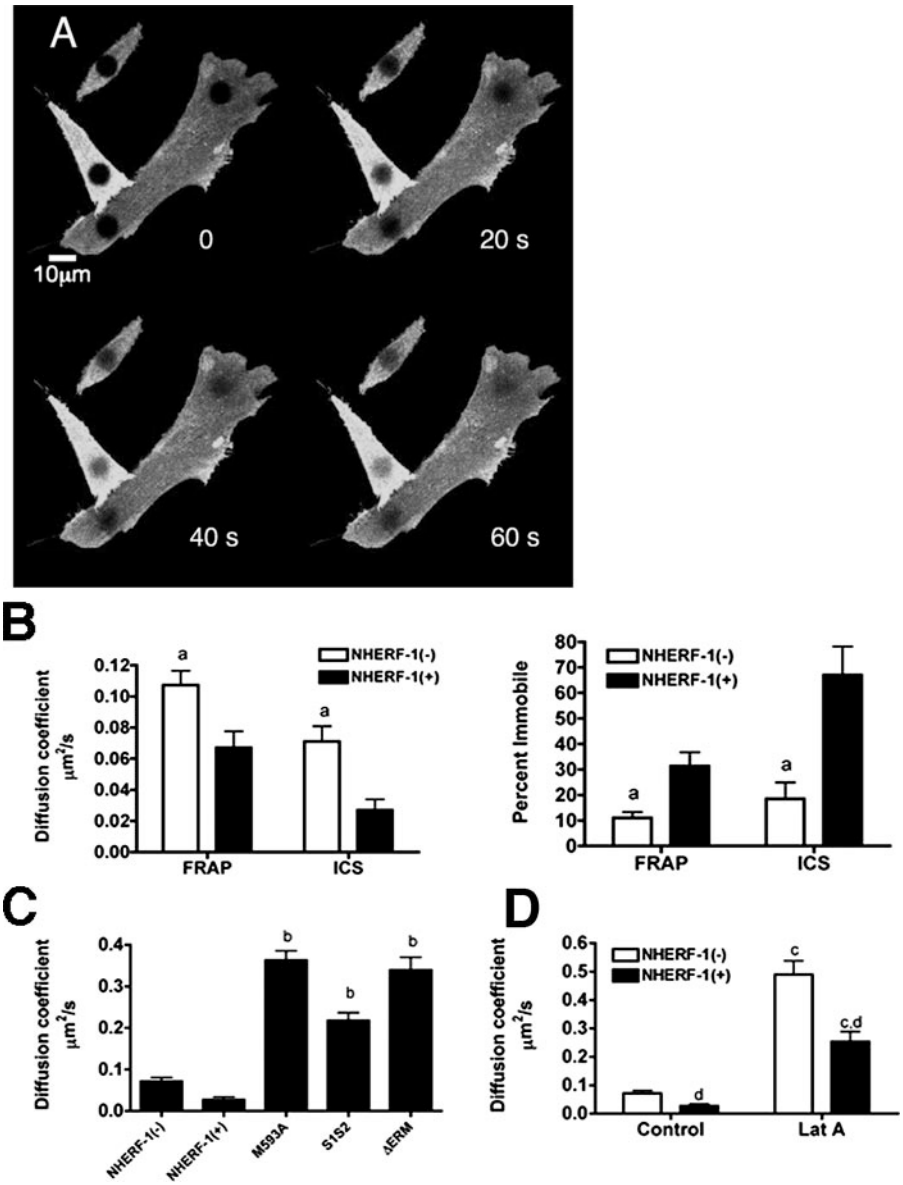

FIGURE 4. **Dynamics of the PTH1R on the plasma membrane of CHO-N10 cells.** *A*, fluorescence recovery after photobleaching. CHO-N10 cells not induced with tetracycline were imaged at 1-s intervals with a Fluoview 1000 confocal microscope. At time 0, several circular spots were bleached (using a 405-nm laser line at 99% power applied for 1 s) where indicated using the SIM scanner of the confocal microscope without interrupting image acquisition. *B*, summary of the diffusion data. *NHERF-1*(−), CHO-N10 cells not induced with tetracycline to express NHERF-1; cells in which the expression of NHERF-1 had been induced are denoted with *NHERF-1*(+). The data represent averages of 5–16 plates of cells. Statistical analysis was done by ANOVA followed by Tukey's *post hoc* tests to determine the statistical significance of the differences between tetracycline-treated and untreated cells. *a*, a statistically significant difference with regard to the NHERF-1(+) state ($p < 0.025$ in all cases). *C*, effects of various mutations on the diffusion of PTH1R. The mutant M593A-PTH1R has a defective PDZ domain binding motif that does not bind PDZ domains efficiently. *S1S2*, cells that were co-transfected with a NHERF-1 mutant in which the sequences of the core binding motifs of both PDZ domains had been mutated to eliminate PTH1R binding. *ΔERM*, cells co-transfected with PTH1R-eGFP and a C-terminal truncation mutant of NHERF-1 that does not possess an ERM binding motif. Diffusion coefficients were determined from ICS data. The data represent a summary of 5–8 cells of at least five independent plates for each condition. Only data from cells treated with tetracycline to induce NHERF-1 expression are presented. Statistical analysis was done by ANOVA followed by Tukey's *post hoc* tests. *b*, statistically significant differences with both basal (*NHERF-1*(−)) and tetracycline-treated (*NHERF-1*(+)) cells ($p < 0.01$ for all cases). *D*, the effects of latrunculin A on the dynamics of PTH1R. CHO-N10 cells were treated with 200 ng/ml latrunculin A 1 h before imaging. Diffusion coefficients were determined from ICS data. The *graph* summarizes results obtained with 5–10 cells from at least five different plates per condition. *c*, statistically significant differences with cells that had not been treated with latrunculin ($p < 0.002$); *d*, significant differences with cells that do not express NHERF-1 ($p < 0.01$).

for two-dimensional diffusion ($D = r^2/(4\tau_d)$, where r is the radius of the bleached spot, and τ_d is the half-life of fluorescence recovery).

Image Correlation Spectroscopy (ICS) and Image Cross-correlation Spectroscopy (ICCS)—These studies were based on the experimental techniques described by Wiseman *et al.* (21–23) and recently reviewed by Bacia and Schwille (24) and Kim *et al.* (25). The technique measures the correlation of an image with itself after a defined latency time τ. This correlation is a function of the mobility of the fluorescent molecules. The experimental design is, in principle, identical to that used for fluorescence correlation spectroscopy, except that in ICS a larger region of the cell is imaged. This allows the acquisition of spatial information that is not available in typical fluorescence correlation spectroscopy experiments. Two different experimental designs were used for these studies. In some cases, the data were collected with a Fluoview 1000 confocal microscope focused onto the plasma membrane of the cell adjacent to the coverslip. In others, the data were obtained using an Olympus-based TIRF system (see below). For confocal microscopy experiments, a small section of the plasma membrane (<50 μm^2) was rapidly scanned (50–60 ms/frame) under low laser power, and up to 300 images were collected. For the TIRF experiments, up to 200 images were obtained consecutively using a 500-ms exposure time. With either experimental set-up, fluorescence loss due to photobleaching of the sample was almost negligible. The image data were exported to ImageJ and analyzed using a plug-in specifically written to calculate the autocorrelation function of the data. This plug-in was based on code developed by A. Tully and E. Levitan (University of Pittsburgh). The resulting autocorrelation data were exported to GraphPad Prism and fit to a single species two-dimensional diffusion model ($G(\tau) = K(1 + \tau/\tau_d)^{-1} + G_0$ where τ_d is the charac-

teristic time constant, K is a proportionality factor, and G_0 is a term that accounts for spatial autocorrelation) as described by Hebert *et al.* (21). The data were also fit to a two-state diffusion model without any significant improvement in the quality of the fit. Therefore, all analyses reported in this paper were done using the single-species diffusion model. For calibration purposes, the diffusion of free intracellular GFP was determined using ICS and FRAP. The values for the diffusion coefficient of GFP obtained by both methods were comparable. ICCS experiments were conducted essentially using the same design, except that images were collected from both green (eGFP) and red (monomeric dsRed) channels. The cross-correlation calculation was performed using an ICCS plug-in for ImageJ developed for this purpose. Fractional binding was calculated from the ratio of the amplitude of the cross-correlation function to the amplitude of the autocorrelation function for PTH1R. These calculations are based on the method described by Kim *et al.* (25).

Total Internal Reflection Microscopy—TIRF microscopy studies were conducted using an Olympus 1X71 equipped with a 150-milliwatt argon laser, an Olympus ×60 TIRF objective, a Princeton CCD camera, and Sutter filter wheels. The imaging work station was controlled with SimplePCI software (Compix, Inc.). Typical exposure times of 500 ms were used for most experiments. For ICS measurements, up to 200 images were collected continuously. For endocytosis experiments, images were taken once every 30 s for up to 20 min. The data collected were exported to ImageJ and analyzed using the appropriate plug-ins.

Endocytosis Studies—These experiments were done using TIRF microscopy. Cells with or without NHERF-1 were imaged at 37 °C at 30-s intervals for 1–2 min before the addition of the ligand. The microscope was refocused after stimulation of the cells, and image acquisition was continued for an additional 20 min at 30-s intervals. Fluorescence intensity data of the whole cell or of specific regions of interest were exported to GraphPad Prism and analyzed by fitting to a single exponential decay.

Statistical Analysis—All multiple comparisons were done using ANOVA followed by Tukey's post-test pairwise comparisons using the analysis routines built in GraphPad Prism. Plates from a minimum of five independent experiments were used for every procedure. Most of the experiments described here were repeated 12 times or more. ICS and ICCS studies were done using ImageJ plug-ins developed in house. These are available upon request.

RESULTS

Expression of NHERF-1 in CHO-N10 Cells—These studies were done using a new cell line, derived from Chinese hamster ovary cells. These cells, termed CHO-N10, express NHERF-1 in a tetracycline-inducible manner. We chose CHO cells as a model system for these studies, because they do not express detectable levels of NHERF-1 (Fig. 1). Fig. 1 also shows the induction of NHERF-1 expression 24 h after the addition of various doses of tetracycline. As shown, the expression of NHERF-1 by CHO-N10 cells is exquisitely sensitive to tetracycline. Therefore, CHO-N10 cells appear to be an ideal system to examine the effects of NHERF-1 expression on the dynamics and biochemistry of its interacting proteins. All experiments reported below were done inducing NHERF-1 expression with 50 ng/ml tetracycline for 24 h.

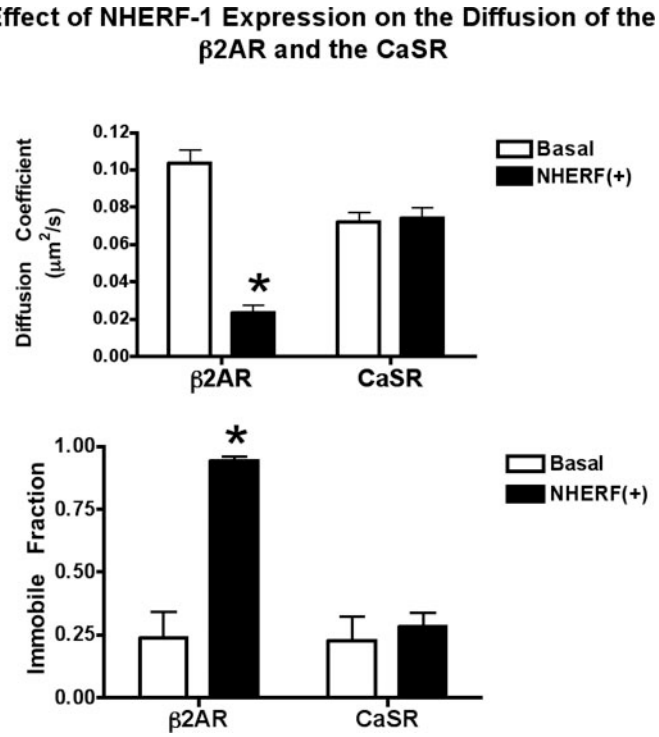

FIGURE 5. **Effects of NHERF-1 expression on the diffusion of β_2AR and CaSR in the plasma membrane of CHO-N10 cells.** CHO-N10 cells were transfected with β_2AR-eGFP or CaSR-eGFP, and NHERF-1 expression was induced with 50 ng/ml tetracycline for 24 h. The diffusion of the fluorescent receptors was examined by TIRF-ICS. One hundred images were collected per set at a rate of 3 images/s. The measured total intensities were corrected for photobleaching using a normalization plug-in for ImageJ. The corrected intensities were fit to a single-component two-dimensional diffusion model to determine the diffusion coefficient and the immobile fraction of the receptor. Statistically significant differences ($p < 0.01$) between basal and tetracycline-induced, NHERF-1-expressing cells are denoted by the *asterisks* ($n = 6$ for all experiments).

GPCRs That Contain C-terminal PDZ Binding Motifs Are Tethered to Actin Stress Fibers—Since NHERF-1 binds GPCR and the cytoskeleton, we first examined the effects of NHERF-1/EBP50 on the distribution of GPCR in live cells transfected with β_2AR-eGFP, PTH1R-eGFP, or CaSR-eGFP. TIRF microscopy revealed that the β_2AR-eGFP construct aggregated on puncta and bundle-like structures that closely resembled cytoskeletal stress fibers only in cells expressing NHERF-1/EBP50 (Fig. 2, *A* and *B*). In contrast, PTH1R-eGFP accumulated in bundles even in the absence of NHERF-1 expression (Figs. 2, *C* and *D*, and 3*A*). The CaSR chimeras were never observed in bundles (Fig. 2, *D* and *E*). Several lines of evidence suggested that these bundle structures were linked to the cytoskeleton. For instance, prolonged serum starvation of the cells reduced significantly the prevalence of receptor bundles. Furthermore, the addition of latrunculin A to disrupt the cytoskeleton rapidly dissipated most of the PTH1R bundles (see, for instance, Fig. 3*B*), such that 15 min after the addition of latrunculin, no bundles were visible. The relative distribution of the receptors in bundles was determined by morphometric analyses. The results of these measurements are summarized in Table 1.

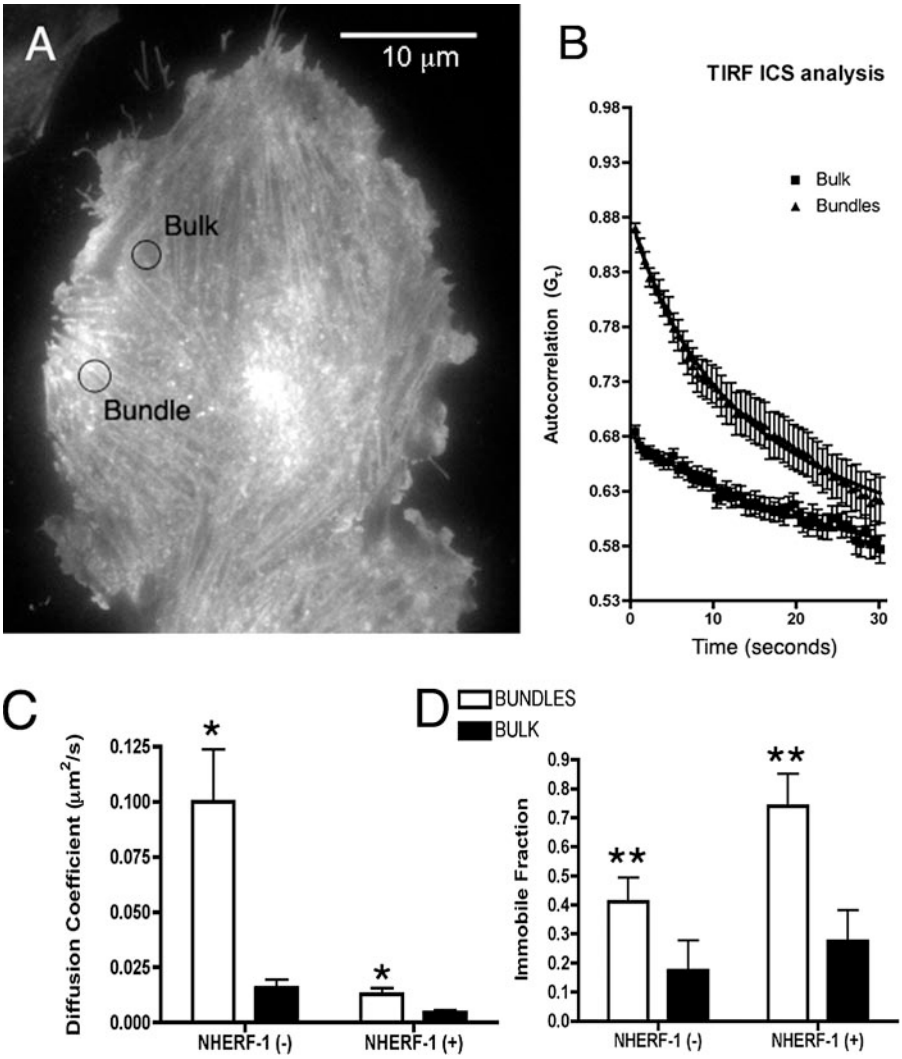

FIGURE 6. **Topological analysis of the diffusion of PTH1R.** CHO-N10 cells were examined using TIRF microscopy. Images (100–300) were collected at 500-ms intervals. The cells were then examined to detect bundle-rich and bulk plasma membrane regions. Small circular sections were selected in these regions (<10-μm diameter; as seen in *A*), and the data were fit to one-species autocorrelation functions. *B*, the first 30 s of the autocorrelation curves calculated for the regions of interest shown in *A*. These results were used to calculate diffusion coefficients (shown in *C*) and immobile fractions (*D*). Six cell plates for each experimental condition were examined. The distribution among "bundle" and "bulk" regions was done based primarily on the local density of bundles on the cell surface within the selected region of interest. Bundle-rich and bulk regions were selected using thresholding algorithms, and the analysis was limited to well defined bundle and bulk regions. Because of these limitations, roughly 30% of the surface of each cell examined was covered. The data were analyzed by ANOVA followed by post-test Tukey's comparisons between the NHERF-1(+) and NHERF-1(−) groups. Relevant significant differences are noted in the *graph* as *asterisks* (*, $p < 0.001$; **, $p < 0.05$). These data were collected from six independent coverslips for each condition (1–3 cells were examined in each).

These results illustrate the significant effects of the expression of NHERF-1 on the subcellular distribution of the β_2AR. The effects of NHERF-1 on the distribution of the PTH1R were much less dramatic although significant. In contrast, NHERF-1 expression had no detectable effects on the distribution of the CaSR. Finally, to demonstrate that these distributions were not peculiar to CHO cells, the distribution of the PTH1R was examined in HEK293, rat osteosarcoma (ROS), and human osteosarcoma (SaOS2) cells. In all cases, a significant fraction of the PTH1R was found in bundle-like structures (data not shown). To determine the relationship between the receptor bundles and the cytoskeleton, CHO-N10 cells expressing PTH1R-eGFP were fixed and stained with TRITC-conjugated phalloidin. Fig. 3*C* shows clearly that the bundles parallel actin fibers. As expected, NHERF-1 co-localized with these fibers.

The data shown in Fig. 1 clearly suggested a major difference in the subcellular distributions of the CaSR on one side and the β_2AR and the PTH1R on the other. We hypothesized that the differences in the distribution of these receptors were a consequence of the fact that the β_2AR and the PTH1R contain a PDZ binding motif at their C terminus, whereas the CaSR does not. Since the PDZ binding motifs of the β_2AR and the PTH1R interact with NHERF-1, we proceeded to examine the relevance of these interactions for the stability of the receptor bundles using the PTH1R as a model. CHO-N10 cells were transfected with 1) M593A-PTH1R-eGFP (a PTH1R-eGFP in which the C-terminal methionine has been mutated to alanine, which results in a dramatic reduction of the affinity of the receptor for NHERF-1 (26)) or 2) wt-PTH1R-eGFP co-transfected with a deletion mutant of NHERF-1 that does not contain the ERM-binding domain (ΔERM-NHERF-1, which has intact PDZ domains and acts as a dominant negative regarding most of the effects of NHERF-1, primarily because it does not interact with the cytoskeleton (18)). In both cases, the PTH1R bundles were still present, albeit much less so than in the cells that expressed wt-PTH1R-eGFP alone (Table 1 and Fig. 3, *D* and *E*). Thus, the binding of the PTH1R to cytoskeletal fibers is mediated to a significant extent by the interaction of the C terminus of the receptor with specific PDZ domain-containing proteins.

NHERF-1 Expression Modulates Receptor Diffusion—We next studied the effects of the cytoskeleton and NHERF-1 expression on PTH1R mobility. Diffusion coefficients were measured using a confocal microscope focused at the plasma membrane closest to the coverslip using FRAP and ICS techniques (Fig. 4). Fig. 4*A* shows a representative FRAP experiment carried out with cells that do not express NHERF-1. The diffusion coefficients and immobile fractions were calculated for several cells from 5–16 plates for each condition. These results are summarized in Fig. 4*B*. The diffusion of the PTH1R was significantly slower, and the fraction of immobile receptors was

significantly greater in cells that expressed NHERF-1. The results obtained with FRAP and ICS were internally consistent; both methods demonstrated that NHERF-1 significantly decreased the diffusion coefficient and mobile fraction of PTH1R (Fig. 4*B*). It should be noted that the numbers obtained with ICS and FRAP were not identical. These differences are not unusual and have been attributed to the existence of confinement zones that have a much greater relative influence in the data collected by ICS, because the region imaged is significantly smaller (27).

To demonstrate that the effects of NHERF-1 on receptor mobility were primarily due to the interaction of PTH1R with NHERF-1, we examined the diffusion of M593A-PTH1R. M593A-PTH1R diffused very rapidly in comparison with wt-PTH1R in the presence of NHERF-1 (Fig. 4*C*). Likewise, wt-PTH1R diffused very rapidly when co-expressed with NHERF-1 mutants that do not bind the receptor (such as S1S2, in which the core binding sequences of the PDZ domains have been scrambled) or that fail to interact with the cytoskeleton (such as ΔERM-NHERF-1) (Fig. 4*C*).

Finally, we examined the role of the cytoskeleton in the lateral mobility of PTH1R (Fig. 4*D*). Blocking actin polymerization with latrunculin A increased dramatically the diffusion coefficient while decreasing the immobile fraction of wt-PTH1R-eGFP. Interestingly, NHERF-1 decreased the diffusion coefficient of PTH1R in latrunculin A-treated cells, suggesting the presence of a macromolecular complex that includes NHERF-1, PTH1R, and other proteins that may interact with the second PDZ domain or with the ERM binding motif of NHERF-1. These observations demonstrate that the restricted mobility of the PTH1R observed in cells that express NHERF-1 is a consequence of two concomitant phenomena: 1) the interactions of the receptor with NHERF-1 and 2) the interactions of NHERF-1 with the cytoskeleton.

Since NHERF-1 also interacts with the β_2AR with high affinity, we predicted that NHERF-1 expression should have similar effects on β_2AR diffusion. The results are shown in Fig. 5. NHERF-1 dramatically reduced the mobility of the β_2AR. Importantly, NHERF-1 had no discernible effects on the diffusion of the CaSR, which was included as a negative control. Therefore, the effects of NHERF-1 are specific and not due to generalized changes in the structure of the cytoskeleton in the vicinity of the plasma membrane. Interestingly, the effects of NHERF-1 on β_2AR mobility were independent of the presence of ligand, thus suggesting that the interactions between the β_2AR and NHERF-1 do not require ligand binding.

Local Effects of NHERF-1 on Receptor Lateral Diffusion—Because the distribution of the PTH1R on the cell surface was not homogeneous, we examined the dynamics of the receptor in different subregions of the cell using TIRF microscopy. "Bundle" and "bulk" regions within each cell were identified based on the concentration of observable bundles within the region of interest (ROI) (Fig. 6*A*). Small (<2.5 μm in diameter) circular ROI were selected within these regions, and the diffusion coefficient of the receptor was measured by ICS. As shown in Fig. 6*B*, the autocorrelation functions of the PTH1R within "bulk" and "bundle" regions were very different. Within the bundles, in the absence of NHERF-1, about 60% of the receptor molecules

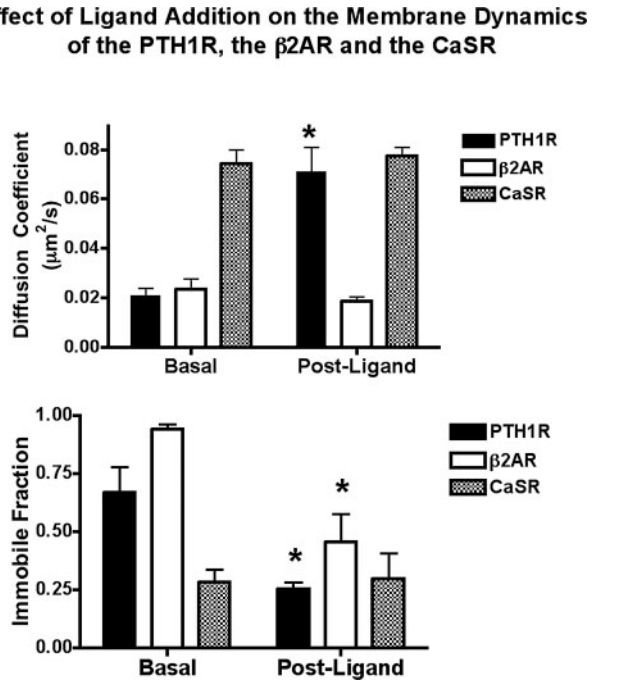

FIGURE 7. **Effects of the addition of ligand on the lateral mobility of cell surface receptors.** CHO-N10 cells were transfected with PTH1R-eGFP, β_2AR-eGFP, or CaSR-eGFP, and NHERF-1 expression was induced with 50 ng/ml tetracycline for 24 h. The diffusion of the fluorescent receptors was examined by TIRF-ICS immediately before and 5 min after the addition of saturating concentrations of ligand (100 nM PTH-(1–34) for the PTH1R, 10 μM isoproterenol for the β_2AR, and 5 mM Ca^{2+} for the CaSR). One hundred images were collected per set at a rate of 3 images/s. The measured total intensities were corrected for photobleaching and receptor endocytosis using a normalization plug-in for ImageJ. The corrected intensities were fit to a single component two-dimensional diffusion model to determine the diffusion coefficient and the immobile fraction of the receptor. The statistical analysis was done by ANOVA followed by post-test Tukey's comparisons. Statistically significant differences between basal and post-ligand were noted ($p < 0.01$, $n = 6$ independent coverslips (1–6 cells examined/coverslip) for each experiment).

diffused with a coefficient of 0.1 $\mu m^2/s$ (Fig. 6*C*). In contrast, the receptor diffused very slowly ($D = 0.019$ $\mu m^2/s$) in the bulk region of the cell. This finding strongly suggests that the receptor diffuses along the bundles. However, this diffusion was still very slow when compared with that observed in the presence of latrunculin A; thus, we conclude that the motion of the receptors along the bundles is limited by the binding of the receptor to the cytoskeleton. NHERF-1 expression drastically reduced the diffusion coefficient of the fast moving component within the bundles without exerting a statistically significant effect on the diffusion coefficient of PTH1R molecules within the bulk membrane (Fig. 6*C*). Conversely, the expression of NHERF-1 increased significantly the immobile fraction of the PTH1R within the bundles. Because the data show that PTH1R bundles coincide with actin stress fibers (Fig. 3*C*), these results suggest that the effects of NHERF-1 on the lateral diffusion of the PTH1R are effectively limited to the population of receptors located in very close proximity to actin fibers.

Perturbation of the Effects of NHERF-1 Expression by the Addition of Ligand—The diffusion data shown in Figs. 4 and 5 suggest that NHERF-1 effectively tethers PTH1R and β_2AR to the cytoskeleton. Inasmuch as the interactions of some GPCR with NHERF-1 appear to be ligand-dependent (28), we hypoth-

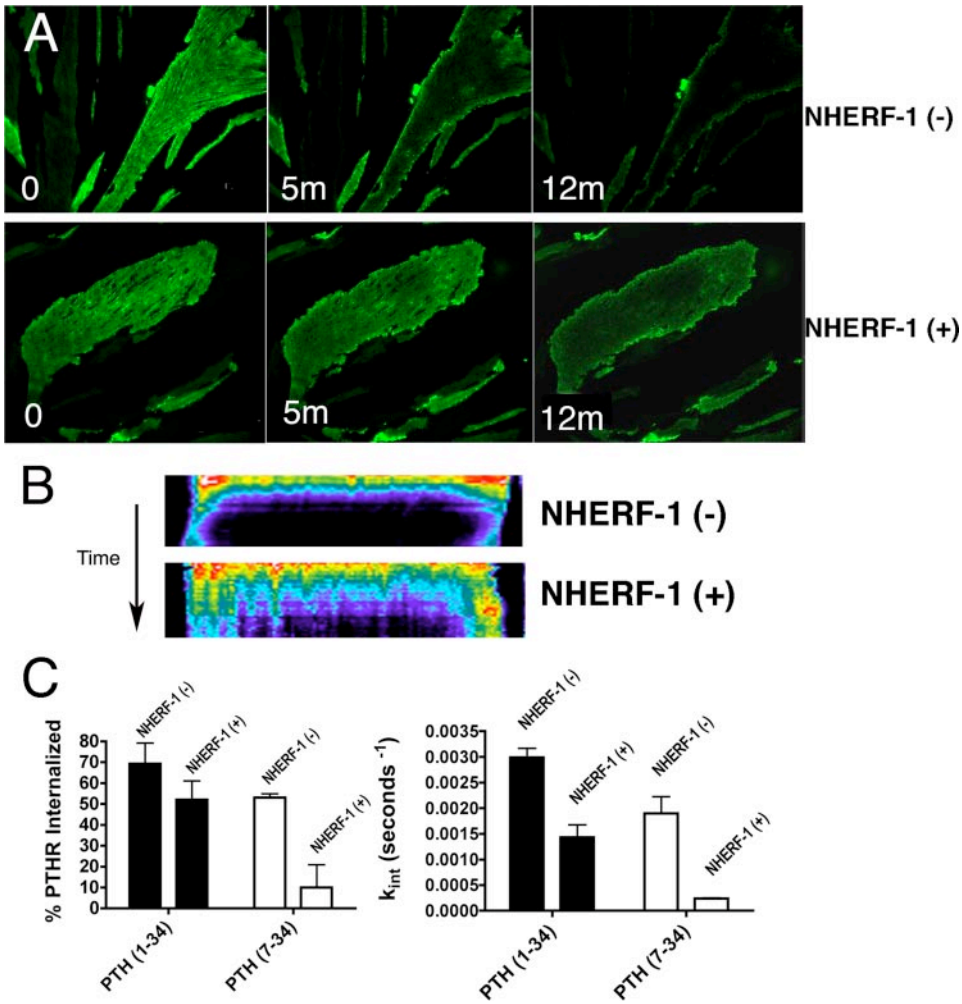

FIGURE 8. **Effects of the expression of NHERF-1 on the internalization of PTH1R.** *A*, CHO-N10 cells treated with vehicle (NHERF$^-$) or tetracycline (NHERF$^+$) were examined by TIRF microscopy after the addition of 100 nM PTH-(1–34). Images were collected at 30-s intervals. The figure shows representative images obtained at the indicated times. *B*, kymograph of the cells shown in *A*. The image data were processed as follows. After correction for photobleaching, a *y* axis maximal projection of the cell was obtained. A pseudocolor look up table was applied to the projection. As shown, the intensity decayed significantly more rapidly in the NHERF$^-$ cell shown in *A*. Furthermore, receptor internalization was somewhat slower at the edges of both cells. *C*, summary of the PTH1R endocytosis data. The data show the summary of 12–18 cells (12 separate coverslips) per condition. The internalization rate constant was calculated fitting the intensity data to a single exponential, whereas the fraction of surface receptors internalized was calculated from the span of the decay function obtained from these fits. ANOVA analyses followed by Tukey's post-test comparisons revealed that NHERF-1 expression had a significant effect on the rate of endocytosis of the PTH1R, independently of the ligand used to induce internalization. Moreover, PTH-(7–34)-induced internalization of the receptor was almost completely blocked by NHERF-1 ($p < 0.001$, $n = 12$).

esized that the addition of ligand would result in changes of the diffusion properties of these receptors. Since its diffusion was insensitive to the expression of NHERF-1, once again we used the CaSR for control purposes. TIRF experiments were done using CHO-N10 cells transiently expressing PTH1R-eGFP, β_2AR-eGFP, or CaSR-eGFP. The results are shown in Fig. 7. The addition of 5 mM calcium did not influence the diffusion of the CaSR. In contrast, the diffusion of the PTH1R was very sensitive to the addition of ligand; the diffusion coefficient of the PTH1R increased almost 4-fold within 5 min of the addition of PTH-(1–34), whereas the immobile fraction was reduced to about half of its original value. The results obtained with the β_2AR were somewhat different. Prior to the addition of ligand, about 95% of the surface β_2AR was essentially immobile. The addition of isoproterenol did not alter the diffusion coefficient of the β_2AR; however, the immobile fraction of the receptor was reduced substantially. These results suggest that ligand induces the dissociation of the β_2AR·NHERF-1 complexes from the cytoskeleton without affecting the binding of NHERF-1 to the receptor.

NHERF-1 Expression Modulates PTH1R Internalization—To investigate the effects of NHERF-1 on receptor traffic, we examined the effects of the addition of ligand on the surface distribution of the PTH1R using TIRF microscopy. In these experiments, images were collected at 30-s intervals after the addition of ligand. PTH-(1–34), a well characterized PTH agonist (18, 26), induced the disappearance of these receptor bundles (Fig. 8*A*). Fig. 8*B* shows a kymograph of the *xy* projections of the cells shown in Fig. 8*A*. Interestingly, the PTH1R internalized significantly more slowly at the edges of the cell. Collected intensity data were fit to a single exponential to estimate an apparent first order rate of internalization. The plateau values from these fits were used to calculate the fraction of internalized receptor. In the presence of PTH-(1–34), 70–80% of the receptors internalized. Strikingly, NHERF-1 expression reduced the rate of internalization of the receptor by about 50% without affecting significantly the fraction of internalized receptors. In contrast, the antagonist PTH-(7–34) induced slower receptor internalization, which was abrogated by the expression of NHERF-1. We conclude that NHERF-1 expression affected differentially receptor internalization, depending on the nature of the ligand used to induce endocytosis.

Effects of NHERF-1 Expression on the Binding of β-Arrestin to the PTH1R—To gain some insight into the mechanisms by which NHERF-1 modulates PTH1R dynamics and internalization, CHO-N10 cells were transfected with PTH1R-eGFP and β-arrestin-1 fused to mRFP (a monomeric variant of the *Discosoma* protein dsRed). These cells were then studied using ICCS analysis, a technique developed to study protein-protein interactions in live cells. This method is based on a time-dependent analysis of the cross-correlation between the fluorescence intensities of two targets labeled with distinct fluorophores (24): proteins that are associated with a common macromolec-

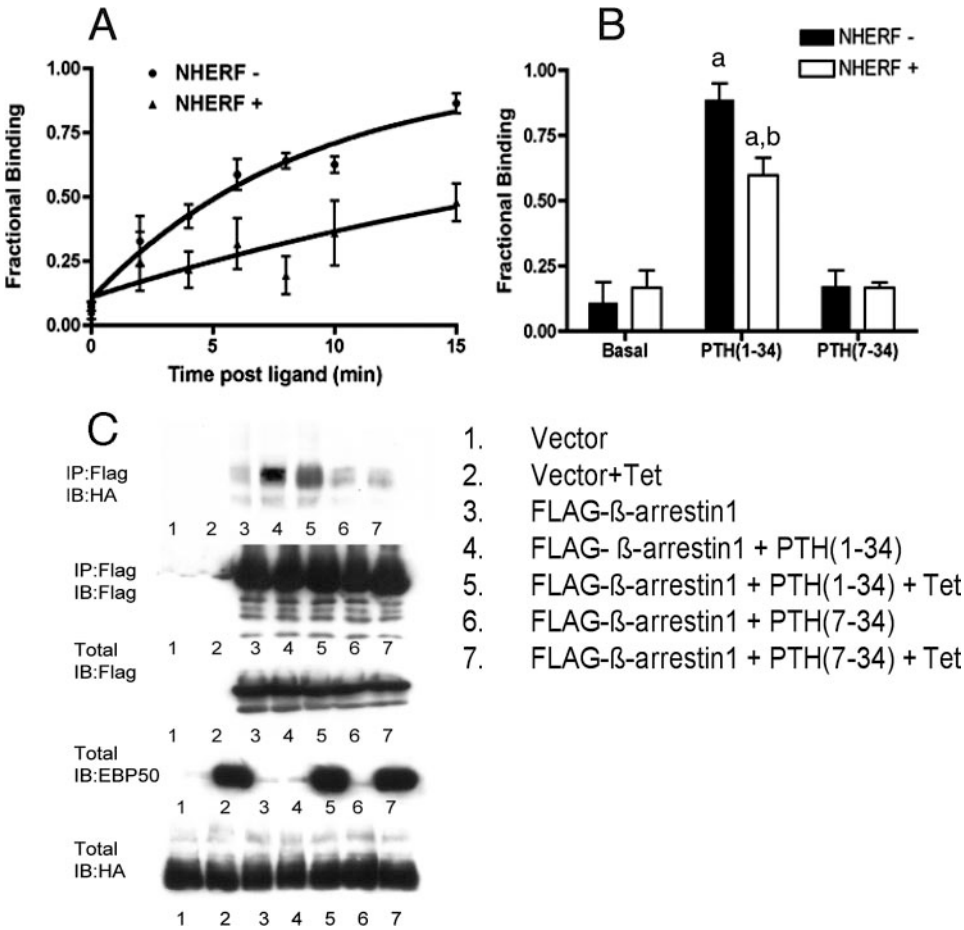

FIGURE 9. **Effects of PTH analogs and NHERF-1 expression on the binding of β-arrestin-1 to PTH1R.** CHO-N10 cells were transfected with PTH1R-eGFP and selected for 20 days with G418. These cells were further transfected with a β-arrestin-1-mRFP construct and treated with vehicle (*NHERF*$^-$) or with tetracycline (*NHERF*$^+$) as described under "Experimental Procedures." The cells were then examined with a confocal microscope focused on the plasma membrane. *A*, kinetics of binding of β-arrestin-1 to PTH1R. The fractional binding was calculated from the autocorrelation and cross-correlation curves as described under "Experimental Procedures." The *solid lines* were obtained by fitting the data to a single exponential. The rate constants obtained were 0.12 and 0.037 min^{-1} for the NHERF$^-$ and NHERF$^+$ conditions, respectively. The difference between these rate constants is statistically significant ($p = 0.002$, $n = 5$). *B*, the fractional binding of PTH1R to arrestin was determined by image cross-correlation spectroscopy 10 min after the addition of the various ligands. The autocorrelation function for PTH1R-eGFP and the cross-correlation function were determined as described under "Experimental Procedures." The fractional binding of PTH1R to arrestin was calculated from the ratio of the amplitudes of the cross-correlation and autocorrelation functions as described by Kim *et al.* (25). The differences among groups were examined by ANOVA followed by pairwise Tukey's test comparisons. *a*, different from preligand basal ($p < 0.05$); *b*, different from NHERF$^-$ ($p < 0.05$). Five independent coverslips were examined for each condition. *C*, CHO-N10 cells were transfected with hemagglutinin-tagged PTH1R and FLAG-tagged β-arrestin-1. Cells were treated with PTH-(1–34) (100 nM) or PTH-(7–34) (1 μM) where stated. Fifteen minutes after the addition of ligand, the cells were lysed, and β-arrestin-1 was immunoprecipitated (*IP*) using agarose-conjugated anti-FLAG antibodies. *IB*, immunoblot.

ular complex diffuse together, whereas those that are not diffuse in random directions with respect to one another. This approach has been previously used to measure dynamic protein-protein association (24, 25).

In order to eliminate experimental artifacts due to signal saturation, we selected cells in which the fluorescence intensities of PTH1R-eGFP and mRFP-β-arrestin-1 were comparable. In all cases, we calculated the cross-correlation function of the same cells, immediately before and at various times after the addition of the ligand. The fractional degree of binding was experimentally determined by measuring the ratio of the amplitudes of the PTH1R autocorrelation curve and the PTH1R-βArrestin cross-correlation curve, as described by Bacia *et al.* (24). The addition of PTH-(1–34) increased substantially the binding of PTH1R to arrestin in a time-dependent manner from a low basal value to almost 100% (Fig. 9*A*), indicative of the formation of a complex that included arrestin and the receptor. NHERF-1 reduced the rate of formation of this complex 3-fold, suggesting that NHERF-1 binding interferes with arrestin recruitment to the receptor. This observation also indicates that NHERF-1 dissociation probably precedes arrestin binding.

Since PTH1R internalization induced by PTH-(7–34) was significantly slower, we examined the interactions of the receptor with β-arrestin-1 after the addition of this ligand. PTH-(7–34) did not increase the cross-correlation between PTH1R and β-arrestin-1 (Fig. 9*B*). To confirm that the ICCS data reported in Fig. 9*B* reflected PTH1R-arrestin interactions, CHO-N10 cells were co-transfected with FLAG-tagged β-arrestin-1 and hemagglutinin-tagged PTH1R. The cells were treated with PTH-(1–34) or PTH-(7–34) for 15 min, and the binding of PTH1R to arrestin was determined by co-immunoprecipitation methods (Fig. 9*C*). As shown, PTH-(1–34) induced the formation of complexes with β-arrestin, whereas PTH-(7–34) did not. This suggests that PTH-(7–34)-induced internalization is arrestin-independent. Because NHERF-1 expression completely blocked PTH-(7–34)-induced PTH1R internalization, we also conclude that NHERF-1 affects PTH1R endocytosis by a dual mechanism: 1) reducing the rate of arrestin binding to the receptor, and 2) blocking arrestin-independent endocytic processes.

DISCUSSION

Direct, functional interactions of GPCRs with the cytoskeleton were initially suggested several years ago (29). We describe here three different modes of interaction of GPCR with the cytoskeleton: 1) some GPCR, such as the β_2AR, are linked to the cytoskeleton via their interactions with NHERF-1; 2) some GPCRs, such as the PTH1R, interact with the cytoskeleton through their interactions with other proteins in addition to NHERF-1; and 3) some GPCRs, such as the CaSR, do not appear to interact with the cytoskeleton at all.

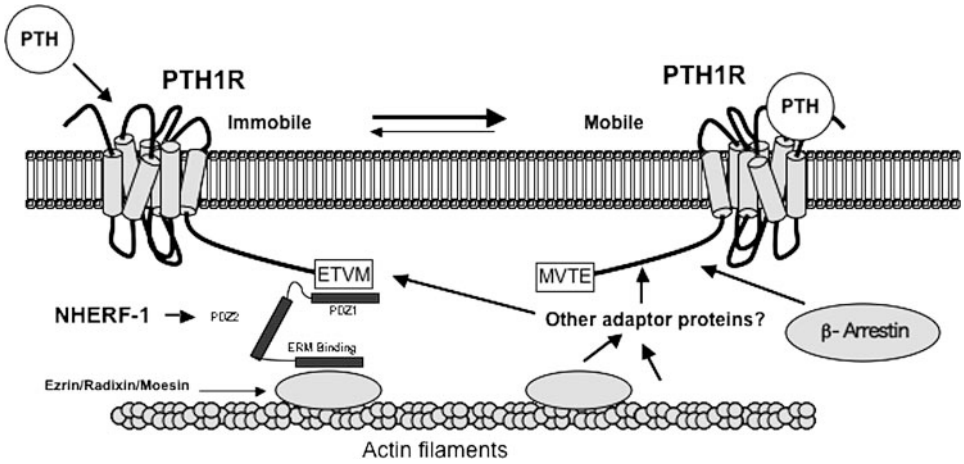

FIGURE 10. **Model describing the interactions of PTH1R with ligand, NHERF-1, the actin cytoskeleton, and arrestin.** The PTH1R is anchored to the actin cytoskeleton by multiple interacting proteins, one of which is NHERF-1. In the absence of NHERF-1, the PTH1R moves rapidly along actin fibers by a mechanism that may involve dissociation from the cytoskeleton. The interaction of NHERF-1 with the ETVM C-terminal sequence immobilizes the PTH1R and tethers it to actin fibers. The addition of ligand to the PTH1R induces the dissociation of NHERF-1 and the binding of β-arrestin. Ligand-induced arrestin binding is significantly slower in the presence of NHERF-1, probably because NHERF-1 dissociation must precede arrestin binding.

The interactions of the β_2AR with the cytoskeleton appeared to be mediated almost exclusively by NHERF-1, as there was no evidence of cytoskeletal localization of the β_2AR in cells that did not express NHERF-1. However, surprisingly, the association of PTH1R to cytoskeletal structures was not strictly dependent on the expression of NHERF-1, suggesting that NHERF-1 is only one of several cellular components mediating the interactions of PTH1R with the actin cytoskeleton. Consistent with this, at least two other cytoskeleton-related proteins have been reported to interact with PTH1R: Tctex-1, a dynein light chain (30), reportedly linked to the actin cytoskeleton (31), and 4.1G, a protein directly associated with actin (32). The binding sites for these two proteins are located near the C terminus of PTH1R, upstream of the PDZ domain binding motif (ETVM), which appears to be excluded (30, 32). These interactions may be sufficient to promote partial binding of PTH1R to the cytoskeleton. However, interference with the C-terminal PDZ domain binding motif significantly decreased the accumulation of PTH1R in bundles, suggesting that other PDZ domain-containing proteins may participate in the linkage of the PTH1R to the cytoskeleton. Nevertheless, our data strongly suggest strong interactions between the PTH1R and NHERF-1 in live cells; the PTH1R becomes effectively immobilized by its interactions with NHERF-1 and the underlying cytoskeletal fibers. The functional consequences of these interactions are probably multiple. The activation of phospholipase C-dependent pathways by PTH1R appears to be regulated by binding to NHERF and the cytoskeleton (16, 33).

Much less is known about the functional consequences of tethering the β_2AR to NHERF-1 and the cytoskeleton, and most of what we know about these is limited to the effects of NHERF-1 on β_2AR traffic. It is clear that β_2AR recycling is tightly regulated by NHERF-1 expression, since disruption of the cytoskeleton impairs β_2AR recycling and increases receptor degradation (34). More recently, it has been reported that the ability of isoproterenol to activate cAMP production is increased by disruption of the cytoskeleton (35), but this observation has not been linked to NHERF-1 expression or function.

The diffusion of the β_2AR and the PTH1R but not the CaSR was strongly influenced by NHERF-1. The expression of NHERF-1 reduced the diffusion coefficient of the β_2AR and the PTH1R while increasing significantly the immobile fraction of these receptors. These results are consistent with the report of Bates *et al.* (27), who showed that the diffusion of the CFTR was also strongly influenced by NHERF-1 binding. These results prove that NHERF-1 immobilizes its targets by linking them to the cytoskeleton.

Our diffusion studies also shed important light on the influence of ligand binding on interactions of GPCR with NHERF-1. We hypothesized that ligands that reduce the affinity for NHERF-1 should increase the lateral mobility of the receptor. That seems to be the case for the PTH1R; ligand binding induced a significant increase of the diffusion coefficient and the mobile fraction of PTH1R in cells that expressed NHERF-1, whereas it was without significant effects in cells that did not. This indicates that, after ligand binding, 1) the interactions of the PTH1R with NHERF-1 and other partners have been altered, and 2) the association of PTH1R with the cytoskeleton has been impaired by either releasing NHERF-1 from the cytoskeleton or by direct disruption of the cytoskeleton. However, the case of the β_2AR is somewhat different. NHERF-1 expression immobilizes non-stimulated β_2AR, strongly suggesting that β_2AR·NHERF-1 complexes exist in the absence of ligand. Five minutes after the addition of ligand, the mobile fraction of the β_2AR was significantly increased without changing its diffusion coefficient. This strongly suggests that the binding of the β_2AR to NHERF-1 is not significantly altered by the addition of ligand, although the association of β_2AR·NHERF-1 complexes to the cytoskeleton probably is. The permanence of β_2AR·NHERF-1 complexes after the addition of ligand is consistent with previously published data. In fact, it was suggested that the interactions of the β_2AR and NHERF-1 were induced by ligand (28). However, more recent work by Cao *et al.* (34) established that GRK5-dependent phosphorylation of Ser^{411} impaired NHERF-1 binding to the β_2AR, suggesting that ligand binding might negatively influence the binding of NHERF-1 to the β_2AR. Thus, the binding of NHERF-1 to the β_2AR appears to be temporally and dynamically regulated by signaling cascades downstream the activation of the receptor. Our results suggest that, at least within 5 min after ligand addition, the β_2AR remains associated to NHERF-1, but the

interactions of NHERF-1 with the cytoskeleton or the integrity of the cytoskeleton itself are altered as a consequence of the treatment. It should be noted that several effects of cAMP and protein kinase A on the disruption of the cytoskeleton have been documented (36–39).

The reduced lateral mobility of membrane proteins induced by NHERF-1 is likely to result in the accumulation of receptors in NHERF-1-enriched regions. Furthermore, the reduced mobility of the receptors should have significant modulatory effects on the traffic of these receptors. It was recently shown that, in HEK293 cells (which express NHERF-1 at very high levels), the interactions of PDZ domain-containing proteins with the C terminus of GPCRs regulate the dynamics of the endocytosis of these receptors by delaying the recruitment of dynamin, inducing abortive events that reduce the efficiency of endocytosis, or selecting subpopulations of clathrin-coated pits (40). Here we show that the interactions with NHERF-1 govern the overall dynamics of receptors that contain C-terminal PDZ binding motifs. We propose that, since endocytic events are initiated randomly on the cell surface and have a finite duration (19), a significant reduction of the lateral mobility of the cargo molecules will probably reduce the probability of accumulation of cargo in clathrin-coated pits, thus reducing the net rate of endocytosis. Furthermore, at least in the case of the PTH1R, the interaction of the receptor with NHERF-1 delays the binding of β-arrestin. Delayed β-arrestin recruitment implies delayed recruitment of AP-2 and clathrin and, as a consequence, delayed recruitment of dynamin to complete the endocytic process. Thus, our findings provide a simple, self-consistent explanation for the reduced rate of endocytosis of GPCR containing C-terminal PDZ binding motifs observed in the presence of NHERF-1. Furthermore, we show that different ligands can induce selective, alternative pathways of GPCR internalization via mechanisms that may or may not involve arrestin and that are tightly regulated by NHERF-1. The general model we propose is shown in Fig. 10. GPCRs that contain a C-terminal PDZ binding motif are tethered to the cytoskeleton via direct interactions with NHERF-1. Some of these, such as the PTH1R, may bind the cytoskeleton via multiple additional interactions that may include other PDZ domain-containing targets. In general, NHERF-1 binding plays a major role in anchoring these receptors to the cytoskeleton, reducing receptor mobility, and dynamically interfering with the binding of arrestin after ligand stimulation. Furthermore, the binding of NHERF-1 to some of these receptors blocks completely arrestin-independent receptor internalization processes, such as PTH-(7–34)-induced PTH1R endocytosis. These data, in conjunction with those of Puthenveedu and von Zastrow (40), suggest that this may be a very general mechanism for the regulation of GPCR trafficking.

Acknowledgments—We thank Drs. Edwin Levitan, Daniel Altschuler, and Lynton Traub for suggestions and critical reviews of the manuscript. We also acknowledge the contributions of Dr. Simon Watkins and the Center for Biological Imaging of the University of Pittsburgh.

REFERENCES

1. Nicolini, C., Baranski, J., Schlummer, S., Palomo, J., Lumbierres-Burgues, M., Kahms, M., Kuhlmann, J., Sanchez, S., Gratton, E., Waldmann, H., and Winter, R. (2006) *J. Am Chem. Soc.* **128,** 192–201
2. Plowman, S. J., Muncke, C., Parton, R. G., and Hancock, J. F. (2005) *Proc. Natl. Acad. Sci. U. S. A.* **102,** 15500–15505
3. Rizzo, M. A., Kraft, C. A., Watkins, S. C., Levitan, E. S., and Romero, G. (2001) *J. Biol. Chem.* **276,** 34928–34933
4. Loebrich, S., Bahring, R., Katsuno, T., Tsukita, S., and Kneussel, M. (2006) *EMBO J.* **25,** 987–999
5. Gaidarov, I., Santini, F., Warren, R. A., and Keen, J. H. (1999) *Nat. Cell Biol.* **1,** 1–7
6. Jacobson, K., Sheets, E. D., and Simson, R. (1995) *Science* **268,** 1441–1442
7. Simson, R., Sheets, E. D., and Jacobson, K. (1995) *Biophys. J.* **69,** 989–993
8. Voltz, J. W., Weinman, E. J., and Shenolikar, S. (2001) *Oncogene* **20,** 6309–6314
9. Wade, J. B., Liu, J., Coleman, R. A., Cunningham, R., Steplock, D. A., Lee-Kwon, W., Pallone, T. L., Shenolikar, S., and Weinman, E. J. (2003) *Am. J. Physiol.* **285,** C1494–C1503
10. Weinman, E. J., Hall, R. A., Friedman, P. A., Liu-Chen, L. Y., and Shenolikar, S. (2006) *Annu. Rev. Physiol.* **68,** 491–505
11. Huang, P., Steplock, D., Weinman, E. J., Hall, R. A., Ding, Z., Li, J., Wang, Y., and Liu-Chen, L. Y. (2004) *J. Biol. Chem.* **279,** 25002–25009
12. Gage, R. M., Matveeva, E. A., Whiteheart, S. W., and von Zastrow, M. (2005) *J. Biol. Chem.* **280,** 3305–3313
13. Rochdi, M. D., and Parent, J. L. (2003) *J. Biol. Chem.* **278,** 17827–17837
14. Cunningham, R., Steplock, D., Shenolikar, S., and Weinman, E. J. (2005) *Am. J. Physiol.* **289,** F933–F938
15. Cunningham, R., Steplock, D., Wang, F., Huang, H., Xiaofei, E., Shenolikar, S., and Weinman, E. J. (2004) *J. Biol. Chem.* **279,** 37815–37821
16. Mahon, M. J., and Segre, G. V. (2004) *J. Biol. Chem.* **279,** 23550–23558
17. Shenolikar, S., Voltz, J. W., Minkoff, C. M., Wade, J. B., and Weinman, E. J. (2002) *Proc. Natl. Acad. Sci. U. S. A.* **99,** 11470–11475
18. Sneddon, W. B., Syme, C. A., Bisello, A., Magyar, C. E., Rochdi, M. D., Parent, J. L., Weinman, E. J., Abou-Samra, A. B., and Friedman, P. A. (2003) *J. Biol. Chem.* **278,** 43787–43796
19. Ehrlich, M., Boll, W., Van Oijen, A., Hariharan, R., Chandran, K., Nibert, M. L., and Kirchhausen, T. (2004) *Cell* **118,** 591–605
20. Rizzo, M. A., Shome, K., Vasudevan, C., Stolz, D. B., Sung, T. C., Frohman, M. A., Watkins, S. C., and Romero, G. (1999) *J. Biol. Chem.* **274,** 1131–1139
21. Hebert, B., Costantino, S., and Wiseman, P. W. (2005) *Biophys. J.* **88,** 3601–3614
22. Wiseman, P. W., Hoddelius, P., Petersen, N. O., and Magnusson, K. E. (1997) *FEBS Lett.* **401,** 43–48
23. Wiseman, P. W., and Petersen, N. O. (1999) *Biophys. J.* **76,** 963–977
24. Bacia, K., Kim, S. A., and Schwille, P. (2006) *Nat. Methods* **3,** 83–89
25. Kim, S. A., Heinze, K. G., Bacia, K., Waxham, M. N., and Schwille, P. (2005) *Biophys. J.* **88,** 4319–4336
26. Sneddon, W. B., Magyar, C. E., Willick, G. E., Syme, C. A., Galbiati, F., Bisello, A., and Friedman, P. A. (2004) *Endocrinology* **145,** 2815–2823
27. Bates, I. R., Hebert, B., Luo, Y., Liao, J., Bachir, A. I., Kolin, D. L., Wiseman, P. W., and Hanrahan, J. W. (2006) *Biophys. J.* **91,** 1046–1058
28. Hall, R. A., Premont, R. T., Chow, C. W., Blitzer, J. T., Pitcher, J. A., Claing, A., Stoffel, R. H., Barak, L. S., Shenolikar, S., Weinman, E. J., Grinstein, S., and Lefkowitz, R. J. (1998) *Nature* **392,** 626–630
29. Sarndahl, E., Lindroth, M., Bengtsson, T., Fallman, M., Gustavsson, J., Stendahl, O., and Andersson, T. (1989) *J. Cell Biol.* **109,** 2791–2799
30. Sugai, M., Saito, M., Sukegawa, I., Katsushima, Y., Kinouchi, Y., Nakahata, N., Shimosegawa, T., Yanagisawa, T., and Sukegawa, J. (2003) *Biochem. Biophys. Res. Commun.* **311,** 24–31
31. Chuang, J. Z., Yeh, T. Y., Bollati, F., Conde, C., Canavosio, F., Caceres, A., and Sung, C. H. (2005) *Dev. Cell* **9,** 75–86
32. Saito, M., Sugai, M., Katsushima, Y., Yanagisawa, T., Sukegawa, J., and Nakahata, N. (2005) *Biochem. J.* **392,** 75–81
33. Mahon, M. J., Donowitz, M., Yun, C. C., and Segre, G. V. (2002) *Nature* **417,** 858–861
34. Cao, T. T., Deacon, H. W., Reczek, D., Bretscher, A., and von Zastrow, M. (1999) *Nature* **401,** 286–290

35. Head, B. P., Patel, H. H., Roth, D. M., Murray, F., Swaney, J. S., Niesman, I. R., Farquhar, M. G., and Insel, P. A. (2006) *J. Biol. Chem.* **281,** 26391–26399
36. Grimaldi, M., Favit, A., and Alkon, D. L. (1999) *J. Biol. Chem.* **274,** 33557–33564
37. Liu, F., Verin, A. D., Borbiev, T., and Garcia, J. G. (2001) *Am. J. Physiol.* **280,** L1309–L1317
38. Perez, V., Bouschet, T., Fernandez, C., Bockaert, J., and Journot, L. (2005) *Eur. J. Neurosci.* **21,** 26–32
39. Szaszi, K., Kurashima, K., Kaibuchi, K., Grinstein, S., and Orlowski, J. (2001) *J. Biol. Chem.* **276,** 40761–40768
40. Puthenveedu, M. A., and von Zastrow, M. (2006) *Cell* **127,** 113

0888-8809/08/$15.00/0
Printed in U.S.A.

Molecular Endocrinology 22(5):1163–1170

doi: 10.1210/me.2007-0461

Regulation of Parathyroid Hormone Type 1 Receptor Dynamics, Traffic, and Signaling by the Na^+/H^+ Exchanger Regulatory Factor-1 in Rat Osteosarcoma ROS 17/2.8 Cells

David Wheeler, Jose Luis Garrido, Alessandro Bisello, Yung Kyu Kim, Peter A. Friedman, and Guillermo Romero

Department of Pharmacology (D.W., J.L.G., A.B., Y.K.K., P.A.F., G.R.), University of Pittsburgh School of Medicine, and the Medical Scientist Training Program (D.W.), University of Pittsburgh School of Medicine, Pittsburgh, Pennsylvania 15261

The effects of the expression of the Na^+/H^+ exchanger regulatory factor-1 (NHERF1) on the distribution, dynamics, and signaling properties of the PTH type 1 receptor (PTH1R) were studied in rat osteosarcoma cells ROS 17/2.8. NHERF1 had a dramatic effect on the subcellular distribution of PTH1R, promoting a substantial relocation of the receptor to regions of the plasma membrane located in very close proximity to cytoskeletal fibers. Direct interactions of NHERF1 with the PTH1R and the cytoskeleton were required for these effects, because they were abolished by 1) PTH1R mutations that impair NHERF1 binding, and 2) NHERF1 mutations that impair binding to the PTH1R or the cytoskeleton. NHERF1 reduced significantly the diffusion of the PTH1R by a mechanism that was also dependent on a direct association of NHERF1 with the PTH1R and the cytoskeleton. NHERF1 increased ligand-dependent production of cAMP and induced ligand-dependent rises in intracellular calcium. These effects on calcium were due to increased calcium uptake, as they were blocked by calcium channel inhibitors and by the addition of EGTA to the medium. These calcium effects were abolished by protein kinase A inhibition but phospholipase C inhibition was without effect. Based on these analyses, we propose that, in ROS cells, the presence of NHERF1 induces PTH-dependent calcium signaling by a cAMP-mediated mechanism that involves local protein kinase A-dependent activation of calcium channels. (*Molecular Endocrinology* 22: 1163–1170, 2008)

THE TYPE 1 PTH receptor (PTH1R) is a G protein-coupled receptor that signals primarily through the activation of adenylyl cyclase and the production of cAMP. However, PTH exhibits remarkable cell- and tissue-specific signaling. In most cells and tissues, the PTH1R signals via the activation of cAMP and intracellular Ca^{2+} release (1, 2). In some cells and heterologous expression systems, for instance, the PTH1R activates both adenylyl cyclase and phospholipase C (PLC). In certain instances, however, the PTH1R couples only to a single pathway and does so in a cell-specific manner. For example, in vascular smooth muscle cells, PTH stimulates adenylyl cyclase but not PLC (3, 4), whereas in keratinocytes (5–7), cardiac myocytes (8, 9), and lymphocytes (10–12), PLC, but not adenylyl cyclase, is activated. The PTH1R may be influenced by the relative levels of expression of specific G proteins (13). Likewise, N-truncated PTH antagonists, whereas failing to elicit detectable downstream signaling, promote PTH1R internalization in some cell types, but not in others (14, 15). Based on the observation that the PTH1R interacts with the Na^+/H^+ exchanger regulatory factor proteins, NHERF1 and NHERF2 (16, 17), a unified model to explain these diverse findings was developed. NHERF1 and NHERF2 are characterized by two tandem N-terminal post-synaptic 95, PSD95 (PDZ) domains that interact primarily with the C-terminal end of many targets, including the PTH1R, regulating their traffic, dynamics, and signaling properties (18–20). NHERF1 and NHERF2 also contain an ezrin-radixin-moesin (ERM) binding motif at the C terminus (20). Because of the multivalent nature of NHERF1 and NHERF2, it has been proposed that these proteins act as scaffolds, bringing together specific target molecules, and mediating the interactions of specific proteins with the cytoskeleton (16, 17).

Previous work established that NHERF1 expression has dramatic effects on the modulation of the responses of PTH1R to various ligands. Some of these are: 1) reduction of the rate of ligand-induced PTH1R endocytosis (21); 2) reduced production of cAMP (16,

First Published Online January 17, 2008

Abbreviations: EGFP, Enhanced green fluorescent protein; ERM, ezrin-radixin-moesin; IBMX, 3-isobutyl-1-methylxanthine; NHERF1, Na^+/H^+ exchanger regulatory factor-1; PDZ, post-synaptic 95, PSD95; PKA, protein kinase A; PLC, phospholipase C; PTH1R, PTH type 1 receptor; TRITC, tetramethylrhodamine isothiocyanate.

***Molecular Endocrinology* is published monthly by The Endocrine Society (http://www.endo-society.org), the foremost professional society serving the endocrine community.**

17); 3) induction of calcium responses (16, 17); and 4) blockade of the receptor internalization effects of N-truncated PTH analogs (14, 15). Because calcium responses and cAMP production appear to be inversely correlated, it has been suggested that NHERF1 induces a signaling switch, impairing the coupling of PTH1R with G_s and promoting the activation of PLC by mechanisms linked to the activation of G_i/G_o (16, 17) or G_q/G_{11} (13, 22). The molecular mechanisms underlying the signaling switch have not been characterized.

Relatively little is known about the mechanisms by which NHERF1 regulates PTH responses in bone cells. NHERF1 is not expressed in rat osteosarcoma ROS 17/2.8 (ROS) cells (16), and in these cells PTH neither activates PLC nor induces calcium-dependent signals. However, PTH(1–34) increased the activity of an activating protein 1-responsive luciferase reporter in ROS cells transfected with NHERF2, suggesting that expression of NHERF2 suffices to induce PKC-dependent responses (16). There is limited additional evidence for a NHERF1 or NHERF2-dependent signaling switch in bone cells. In fact, PLC-independent activation of PKC has been described in bone (23). In this paper we examine the influence of NHERF1 expression on the distribution, dynamics, and signaling events downstream of the PTH1R in ROS cells. Our data show that stable expression of NHERF1 alters significantly the distribution and diffusion of PTH1R, concomitantly inducing the appearance of calcium responses to stimulation with PTH. However, in contrast with the observations made in other cell systems, the induction of calcium responses by NHERF1 in ROS cells is not due to the activation of PLC. We show here that the elevation of intracellular calcium is a consequence of the activation of calcium channels by a mechanism mediated by protein kinase A (PKA) and requiring NHERF1. A novel model for the physiological role of NHERF1 in PTH1R signaling is proposed.

RESULTS

NHERF1 Regulates the Distribution of the PTH1R

Examination of a PTH1R-enhanced green fluorescent protein (EGFP) construct by confocal microscopy revealed a uniform surface distribution of the receptor on the surface of ROS cells (Fig. 1A). Actin fibers were

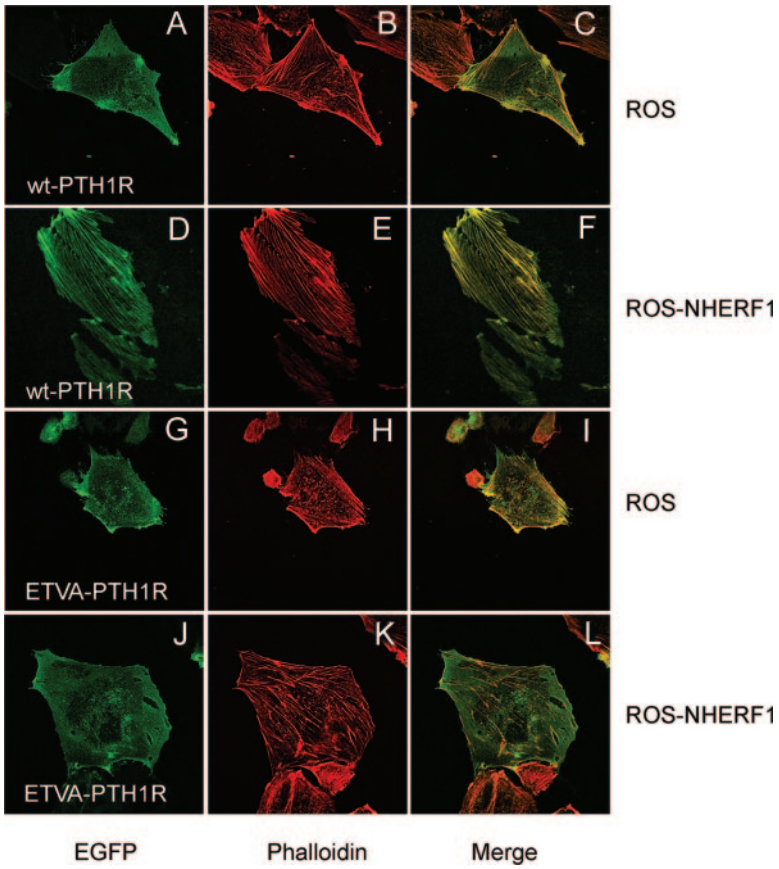

Fig. 1. NHERF1 Regulates the Distribution of the PTH1R

ROS and ROS-NHERF1 cells were transfected with PTH1R-EGFP and examined by confocal microscopy. The images shown were obtaining by focusing the microscope onto the plasma membrane adjacent to the coverslip. PTH1R-EGFP (wild-type and the ETVA mutant) images are shown in panels A, D, G, and J. Actin fibers stained with TRITC-phalloidin are shown in panels B, E, H, and K. Panels C, F, I, and L show the merged images. Colocalization of the *green* and *red* labels is shown in *yellow*. wt, Wild type.

stained with phalloidin-tetramethylrhodamine isothiocyanate (TRITC) (Fig. 1B) to investigate the colocalization of the PTH1R and the cytoskeleton. As shown in Fig. 1C, there was no colocalization of the receptor with actin fibers in the parental ROS cells. To examine the effects of NHERF1 expression on the distribution of the PTH1R, ROS cells were transfected with human NHERF1. NHERF1 expression was verified by Western blotting and immunocytochemistry (data not shown). Stably transfected cells were selected (ROS-NHERF1 cells) and further transfected with PTH1R-EGFP, and the distribution of the receptor was examined. In marked contrast with the results obtained with ROS cells, PTH1R-EGFP was organized around actin fibers (Fig. 1, D–F). To confirm that the interactions of PTH1R and NHERF1 were responsible for the reorganization of the receptor and its colocalization with the actin cytoskeleton, ROS and ROS-NHERF1 cells were transfected with M593A-PTH1R-EGFP (ETVA-PTH1R). This mutated receptor has a defective PDZ-binding motif and does not bind NHERF1 (15). As shown (Fig. 1, G–L), the distribution of ETVA-PTH1R was identical in ROS and ROS-NHERF1 cells. Furthermore, the colocalization with actin fibers was lost in the mutant receptor. Thus, binding of the PTH1R to the actin cytoskeleton requires an intact PDZ-recognition domain and the presence of NHERF1. To confirm that these results were not a consequence of the overexpression of the receptor, the experiments were reproduced by immunocytochemistry using antibodies against the PTH1R. The results shown in Fig S2 (published as supplemental data on The Endocrine Society's Online web site at http://mend.endojournals.org), demonstrate that the endogenous receptor is also organized around actin fibers in ROS-NHERF1 cells.

NHERF1 Reduces the Mobility of the PTH1R

The diffusion of PTH1R-EGFP was studied in ROS and ROS-NHERF1 cells by image correlation spectroscopy. As shown in Fig. 2, in ROS cells 80% of the PTH1R was readily mobile and diffused with a diffusion coefficient of about 0.15 μm^2/sec. In contrast, in ROS-NHERF1 cells, most of the receptor molecules (80%) were immobile, and those receptors that diffused did so with a diffusion coefficient of 0.045 μm^2/sec. Importantly, the expression of NHERF1 mutants that do not bind the PTH1R (S1S2, in which the core of the PDZ domains 1 and 2 has been scrambled), or that bind the receptor but fail to attach to the cytoskeleton (ΔERM, where the ERM-binding domain of NHERF1 has been deleted) had no detectable effects on the mobility of the receptor. These data demonstrate that immobilization of the PTH1R by NHERF1 is the result of specific tethering of the receptor to the actin cytoskeleton.

NHERF1 Regulates PTH1R Signaling

It has been proposed that NHERF1 induces a signaling switch in the responses of the PTH1R to hormone (16, 17). According to the signaling switch hypothesis, NHERF1 promotes the coupling of the PTH1R to pertussis toxin-sensitive PLC activity with a concomitant reduction in the production of hormone-dependent cAMP. To test this model, we examined the production of cAMP and changes in the intracellular concentration of Ca^{2+} in ROS and ROS-NHERF1 cells. Figure 3 shows a comparison of the cAMP responses induced by 100 nM PTH(1–34) and forskolin (100 μM) in ROS and ROS-NHERF1 cells. The data demonstrate clearly that NHERF1 expression increased rather than diminished cAMP production. These differences are not due to different levels of adenylyl cyclase expression, because both cell types exhibited comparable responses to forskolin. Radioligand binding studies using the PTH analog [^{125}I][Nle^{8,18},Tyr^{34}]PTH(1–34)NH_2 demonstrated that ROS and ROS-NHERF1 cells expressed comparable numbers of receptors on the surface (ROS: 10.8 ± 1.6 nmol/mg protein; ROS-

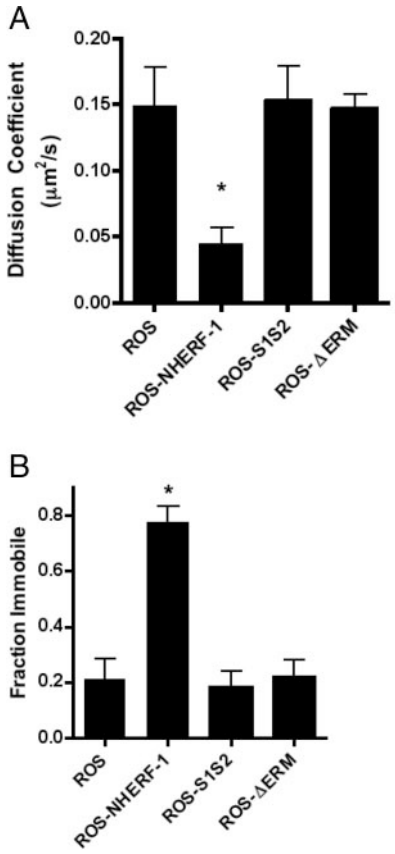

Fig. 2. NHERF1 Regulates the Diffusion of the PTH1R

ROS and ROS-NHERF1 cells were transfected with PTH1R-EGFP and the diffusion of the PTH1R was examined by image correlation spectroscopy as described in the text. Autocorrelation data were fit to a model assuming a single mobile species. A, The diffusion coefficient was calculated from the autocorrelation data. B, The immobile fraction was calculated from the autocorrelation function fitted to the imaging data. *, Statistically significant differences with all other samples in the data set ($P < 0.01$; n = 6).

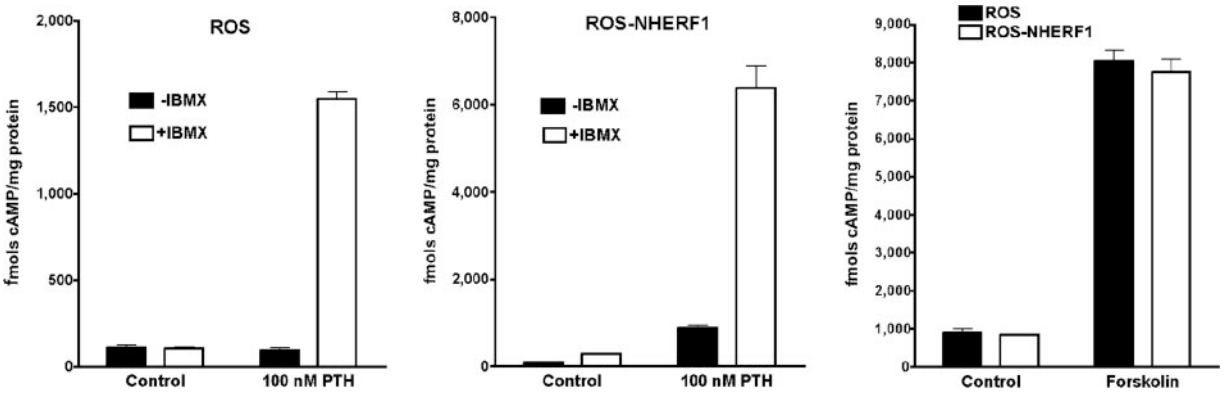

Fig. 3. NHERF1 Modulates PTH-Induced cAMP Production

ROS and ROS-NHERF1 cells were prelabeled with tritiated adenine and treated with PTH(1–34) in the presence or absence of IBMX. * and ** denote statistically significant differences with the control and control + IBMX samples (*, $P < 0.001$; **, $P < 0.01$; n = 3).

NHERF1: 13.6 ± 2.2 nmol/mg protein) (Fig. S1, published as supplemental data).

Because the increased cAMP production observed in the ROS-NHERF1 cells was inconsistent with the predictions of the signaling switch model, we also examined PTH(1–34)-induced changes of intracellular Ca^{2+}. The data shown in Fig. 4 demonstrate robust Ca^{2+} responses to 100 nM PTH(1–34) but only in the ROS-NHERF1 cells (Fig. 4, A and B). These Ca^{2+} responses were remarkable on two accounts. First, they appeared to be relatively slow in comparison with typical PLC-mediated responses (see Fig. 6B); second, the Ca^{2+} response was biphasic, with a slow increase in Ca^{2+} after the initial spike (Fig. 4A). The secondary rise in Ca^{2+} was not a consequence of reduced cell integrity because it was absent in the parental ROS cells. The Ca^{2+} responses depicted in Fig. 4A were due to the entry of extracellular Ca^{2+}, as they were blocked by addition of 5 mM EGTA to the extracellular medium 5 min before the addition of PTH(1–34) (Fig. 4C). Furthermore, the voltage-dependent Ca^{2+}-channel blockers nifedipine and verapamil abolished the Ca^{2+} responses induced by PTH (Fig. 4, D and E).

To further define the mechanism of PTH-induced Ca^{2+} entry, PLC activity was inhibited with U73122 (24).

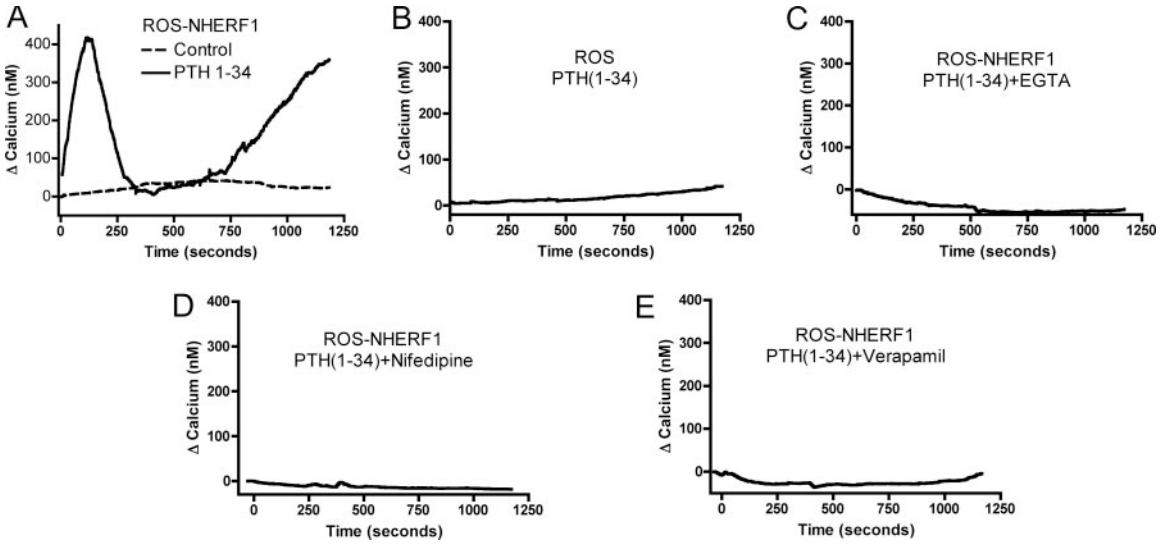

Fig. 4. NHERF1 Modulates PTH-Regulated Intracellular Ca^{2+} by a Mechanism Mediated by Voltage-Dependent Ca^{2+} Channels

ROS-NHERF1 (A) and ROS (B) cells were preloaded with Fluo4 AM. Cells were treated with 100 nM PTH(1–34), and changes in the intracellular Ca^{2+} concentration were recorded from the changes in fluorescence at 1-sec intervals for up to 20 min. Actual [Ca^{2+}] concentrations were determined as described in *Materials and Methods*. C, ROS-NHERF1 cells were pretreated with 5 mM EGTA 5 min before stimulation with PTH (1–34). D, ROS-NHERF1 cells were pretreated with 5 μM nifedipine 15 min before the experiment. E, ROS-NHERF1 cells were pretreated with 10 μM verapamil 15 min before the experiment. The figure shows representative traces of experiments that were reproduced at least three times. Calcium traces from 8–12 cells were recorded simultaneously in each experiment.

Even at rather high concentrations (10 μM), U73122 had only minor effects on the PTH-induced entry of Ca^{2+} in ROS-NHERF1 cells (Fig. 5A). At these concentrations, U73122 completely blocked carbachol-induced Ca^{2+} responses (Fig. 5B). These studies strongly suggest that PLC activation was not involved in PTH-stimulated Ca^{2+} entry. To test the involvement of a classical cAMP-PKA-dependent mechanism, the cells were pretreated with the PKA inhibitor H89 (10 μM, 10 min) before exposure to the ligand. As shown in Fig. 5C, H89 abolished PTH-induced Ca^{2+} entry. Consistent with this, treatment of the cells with forskolin elicited a transient Ca^{2+} response in ROS-NHERF1 cells (Fig. 5D). Remarkably, ROS cells did not display an equivalent response to forskolin, indicating that NHERF1 is required for cAMP-dependent Ca^{2+} entry. These data strongly suggest that PKA activation is necessary, but not sufficient, for the activation of Ca^{2+} entry.

The actual role of NHERF1 in the generation of the Ca^{2+} responses observed in ROS-NHERF1 cells was further explored using a C-terminal NHERF1 truncation mutant missing most of the ERM-binding motif (ΔERM). As shown in Fig. 6A, ΔERM did not elicit any Ca^{2+} responses, unlike full-length NHERF1. Furthermore, transfection of ROS-NHERF1 cells with the ΔERM mutant blocked the Ca^{2+} responses induced by PTH treatment. We conclude from these results that the binding of PTH1R to the cytoskeleton is required for the observed NHERF1 effects on Ca^{2+} entry.

DISCUSSION

There are multiple signaling pathways downstream of the PTH1R. Abundant evidence shows the activation of cAMP- and Ca^{2+}-mediated responses, and the nature and magnitude of these responses are cell and tissue dependent (2, 13, 14, 16, 17, 22, 25). These remarkable variations in the signals triggered by PTH have received substantial attention in the last few years. Some insight as to the origins of these variations emerged from the discovery of the NHERF1/EBP50 family of scaffolding proteins. Mahon *et al.* (16) reported that NHERF2, a protein very closely related to NHERF1, reduced cAMP responses to PTH and promoted the activation of PLC by a Pertussis toxin-sensitive mechanism. These observations were extended to NHERF1 (17). Thus, a signaling switch mechanism was proposed. According to this model, the two PDZ domains of NHERF1/2 interact with the C terminus of the PTH1R and PLCβ, while tethering this complex to the cytoskeleton. The formation of this complex presumably switches the signaling mode of the PTH1R from a G_s-based activation of adenylyl cyclase to a G_i-dependent inhibition of cAMP production and activation of PLCβ. Thus, the PTH1R, in the presence of NHERF1, would signal via the activation of Ca^{2+}-dependent processes.

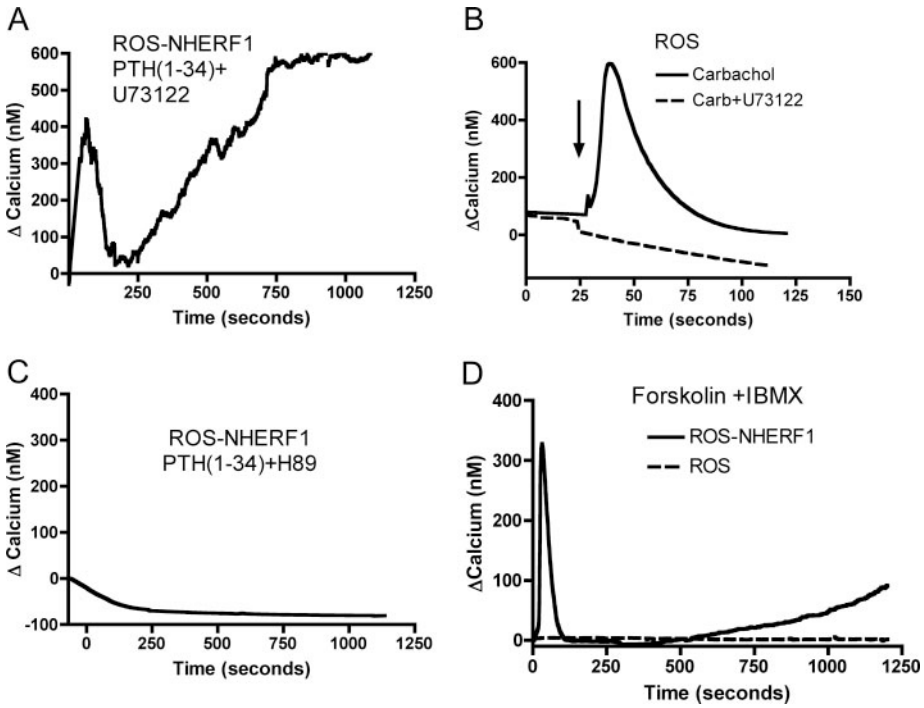

Fig. 5. PTH-Dependent Ca^{2+} Entry Is Mediated by PKA Activation and Independent of PLC Activity

Calcium entry experiments were performed as described for Fig. 4. A, Cells were preincubated with 10 μM U73122 15 min before the addition of PTH. B, Cells were preincubated with 15 μM U73122 15 min before treatment with carbachol. C, H89 (15 μM) was added to the cells 20 min before stimulation with PTH(1–34). D, Cells were stimulated with forskolin (20 μM) after preincubation with 250 μM IBMX for 20 min.

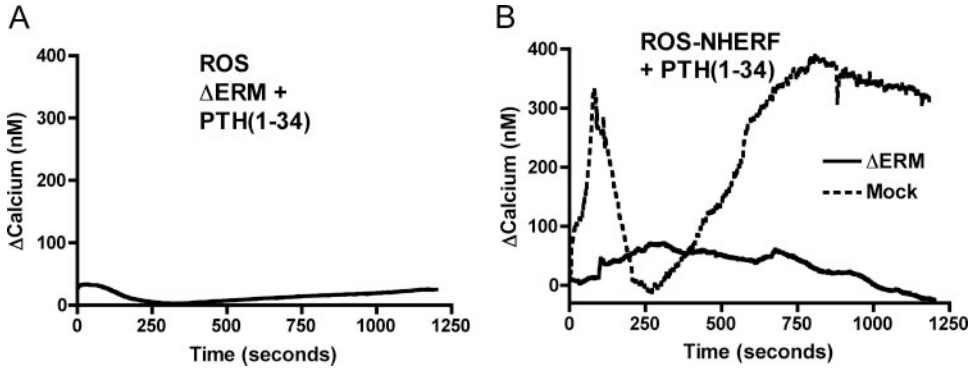

Fig. 6. PTH-Induced, NHERF1-Dependent Ca^{2+} Entry Requires the Binding of PTH1R and NHERF1 to the Cytoskeleton

ROS and ROS-NHERF1 cells were transiently transfected with ΔERM-NHERF1 24 h before the experiments. The cells were stimulated with 100 nM PTH(1–34), and the intracellular [Ca^{2+}] was monitored as described in Fig. 4.

The generality of the signaling switch model has not been well established. In fact, several lines of evidence suggest that the proposed NHERF1-dependent G_s-to-G_i coupling change is not necessary for the stimulation of substantial Ca^{2+}-dependent responses to PTH. For instance, some cells that express NHERF1 at very high levels, such as osteoblast-like UMR-106 cells (our unpublished observations), produce large amounts of cAMP in response to PTH (26). Furthermore, several G protein-coupled receptors primarily linked to G_s and cAMP production elicit Ca^{2+} entry via the activation of voltage-dependent Ca^{2+} channels (27). Finally, work with signaling-selective PTH analogs demonstrated that PKC-dependent pathways may be activated by the PTH1R without concomitant activation of PLC-dependent phosphatidylinositol hydrolysis (23), suggesting PLC-independent Ca^{2+}-dependent responses. In this study we address the mechanism by which NHERF1 induces PTH-dependent Ca^{2+} signaling in a well-established bone cell model, the rat osteosarcoma ROS 17/2.8 cell line.

Remarkably, the present results diverge substantially from those reported for other cell systems (13, 16, 22, 25). Our data indicate that NHERF1 increases PTH-dependent cAMP accumulation, and that this effect is accompanied by Ca^{2+} entry. Importantly, NHERF1 is absolutely required for PTH-induced Ca^{2+} entry in ROS cells. However, the entry of Ca^{2+} into ROS-NHERF1 cells is qualitatively different from the responses reported in opossum kidney (OK) cells (17). Whereas the response to PTH appears as a single Ca^{2+} spike that has a duration of less than 50 sec in OK cells, the PTH response in ROS-NHERF1 cells is biphasic, with an initial spike that has a duration of 200–250 sec and a second, sustained phase that appears to plateau after 15 min (Figs. 4A and Fig. 5A). Furthermore, the mechanisms by which PTH induces Ca^{2+} entry in the ROS-NHERF1 cells differs from that in OK cells. In OK cells, G_i-dependent activation of PLC appears to be involved in the pathway, whereas in ROS-NHERF1 cells the mechanism is PKA mediated.

An important question is: because PTH increases cAMP levels in both ROS and ROS-NHERF1 cells, why is Ca^{2+} entry observed exclusively in the latter? We propose that the answer to this question lies in the subcellular distribution and membrane dynamics of the PTH1R and its signaling targets in cells that express NHERF1. First, NHERF1 is not serving a simple scaffolding role by bringing together proteins targeted by NHERF1's PDZ domains. This is evident from the fact that ΔERM-NHERF1 fails to transduce Ca^{2+} signals (Fig. 6A). These data clearly demonstrate that the attachment of NHERF1 to the cytoskeleton is absolutely required for its role in the promotion of Ca^{2+} entry in ROS-NHERF1 cells. This conclusion is further strengthened by the fact that ΔERM-NHERF1 inhibits the effects of the expression of the full-length NHERF1, acting as a dominant-negative mutant (Fig. 6B). Second, in the absence of IBMX (*i.e.* under physiological conditions) very little cAMP accumulates in ROS cells. In fact, the data shown in Fig. 3 suggest that, 20 min after the addition of PTH, the levels of cAMP are indistinguishable from the basal state in the parental ROS cells. In contrast, even in the absence of IBMX, PTH elicits cAMP production to some detectable degree in ROS-NHERF1 cells. Third, the PTH1R distribution and diffusion data shown in Figs. 1 and 2 demonstrate clearly that NHERF1 tethers the PTH1R to the cytoskeleton, promoting the accumulation of the receptor in the vicinity of actin fibers, where the PTH1R is immobilized. Therefore, even though the average intracellular concentration of cAMP may not substantially increase after stimulation, the local concentration of cAMP may rise dramatically in the vicinity of the cytoskeletal fibers. And finally, as shown in Fig. 5D, forskolin cannot induce Ca^{2+} entry in the absence of NHERF1. Taken together, these data clearly suggest that the scaffolding function of NHERF1 is an absolute requirement for the cAMP-dependent entry of Ca^{2+} in ROS cells. Furthermore, several known A kinase-anchoring proteins link PKA to the cytoskeleton, such as ezrin (28), which also interacts with NHERF1 via the C-terminal ERM-binding motif of NHERF1. We propose an alternative model for PTH-dependent activation of Ca^{2+} entry in cells that express NHERF1/2. According to this model, NHERF1

forms a scaffolding complex with the PTH1R and ERM proteins, such as ezrin or radixin. This complex accumulates along actin fibers running parallel to the surface of the cell. Upon the activation of the receptor, G_s-dependent adenylyl cyclase produces high local concentrations of cAMP, which, in turn, activate PKA locally, inducing the phosphorylation of voltage-dependent Ca^{2+} channels, thus allowing Ca^{2+} entry. PTH-dependent PLC activation may occur or not, but our data suggest that PLC activity is not required for the Ca^{2+} entry process.

MATERIALS AND METHODS

ROS and ROS-NHERF1 Cells

ROS 17/2.8 cells were grown in DMEM/F12 medium supplemented with 10% fetal calf serum. ROS-NHERF1 cells were generated by transfection of the parental cell line with human NHERF1 subcloned in the multiple cloning site of the plasmid pCDNA3.1/Hygro (Stratagene, La Jolla, CA). Stable transfectants were selected with hygromycin (up to 150 μg/ml) over a period of 4 wk. The expression of NHERF1 was determined by Western blotting using a specific anti-NHERF1 antibody (Upstate Biotechnology, Inc., Lake Placid, NY). ROS-NHERF1 cells were further characterized by measuring the levels of expression of PTH1R and the dissociation constant (K_d) for PTH(1–34). Both cell lines expressed similar levels of PTH1R (ROS: 10.8 $\pm$ 1.6 nmol/mg protein; ROS-NHERF1: 13.6 $\pm$ 2.2 nmol/mg protein). Likewise, the K_d of PTH(1–34) was the same in both cell lines (see Fig S1).

Immunocytochemistry

Cells were cultured on glass coverslips, transfected with wild-type PTH1R-EGFP or ETVA-PTH1R-EGFP, and allowed to grow until 80% confluence. The coverslips were washed in PBS and fixed for 20 min in 4% paraformaldehyde in PBS at 4 C. Cells were permeabilized with 5% nonfat milk, 0.1% Triton X-100 for 1 h at 4 C and then stained with phalloidin-TRITC (3 nM) overnight at 4 C. For the detection of endogenous receptors, untransfected cells were simultaneously incubated with anti-PTH1R antibody E-17 (Santa Cruz Biotechnology, Inc., Santa Cruz, CA) and a dilution of 1:100. Bound antibody was detected with an Alexa488-conjugated antigoat IgG. The cells were then washed four times with PBS, mounted with gelvatol, and examined by confocal microscopy using an Olympus Fluoview 1000 instrument (Olympus Corp., Lake Success, NY). Colocalization was measured using the image correlation plug-ins of Image J.

Adenylate Cyclase Activity

cAMP accumulation was determined as described previously (14). Briefly, cells cultured in 24-well plates were labeled with 0.5 μCi of [^{3}H]adenine for 2 h. The cells were then treated with vehicle or 100 nM PTH(1–34) for 5 min. IBMX (250 μM) was included where indicated. The reaction was terminated by addition of 1 M trichloroacetic acid followed by neutralization with KOH. cAMP was isolated by the two-column method (29).

Measurement of the Diffusion Coefficient of the PTH1R

These studies were done by total internal reflection-image correlation spectroscopy as described previously (21). The technique is based on the analysis of the correlation of an image with itself after a certain lag time τ. This correlation is a function of the mobility of the fluorescent molecules (30, 31). Cells were transfected with PTH1R-EGFP and examined 24 h after transfection. Cell images were collected by total internal reflection microscopy at 200-msec intervals. Up to 300 images were obtained for each experiment. Fluorescence loss due to photobleaching of the sample was almost negligible. The image data were exported to ImageJ and analyzed using a plug-in specifically written to calculate the autocorrelation function of the data (21). The resulting autocorrelation data were exported into GraphPad Prism and fit to a single species two-dimensional diffusion model [$G(\tau) = K(1 + \tau/\tau_d)^{-1} + G_0$ where τ_d is the characteristic time constant, K is a proportionality factor, and G_D is a term that accounts for spatial autocorrelation]. The diffusion coefficient was calculated from the Stokes-Einstein equation [$D = r^2/(4\tau_d)$].

Determination of Intracellular Ca^{2+}

ROS and ROS-NHERF1 cells cultured in Mattek dishes were loaded with the calcium-sensitive dye Fluo4 AM in serum-free medium for 20–30 min. The final loading concentration of the dye was 4 μM. All calcium measurements were done using DMEM/F12 containing 20 mM HEPES (pH 7.4) at 37 C in an Olympus IX70 inverted microscope equipped with a temperature-controlled chamber (Harvard Apparatus, Inc., South Natick, MA) and a Orca ER camera (Hamamatsu Photonic Systems Corp., Bridgewater, NJ). The intracellular Ca^{2+} concentration was determined using the expression $F = [F_{max} - F_{min})/(1 + ([Ca^{2+}]/K_d)]$ where F is the measured fluorescence intensity, F_{max} is the fluorescence measured after addition of ionomycin (which equilibrates the interior of the cell with the extracellular medium), F_{min} is the fluorescence measured after addition of 10 mM EGTA, and K_d is the dissociation equilibrium constant of the dye-Ca^{2+} complex (0.19 μM) (32).

Statistical Analysis

All curve-fitting analyses were done using GraphPad Prism (GraphPad Software, Inc., San Diego, CA). All experiments reported were reproduced at least three times and done by triplicate. The calcium concentration traces shown in Figs. 4–6 are representative, and some cell-to-cell variations were observed. Statistical comparisons of multiple samples were done by ANOVA followed by posttest comparisons using Tukey's method. Pairs of samples were compared using Student's *t* tests.

Acknowledgments

Received October 8, 2007. Accepted January 8, 2008.

Address all correspondence and requests for reprints to: Guillermo Romero, University of Pittsburgh School of Medicine, Department of Pharmacology and Medicine, W1345 Biomedical Science Tower, Pittsburgh, Pennsylvania 15261. E-mail: ggr@pitt.edu.

This work was supported by Grant DK-69998 from the National Institutes of Health (to P.A.F.), and an internal grant from the Office of the Senior Vice Chancellor for the Health Sciences, University of Pittsburgh (to G.R.).

Disclosure Statement: All authors have nothing to disclose.

REFERENCES

1. Abou-Samra AB, Juppner H, Force T, Freeman MW, Kong XF, Schipani E, Urena P, Richards J, Bonventre JV, Potts Jr JT, Kronenberg HM, Segre GV 1992 Expression cloning of a common receptor for parathyroid hormone

and parathyroid hormone-related peptide from rat osteoblast-like cells: a single receptor stimulates intracellular accumulation of both cAMP and inositol trisphosphates and increases intracellular free calcium. Proc Natl Acad Sci USA 89:2732–2736
2. Bringhurst FR, Juppner H, Guo J, Urena P, Potts Jr JT, Kronenberg HM, Abou-Samra AB, Segre GV 1993 Cloned, stably expressed parathyroid hormone (PTH)/PTH-related peptide receptors activate multiple messenger signals and biological responses in LLC-PK1 kidney cells. Endocrinology 132:2090–2098
3. Maeda S, Wu S, Juppner H, Green J, Aragay AM, Fagin JA, Clemens TL 1996 Cell-specific signal transduction of parathyroid hormone (PTH)-related protein through stably expressed recombinant PTH/PTHrP receptors in vascular smooth muscle cells. Endocrinology 137:3154–3162
4. Wu S, Pirola CJ, Green J, Yamaguchi DT, Okano K, Jueppner H, Forrester JS, Fagin JA, Clemens TL 1993 Effects of N-terminal, midregion, and C-terminal parathyroid hormone-related peptides on adenosine 3′,5′-monophosphate and cytoplasmic free calcium in rat aortic smooth muscle cells and UMR-106 osteoblast-like cells. Endocrinology 133:2437–2444
5. Orloff JJ, Ganz MB, Ribaudo AE, Burtis WJ, Reiss M, Milstone LM, Stewart AF 1992 Analysis of PTHRP binding and signal transduction mechanisms in benign and malignant squamous cells. Am J Physiol 262:E599–E607
6. Orloff JJ, Kats Y, Urena P, Schipani E, Vasavada RC, Philbrick WM, Behal A, Abou-Samra AB, Segre GV, Juppner H 1995 Further evidence for a novel receptor for amino-terminal parathyroid hormone-related protein on keratinocytes and squamous carcinoma cell lines. Endocrinology 136:3016–3023
7. Whitfield JF, Chakravarthy BR, Durkin JP, Isaacs RJ, Jouishomme H, Sikorska M, Williams RE, Rixon RH 1992 Parathyroid hormone stimulates protein kinase C but not adenylate cyclase in mouse epidermal keratinocytes. J Cell Physiol 150:299–303
8. Rampe D, Lacerda AE, Dage RC, Brown AM 1991 Parathyroid hormone: an endogenous modulator of cardiac calcium channels. Am J Physiol 261:H1945–H1950
9. Schluter KD, Weber M, Piper HM 1995 Parathyroid hormone induces protein kinase C but not adenylate cyclase in adult cardiomyocytes and regulates cyclic AMP levels via protein kinase C-dependent phosphodiesterase activity. Biochem J 310:439–444
10. Atkinson MJ, Hesch RD, Cade C, Wadwah M, Perris AD 1987 Parathyroid hormone stimulation of mitosis in rat thymic lymphocytes is independent of cyclic AMP. J Bone Miner Res 2:303–309
11. Klinger M, Alexiewicz JM, Linker-Israeli M, Pitts TO, Gaciong Z, Fadda GZ, Massry SG 1990 Effect of parathyroid hormone on human T cell activation. Kidney Int 37: 1543–1551
12. Whitfield JF, MacManus JP, Youdale T, Franks DJ 1971 The roles of calcium and cyclic AMP in the stimulatory action of parathyroid hormone on thymic lymphocyte proliferation. J Cell Physiol 78:355–368
13. Cheung R, Erclik MS, Mitchell J 2005 Increased expression of G11α in osteoblastic cells enhances parathyroid hormone activation of phospholipase C and AP-1 regulation of matrix metalloproteinase-13 mRNA. J Cell Physiol 204:336–343
14. Sneddon WB, Magyar CE, Willick GE, Syme CA, Galbiati F, Bisello A, Friedman PA 2004 Ligand-selective dissociation of activation and internalization of the parathyroid hormone (PTH) receptor: conditional efficacy of PTH peptide fragments. Endocrinology 145:2815–2823
15. Sneddon WB, Syme CA, Bisello A, Magyar CE, Rochdi MD, Parent JL, Weinman EJ, Abou-Samra AB, Friedman PA 2003 Activation-independent parathyroid hormone receptor internalization is regulated by NHERF1 (EBP50). J Biol Chem 278:43787–43796
16. Mahon MJ, Donowitz M, Yun CC, Segre GV 2002 Na(+)/H(+) exchanger regulatory factor 2 directs parathyroid hormone 1 receptor signalling. Nature 417:858–861
17. Mahon MJ, Segre GV 2004 Stimulation by parathyroid hormone of a NHERF-1-assembled complex consisting of the parathyroid hormone I receptor, phospholipase Cβ, and actin increases intracellular calcium in opossum kidney cells. J Biol Chem 279:23550–23558
18. Weinman EJ, Steplock D, Tate K, Hall RA, Spurney RF, Shenolikar S 1998 Structure-function of recombinant Na/H exchanger regulatory factor (NHE-RF). J Clin Invest 101:2199–2206
19. Weinman EJ, Steplock D, Wang Y, Shenolikar S 1995 Characterization of a protein cofactor that mediates protein kinase A regulation of the renal brush border membrane Na(+)-H+ exchanger. J Clin Invest 95:2143–2149
20. Weinman EJ, Hall RA, Friedman PA, Liu-Chen LY, Shenolikar S 2006 The association of NHERF adaptor proteins with G protein-coupled receptors and receptor tyrosine kinases. Annu Rev Physiol 68:491–505
21. Wheeler D, Sneddon WB, Wang B, Friedman PA, Romero G 2007 NHERF-1 and the cytoskeleton regulate the traffic and membrane dynamics of G protein-coupled receptors. J Biol Chem 282:25076–25087
22. Offermanns S, Iida-Klein A, Segre GV, Simon MI 1996 Gαq family members couple parathyroid hormone (PTH)/PTH-related peptide and calcitonin receptors to phospholipase C in COS-7 cells. Mol Endocrinol 10:566–574
23. Yang D, Guo J, Divieti P, Bringhurst FR 2006 Parathyroid hormone activates PKC-δ and regulates osteoblastic differentiation via a PLC-independent pathway. Bone 38:485–496
24. Jin W, Lo TM, Loh HH, Thayer SA 1994 U73122 inhibits phospholipase C-dependent calcium mobilization in neuronal cells. Brain Res 642:237–243
25. Schwindinger WF, Fredericks J, Watkins L, Robinson H, Bathon JM, Pines M, Suva LJ, Levine MA 1998 Coupling of the PTH/PTHrP receptor to multiple G-proteins. Direct demonstration of receptor activation of Gs, Gq/11, and Gi(1) by [α-32P]GTP-γ-azidoanilide photoaffinity labeling. Endocrine 8:201–209
26. Gray TK, Flynn TC, Gray KM, Nabell LM 1987 17β-Estradiol acts directly on the clonal osteoblastic cell line UMR106. Proc Natl Acad Sci USA 84:6267–6271
27. Picotto G, Massheimer V, Boland R 1997 Parathyroid hormone stimulates calcium influx and the cAMP messenger system in rat enterocytes. Am J Physiol 273:C1349–C1353
28. Dransfield DT, Bradford AJ, Smith J, Martin M, Roy C, Mangeat PH, Goldenring JR 1997 Ezrin is a cyclic AMP-dependent protein kinase anchoring protein. EMBO J 16:35–43
29. Salomon Y, Londos C, Rodbell M 1974 A highly sensitive adenylate cyclase assay. Anal Biochem 58:541–548
30. Wiseman PW, Petersen NO 1999 Image correlation spectroscopy. II. Optimization for ultrasensitive detection of preexisting platelet-derived growth factor-β receptor oligomers on intact cells. Biophys J 76:963–977
31. Wiseman PW, Squier JA, Ellisman MH, Wilson KR 2000 Two-photon image correlation spectroscopy and image cross-correlation spectroscopy. J Microsc 200:14–25
32. Woodruff ML, Sampath AP, Matthews HR, Krasnoperova NV, Lem J, Fain GL 2002 Measurement of cytoplasmic calcium concentration in the rods of wild-type and transducin knock-out mice. J Physiol 542:843–854

Molecular Endocrinology **is published monthly by The Endocrine Society (http://www.endo-society.org), the foremost professional society serving the endocrine community.**

Calcium/Calmodulin-Dependent Protein Kinase (CaMK) IV Mediates Nucleocytoplasmic Shuttling and Release of HMGB1 during Lipopolysaccharide Stimulation of Macrophages[1]

Xianghong Zhang,[2]* David Wheeler,[2]* Ying Tang,* Lanping Guo,* Richard A. Shapiro,* Thomas J. Ribar,[†] Anthony R. Means,[†] Timothy R. Billiar,* Derek C. Angus,[‡] and Matthew R. Rosengart[3]*[‡]

The chromatin-binding factor high-mobility group box 1 (HMGB1) functions as a proinflammatory cytokine and late mediator of mortality in murine endotoxemia. Although serine phosphorylation of HMGB1 is necessary for nucleocytoplasmic shuttling before its cellular release, the protein kinases involved have not been identified. To investigate if calcium/calmodulin-dependent protein kinase (CaMK) IV serine phosphorylates and mediates the release of HMGB1 from macrophages (Mϕ) stimulated with LPS, RAW 264.7 cells or murine primary peritoneal Mϕ were incubated with either STO609 (a CaMKIV kinase inhibitor), KN93 (a CaMKIV inhibitor), or we utilized cells from which CaMKIV was depleted by RNA interference (RNAi) before stimulation with LPS. We also compared the LPS response of primary Mϕ isolated from CaMKIV$^{+/+}$ and CaMKIV$^{-/-}$ mice. In both cell types LPS induced activation and nuclear translocation of CaMKIV, which preceded HMGB1 nucleocytoplasmic shuttling. However, Mϕ treated with KN93, STO609, or CaMKIV RNAi before LPS showed reduced nucleocytoplasmic shuttling of HMGB1 and release of HMGB1 into the supernatant. Additionally, LPS induced serine phosphorylation of HMGB1, which correlated with an interaction between CaMKIV and HMGB1 and with CaMKIV phosphorylation of HMGB1 in vitro. In cells, both HMGB1 phosphorylation and interaction with CaMKIV were inhibited by STO609 or CaMKIV RNAi. Similarly, whereas CaMKIV$^{+/+}$ Mϕ showed serine phosphorylation of HMGB1 in response to LPS, this phosphorylation was attenuated in CaMKIV$^{-/-}$ Mϕ. Collectively, our results demonstrate that CaMKIV promotes the nucleocytoplasmic shuttling of HMGB1 and suggest that the process may be mediated through CaMKIV-dependent serine phosphorylation of HMGB1. ***The Journal of Immunology,*** **2008, 181: 5015–5023.**

High-mobility group box 1 (HMGB1)[4] was initially identified as an architectural chromatin-binding factor that bends DNA and directs protein assembly on specific DNA targets. Recently it has been demonstrated to function as a proinflammatory cytokine and late mediator of mortality in murine endotoxemia and sepsis (1–3). HMGB1 appeared 8 h poststimulation and plateaued at 16–32 h, a time course very distinct from the acute rise and fall of early mediators of severe sepsis and septic shock (TNF-α, IL-1β) (3). Recombinant HMGB1 mimicked the lethality of high-dose LPS and induced the release of TNF-α by macrophages (Mϕ) (3). Anti-HMGB1 Abs conferred a dose-dependent protection in animal models of endotoxemia, even when the first dose of anti-HMGB1 Abs was delayed for at least 2 h (2, 3). Human studies have revealed that systemic HMGB1 levels are markedly elevated in patients that die of sepsis and during hemorrhagic shock (4, 5).

In the context of sepsis, current data indicate that HMGB1 is released by activated monocytes and Mϕ via an active process that involves shuttling the protein from nucleus to cytoplasm (3, 6, 7). Acetylation of HMGB1 and of the histones to which it binds appears to be essential for its release (8). HMGB1 contains two nuclear localization signals (NLS) and two putative nuclear export signals, suggesting that HMGB1 shuttles between the nucleus and cytoplasm through a tightly controlled mechanism (6). Recently, serine phosphorylation has been demonstrated to be a requisite step for this process, although neither the kinase nor the mechanisms controlling nucleocytoplasmic shuttling have been identified (9). Considering the data suggesting that HMGB1 may serve as a target to reduce mortality from sepsis, identifying the mechanisms responsible for inducing and controlling its release is important.

We have recently demonstrated the integral role for members of the family of multifunctional calcium/calmodulin-dependent protein kinases (CaMKI, II, IV) in the release of HMGB1 by hepatocytes subjected to oxidant stress and hepatocellular injury in an in vivo model of hepatic ischemia/reperfusion, although we have yet to identify the specific members involved (10). The multifunctional CaMKs are serine/threonine kinases sensitive to changes in

*Department of Surgery, University of Pittsburgh, Pittsburgh, PA 15213; [†]Department of Pharmacology and Cancer Biology, Duke University, Durham, NC 27710; and [‡]Department of Critical Care Medicine, University of Pittsburgh, Pittsburgh, PA 15213

Received for publication October 15, 2007. Accepted for publication July 22, 2008.

The costs of publication of this article were defrayed in part by the payment of page charges. This article must therefore be hereby marked *advertisement* in accordance with 18 U.S.C. Section 1734 solely to indicate this fact.

[1] This work was supported by Grant 1KL2 RR024154-01 (to M.R.R.) from the National Center for Research Resources (NCRR), a component of the National Institutes of Health (NIH), and the NIH Roadmap for Medical Research. This work was also supported by NIH grant DK074701 (to A.R.M.).

[2] X.Z. and D.W. contributed equally to this work.

[3] Address correspondence and reprint requests to Dr. Matthew R. Rosengart, Department of Surgery, University of Pittsburgh, 200 Lothrop Street, Pittsburgh, PA 15213. E-mail address: rosengartmr@upmc.edu

[4] Abbreviations used in this paper: HMGB1, high-mobility group box 1; CaMK, calcium/calmodulin-dependent protein kinase; Mϕ, macrophage; NLS, nuclear localization signal; RNAi, RNA interference; siRNA, small interfering RNA.

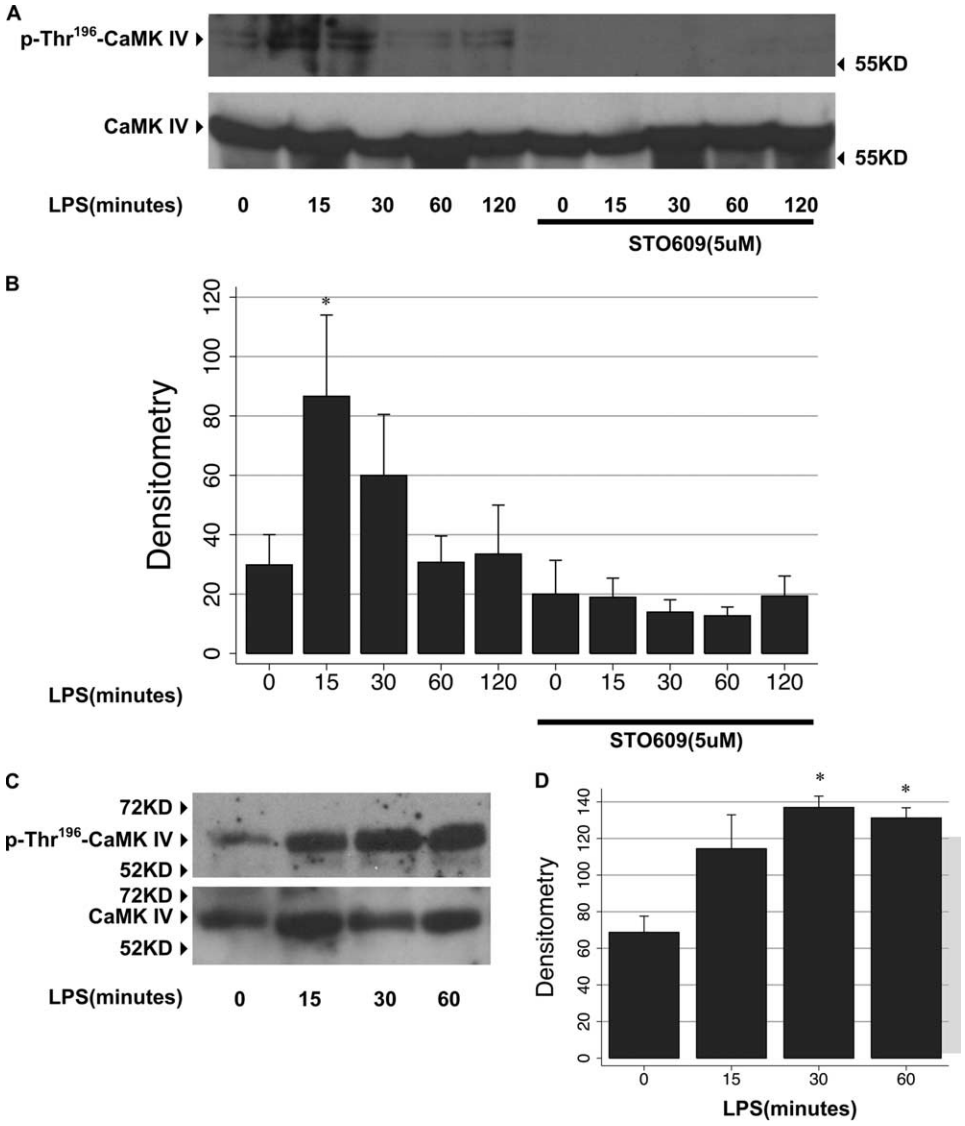

FIGURE 1. LPS activates CaMKIV. *A*, RAW 264.7 cells were treated with LPS (10 ng/ml) for the durations of 15, 30, 60, and 120 min, at which time total cell lysate was harvested, subjected to immunoblot analysis, and probed for p-Thr^{196}-CaMKIV. Parallel populations were treated with STO609 (5 μM) for 1 h before LPS stimulation and subjected to similar immunoblot analysis. Each blot was stripped and reprobed with anti-CaMKIV Ab to confirm equal loading. Representative blot of three individual experiments. *B*, Densitometry represents means $\pm$ SEM OD of individual p-Thr^{196}-CaMKIV immunoblots ($n = 3$); $*$, $p < 0.05$ vs control, unstimulated cells. *C*, Murine peritoneal Mϕ were exposed to similar experimental conditions, and p-Thr^{196}-CaMKIV and total CaMKIV were assessed by SDS-PAGE as previously described. Representative blot of three individual experiments. *D*, Densitometry represents means $\pm$ SEM OD of individual p-Thr^{196}-CaMKIV immunoblots ($n = 3$); $*$, $p < 0.05$ vs control, unstimulated cells.

intracellular [Ca^{2+}] that coordinate a variety of cellular functions, including gene expression, cell cycle progression, apoptosis, differentiation, and ischemic tolerance (11, 12). Whereas isoforms of CaMKI and CaMKII are expressed in all mammalian cells, CaMKIV is present in only selective tissues, which include the bone marrow (13). CaMKIV is activated and translocates into the nucleus upon its phosphorylation by an upstream CaMKK in the cytoplasm (14, 15). The nuclear, autonomously active form of CaMKIV phosphorylates a number of proteins involved in the regulation of transcription (16). Additionally, it has recently been shown that CaMKIV is a component of a signaling cascade initiated by LPS activation of TLR4 that facilitates survival of dendritic cells by phosphorylating CREB and regulating expression of the Bcl-2 gene (17). These observations suggested to us that CaMKIV would be an attractive candidate kinase to phosphorylate HMGB1 in macrophages and facilitate its translocation from nucleus to cytoplasm in response to LPS.

Materials and Methods

Reagents

Escherichia coli 0111:B4 LPS was obtained from Sigma-Aldrich. KN93, obtained from Calbiochem, was dissolved in sterile DMSO at a concentration of 10 mM. STO690 was obtained from Calbiochem. STO609 is selective for CaMKK: it has an in vitro IC_{50} of 0.13–0.38 μM for CaMKK and 32 μM for CaMKII with little or no inhibition of CaMKI, CaMKIV, protein kinase A, protein kinase C, ERK, or myosin light chain kinase (18). mAb against autonomously active, Thr^{196}-phosphorylated CaMKIV (anti-p-Thr^{196}-CaMKIV) was the generous gift of Dr. Naohito Nozaki (Kanagawa, Japan). Abs against total CaMKIV and HMGB1 were obtained from Abcam. Ab against phosphoserine was obtained from Promega. Ab against FLAG epitope was obtained from Sigma-Aldrich. DAPI was obtained from Molecular Probes.

Cell isolation and treatment

Murine monocyte/macrophage-like cells (RAW 264.7, American Type Culture Collection) were grown in DMEM (BioWhittaker) supplemented with 10% FCS (Sigma-Aldrich), 50 U/ml penicillin, and 50 μg/ml streptomycin (Cellgro/Mediatech). Primary murine peritoneal Mϕ were isolated by lavaging the peritoneal cavity with five 3-ml aliquots of sterile PBS. After centrifugation at 300 $\times$ *g* for 10 min, the Mϕ were resuspended in RPMI 1640 with 10% FCS, 50 U/ml penicillin, and 50 μg/ml streptomycin. Selected cells were pretreated with varying concentrations of KN93 (5, 10, 20 μM) or STO609 (1, 2, 5, 10, 20 μM) for 1 h or subjected to RNA interference (RNAi) using nontarget or CaMKIV small interfering RNA (siRNA) (see below). Selected cells were then treated with increasing doses of LPS (1, 10, 100 ng/ml).

Transfection of fluorescein-labeled cyclophilin, nontarget, and CaMKIV siRNA

RAW 264.7 cells (2×10^4) or murine peritoneal Mϕ (1×10^5) were plated in 0.5 ml of growth medium (without antibiotics) in each well of a 24-well

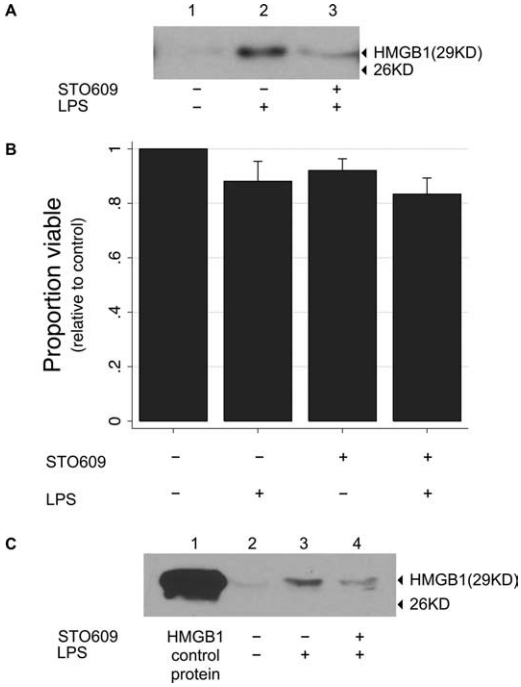

FIGURE 2. CaMK kinase cascade mediates LPS-induced HMGB1 release. *A*, RAW 264.7 cells were treated with LPS (100 ng/ml) for 16 h, at which time cellular supernatant was harvested, subjected to immunoblot analysis, and probed for HMGB1. Parallel populations were pretreated with STO609 (5 μM) for 1 h before LPS stimulation and subjected to similar immunoblot analysis. Representative blot of three individual experiments. *B*, RAW 264.7 cells were subjected to similar conditions as described above. Cell viability was evaluated by MTT assay and is shown as means ± SEM fold change relative to control, untreated cell population ($n = 4$). *C*, Murine peritoneal Mϕ were isolated and treated with LPS and STO609 as previously described. The supernatant was harvested, subjected to Western blot analysis, and probed for HMGB1. Representative blot of three individual experiments.

plate, resulting in 30% or 80% confluence, respectively. Fluorescein-labeled cyclophilin control siRNA, nontarget siRNA, and CaMKIV siRNA obtained from Dharmacon were added to 50 μl serum-free DMEM in a final concentration of 25 nM. We utilized the SMARTpool siRNA from Dharmacon that incorporates four separate siRNA sequences for CaMKIV: 5′-GAGAUCCUCUGGGCGAUUUUU3-′, 5′-UCAAGGAAAUAUUCGAAACUU3-′, 5′-GGUGCUACAUCCAUUGUGUUU3-′, and 5′-GGGAUGAAGUGUCUUUAAAUU3-′. In a separate tube, 3 μl HiPerFect was diluted in 50 μl serum-free DMEM and incubated at room temperature for 5 min. These two solutions were combined, and the final transfection mixture was incubated for 20 min at room temperature. This transfection mixture was applied to each well and incubated for 6 h, after which it was replaced by 500 μl of cell medium and incubated for 72 h. Transfection efficiency was determined at 24 h by fluorescence microscopy. For each experiment at least three microscopic visual fields (×200 magnification) were counted to facilitate calculation of the ratio of fluorescent cyclophilin-expressing cells to nonfluorescent cells. Inhibition of each targeted protein was determined by immunoblot or RT-PCR. All experiments and cell number determinations were performed in triplicate.

Plasmid construction and transfection

Plasmids encoding a constitutively active CaMKIV (CaMKIV-dCT) or a kinase-inactive CaMKIV-dCTK75E mutant were the generous gifts of Dr. Douglas Black (19). CaMKIV-dCT contains a C-terminally truncated version of the human CaMKIV-encoding gene, truncated to Leu^{317}, and an N-terminal FLAG epitope (19, 20). CaMKIV-dCTK75E was constructed by changing Lys^{75} to glutamate in CaMKIV-dCT, which negatively affects ATP binding at the catalytic site (19, 20). For transient transfection, RAW 264.7 cells were seeded in a 24-well plate at 3×10^5 cells/well. After 2 h of adhesion, Mϕ were transfected with 1 μg of plasmid CaMKIV-dCT or CaMKIV-dCTK75E using the Lipofectamine 2000 reagent according to the instructions specified by the manufacturer (Invitrogen). Following transfection, cells were handled as detailed in the figure legends.

Cellular protein extraction

Total cellular protein was extracted at 4°C in 500 μl of lysis buffer (20 mM Tris, 137 mM NaCl, 2 mM EDTA, 10% glycerol, 1% Triton X-100, 1 μM sodium orthovanadate, 100 μM DTT, 200 μM PMSF, 10 μg/ml leupeptin, 0.15 U/ml aprotinin, 50 mM sodium fluoride, 10 mM sodium pyrophosphate, 2.5 μg/ml pepstatin A, 1 mM benzamidine, and 40 mM α-glycerophosphate). Protein concentration was determined using a bicinchoninic acid protein assay (Pierce).

Nuclear and cytoplasmic protein isolation

Cells were harvested and washed with PBS, followed by centrifugation at $300 \times g$ for 10 min. The cell pellet was lysed with NE-PER nuclear and cytoplasmic extraction reagent according to the instructions specified by the manufacturer (Thermo Scientific).

Immunoprecipitation

Equal amounts of cellular protein obtained from each experimental condition were used for immunoprecipitation. Five microliters of Ab was added to 500

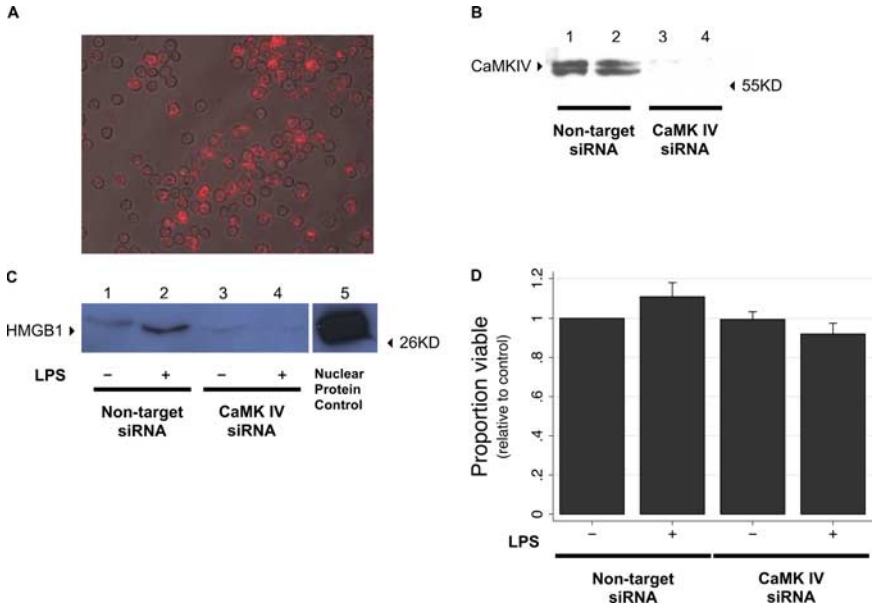

FIGURE 3. CaMKIV mediates LPS-induced HMGB1 release. *A*, RAW 264.7 cells were transfected with fluorescent cyclophilin B siRNA for 24 h and imaged by confocal microscopy. Transfection efficiency was determined by determining the ratio of fluorescent cells to total number of cells. *B*, RAW 264.7 cells were transfected with either nontarget (NT) or CaMKIV siRNA for 72 h, at which time total cell lysate was harvested, subjected to immunoblot analysis, and probed for CaMKIV. Representative blots of three individual experiments. *C*, RAW 264.7 cells were transfected with either NT or CaMKIV siRNA for 72 h and then stimulated with LPS (100 ng/ml) for 16 h. The supernatant was harvested, subjected to immunoblot analysis, and probed for HMGB1. Representative blots of three individual experiments. *D*, RAW 264.7 cells were subjected to similar conditions as described above. Cell viability was evaluated by MTT assay and is shown as means ± SEM fold change relative to control, untreated NT cell population ($n = 4$).

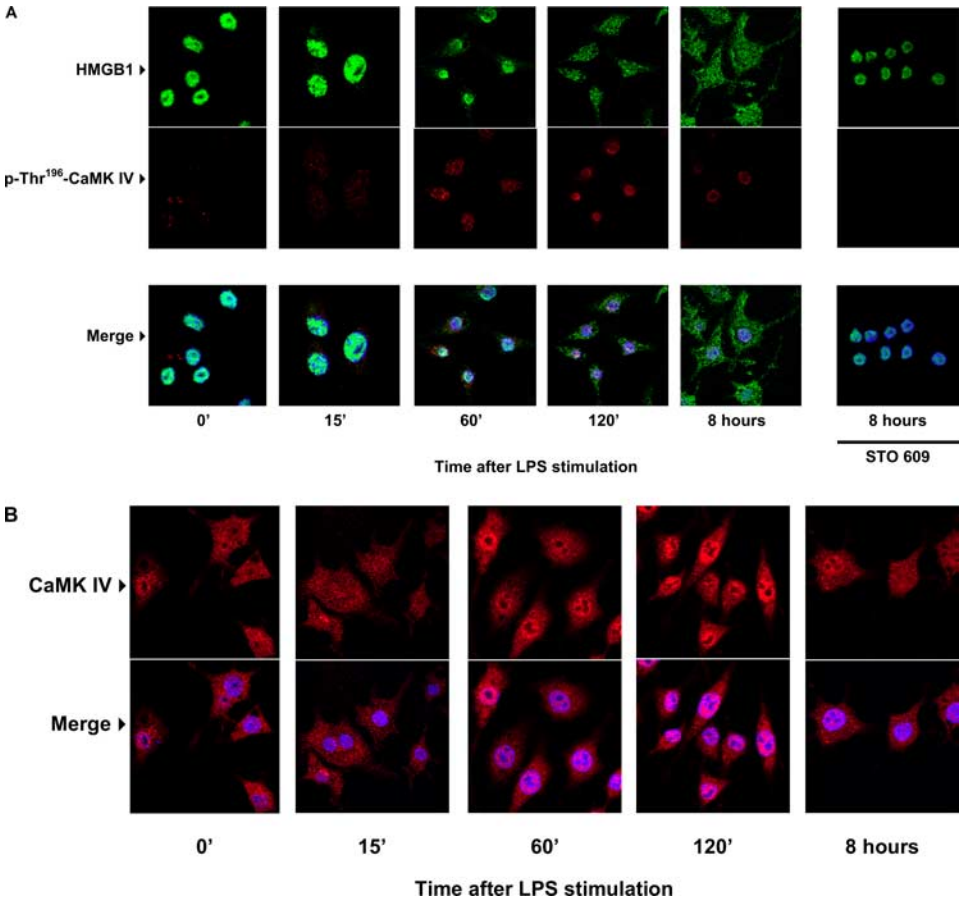

FIGURE 4. Spatial and temporal relationship of LPS-induced CaMKIV Thr[196] phosphorylation and HMGB1 nucleocytoplasmic shuttling. *A*, RAW 264.7 cells were stimulated with LPS (100 ng/ml) for 15 min and 1, 2, and 8 h, at which time they were fixed, permeabilized, stained for HMGB1 (green) or p-Thr[196]-CaMKIV (red), and imaged by confocal microscopy at ×630. Green, HMGB1; red, p-Thr[196]-CaMKIV; blue, DAPI. Representative image of three individual experiments. *B*, RAW 264.7 cells were subjected to similar conditions as described above, stained for total CaMKIV, and imaged by confocal microscopy at ×630. Red, CaMKIV; blue, DAPI. Representative image of three individual experiments.

μg of isolated cellular protein within lysis buffer and incubated at 4°C overnight on a rotator. Fifty microliters of 50% slurry of prewashed protein G-agarose beads (Abcam) were then added to each sample, followed by incubation for an additional 2 h at 4°C. The samples were spun briefly in a microcentrifuge at 14,000 rpm and washed four times in lysis buffer. Samples were then resuspended in 30 μl of lysis buffer for future analysis.

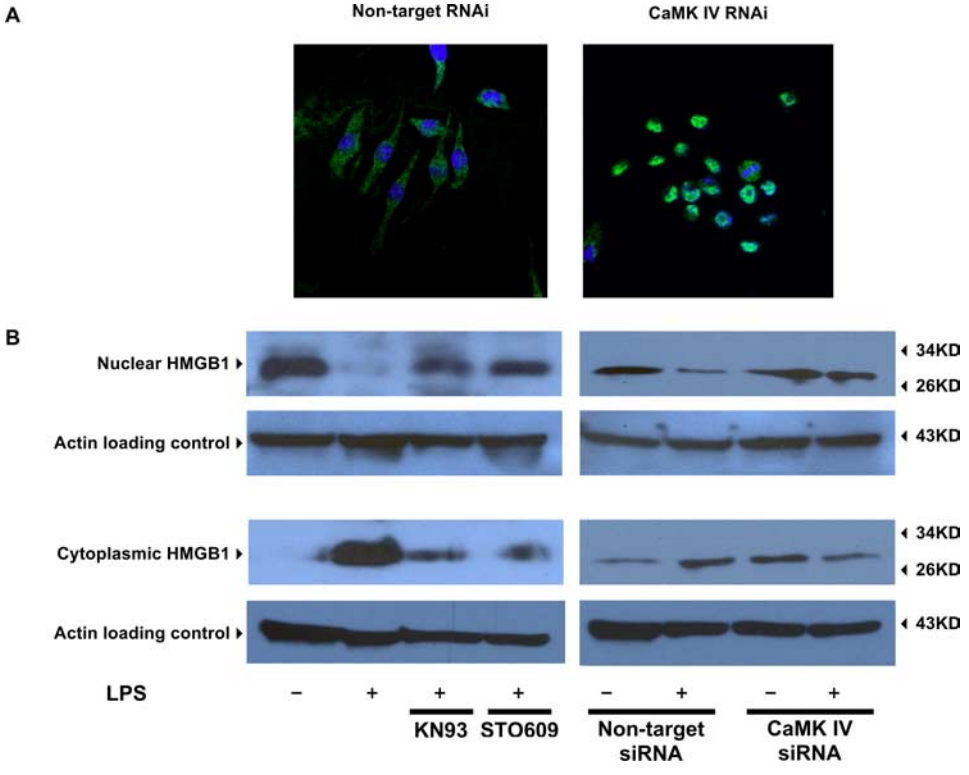

FIGURE 5. CaMKIV mediates HMGB1 nucleocytoplasmic shuttling. *A*, RAW 264.7 cells underwent RNAi using nontarget (NT) siRNA or CaMKIV siRNA. Cells were stimulated with LPS (100 ng/ml) for 8 h and then fixed, permeabilized, stained for HMGB1 (green), and imaged by confocal microscopy at ×630. Green, HMGB1; blue, DAPI. Representative image of three individual experiments. *B*, RAW 264.7 cells were subjected to STO609 (5 μM) or KN93 (10 μM) or underwent NT or CaMKIV RNAi before stimulation with LPS (100 ng/ml) as detailed above. Nuclear and cytoplasmic protein were isolated, subjected to immunoblot analysis, and probed for HMGB1. Representative blots of three separate experiments.

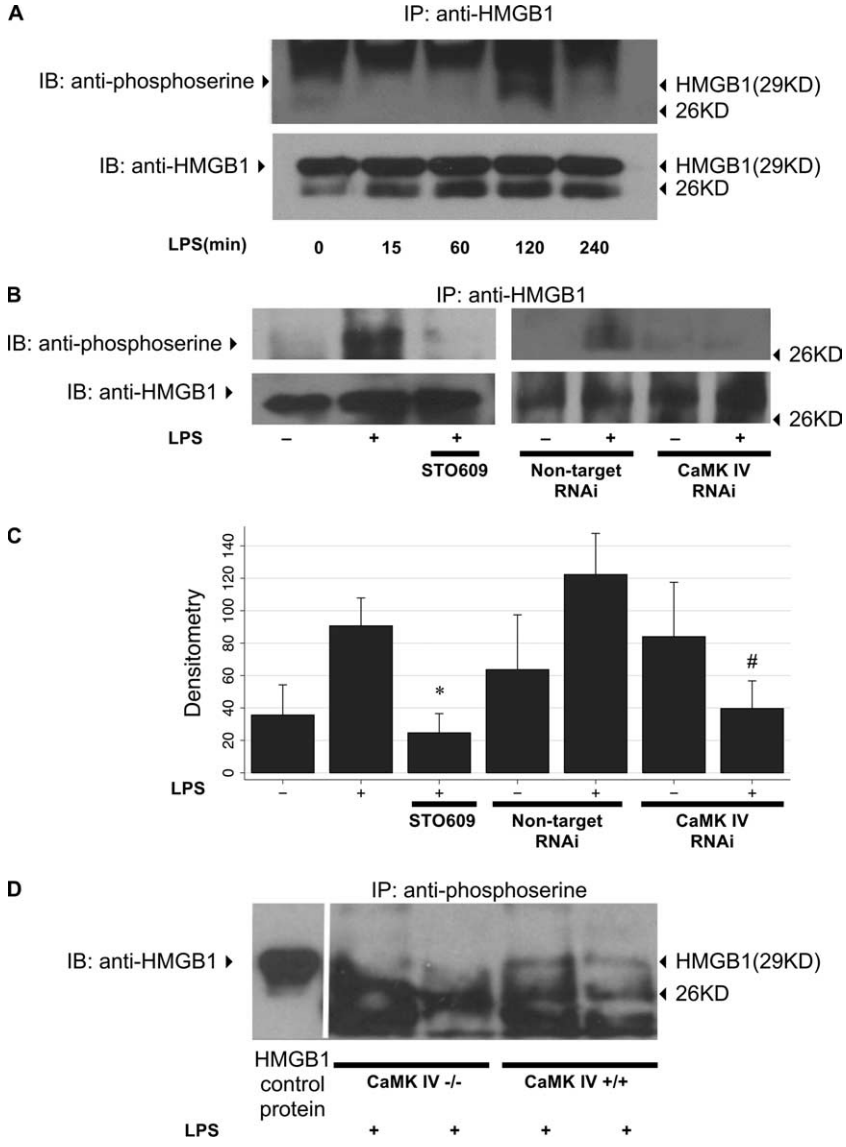

FIGURE 6. CaMKIV mediates serine phorphorylation of HMGB1. *A*, RAW 264.7 cells were stimulated with LPS (100 ng/ml) for 15 min and 1, 2, and 4 h, at which point total cell lysate was harvested, immunoprecipitated for HMGB1, subjected to immunoblot analysis, and probed for phosphorylated serine residues. Each membrane was stripped and probed with anti-HMGB1 Ab to confirm equal loading. *B*, Murine peritoneal Mϕ were stimulated with LPS (100 ng/ml) for 2 h either in the presence or absence of STO609 (5 μM) or after CaMKIV RNAi. Total cell lysate was harvested, immunoprecipitated for HMGB1, subjected to immunoblot analysis, and probed for phosphorylated serine residues. Each membrane was stripped and probed with anti-HMGB1 Ab to confirm equal loading. *C*, Densitometry represents means ± SEM OD of individual phosphoserine HMGB1 immunoblots ($n = 4$); *, $p < 0.05$ vs LPS stimulated Mϕ; #, $p < 0.05$ vs LPS stimulated nontarget RNAi Mϕ. *D*, Peritoneal Mϕ, isolated from CaMKIV$^{-/-}$ or CaMKIV$^{+/+}$ mice, were exposed to LPS 100 ng/ml for 2 h, at which point total cell lysate was harvested, immunoprecipitated for phosphoserine, subjected to immunoblot analysis, and probed for HMGB1.

Immunoblots

Total cellular protein was electrophoresed in a 10% SDS-PAGE gel and transferred to a Hybond ECL nitrocellulose membrane (Amersham Pharmacia Biotech). The membrane was blocked for 1 h at room temperature with 5% milk and was then incubated with primary Ab for 12 h at 4°C. Blots were then incubated in a HRP-conjugated secondary Ab against the primary Ab at room temperature for 1 h. The blot was developed using the SuperSignal chemiluminescent substrate (Pierce) and exposed on KAR-5 film (Eastman Kodak). In addition to utilizing the primary anti-threonine phosphorylated (Thr^{196}) CaMKIV Ab, the active threonine phosphorylated form of CaMKIV was determined using CaMK-immunoprecipitated protein. Densitometry was performed by the National Institutes of Health (Bethesda, MD) image program to quantify OD.

Immunocytochemistry and confocal microscopy

Cells were cultured on glass coverslips until 80% confluent. The coverslips were washed in PBS and fixed for 20 min in 4% paraformaldehyde in PBS at 4°C. Cells were permeabilized with 5% BSA, 0.1% Triton X-100 for 1 h at 4°C and then stained with the appropriate Ab (1 μg/ml) overnight at 4°C. Cells were further treated with anti-rabbit IgG conjugated with FITC (1/1000), anti-mouse IgG conjugated with tetramethylrhodamine isothiocyanate (1/1000), and DAPI (5 mg/ml) in 5% nonfat milk for an additional 2 h at room temperature. The cells were then washed four times with PBS, mounted with Gel/Mount (Biomeda) and examined by confocal microscopy.

In vitro kinase assay

Recombinant HMGB1 (1 μg) was incubated in the presence or absence of activated p-Thr^{196}-CaMKIV (25 ng) for 10 min at 30°C with the following additions: 10 mM $MgCl_2$, 0.2 mM ATP, 1 mM $CaCl_2$, and 1 μM CaM. Reactions were terminated by boiling in SDS-2-ME dissociation solution, subjected to 10% SDS-PAGE, and probed with anti-phosphoserine, anti-CaMKIV, or anti-HMGB1 Ab.

Cell viability and morphologic features

Representative cell populations from each condition were examined under light microscopy. Cell viability was also confirmed by MTT assay. Cells were incubated in 96-well plates (Costar). After a 24-h incubation in 100 μl RPMI 1640 medium containing the stimulus, 50 μl of a 5 mg/ml MTT (Sigma-Aldrich) solution in PBS was added, and cells were incubated at 37°C for 2 h. The cells were then lysed by addition of 100 μl per well extraction buffer (20% (w/v) SDS, 50% (v/v) *N*,*N*-dimethyl formamide, 2% (v/v) acetic acid (pH 4.7)). After overnight incubation with extraction buffer, the OD at 562 nm was measured.

Statistic analysis

Values are expressed as means ± SEM. Groups are compared by Mann-Whitney. A p value of <0.05 was considered statistically significant.

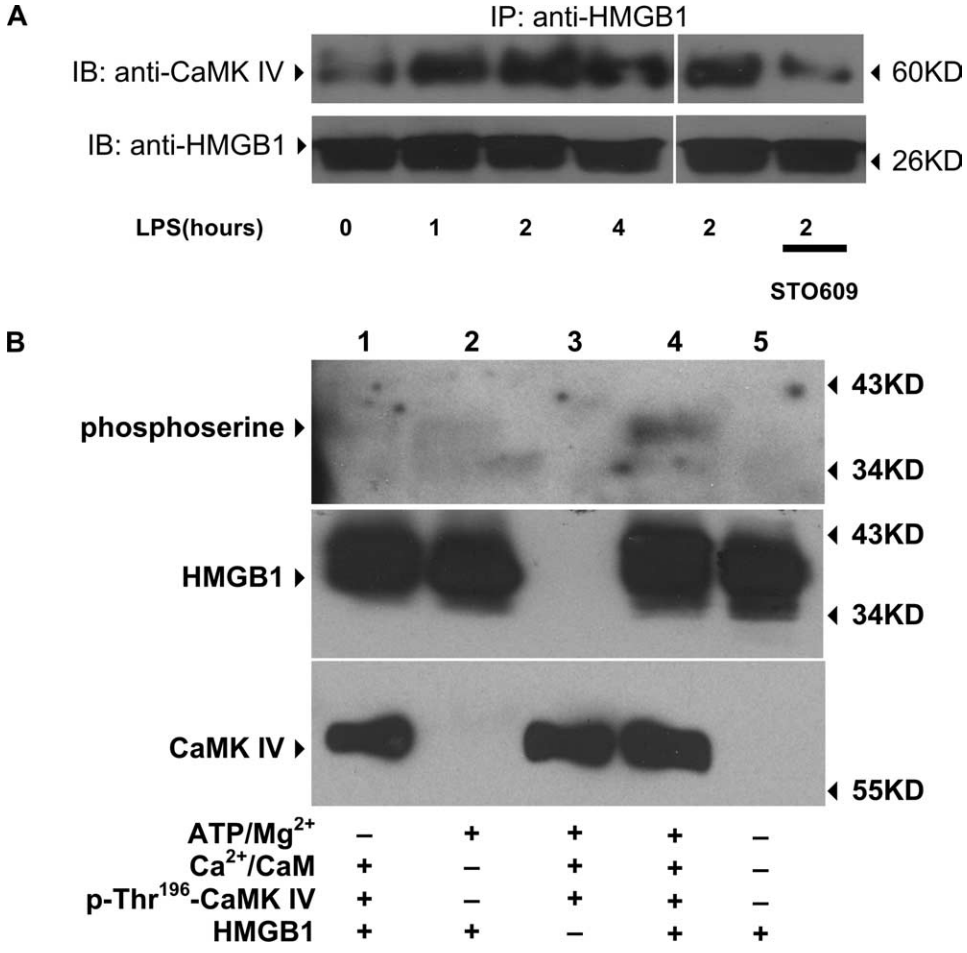

FIGURE 7. CaMKIV directly serine phosphorylates HMGB1. *A*, RAW 264.7 cells were stimulated with LPS (100 ng/ml) either in the presence or absence of STO609 (5 μM) for 1, 2, and 4 h, at which point total cell lysate was harvested, immunoprecipitated for HMGB1, subjected to immunoblot analysis, and probed for CaMKIV. Representative blots of three separate experiments. *B*, Recombinant HMGB1 (1 μg) was incubated in the presence or absence of activated p-Thr^{196}-CaMKIV (25 ng) for 10 min at 30°C with the following additions: 10 mM $MgCl_2$, 0.2 mM ATP, 1 mM $CaCl_2$, and 1 μM CaM. Reactions were terminated by boiling in SDS-2-ME dissociation solution, subjected to 10% SDS-PAGE, and probed with anti-phosphoserine Ab. Representative blots of three separate experiments.

Results

LPS activates CaMKIV

The phosphorylation of CaMKIV on Thr^{196} generates an autonomously active p-CaMKIV (11). We first established the time course for CaMKIV activation in RAW 264.7 cells following LPS stimulation. LPS activated CaMKIV, with Thr^{196} phosphorylation occurring at 15 min and returning toward baseline by 60 min after stimulation (Fig. 1*A*). Upstream inhibition of CaMKIV kinase with STO609 prevented CaMKIV phosphorylation (Fig. 1*A*). We did observe two bands in our assessment of CaMKIV phosphorylation, and two CaMKIV isoforms have been described (21). This time course of CaMKIV phosphorylation was consistent across all independent experiments, yielding a mean CaMKIV activation time course that peaked 15–30 min after LPS (Fig. 1*B*). We repeated these experiments with primary peritoneal Mϕ. LPS induced Thr^{196} phosphorylation of CaMKIV within 15–30 min (Fig. 1*C*). However, even at 60 min after LPS exposure, CaMKIV remained phosphorylated (Fig.1, *C* and *D*). Again, CaMKIV activation was dependent upon CaMKIV kinase, as inhibition with STO609 markedly reduced the LPS-induced increase in p-Thr^{196}-CaMKIV (data not shown).

The CaM kinase cascade mediates LPS-induced HMGB1 release

Consistent with previous studies, we found that LPS induced the release of HMGB1 by RAW 264.7 cells, with detectable concentrations of supernatant HMGB1 occurring as early as 8 h (data not shown) and peaking at 16 h after LPS stimulation as shown (Fig. 2*A*, *lanes 1 and 2*). Incubation with STO609 markedly reduced supernatant HMGB1 concentration (Fig. 2*A*, *lane 3*). As shown in Fig. 2*B*, the HMGB1 release was not due to differential cell death since similar cell viability was observed for treated cell populations.

We confirmed that the CaM kinase cascade also mediated LPS-induced HMGB1 release in primary peritoneal Mϕ. Similar to RAW 264.7 cells, LPS induced HMGB1 release by peritoneal Mϕ that was inhibited by upstream CaM kinase inhibition with STO609 (Fig. 2*C*).

CaMKIV mediates LPS-induced HMGB1 release

The previous observations suggested that the CaM kinase cascade is integral to LPS-induced Mϕ HMGB1 release. We utilized RNAi to study the individual role of downstream CaMKIV in these events. As determined by fluorescent microscopy, cell transfection with fluorescent cyclophilin B siRNA was efficacious (Fig. 3*A*) and, as determined by SDS-PAGE, CaMKIV RNAi markedly reduced CaMKIV expression (Fig. 3*B*). Control, nontarget RNAi-treated cells released HMGB1 in response to LPS similar to untreated RAW 264.7 cells and peritoneal Mϕ (Fig. 3*C*, *lanes 1 and 2*). By contrast, CaMKIV RNAi almost completely inhibited LPS-induced HMGB1 release (Fig. 3*C*, *lanes 3 and 4*). The effects of CaMKIV RNAi were not related to cell death, as the MTT assay demonstrated similar viability for all cells regardless of how they were treated (Fig. 3*D*).

CaMKIV mediates nuclear export of HMGB1 after LPS stimulation

HMGB1 release is an active process by which HMGB1 is shuttled from nucleus to cytoplasm and then out of the cell. Because most

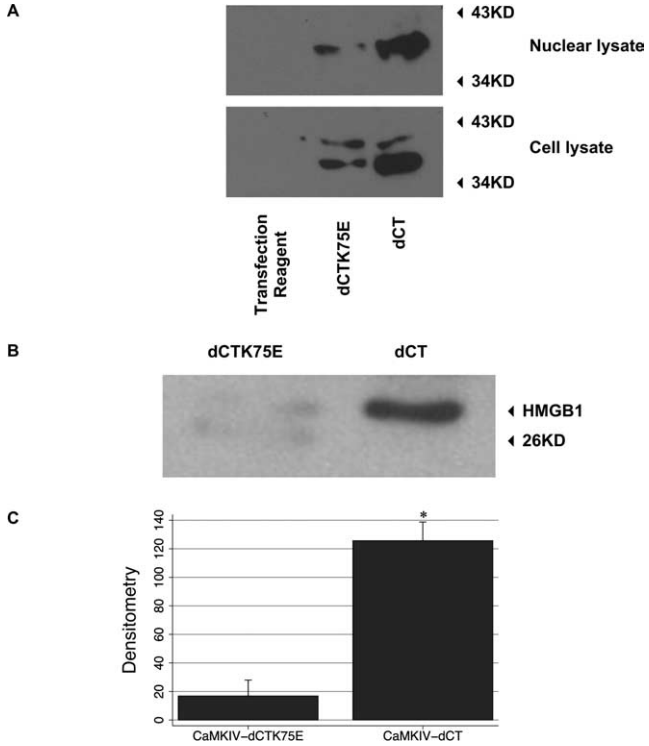

FIGURE 8. Active CaMKIV is sufficient for HMGB1 release. *A*, RAW 264.7 cells were transfected with either a constitutively active CaMKIV-dCT or a kinase-dead mutant CaMKIV-dCTK75E. Eight hours later, total cell lysate or nuclear protein was isolated, resolved by SDS-PAGE, and probed for kinase expression using an anti-FLAG Ab. Representative blots of three separate experiments. *B*, RAW 264.7 cells were transfected with the indicated kinase construct as detailed above. After 24 h, the supernatant was harvested, resolved by SDS-PAGE, and probed with an anti-HMGB1 Ab. Representative blots of three separate experiments. *C*, Densitometry represents means ± SEM OD of individual supernatant HMGB1 immunoblots ($n = 3$); *, $p = 0.03$ vs CaMKIV-dCTK75E.

of the identified functions of CaMKIV occur within the nucleus, we hypothesized that CaMKIV plays an integral role in the translocation of HMGB1 from nucleus to cytoplasm. We initially explored the spatial and temporal relationships of CaMKIV phosphorylation and HMGB1 release. As shown in Fig. 4*A*, HMGB1 (green) is predominantly intranuclear under basal, unstimulated conditions (Fig. 4*A*, *top row*). Within 120 min of LPS stimulation, HMGB1 is observed within the cytoplasm and continues to increase within the cytoplasm over the ensuing 8 h (Fig. 4*A*, *top row*). Unstimulated RAW 264.7 cells demonstrate minimal CaMKIV Thr^{196} phosphorylation (red), but within 15 min of LPS stimulation, phosphorylation increases and continues to increase with time, peaking at 120 min after LPS stimulation (Fig. 4*A*, *middle row*). Although some active CaMKIV is apparent within the cytoplasm, most of this p-Thr^{196}-CaMKIV seems to be concentrated within the nucleus. This localization appears to result from translocation of active CaMKIV to the nucleus as demonstrated by the increased fluorescence of both p-Thr^{196}-CaMKIV (Fig. 4*A*, *middle row*) and total CaMKIV (Fig. 4*B*, *top row*) within the nucleus after LPS stimulation. Inhibition of CaMKIV kinase with STO609 inhibits the Thr^{196} phosphorylation of CaMKIV and the translocation of HMGB1 to the cytoplasm (Fig. 4*A*, *last column*).

To confirm that this translocation process was CaMKIV dependent, we conducted similar experiments using cells treated with CaMKIV RNAi. RAW 264.7 cells transfected with control, non-target siRNA demonstrated nucleocytoplasmic shuttling of HMGB1 (green) at 8 h after LPS stimulation (Fig. 5*A*, *left*). On the other hand, CaMKIV RNAi inhibited LPS-induced HMGB1 translocation with strong nuclear and minimal cytoplasmic staining of HMGB1 at 8 h after LPS stimulation (Fig. 5*A*, *right*). This inhibition was similar to that induced by pretreatment with the CaMKIV kinase inhibitor STO609 (Fig. 4*A*, *last column*).

We confirmed these immunofluorescent microscopic observations by analyzing the HMGB1 concentration of nuclear and cytoplasmic protein isolated from Mϕ subjected to similar conditions as detailed above. As shown in Fig. 5*B*, LPS induced the translocation of HMGB1 from the nucleus to the cytoplasm. By comparison to LPS-stimulated Mϕ, there was a significant reduction in HMGB1 translocation to the cytoplasm in response to either KN93 (which inhibits CaMKIV) or STO609 (which inhibits CaMKIV kinase) (Fig. 5*B*). Similarly, by comparison to control, nontarget RNAi, CaMKIV RNAi reduced the LPS-induced nucleocytoplasmic shuttling of HMGB1 (Fig. 5*B*). These results confirm our idea that a CaMKK/CaMKIV cascade regulates LPS-induced nuclear-to-cytoplasmic translocation of HMGB1.

CaMKIV directly serine phosphorylates HMGB1 after LPS stimulation

Our results demonstrate that CaMKIV mediates LPS-induced HMGB1 release, in part, through processes guiding the nuclear exportation of HMGB1. Recently, HMGB1 translocation to the cytoplasm has been demonstrated to require serine phosphorylation within its NLSs (9). We first confirmed that LPS induced serine phosphorylation of HMGB1. As shown in Fig. 6*A*, stimulation of RAW 264.7 cells with LPS results in serine phosphorylation of HMGB1 within 2 h. Additionally, this phosphorylation event may require CaMKIV, as preincubation of primary peritoneal Mϕ with STO609 inhibited LPS-induced serine phosphorylation of HMGB1 (Fig. 6*B*). Similarly, CaMKIV RNAi treatment of Mϕ also reduced LPS-induced HMGB1 serine phosphorylation (Fig. 6*B*), and the mean degree of inhibition determined by densitometry is illustrated in Fig. 6*C*. Finally, we compared the degree of serine phosphorylated HMGB1 in peritoneal Mϕ isolated from either $CaMKIV^{+/+}$ or $CaMKIV^{-/-}$ mice. As shown in Fig. 6*D*, control $CaMKIV^{+/+}$ Mϕ show serine phosphorylation of HMGB1 after LPS stimulation, whereas the extent of this induced HMGB1 phosphorylation is reduced in $CaMKIV^{-/-}$ Mϕ.

Our immunocytochemistry data suggest colocalization of CaMKIV and HMGB1 after LPS stimulation, and thus we investigated whether CaMKIV interacts with HMGB1. As shown in Fig. 7*A*, LPS stimulation markedly increased the degree to which HMGB1 coimmunoprecipitated with CaMKIV. One hour after stimulation with LPS, CaMKIV and HMGB1 coimmunoprecipitation was markedly increased and peaked by 2 h. Reciprocal coimmunoprecipitation experiments yielded similar results (data not shown). These LPS-stimulated interactions likely require the phosphorylation and activation of CaMKIV, as preincubation of cells with STO609 before addition of LPS inhibited the coimmunoprecipitation of HMGB1 with CaMKIV (Fig. 7*A*).

To determine whether CaMKIV could directly serine phosphorylate HMGB1 we conducted in vitro kinase assays. Active p-Thr^{196}-CaMKIV was unable to phosphorylate HMGB1 in the absence of Mg^{2+}/ATP (Fig. 7*B*, *lane 1*). Similarly, in the absence of p-Thr^{196}-CaMKIV, there was minimal serine phosphorylation of HMGB1 (Fig. 7*B*, *lane 2*). However, activated p-Thr^{196}-CaMKIV, in combination with Mg^{2+}/ATP, was able to serine phosphorylate HMGB1 (Fig. 7*B*, *lane 4*).

Active CaMKIV is sufficient for HMGB1 release

To assess whether active CaMKIV is sufficient for HMGB1 release, we transfected RAW 264.7 cells with plasmids expressing either a truncated, constitutively active form of CaMKIV (CaMKIV-dCT) or a similarly truncated kinase-inactive mutant of CaMKIV (CaMKIV-dCTK75E). Both plasmids were successfully transfected and expressed, although expression of the active CaMKIV-dCT was greater than that of CaMKIV-dCTK75E (Fig. 8*A*), confirming previously published observations that substitutions that disrupt kinase activity, including K75E, result in less protein expression in mammalian cells compared with wild-type CaMKIV-dCT (Fig. 8*A*) (20). As shown in Fig. 8*B*, expression of the active CaMKIV-dCT induced the secretion of HMGB1 from the cells, whereas CaMKIV-dCTK75E failed to do so (Fig. 8*B*). This 6-fold induction of HMGB1 release in response to CaMKIV-dCT was highly reproducible in three independent experiments (Fig. 8*C*).

Discussion

During sepsis, perturbations in cellular calcium homeostasis are postulated to mediate the aberrant inflammation underlying organ dysfunction and death (22, 23). Recently, HMGB1, an architectural chromatin-binding factor that bends DNA and directs protein assembly on specific DNA targets, has been demonstrated to function as a late mediator of mortality in murine endotoxemia and sepsis (1–3). Monocytes and Mϕ have been demonstrated to be a primary source of HMGB1, and evidence is accumulating that production of this inflammatory mediator is Ca^{2+} dependent. Herein, we characterize that LPS-induced HMGB1 release is mediated by a Ca^{2+}-dependent signaling cascade involving a CaMKIV kinase and CaMKIV. Our data suggest that this series of reactions may terminate in the nucleus where CaMKIV phosphorylates HMGB1, an event that is required to facilitate the translocation of HMGB1 from nucleus to cytoplasm (24).

Substantial work has been conducted to elucidate the mechanisms by which HMGB1 is released, in part, because interventions that inhibit systemic HMGB1 concentrations reduce mortality in murine models of sepsis (2). Current data support an active process initiated by HMGB1-histone disengagement, HMGB1 hyperacetylation, and shuttling of the protein from nucleus to cytoplasm (6). Recently, serine phosphorylation of HMGB1 has been demonstrated to be essential for this translocation event, although the kinase responsible had not been identified (9). We hypothesized that CaMKIV mediates this process, in part, because this enzyme has been shown to function downstream of TLR4 in the pathway by which LPS induces the Ca^{2+}-dependent survival of dendritic cells (17). Additionally, prior studies demonstrated that activation of CaMKIV by Ca^{2+}/CaM and threonine phosphorylation (Thr^{196} in mice, Thr^{200} in humans) by an upstream CaMK kinase generates increased and autonomous CaMKIV activity that enables the kinase to translocate to the nucleus where it modulates gene expression (11, 25, 26).

Indeed, our data demonstrate that LPS induces this Thr^{196}-phosphorylated and autonomous species of CaMKIV in Mϕ, which then enters the nucleus where it interacts with and phosphorylates HMGB1. The evidence to support this contention is as follows: 1) CaMKIV translocation to the nucleus preceded HMGB1 translocation to the cytoplasm; 2) CaMKIV RNAi reduced cytoplasmic HMGB1 concentration by retaining HMGB1 in the nucleus; 3) CaMKIV coimmunoprecipitated with HMGB1 in response to LPS; and 4) activated CaMKIV directly phosphorylated HMGB1 in in vitro kinase assays. The modest degree of HMGB1 phosphorylation observed in our in vitro kinase assay suggests that, perhaps, additional protein components may be necessary to assemble a signaling complex that facilitates CaMKIV phosphorylation of HMGB1. The minimum consensus CaMKIV substrate recognition sequence Hyd-X-R-X-X-(S/T) provides only a rough template for CaMKIV-mediated phosphorylation. In HMGB1 only Ser^{39} and Ser^{46} in NLS1 meet the hydrophobic requirement at the −5 position amino acid, and Ser^{46} carries a lysine substitution at −3, which is also present in the well-characterized substrate oncoprotein 18 (27).

Interestingly, HMGB1 has two NLS sequences, and current evidence suggests that phosphorylation of both sequences is important for the cytoplasmic localization of HMGB1 (9). Our data support a role for CaMKIV in the mechanism that controls the nuclear export of HMGB1 (9). Regarding this mechanism, Bianchi et al. contend that the strength of HMGB1-histone binding is inversely related to the histone acetylation status, and that increased histone acetylation may enable HMGB1-histone disengagement and subsequent cellular release of HMGB1 (6, 8). The CaMKs have been demonstrated to modulate the nuclear export of various class II histone deacetylases HDAC4 and HDAC5, a process that could favor histone acetylation (28–31). Additionally, HMGB1 requires direct hyperacetylation before export from the nucleus (8). Further investigation of how CaMKIV activation and histone and HMGB1 acetylation are related will be an important aspect of future studies on HMGB1 nuclear export.

Although LPS stimulation of TLR4 can clearly activate CaMKIV, as shown here and in a prior study, the signaling events that occur between receptor ligation and CaMKIV activation have yet to be determined (17). Prior studies have established the dependency of monocyte/Mϕ function on Ca^{2+} transients and CaM activation, and although it remains unclear precisely how the Ca^{2+} transients are generated, the multifunctional CaMKs respond to relatively small changes in intracellular [Ca^{2+}] (32). Regarding CaMKIV activation and generation of autonomous activity, published data have established a requirement for binding of the Ca^{2+}/CaM complex to both CaMKK and CaMKIV (11, 12, 25). We note the presence of nuclear and cytoplasmic activated CaMKIV in resting cells and an increasing concentration of activated and total CaMKIV within the nucleus after LPS stimulation. These observations support a LPS-mediated increase in the cytoplasmic Ca^{2+} signal that is sufficient to activate CaMKIV and induce its nuclear translocation. Alternatively, it is possible that CaMK may be activated by reactive oxygen species in the absence of a Ca^{2+} rise. For example, Howe et al. suggested that IκB phosphorylation in lymphocytes in response to hydrogen peroxide is mediated by Ca^{2+}-independent activation of CaMKs (33, 34). Hence, additional studies are necessary to determine the spatiotemporal patterns of Ca^{2+} signaling and CaMKIV activation following LPS stimulation as well as the TLR4 dependence of such events.

In summary, CaMKIV kinase/CaMKIV mediates Mϕ LPS-induced HMGB1 production by translocating to the nucleus after activation and phosphorylating HMGB1 in a manner that enables nuclear export of HMGB1 that must occur in order for the protein to be secreted from the cell. The combined observations of investigations conducted by our laboratories and those of others are beginning to highlight the integral role of the CaMK transduction cascade in Mϕ function and cytokine production and inflammation. Future studies will elucidate the sites on both proteins that participate in the CaMKIV-HMGB1 interaction and serine phosphorylation of HMGB1. Interestingly, precedent exists for CaMKIV forming a stable complex with PP2A that is competitive with Ca^{2+}/CaM and CaMKKβ, one of the two CaMKKs that has been shown to form stable complexes with CaMKIV and PP2A or

AMPK (15, 35). In the latter but not the former case, the interaction requires the "RP" domain of CaMKKβ (35). Perhaps, HMGB1 will also utilize a unique sequence of CaMKKβ to form a complex. At any rate, these combined observations suggest that modulation of CaMKK and/or CaMKIV activity may be of potential utility in diseases characterized by heightened and aberrant inflammation.

Acknowledgments

Special thanks to Dr. Naohito Nozaki, who provided the monoclonal anti-p-Thr^{196}-CaMKIV Abs, and Dr. Douglas Black, who provided the CaMKIV-dCT and CaMKIV-dCTK75E plasmids. Without the gracious assistance of these individuals, a considerable portion of this work would not be possible.

Disclosures

The authors have no financial conflicts of interest.

References

1. Wang, H., H. Yang, C. J. Czura, A. E. Sama, and K. J. Tracey. 2001. HMGB1 as a late mediator of lethal systemic inflammation. *Am. J. Respir. Crit. Care Med.* 164: 1768–1773.
2. Yang, H., M. Ochani, J. Li, X. Qiang, M. Tanovic, H. E. Harris, S. M. Susarla, L. Ulloa, H. Wang, R. DiRaimo, et al. 2004. Reversing established sepsis with antagonists of endogenous high-mobility group box 1. *Proc. Natl. Acad. Sci. USA* 101: 296–301.
3. Wang, H., O. Bloom, M. Zhang, J. M. Vishnubhakat, M. Ombrellino, J. Che, A. Frazier, H. Yang, S. Ivanova, L. Borovikova, et al. 1999. HMG-1 as a late mediator of endotoxin lethality in mice. *Science* 285: 248–251.
4. Angus, D. C., L. Yang, L. Kong, J. A. Kellum, R. L. Delude, K. J. Tracey, and L. Weissfeld. 2007. Circulating high-mobility group box 1 (HMGB1) concentrations are elevated in both uncomplicated pneumonia and pneumonia with severe sepsis. *Crit. Care Med.* 35: 1061–1067.
5. Ombrellino, M., H. Wang, M. S. Ajemian, A. Talhouk, L. A. Scher, S. G. Friedman, and K. J. Tracey. 1999. Increased serum concentrations of high-mobility-group protein 1 in haemorrhagic shock. *Lancet* 354: 1446–1447.
6. Bonaldi, T., F. Talamo, P. Scaffidi, D. Ferrera, A. Porto, A. Bachi, A. Rubartelli, A. Agresti, and M. E. Bianchi. 2003. Monocytic cells hyperacetylate chromatin protein HMGB1 to redirect it towards secretion. *EMBO J.* 22: 5551–5560.
7. Gardella, S., C. Andrei, D. Ferrera, L. V. Lotti, M. R. Torrisi, M. E. Bianchi, and A. Rubartelli. 2002. The nuclear protein HMGB1 is secreted by monocytes via a non-classical, vesicle-mediated secretory pathway. *EMBO Rep.* 3: 995–1001.
8. Scaffidi, P., T. Misteli, and M. E. Bianchi. 2002. Release of chromatin protein HMGB1 by necrotic cells triggers inflammation. *Nature* 418: 191–195.
9. Youn, J. H., and J. S. Shin. 2006. Nucleocytoplasmic shuttling of HMGB1 is regulated by phosphorylation that redirects it toward secretion. *J. Immunol.* 177: 7889–7897.
10. Tsung, A., J. R. Klune, X. Zhang, G. Jeyabalan, Z. Cao, X. Peng, D. B. Stolz, D. A. Geller, M. R. Rosengart, and T. R. Billiar. 2007. HMGB1 release induced by liver ischemia involves Toll-like receptor 4 dependent reactive oxygen species production and calcium-mediated signaling. *J. Exp. Med.* 204: 2913–2923.
11. Soderling, T. R. 1999. The Ca-calmodulin-dependent protein kinase cascade. *Trends Biochem. Sci.* 24: 232–236.
12. Braun, A. P., and H. Schulman. 1995. The multifunctional calcium/calmodulin-dependent protein kinase: from form to function. *Annu. Rev. Physiol.* 57: 417–445.
13. Kitsos, C. M., U. Sankar, M. Illario, J. M. Colomer-Font, A. W. Duncan, T. J. Ribar, T. Reya, and A. R. Means. 2005. Calmodulin-dependent protein kinase IV regulates hematopoietic stem cell maintenance. *J. Biol. Chem.* 280: 33101–33108.
14. Lemrow, S. M., K. A. Anderson, J. D. Joseph, T. J. Ribar, P. K. Noeldner, and A. R. Means. 2004. Catalytic activity is required for calcium/calmodulin-dependent protein kinase IV to enter the nucleus. *J. Biol. Chem.* 279: 11664–11671.
15. Anderson, K. A., P. K. Noeldner, K. Reece, B. E. Wadzinski, and A. R. Means. 2004. Regulation and function of the calcium/calmodulin-dependent protein kinase IV/protein serine/threonine phosphatase 2A signaling complex. *J. Biol. Chem.* 279: 31708–31716.
16. Chow, F. A., K. A. Anderson, P. K. Noeldner, and A. R. Means. 2005. The autonomous activity of calcium/calmodulin-dependent protein kinase IV is required for its role in transcription. *J. Biol. Chem.* 280: 20530–20538.
17. Illario, M., M. L. Giardino-Torchia, U. Sankar, T. J. Ribar, M. Galgani, L. Vitiello, A. M. Masci, F. R. Bertani, E. Ciaglia, et al. 2008. Calmodulin-dependent kinase IV links Toll-like receptor 4 signaling with survival pathway of activated dendritic cells. *Blood* 111: 723–731.
18. Tokumitsu, H., H. Inuzuka, Y. Ishikawa, M. Ikeda, I. Saji, and R. Kobayashi. 2002. STO-609, a specific inhibitor of the Ca^{2+}/calmodulin-dependent protein kinase kinase. *J. Biol. Chem.* 277: 15813–15818.
19. Xie, J., and D. L. Black. 2001. A CaMK IV responsive RNA element mediates depolarization-induced alternative splicing of ion channels. *Nature* 410: 936–939.
20. Chatila, T., K. A. Anderson, N. Ho, and A. R. Means. 1996. A unique phosphorylation-dependent mechanism for the activation of Ca^{2+}/calmodulin-dependent protein kinase type IV/GR. *J. Biol. Chem.* 271: 21542–21548.
21. Sun, Z., R. L. Means, B. LeMagueresse, and A. R. Means. 1995. Organization and analysis of the complete rat calmodulin-dependent protein kinase IV gene. *J. Biol. Chem.* 270: 29507–29514.
22. Zaloga, G. P., and B. Chernow. 1987. The multifactorial basis for hypocalcemia during sepsis: studies of the parathyroid hormone-vitamin D axis. *Ann. Intern. Med.* 107: 36–41.
23. Zaloga, G. P., A. Sager, K. W. Black, and R. Prielipp. 1992. Low dose calcium administration increases mortality during septic peritonitis in rats. *Circ. Shock* 37: 226–229.
24. Sparatore, B., M. Passalacqua, M. Patrone, E. Melloni, and S. Pontremoli. 1996. Extracellular high-mobility group 1 protein is essential for murine erythroleukaemia cell differentiation. *Biochem. J.* 320: 253–256.
25. Tokumitsu, H., and T. R. Soderling. 1996. Requirements for calcium and calmodulin in the calmodulin kinase activation cascade. *J. Biol. Chem.* 271: 5617–5622.
26. Corcoran, E. E., and A. R. Means. 2001. Defining Ca^{2+}/calmodulin-dependent protein kinase cascades in transcriptional regulation. *J. Biol. Chem.* 276: 2975–2978.
27. White, D. J., D. L. Maass, B. Sanders, and J. W. Horton. 2002. Cardiomyocyte intracellular calcium and cardiac dysfunction after burn trauma. *Crit. Care Med.* 30: 14–22.
28. Miska, E. A., E. Langley, D. Wolf, C. Karlsson, J. Pines, and T. Kouzarides. 2001. Differential localization of HDAC4 orchestrates muscle differentiation. *Nucleic Acids Res.* 29: 3439–3447.
29. Davis, F. J., M. Gupta, B. Camoretti-Mercado, R. J. Schwartz, and M. P. Gupta. 2003. Calcium/calmodulin-dependent protein kinase activates serum response factor transcription activity by its dissociation from histone deacetylase, HDAC4: implications in cardiac muscle gene regulation during hypertrophy. *J. Biol. Chem.* 278: 20047–20058.
30. Chawla, S., P. Vanhoutte, F. J. Arnold, C. L. Huang, and H. Bading. 2003. Neuronal activity-dependent nucleocytoplasmic shuttling of HDAC4 and HDAC5. *J. Neurochem.* 85: 151–159.
31. McKinsey, T. A., C. L. Zhang, J. Lu, and E. N. Olson. 2000. Signal-dependent nuclear export of a histone deacetylase regulates muscle differentiation. *Nature* 408: 106–111.
32. Anderson, K. A., R. L. Means, Q. H. Huang, B. E. Kemp, E. G. Goldstein, M. A. Selbert, A. M. Edelman, R. T. Fremeau, and A. R. Means. 1998. Components of a calmodulin-dependent protein kinase cascade: molecular cloning, functional characterization and cellular localization of Ca^{2+}/calmodulin-dependent protein kinase kinase β. *J. Biol. Chem.* 273: 31880–31889.
33. Howe, C. J., M. M. LaHair, J. A. Maxwell, J. T. Lee, P. J. Robinson, O. Rodriguez-Mora, J. A. McCubrey, and R. A. Franklin. 2002. Participation of the calcium/calmodulin-dependent kinases in hydrogen peroxide-induced IκB phosphorylation in human T lymphocytes. *J. Biol. Chem.* 277: 30469–30476.
34. Howe, C. J., M. M. Lahair, J. A. McCubrey, and R. A. Franklin. 2004. Redox regulation of the calcium/calmodulin-dependent protein kinases. *J. Biol. Chem.* 279: 44573–44581.
35. Anderson, K. A., T. J. Ribar, F. Lin, P. K. Noeldner, M. F. Green, M. J. Muehlbauer, L. A. Witters, B. E. Kemp, and A. R. Means. 2008. Hypothalamic CaMKK2 contributes to the regulation of energy balance. *Cell Metab.* 7: 377–388.

Role of Phospholipase D in Parathyroid Hormone Type 1 Receptor Signaling and Trafficking

José Luis Garrido,* David Wheeler,* Luis Leiva Vega, Peter A. Friedman, and Guillermo Romero

Department of Pharmacology and Chemical Biology (J.L.G., D.W., L.L.V., P.A.F., G.R.) and the Medical Scientist Training Program (D.W.), University of Pittsburgh School of Medicine, Pittsburgh, Pennsylvania 15261

The role of phospholipase D (PLD) in the regulation of the traffic of the PTH type 1 receptor (PTH1R) was studied in Chinese hamster ovary cells stably transfected with a human PTH1R (CHO-R3) and in rat osteosarcoma 17/2.8 (ROS) cells. PTH(1–34) increased total PLD activity by 3-fold in CHO-R3 cells and by 2-fold in ROS cells. Overexpression of wild-type (WT) PLD1 and WT-PLD2 increased basal PLD activity in CHO-R3 but not in ROS cells. Ligand-stimulated PLD activity greatly increased in CHO-R3 cells transfected with WT-PLD1 and WT-PLD2. However, only WT-PLD2 expression increased PTH-dependent PLD activity in ROS cells. Expression of the catalytically inactive mutants R898K-PLD1 (DN-PLD1) and R758K-PLD2 (DN-PLD2) inhibited ligand-dependent PLD activity in both cell lines. PTH(1–34) induced internalization of the PTH1R with a concomitant increase in the colocalization of the receptor with PLD1 in intracellular vesicles and in a perinuclear, ADP ribosylation factor-1-positive compartment. The distribution of PLD1 and PLD2 remained unaltered after PTH treatment. Expression of DN-PLD1 had a small effect on endocytosis of the PTH1R; however, DN-PLD1 prevented accumulation of the PTH1R in the perinuclear compartment. Expression of DN-PLD2 significantly retarded ligand-induced PTH1R internalization in both cell lines. The differential effects of PLD1 and PLD2 on receptor traffic were confirmed using isoform-specific short hairpin RNA constructs. We conclude that PLD1 and PLD2 play distinct roles in regulating PTH1R traffic; PLD2 primarily regulates endocytosis, whereas PLD1 regulates receptor internalization and intracellular receptor traffic. **(*Molecular Endocrinology* 23: 2048–2059, 2009)**

PTH regulates calcium and phosphate homeostasis by acting primarily on target cells in bone and kidney. PTH function is mediated by the PTH type 1 receptor (PTH1R), a member of the B family of G protein-coupled receptors (GPCR). Agonist binding to the PTH1R leads to activation of adenylyl cyclase and phosphatidylinositol-specific phospholipase C (1–3). PTH binding to the PTH1R results in the internalization of the ligand-receptor complex via clathrin-coated pits by a mechanism that involves arrestin (4–7). Recent data suggest that regulated GPCR endocytosis is a complex multistep process that involves the catalytic action of several lipid-modifying enzymes (8, 9).

Phospholipases D (PLD) hydrolyze phosphatidylcholine to generate choline and the bioactive lipid phosphatidic acid. These enzymes have been implicated in signal transduction, membrane trafficking, transformation, and cytoskeletal reorganization (10–15). Two mammalian PLD isoforms have been identified, PLD1 (10) and PLD2 (16). Both are expressed in a wide but selective variety of tissues and cells (17, 18). Numerous reports based on overexpression have proposed that PLD2 acts at the plasma membrane to regulate cortical cytoskeletal reorganization, endocytosis, and receptor signaling (14, 19–23). Overexpression of catalytically inactive mutants of

ISSN Print 0888-8809 ISSN Online 1944-9917
Printed in U.S.A.

doi: 10.1210/me.2008-0436 Received November 18, 2008. Accepted September 2, 2009.
First Published Online October 16, 2009
* J.L.G. and D.W. contributed equally to the completion of this work and should, therefore, be considered as co-first authors.

Abbreviations: ARF1, ADP ribosylation factor-1; DN, dominant negative; EEA1, early endosome antigen 1; EGFP, enhanced green fluorescent protein; FACS, fluorescence-activated cell sorting; GPCR, G protein-coupled receptor; HA, hemagglutinin; PA, phosphatidic acid; PLD, phospholipase D; PTH1R, PTH type 1 receptor; shRNA, short hairpin RNA; TLC, thin-layer chromatography; WT, wild type.

PLD1 inhibited the down-regulation of epidermal growth factor receptor in response to epidermal growth factor (24), and expression of a catalytically inactive mutant of PLD2 perturbed agonist-induced internalization of angiotensin (19) and μ-opioid receptors (13). Phagocytosis was also inhibited by expression of truncated or catalytically inactive PLD2 (25, 26).

Previous work showed that PTH stimulates PLD activity in UMR-106 osteoblastic cells (27). The pathway appears to involve the heterotrimeric G proteins $G_{12/13}$ and the subsequent activation of RhoA (27). However, the physiological role of PLD activation in PTH function has not been established.

In the present study, we investigated the role of PLD activity in PTH1R internalization using two cells models: CHO cells that express an HA-tagged human PTH1R (CHO-R3 cells) and rat osteosarcoma ROS 17/2.8 (ROS) cells, which express endogenous PTH receptors. We show here that PTH(1–34) activates both PLD1 and PLD2 in CHO-R3 cells, although activating primarily the PLD2 isoform in ROS cells. We further demonstrate that both PLD1 and PLD2 play an important role in the regulation of PTH1R traffic; although PLD2 activity is essential for PTH1R endocytosis, PLD1 regulates the intracellular traffic of the receptor.

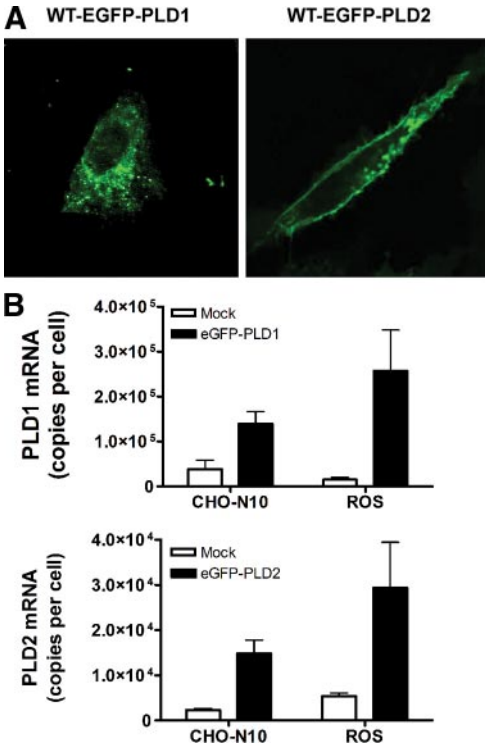

FIG. 1. Localization of EGFP-PLD and EGFP-PLD2 in CHO-R3 cells. A, CHO-R3 cells were transiently transfected with PLD1-EGFP or PLD2-EGFP expression plasmids. Forty-eight hours later, images were captured by confocal microscopy (Olympus Fluoview 1000). EGFP fluorescence was used to determine the subcellular localization of the transfected proteins. B, The expression of endogenous and transfected PLD1 and PLD2 in CHO-R3 and ROS cells was determined by quantitative RT-PCR. The numbers of copies reported in the figure were obtained using standard curves generated by serial dilutions of plasmid DNA coding for the WT human PLD1 and mouse PLD2.

Results

PTH(1–34) stimulates PLD activity in CHO-R3 and ROS cells

The intracellular distribution of PLD in cultured CHO-R3 cells was investigated by immunofluorescence and confocal microscopy. The subcellular distributions of enhanced green fluorescent protein (EGFP)-PLD1 and EGFP-PLD2 are shown in Fig. 1A. PLD1 localizes primarily to endosomal vesicles and to a perinuclear region, as reported previously by us and others (28–30). Some localization of EGFP-PLD1 on the plasma membrane was observed occasionally. In contrast, PLD2 was detected primarily in the plasma membrane and vesicles close to plasma membrane as described (16). Identical results were obtained with ROS 17/2.8 cells.

The expression of PLD1 and PLD2 in CHO and ROS cells was determined by quantitative RT-PCR. The data, shown in Fig. 1B, confirm the endogenous expression of PLD1 and PLD2 in both cell lines. We also determined the levels of expression of PLD1 and PLD2 after transfection with our PLD-EGFP constructs. The endogenous mRNA levels for both PLDs were comparable for CHO-R3 and ROS cells. The number of copies of PLD1 mRNA was 3.8×10^4 in CHO-R3 cells and 1.5×10^4 in ROS cells. PLD2 mRNA was significantly less abundant (2300 and 5300 copies for CHO-R3 and ROS cells, respectively). As shown in Fig. 1B, transfection with EGFP-PLD1 and EGFP-PLD2 increased expression by 4- to 20-fold. Actual protein levels could not be determined because of the lack of good specific antibodies. Similar transfection efficiencies were observed for CHO-R3 and ROS cells in all experiments.

PTH(1–34) increased PLD activity about 2.2-fold in CHO-R3 cells in a time-dependent manner (Fig. 2A). Similar but less dramatic results were observed in ROS cells (Fig. 2B). To determine which PLD isoforms are stimulated by PTH treatment, CHO-R3 and ROS cells were transfected with either wild-type (WT)-EGFP-PLD1 or WT-EGFP-PLD2 and treated with PTH(1–34) for 30 min. Both PLD constructs increased basal PLD activity in CHO-R3 cells (Fig. 2C) but had no significant effects on the basal PLD activity of ROS cells (Fig. 2D). PTH(1–34) treatment produced a pronounced increase in PLD activity in CHO-R3 cells transfected with either WT construct (Fig. 2C). In contrast, only ROS cells transfected with WT-EGFP-PLD2 showed an increased response to the addition of ligand (Fig. 2D). These results suggest that the

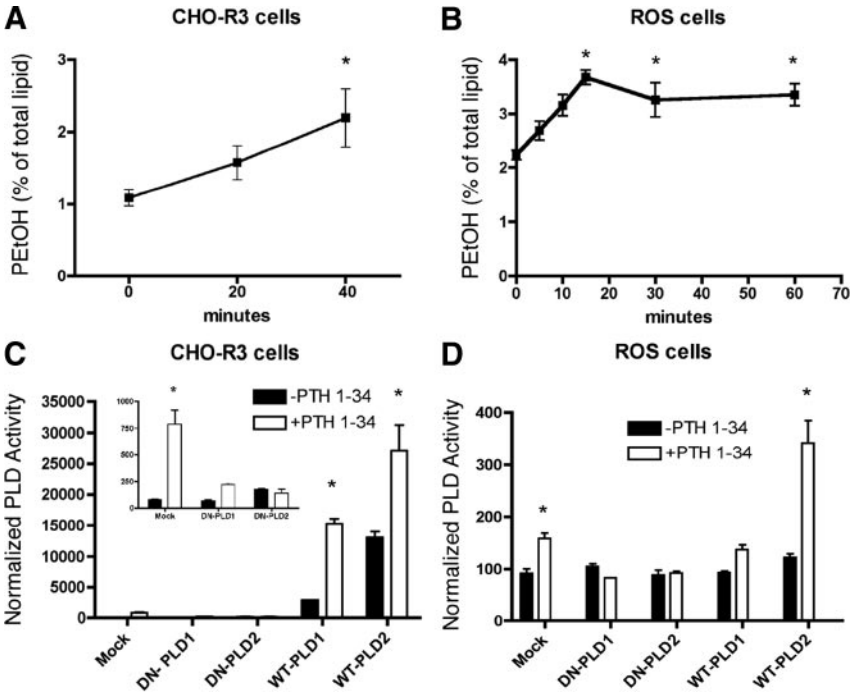

FIG. 2. PTH1R-mediated PLD activation. A, Time course of the activation of PLD by PTH(1–34) (100 nM) in CHO-R3 cells. B, Time course of the activation of PLD by PTH(1–34) (100 nM) in ROS 17/2.8 cells. C, CHO-R3 cells stably expressing HA-PTH1R (control) were transfected with EGFP-tagged WT-PLD1 and -PLD2 and with the EGFP-tagged mutants K898R-PLD1 (DN-PLD1) and R758K-PLD2 (DN-PLD2). Cells were stimulated with PTH(1–34) for 30 min. Graphs represents a mean ± SE of three independent experiments. The *inset* shows only the mock, DN-PLD1, and DN-PLD2 data. D, ROS cells were transfected with EGFP-tagged WT and mutant PLDs and treated with PTH(1–34). The graph represents a mean ± SE of three independent experiments. *, $P < 0.05$ compared with the respective controls (time = 0 for the kinetics experiments shown in A and B and untreated cells for the data shown in C and D).

PTH1R can activate both PLD1 and PLD2 in CHO cells but activates preferentially PLD2 in ROS cells. Interestingly, the effects were much greater in CHO-R3 cells than in ROS cells. This is possibly a consequence of the much larger number of receptors expressed in the CHO-R3, which express 650,000 receptors per cell (31), whereas the ROS cells express about 72,000 endogenous receptors per cell (32). Transfection of the catalytically inactive (dominant-negative, or DN) mutants DN-PLD1 or DN-PLD2 blocked PTH-induced PLD activity in both cell lines (Fig. 2, C and D).

PLD activity regulates PTH1R traffic

A cell sorting-based assay was developed to investigate the role of PLD in the regulation of PTH1R internalization. This assay makes use of a human PTH1R tagged with an hemagglutinin (HA) epitope near the N terminus. This epitope faces the extracellular milieu such that only the receptor expressed on the surface of the cell is accessible to anti-HA antibodies added to intact, nonpermeabilized cells. Upon receptor internalization, the immunoreactivity of the cells decreases as a function of time. This time-dependent change is then detected by fluorescence-activated cell sorting (FACS) or by indirect immunofluorescence. A representative FACS experiment performed with CHO-R3 cells is shown in Fig. 3 (see *Materials and Methods* for a complete description of the protocol). Figure 3A shows the selection of appropriate gates to detect the HA-tagged receptor. These gates were obtained by 1) transfecting cells with untagged receptors or 2) omitting the HA-specific primary antibody. Figure 3B shows histograms of the data shown in Fig. 3A. The 10-min points are omitted for the sake of clarity. As shown, the fluorescence of the cells decreases as a function of time after the addition of PTH(1–34).

The effects of PLD on ligand-induced internalization of the PTH1R in CHO-R3 cells are shown in Fig. 4. WT-PLD2 had no effects on the internalization of the PTH1R (Fig. 4A). DN-PLD2, in contrast, significantly slowed receptor internalization (Fig. 4A). Both WT- and DN-PLD1 decreased the rate of PTH1R internalization after addition of ligand (Fig. 4B). Importantly, the level of expression of the HA-tagged receptors in cells that overexpressed WT-PLD1 or DN-PLD1 was significantly reduced (Fig. 4C). Thus, we conclude that the activities of PLD1 and PLD2 modulate the rate of PTH1R internalization; furthermore, we conclude that regulated PLD1 activity is required for efficient traffic of the PTH1R to the plasma membrane.

Confocal studies on the regulation of the traffic of the PTH1R by PLD1 and PLD2

PTH1R traffic was further studied by confocal microscopy. CHO-R3 cells were treated with PTH(1–34) for various times and fixed, and the distribution of the HA-tagged PTH1R was determined using anti-HA antibodies and a tetramethylrhodamine-conjugated secondary antibody. Transfections with empty vectors were used as controls. The distribution of EGFP-PLD1 was determined from the GFP fluorescence of the cells. The data are shown in Fig. 5. Before the addition of PTH(1–34), the receptor was expressed on the cell surface and in intracellular vesicles. WT-PLD1 and DN-PLD1 were primarily localized to the cytosol or to intracellular vesicles, some of which were also decorated with the PTH1R. Significant reorganization of the PTH1R and PLD labels was ob-

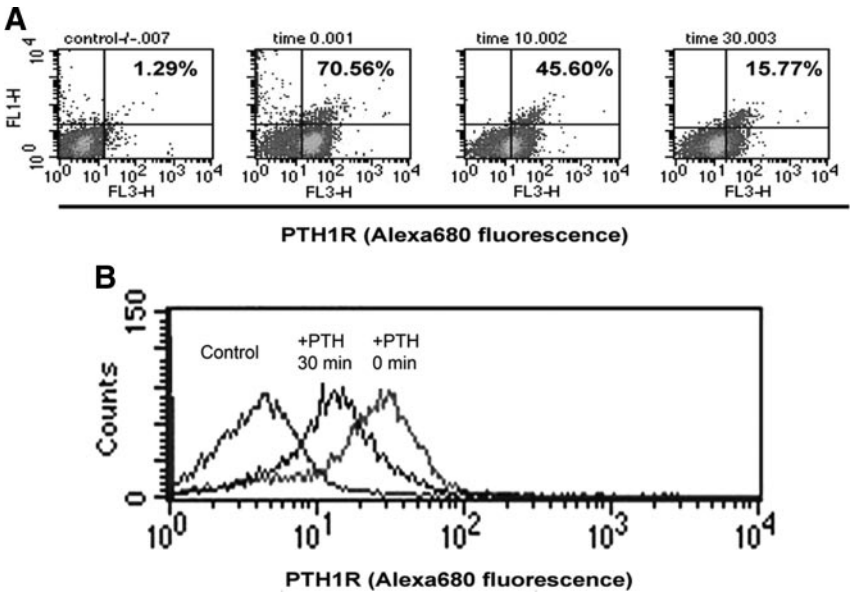

FIG. 3. FACS analysis of the internalization of the PTH1R. A, Representative traces showing control cells (CHO cells not expressing HA-tagged PTH1R, *left*) and CHO-R3 cells after various times (0, 10, or 30 min) of incubation with 100 nM PTH(1–34). B, Histogram representation of the data shown in A. The 10-min point has been eliminated for the sake of clarity.

served within 10 min of the addition of ligand; the PTH1R disappeared from the membrane and was localized to vesicles (probably early endosomes, see Fig. 9) that were also decorated with PLD1. Thirty minutes after ligand addition, the PTH1R accumulated in the perinuclear compartment. Importantly, WT-PLD1-EGFP colocalized with the receptor in this perinuclear compartment (Fig. 5A).

The intracellular distribution of DN-PLD1 was somewhat different. DN-PLD1 was seldom found in perinuclear compartments before or after addition of PTH(1–34). The expression of DN-PLD1 significantly affected the traffic of the internalized receptor. Receptor internalization appeared to be slower, and the accumulation of the internalized PTH1R in the perinuclear region was never observed. Rather, the internalized receptor remained in small intracellular vesicles, where it colocalized abundantly with DN-EGFP-PLD1 (Fig. 5B, 30 min). A quantitative description of these phenomena was obtained by calculating the Pearson correlation coefficient of the red and green fluorescence of images obtained from 35–45 cells from at least 5 independent experiments. The correlation between PTH1R and WT-PLD1 increased significantly as a function of time ($P < 0.01$), indicative of a time-dependent accumulation of both labels in common cellular compartments (Fig. 5C). A much slower, but similar, phenomenon was observed with DN-PLD1. The increased colocalization between PTH1R and DN-PLD1 only became significant 30 min after the addition of ligand (Fig. 5C).

In parallel studies, CHO-R3 cells were transfected with WT- and DN-PLD2 and stimulated with PTH(1–34) for 10 and 30 min. In nontransfected or WT-PLD2-transfected cells, the PTH1R showed a vesicular distribution 10 and 30 min after treatment with PTH(1–34). Significant accumulation of the receptor in the perinuclear compartment was visible after 30 min (Fig. 6A). However, most of the PLD2 remained at the plasma membrane, although a small fraction of the PLD2 trafficked with the PTH1R to the perinuclear compartment. In marked contrast, little internalization of the receptor was apparent even after 30 min in cells that were transfected with DN-PLD2. In fact, a significant fraction of the cells expressing DN-PLD2 did not internalize the receptor at all (Fig. 6B).

In contrast to PLD1, which colocalized with the internalized PTH1R in vesicles and in the perinuclear compartment, the distribution of WT-EGFP-PLD2 remained unchanged after PTH1R stimulation, independently of the traffic of the receptor. A quantitative analysis of the colocalization data are shown in Fig. 6C. The Pearson correlation coefficient of the fluorescent images obtained with the WT-PLD2 construct and the HA-tagged receptor decreased as a function of time as a consequence of the disappearance of the PTH1R from the plasma membrane surface and the retention of the PLD2 construct on the surface (Fig. 6C). In contrast, the correlation coefficients of the fluorescent images obtained with the DN construct remained approximately constant, indicative of the much slower internalization of the PTH1R.

PTH1R internalization in ROS cells

To examine the regulation of PTH1R endocytic traffic in a more physiologically relevant cellular system, we investigated ligand-induced redistribution of the PTH1R in ROS cells. This was done using ROS cells transfected with HA-tagged human PTH1R.

As shown in Fig. 7, HA-tagged PTH1R was localized primarily on the plasma membrane of untreated ROS cells. Occasionally, a fraction of the receptor was found in a perinuclear compartment, which was also decorated with ADP ribosylation factor-1 (ARF1), consistent with the Golgi compartment. Thirty minutes after treatment with PTH(1–34), the plasma membrane receptor had accumulated in numerous intracellular vesicles and the Golgi compartment.

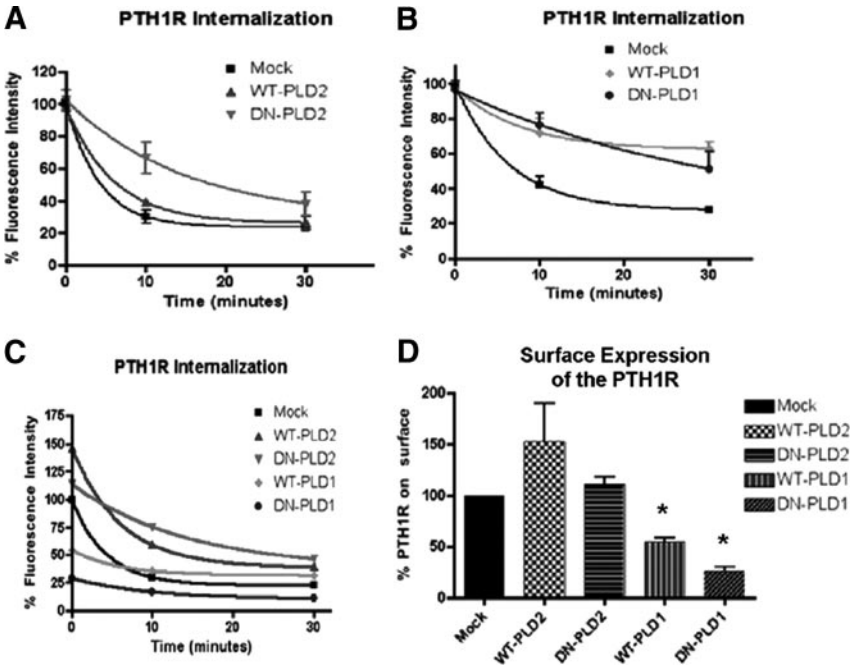

FIG. 4. Phospholipase D activity regulates PTH1R internalization and traffic. A, CHO-R3 cells stably expressing HA-PTH1R were transiently transfected with EGFP-PLD2 (WT) or R758K-PLD2 (DN). Forty-eight hours after transfection, cells were stimulated with PTH(1–34) for 0, 10, or 30 min and analyzed by FACS using a specific anti-HA antibody. Cells successfully transfected were identified by GFP fluorescence. Only GFP-positive cells were used in the analysis. The data shown have been normalized to the initial integrated cell fluorescence. B, Same as A, except that WT and R898K (DN) PLD1 were used. C, PTH1R internalization data normalized to the mock transfection values. Notice the much lower starting points of the cells that express WT- and DN-PLD1. D, Expression of the PTH1R on the cell membrane is inhibited by overexpression of WT- and DN-PLD1. CHO-R3 cells transfected with PLD1 were examined by FACS after 48 h. The total cell-associated PTH1R fluorescence of the transfected cells was compared with the fluorescence of paired, mock transfected cells or to that of nontransfected cells. Both comparisons yielded identical results. The data shown represent the averages from three different experiments. *, $P < 0.01$ *vs.* mock.

Further details of the endocytic traffic of the PTH1R in ROS cells are illustrated in Fig. 8. Some colocalization of the PTH1R with early endosome antigen 1 (EEA1) was observed even under basal conditions (red-green correlation coefficient, 0.34 ± 0.112) (Fig. 8). However, addition of PTH(1–34) increased significantly the colocalization of the PTH1R with EEA1 (red-green correlation coefficient, 0.857 ± 0.097) (Fig. 8). This demonstrates that the receptor traffics via the standard endocytic pathway. Figure 9 shows that DN-PLD2 impairs the endocytosis of the PTH1R in ROS cells in a manner analogous to that described for CHO-R3 cells. Transfection with DN-PLD1 greatly reduced the expression of the HA-tagged PTH1R on the surface in ROS cells, precluding the analysis of the effects of DN-PLD1 on receptor internalization (data not shown).

To confirm that the results obtained by overexpression of catalytically inactive PLD were a consequence of reduced PLD activity, we generated ROS-derived cell lines that expressed short hairpin RNA (shRNA) targeted against PLD1 and PLD2 in a stable manner. PLD expression was determined by semiquantitative PCR. The constructs used reduced PLD1 and PLD2 expression by at least 90% in a specific manner (Fig. 10A). PTH1R internalization was determined using the cell-sorting protocol described in *Materials and Methods*. The knockdown of PLD1 reduced PTH1R expression on the surface by about 50% and reduced the rate of PTH1R internalization (Fig. 10, B and C), confirming the DN-PLD1 data. Likewise, PLD2 knockdown significantly reduced PTH1R internalization (Fig. 10, B and D). Importantly, expression of mouse WT-PLD2 or addition of exogenous phosphatidic acid normalized PTH1R internalization (Fig. 10D). Transfection of the cells expressing PLD2-targeted shRNA with human WT-PLD1, however, did not rescue the effects of PLD2 knockdown on PTH(1–34)-induced internalization of the receptor. These data confirm that PLD2 activation is required for PTH1R internalization, whereas PLD1 activity affects both internalization and traffic of the PTH1R to the cell surface.

Phospholipase D activity is required to couple PTH1R activation to ERK phosphorylation

Previous work from our lab demonstrated that PLD activity is required to couple the function of several cell surface receptors to the activation of the ERK cascade (14, 15, 33–36). In this work, we extended this paradigm to PTH1R signaling in CHO-R3 cells. The data obtained are summarized in Fig. 10. Expression of WT-PLD1 had a small effect on the basal level of phosphorylation of ERK. The expression of WT-PLD2 did not alter the effects of PTH(1–34) on ERK phosphorylation. Importantly, the expression of the DN mutants DN-PLD1 and DN-PLD2, both of which block PTH-induced PLD activation, also abolished the effects of PTH on ERK phosphorylation. We conclude, therefore, that the activation of PLD and the generation of phosphatidic acid are required for the activation of the ERK cascade by PTH.

Discussion

Agonist-induced activation of PLD plays an important role in regulating numerous signal transduction pathways. These include receptor internalization (19, 24, 37),

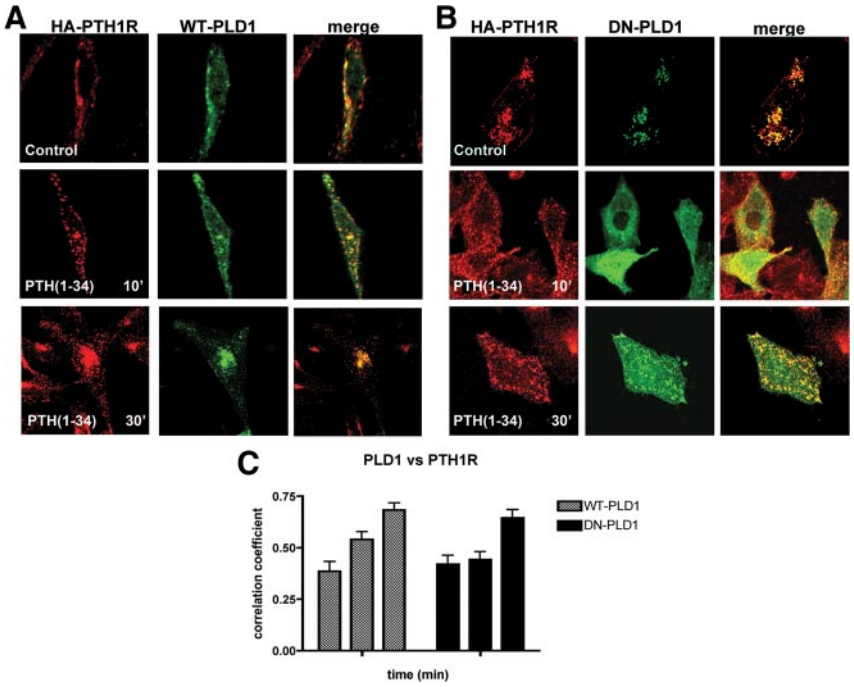

FIG. 5. PLD1 alters PTH1R traffic in CHO cells. CHO-R3 were transiently transfected with WT EGFP-PLD1 (A) or EGFP-tagged K898R-PLD1 (DN-PLD1; (B). Forty-eight hours after transfection, the cells were stimulated with PTH(1–34) for 0, 10, or 30 min. Cells were visualized using an anti-HA antibody and analyzed by confocal microscopy. Representative images are shown from more than 45 cells analyzed across four independent experiments. C, Correlation coefficients were calculated at different times for regions comprising most of the cell. The graph represents the mean ± SE of four independent experiments. More than 35 individual cells were analyzed for each data point.

receptor desensitization and resensitization, and protein phosphorylation (14, 22, 23, 34, 38). Several members of the GPCR family activate PLD (27, 35, 36, 39–41). The PTH1R activates PLD in kidney (3) and bone (27). However, the physiological significance of this activity has not been elucidated. We show here that PLD activity regulates the traffic of the PTH1R to the plasma membrane, PTH1R endocytosis, and PTH-dependent ERK phosphorylation.

Mammalian cells express two main forms of PLD (10, 16, 42). Both PLD isoforms display distinct subcellular distributions and modes of regulation. PLD1 localizes to intracellular vesicles and was implicated initially in various aspects of vesicular traffic (28–30). PLD2 is expressed primarily at the plasma membrane and was identified as the main target for receptor-mediated activation and a regulator of ligand-dependent endocytosis (13, 14, 19, 35, 37). Subsequent work, however, suggests that PLD1 may play additional roles in specific signaling pathways. Recent evidence shows that a small fraction of PLD1 localizes to the plasma membrane where it contributes to mediating specific signaling events (43, 44). We investigated the activation of specific PLD isoforms by the PTH1R using two complementary approaches based on the overexpression of WT and DN mutants. Our results demonstrate cell-dependent specificity in the activation of PLD1 and PLD2 by the PTH1R. Whereas both PLD1 and PLD2 appear to be targets in CHO-R3 cells, only PLD2 seems to be activated by the PTH1R in ROS osteosarcoma cells. However, the expression of catalytically inactive mutants of both isoforms significantly inhibited PTH-induced PLD activity suggesting, superficially, that the activation of both PLDs by the PTH1R follow common signaling pathways. This, however, is not necessarily the case, as will be discussed below.

Activation of PLD2 by the PTH1R is consistent with several reports linking receptor-dependent PLD activation to the PLD2 isoform. (13, 15, 19, 23, 35, 37, 41). In contrast, whereas PLD2 is expressed at the plasma membrane, PLD1 is mostly confined to the cytosol and intracellular membranes in CHO-R3 and ROS cells. However, localization of the PTH1R with PLD1 increases significantly after the addition of ligand owing primarily to the accumulation of PTH1R in endosomes enriched in PLD1. It is possible, therefore, that the PTH1R activates PLD1 and PLD2 in different compartments and in a distinct temporal pattern; PLD2 is activated early and at the plasma membrane, whereas PLD1 activation may occur only after the receptor is internalized and translocated to endosomes.

Interestingly, although PTH effectively activated PLD1 in CHO-R3 cells, we did not find evidence of PTH1R-dependent activation of PLD1 in ROS cells. The cell and tissue specificity of the responses to PTH1R ligands has been abundantly described (3, 5, 45, 46). One explanation for this specificity is based the relative levels of expression of NHERF1 (5, 46). However, neither CHO-R3 (7) nor ROS cells (46, 47) express endogenous NHERF1. Therefore, different levels of NHERF1 expression cannot explain these results.

Importantly, our data demonstrate that altered PLD1 activity, caused by overexpression of the WT protein, by expression of a DN construct, or by shRNA knockdown, significantly reduces the plasma membrane expression of the PTH1R. This result strongly suggests that regulated PLD1 activity is required for the normal traffic of the receptor to the surface. Whether this finding can be extrapolated to other receptors remains to be determined. Nevertheless, this result raises an important issue; studies

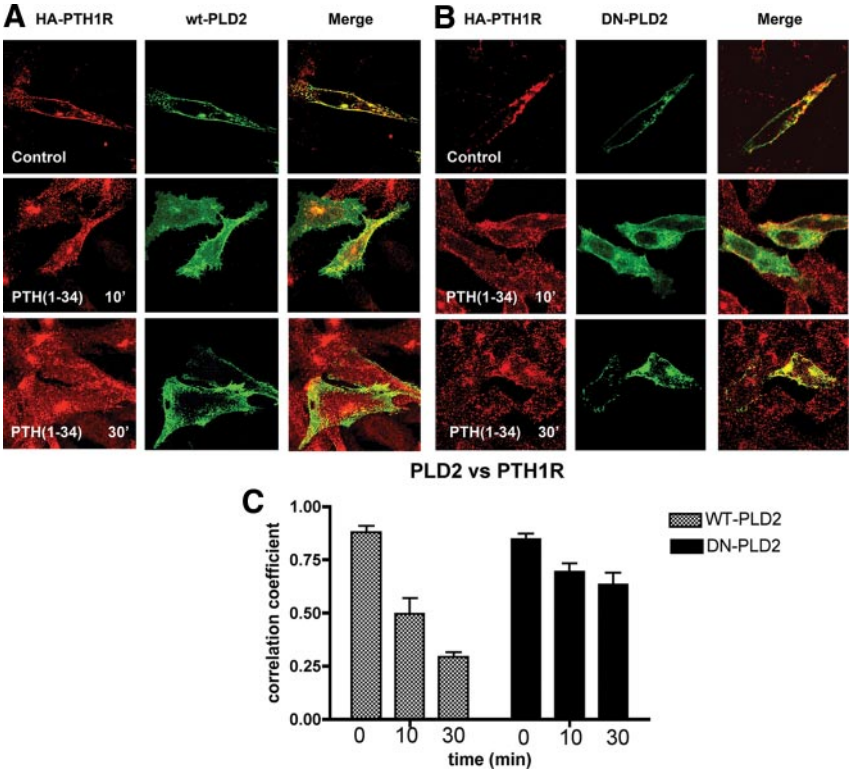

FIG. 6. PLD2 delays PTH1R endocytosis in CHO cells. CHO-R3 cells were transiently transfected with WT EGFP-PLD2 (A) or EGFP-tagged K758R-PLD2 (DN-PLD2; B). Forty-eight hours after transfection, the cells were stimulated with PTH(1–34) for 0, 10, or 30 min. Cells were visualized using an anti-HA antibody and analyzed by confocal microscopy. Representative images are shown from more than 45 cells analyzed across four independent experiments. C, Correlation coefficients were calculated at different times for regions comprising most of the cell. The graph represents the mean ± SE of four independent experiments. At least 35 individual cells were analyzed for each data point.

in which receptor-mediated PLD1 activation is perturbed by expression of a DN or by shRNA techniques must be carefully controlled, because reduced surface expression of the receptor may be a consequence of the perturbation of PLD1 activity. Thus, the mechanism by which PLD1 knockdown and expression of DN-PLD1 impair receptor-mediated PLD activation is not necessarily a consequence of the interference of these treatments with stimulation of endogenous PLD. We cannot distinguish between these alternative explanations at present.

Ligand-induced internalization of GPCR plays a major role in the regulation of signal transduction pathways, either by propagating (48, 49) or terminating (50) signals. Our data strongly support the hypothesis that PLD activation regulates PTH1R internalization, thereby contributing to signal termination. DN-PLD2 expression significantly reduced the rate of receptor internalization in CHO-R3 and ROS cells. The expression of WT-PLD2 was without effect. This is the first time that the activation of PLD2 has been linked to the internalization of the PTH1R. This observation, however, is consistent with results obtained with other receptor systems and in diverse cell lines (13, 19, 21, 24, 37).

The role of PLD1 on PTH1R internalization is somewhat different. Both WT- and DN-PLD1 significantly reduced the level of expression of the PTH1R on the cell surface. In CHO-R3 cells, plasma membrane expression of the PTH1R was reduced by 50 and

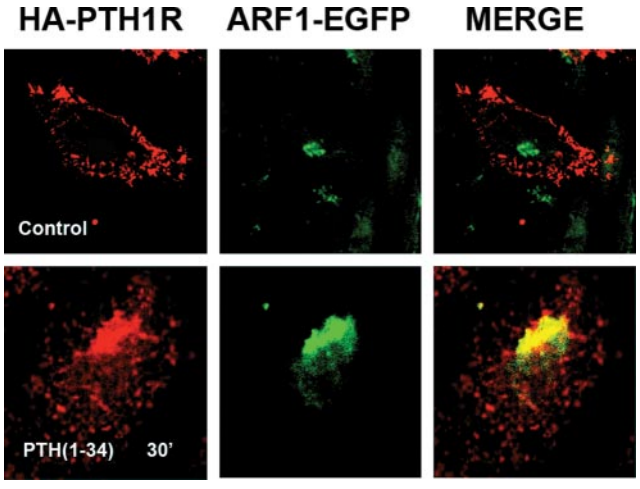

FIG. 7. PTH1R colocalizes with ARF1 after PTH(1–34) treatment. CHO-R3 cells were transfected with ARF1-EGFP and stimulated with PTH(1–34) (100 nM) for 0 or 30 min. The cells were then fixed, permeabilized, immunostained with anti-HA antibodies, and analyzed by confocal microscopy. Representative images are shown from more than 25 cells analyzed per slide across three independent experiments.

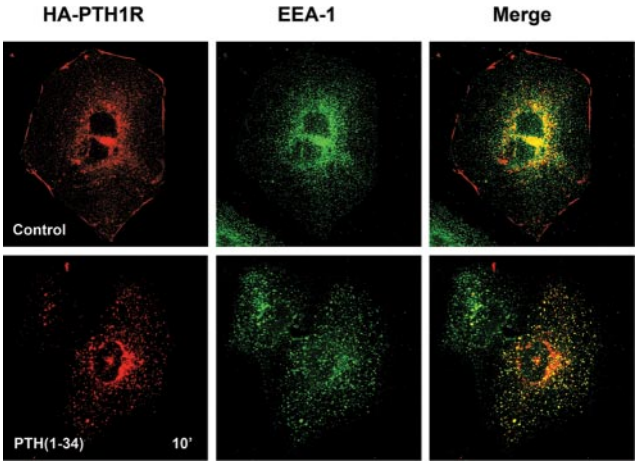

FIG. 8. Internalized PTH1R colocalizes transiently with EEA1. CHO-R3 cells were stimulated with PTH(1–34) (100 nM) for 0, 10, or 30 min. The cells were then fixed, permeabilized, immunostained with anti-HA and anti-EEA1 antibodies, and analyzed by confocal microscopy. Representative images are shown from more than 25 cells analyzed per slide across three independent experiments, each in duplicate.

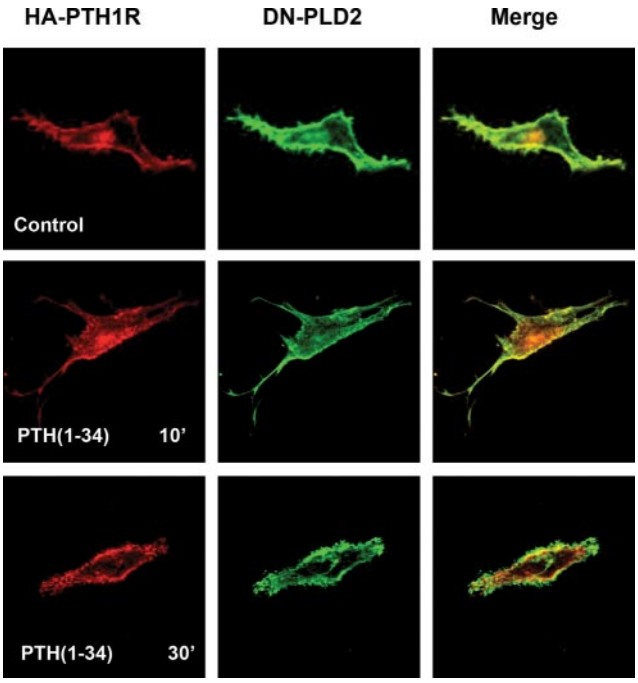

FIG. 9. Inhibition of PTH1R endocytosis by DN-PLD2 in ROS 17/2.8 cells. ROS cells coexpressing HA-PTH1R (control) and EGFP-tagged DN-PLD2 mutant were treated with PTH(1–34) for 0, 10, or 30 min and analyzed by confocal microscopy. Representative images are shown from more than 25 cells analyzed per slide across three independent experiments, each in duplicate.

75% by WT-PLD1 and DN-PLD1, respectively, whereas in ROS cells, HA-tagged PTH1R was essentially undetectable in cells transfected with either WT-PLD1 or DN-PLD1. In independent experiments, PLD1 knockdown using shRNA reduced surface PTH1R expression by about 50% in ROS cells, whereas PLD2 knockdown had no effects. These observations imply that PLD1 plays an important role in regulating the traffic of the receptor to the plasma membrane and thus contributing to signal propagation. The precise function of PLD1 in PTH1R traffic, however, remains to be elucidated.

In addition, PLD1 function also regulates the traffic of the internalized receptor. Internalized receptor accumulates initially in endosomes (Fig. 8) and, after several minutes, in a perinuclear compartment (Figs. 5–7). Because this compartment is also decorated with ARF1 (Fig. 7), we conclude it is the Golgi apparatus. In CHO-R3 cells, PLD1 accompanies the receptor throughout this process (see Fig. 5). However, in cells expressing DN-PLD1, accumulation of the receptor in the Golgi was not observed. Thus, we conclude that in the absence of PLD1 activity, the traffic of the PTH1R is interrupted, such that the receptor never reaches the Golgi.

The present data also demonstrate the requirement for PLD activity in the regulation of the ERK cascade by PTH(1–34). PTH treatment induced ERK phosphorylation, as described previously (51), and this effect was inhibited by overexpression of DN-PLD2 (Fig. 11). WT- and DN-PLD1 had similar effects, but because of the reduced expression of PTH1R on the surface of cells transfected with exogenous PLD1, we cannot conclude that the effects of PLD1 are related to the coupling of the ERK cascade to PTH1R function. The effects of DN-PLD2 on ERK phosphorylation are consistent with the reduced internalization of the PTH1R caused by expression of this mutant protein. Several lines of evidence link endocytosis to the activation of the ERK cascade. These include specific roles for β-arrestins as scaffolds (48, 50, 52) and other less characterized effects of endocytic traffic (53–56). More recently, a specific role for PA as a scaffold for the coupling of the ERK cascade has emerged. This model is based on the fact that Son of Sevenless (SOS; a Ras guanine-nucleotide exchange factor), Raf-1, and kinase supressor of Ras 1 (a scaffolding protein that binds ERK1/2 and MAPK/ERK kinase 1) contain specific binding sites for phosphatidic acid and require phosphatidate binding for function (14, 15, 23, 33, 57). Our data are compatible with both of these models, and some additional work will be required to determine the mechanisms by which PLD activation is required for induction of the ERK cascade by PTH.

Finally, the details of how PTH activates PLD remain incompletely understood. A mechanism mediated by $G_{12/13}$ and RhoA has been proposed to be responsible for the activation of PLD in UMR-106 cells (27). This scheme, however, is somewhat paradoxical because stimulation of cells with PTH leads to the accumulation of cAMP, which in turn inhibits RhoA activity by direct phosphorylation (58). This effect has been linked to inhibition of PLD in neutrophils (59) and to overall cytoskeletal reorganization (58, 60). Thus, it remains unclear how PTH induces RhoA activation in a cAMP background. GPCR may activate PLD function by several other mechanisms. These include activation of small GTPases of the ARF family (61), or formation of macromolecular complexes that include PLD2 and the small GTPase Ral (37). Some GPCR, such as the μ-opioid receptor, interact directly with PLD2, although the regulation of PLD activity by this assembly still requires the activation of ARF GTPases (13). The potential role of these alternative mechanisms on PTH-dependent PLD activation remains to be explored.

Materials and Methods

Cell culture and transfection

ROS 17/2.8 cells were grown in DMEM/F12 medium supplemented with 10% fetal bovine serum (Invitrogen, Carlsbad, CA) and 1% penicillin/streptomycin solution at 37 C, 5% CO_2.

Chinese hamster ovary cells stable expressing HA-tagged human PTH1R, CHO-N10-R3, were maintained in Ham's F-12

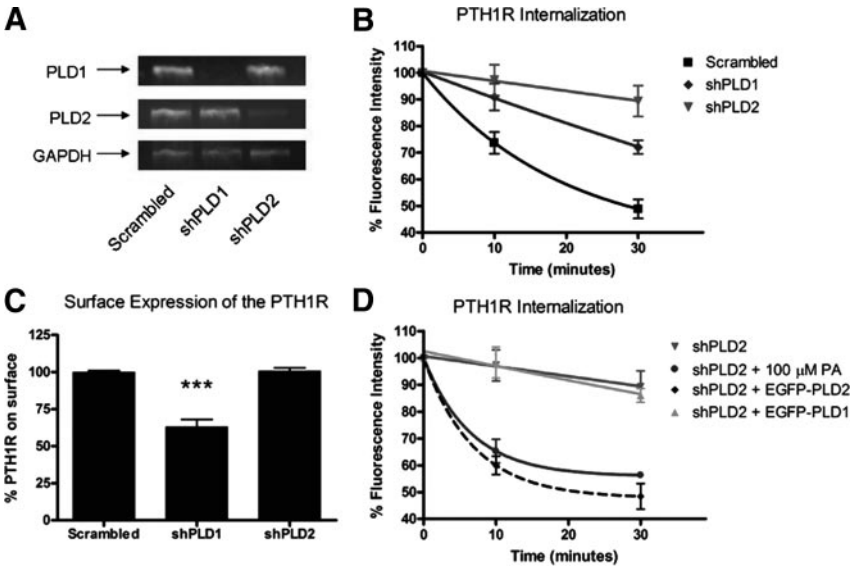

FIG. 10. Knockdown of PLD1 and PLD2 affects differentially the traffic of the PTH1R in ROS 17/2.8 cells. A, Knockdown of PLD1 and PLD2 with shRNA. ROS cells were transfected with plasmids coding for PLD1- and PLD2-specific shRNA (shPLD2) or with a plasmid coding for a scrambled shRNA construct. Transfected cells were selected with G418 for at least 2 wk. PLD1 and PLD2 expression was measured using semiquantitative PCR. Glyceraldehyde 3-phosphate dehydrogenase (GAPDH) expression was used as internal control. As shown, the transfected cells express reduced levels of PLD1 or PLD2 mRNA. B, Knockdown of PLD1 and PLD2 reduces the rate of internalization of the PTH1R. C, PLD1 knockdown reduces the expression of the PTH1R on the surface. D, Treatment with PA (100 μM dioleoyl PA) or overexpression of mouse WT-PLD2 reverts the effects of PLD2 knockdown on PTH1R internalization. In contrast, expression of human PLD1 cannot normalize PTH1R internalization. ***, $P < 0.005$.

medium (Mediatech Inc., Herndon, VA) with 10% fetal bovine serum. Transient transfection was performed using FUGENE 6 (Roche, Indianapolis, IN) according to the manufacturer's instructions. All experiments were performed 48 h after transfection.

Plasmids encoding scrambled shRNA, rat PLD1 shRNA, and rat PLD2 shRNA were described previously (19). The sequences used to silence PLD1 and PLD2 were ^{547}CTGGAAGAT TACTTGACAA (for PLD1) and ^{723}GGACTCC TTCCTGCTGTACA (for PLD2). PLD2 rescue experiments were performed using a mouse EGFP-PLD2 construct with a single nucleotide substitution (^{730}T→A). Expression of the rescue construct was verified measuring EGFP fluorescence. ROS cells stably expressing each shRNA were selected using 500 μg/ml G418 (Invitrogen).

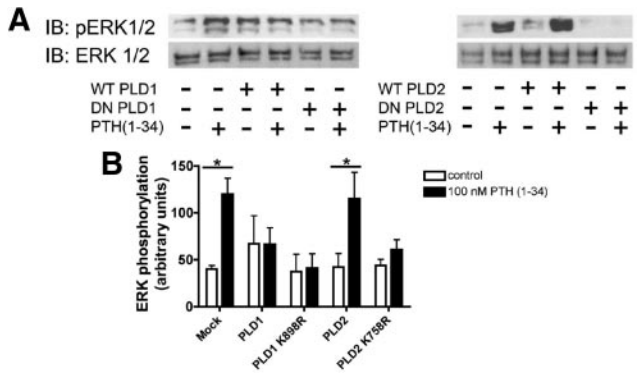

FIG. 11. PLD activity is necessary for PTH-dependent ERK phosphorylation. CHO-R3 cells were transfected with empty vector (mock), WT-, or DN-PLD1 and -PLD2 where indicated. Forty-eight hours after transfection, the cells were treated with 100 nM PTH(1–34) for 15 min. After incubation, the cells were scraped in Laemmli buffer. Extracted proteins were resolved by SDS-PAGE. Phosphorylated ERK (pERK) and total ERK were determined by immunoblotting (IB). A, Representative blot; B, summary of results obtained from three independent experiments. *, $P < 0.05$; **, $P < 0.01$ for the depicted comparisons.

PLD mutants

WT and catalytically inactive variants of PLD1 and PLD2 (K898R-PLD1 and K758R-PLD2) were previously described (14, 15) and fused to green fluorescent protein by subcloning into pEFGP-C1. Transfection efficiency was estimated from fluorescence microscopy data by determining the fraction of cells expressing the green fluorescent constructs. Transfection efficiency was better than 30% in all experiments.

PLD assays

Cells cultivated in six-well plates at 75% confluence were serum starved and labeled overnight with [^{3}H]palmitate (5 mCi/ml) in culture medium containing 0.1% BSA. Cells were stimulated with PTH(1–34) (100 nM) in the presence of 0.5% ethanol for the indicated times. At the end of the incubation, the cells were scraped and transferred to Eppendorf tubes, and the reaction was stopped by addition of chloroform/methanol (1:1). The lipid phase was extracted and developed by thin-layer chromatography (TLC) on silica gel 60 plates using ethyl acetate/trimethylpentane/acetic acid (9:5:2) as solvent. The position of major phospholipids was determined using standards (Avanti Biochemicals, Birmingham, AL) and autoradiography. The TLC plates were developed by autoradiography, and the radioactivity associated with each band was estimated by densitometry and quantified using ImageJ. In some cases, the TLC plates were scraped, and the total amount of radioactivity associated with each lipid species was determined by liquid scintillation counting. The data are expressed as band intensity/number of counts associated with the phosphatidylethanol spot normalized by total intensity/number of counts of lipid loaded.

RT-PCR

Quantification of PLD mRNA was conducted as previously described (35). Briefly, total cellular RNA was isolated using Trizol (Invitrogen) and transcribed into cDNA using a Clontech (Palo Alto, CA) Advantage RT-for-PCR kit. The resulting cDNA was used to amplify PLD1, PLD2, and GAPDH as described previously (35). PCR products were resolved using a 1.5% agarose gel, digitally photographed, and measured using ImageJ (National Institutes of Health, Bethesda, MD). Quantitative real-time PCR was performed on an Applied BioSystems (Foster City, CA) StepOne real-time PCR system using SYBR Green (QIAGEN, Valencia, CA) with the primers previously described. Negative control wells containing nuclease-free water instead of cDNA were used to check for amplicon contami-

nation. All samples were run in duplicate and normalized using GAPDH. A standard curve was generated using 10-fold dilutions of EGFP-PLD1 and EGFP-PLD2 plasmid. Both standard curves had a correlation coefficient greater than 0.98. Total copy number of each target was extrapolated from the standard curve. Copy number per cell was calculated by dividing the total copy number by the cell count and adjusting for transfection efficiency.

Immunocytochemistry and confocal microscopy

Cells were cultured on glass coverslips, transfected with the desired plasmids, and allowed to grow until 80% confluent. The coverslips were washed in PBS and fixed for 10 min in 4% paraformaldehyde in PBS at room temperature. Cells were permeabilized with 0.1% Triton X-100 in PBS for 10 min at room temperature. The samples were blocked with 3% BSA in PBS and then stained with either anti-HA, anti-EEA1, or anti ARF1 antibodies in 1% BSA in PBS for 2 h at room temperature. The samples were washed three times with PBS and incubated with respective secondary antibody (antimouse IgG or antirabbit IgG conjugated with either tetraethylrhodamine or fluorescein isothiocyanate). The cells were then washed with PBS (3×), mounted with gelvatol, and examined. An Olympus Fluoview 1000 confocal microscope was used for all experiments.

FACS

CHO-R3 cells were transiently transfected with EGFP fusion constructs of WT-PLD1, DN-PLD1, WT-PLD2, and DN-PLD2, as described above, using Fugene6. Forty-eight hours after transfection, the cells were switched to serum-free F-12 medium and stimulated with PTH(1–34) (100 nM) for 0, 10, or 30 min. After incubation, the cells were washed with PBS (pH 7.4) and fixed with 0.5% *p*-formaldehyde in PBS for 5 min at 4 C. The cells were washed with PBS and incubated with 3% BSA in PBS for 30 min to block nonspecific antibody binding. Subsequently, the cells were incubated with rabbit anti-HA antibody [Covance (Madison, WI) HA.11, 1:200] and antirabbit-Alexa-680 (Invitrogen; 1:500) for 1.5 h at room temperature, respectively. Finally, cells were scraped and analyzed by FACS. EGFP/cherryFP fluorescence was used to gate cells transfected with the PLD or shRNA constructs.

Statistical analysis

Each experiment was repeated at least three times. Statistical significance was determined using ANOVA followed by column statistic comparisons using the analysis routines built in GraphPad Prism. Quantitative image analyses were performed using ImageJ. Colocalization analyses were done using the ImageJ built-in plug-ins for Pearson correlation. The Pearson correlation coefficient is defined as the ratio of the covariance of the red and green color images divided by the product of the SD of the normalized image intensities. Differences with $P \leq 0.05$ were considered significant.

Acknowledgments

Address all correspondence and requests for reprints to: Dr. Guillermo Romero Department of Pharmacology and Chemical Biology, E1355 Biomedical Research Tower University of Pittsburgh, Pittsburgh, Pennsylvania 15261. E-mail: ggr@pitt.edu.

This work was supported by DK-54171 from the National Institutes of Health (to P.A.F.) and by a grant from the Office of the senior Vice Chancellor for the Health Sciences of the University of Pittsburgh (to G.R.). D.W. was supported by Training Grants GM-08424 and DK-083211.

Disclosure Summary: The authors have nothing to disclose.

References

1. **Abou-Samra AB, Jüppner H, Force T, Freeman MW, Kong XF, Schipani E, Urena P, Richards J, Bonventre JV, Potts Jr JT, Kronenberg HM, Segre GV** 1992 Expression cloning of a common receptor for parathyroid hormone and parathyroid hormone-related peptide from rat osteoblast-like cells: a single receptor stimulates intracellular accumulation of both cAMP and inositol trisphosphates and increases intracellular free calcium. Proc Natl Acad Sci USA 89:2732–2736
2. **Offermanns S, Iida-Klein A, Segre GV, Simon MI** 1996 Gαq family members couple parathyroid hormone (PTH)/PTH-related peptide and calcitonin receptors to phospholipase C in COS-7 cells. Mol Endocrinol 10:566–574
3. **Friedman PA, Gesek FA, Morley P, Whitfield JF, Willick GE** 1999 Cell-specific signaling and structure-activity relations of parathyroid hormone analogs in mouse kidney cells. Endocrinology 140:301–309
4. **Ferrari SL, Behar V, Chorev M, Rosenblatt M, Bisello A** 1999 Endocytosis of ligand-human parathyroid hormone receptor 1 complexes is protein kinase C-dependent and involves β-arrestin2. Real-time monitoring by fluorescence microscopy. J Biol Chem 274:29968–29975
5. **Sneddon WB, Magyar CE, Willick GE, Syme CA, Galbiati F, Bisello A, Friedman PA** 2004 Ligand-selective dissociation of activation and internalization of the parathyroid hormone (PTH) receptor: conditional efficacy of PTH peptide fragments. Endocrinology 145:2815–2823
6. **Vilardaga JP, Krasel C, Chauvin S, Bambino T, Lohse MJ, Nissenson RA** 2002 Internalization determinants of the parathyroid hormone receptor differentially regulate β-arrestin/receptor association. J Biol Chem 277:8121–8129
7. **Wheeler D, Sneddon WB, Wang B, Friedman PA, Romero G** 2007 NHERF-1 and the cytoskeleton regulate the traffic and membrane dynamics of G protein-coupled receptors. J Biol Chem 282:25076–25087
8. **De Camilli P, Emr SD, McPherson PS, Novick P** 1996 Phosphoinositides as regulators in membrane traffic. Science 271:1533–1539
9. **Roth MG** 1999 Lipid regulators of membrane traffic through the Golgi complex. Trends Cell Biol 9:174–179
10. **Hammond SM, Altshuller YM, Sung TC, Rudge SA, Rose K, Engebrecht J, Morris AJ, Frohman MA** 1995 Human ADP-ribosylation factor-activated phosphatidylcholine-specific phospholipase D defines a new and highly conserved gene family. J Biol Chem 270:29640–29643
11. **Morris AJ, Engebrecht J, Frohman MA** 1996 Structure and regulation of phospholipase D. Trends Pharmacol Sci 17:182–185
12. **Kam Y, Exton JH** 2001 Phospholipase D activity is required for actin stress fiber formation in fibroblasts. Mol Cell Biol 21:4055–4066
13. **Koch T, Brandenburg LO, Schulz S, Liang Y, Klein J, Hollt V** 2003 ADP-ribosylation factor-dependent phospholipase D2 activation is required for agonist-induced μ-opioid receptor endocytosis. J Biol Chem 278:9979–9985
14. **Rizzo MA, Shome K, Vasudevan C, Stolz DB, Sung TC, Frohman MA, Watkins SC, Romero G** 1999 Phospholipase D and its product, phosphatidic acid, mediate agonist-dependent raf-1 translocation to the plasma membrane and the activation of the mitogen-activated protein kinase pathway. J Biol Chem 274:1131–1139

15. **Rizzo MA, Shome K, Watkins SC, Romero G** 2000 The recruitment of Raf-1 to membranes is mediated by direct interaction with phosphatidic acid and is independent of association with Ras. J Biol Chem 275:23911–23918
16. **Colley WC, Sung TC, Roll R, Jenco J, Hammond SM, Altshuller Y, Bar-Sagi D, Morris AJ, Frohman MA** 1997 Phospholipase D2, a distinct phospholipase D isoform with novel regulatory properties that provokes cytoskeletal reorganization. Curr Biol 7:191–201
17. **Gibbs TC, Meier KE** 2000 Expression and regulation of phospholipase D isoforms in mammalian cell lines. J Cell Physiol 182:77–87
18. **Meier KE, Gibbs TC, Knoepp SM, Ella KM** 1999 Expression of phospholipase D isoforms in mammalian cells. Biochim Biophys Acta 1439:199–213
19. **Du G, Huang P, Liang BT, Frohman MA** 2004 Phospholipase D2 localizes to the plasma membrane and regulates angiotensin II receptor endocytosis. Mol Biol Cell 15:1024–1030
20. **Arneson LS, Kunz J, Anderson RA, Traub LM** 1999 Coupled inositide phosphorylation and phospholipase D activation initiates clathrin-coat assembly on lysosomes. J Biol Chem 274:17794–17805
21. **Koch T, Brandenburg LO, Liang Y, Schulz S, Beyer A, Schröder H, Höllt V** 2004 Phospholipase D2 modulates agonist-induced μ-opioid receptor desensitization and resensitization. J Neurochem 88:680–688
22. **Lehman N, Ledford B, Di Fulvio M, Frondorf K, McPhail LC, Gomez-Cambronero J** 2007 Phospholipase D2-derived phosphatidic acid binds to and activates ribosomal p70 S6 kinase independently of mTOR. FASEB J 21:1075–1087
23. **Zhao C, Du G, Skowronek K, Frohman MA, Bar-Sagi D** 2007 Phospholipase D2-generated phosphatidic acid couples EGFR stimulation to Ras activation by Sos. Nat Cell Biol 9:706–712
24. **Shen Y, Xu L, Foster DA** 2001 Role for phospholipase D in receptor-mediated endocytosis. Mol Cell Biol 21:595–602
25. **Corrotte M, Chasserot-Golaz S, Huang P, Du G, Ktistakis NT, Frohman MA, Vitale N, Bader MF, Grant NJ** 2006 Dynamics and function of phospholipase D and phosphatidic acid during phagocytosis. Traffic 7:365–377
26. **Iyer SS, Barton JA, Bourgoin S, Kusner DJ** 2004 Phospholipases D1 and D2 coordinately regulate macrophage phagocytosis. J Immunol 173:2615–2623
27. **Singh AT, Gilchrist A, Voyno-Yasenetskaya T, Radeff-Huang JM, Stern PH** 2005 Gα12/Gα13 subunits of heterotrimeric G proteins mediate parathyroid hormone activation of phospholipase D in UMR-106 osteoblastic cells. Endocrinology 146:2171–2175
28. **Toda K, Nogami M, Murakami K, Kanaho Y, Nakayama K** 1999 Colocalization of phospholipase D1 and GTP-binding-defective mutant of ADP-ribosylation factor 6 to endosomes and lysosomes. FEBS Lett 442:221–225
29. **Du G, Altshuller YM, Vitale N, Huang P, Chasserot-Golaz S, Morris AJ, Bader MF, Frohman MA** 2003 Regulation of phospholipase D1 subcellular cycling through coordination of multiple membrane association motifs. J Cell Biol 162:305–315
30. **Lucocq J, Manifava M, Bi K, Roth MG, Ktistakis NT** 2001 Immunolocalisation of phospholipase D1 on tubular vesicular membranes of endocytic and secretory origin. Eur J Cell Biol 80:508–520
31. **Wang B, Bisello A, Yang Y, Romero GG, Friedman PA** 2007 NHERF1 regulates parathyroid hormone receptor membrane retention without affecting recycling. J Biol Chem 282:36214–36222
32. **Yamamoto I, Shigeno C, Potts Jr JT, Segre GV** 1988 Characterization and agonist-induced down-regulation of parathyroid hormone receptors in clonal rat osteosarcoma cells. Endocrinology 122:1208–1217
33. **Andresen BT, Rizzo MA, Shome K, Romero G** 2002 The role of phosphatidic acid in the regulation of the Ras/MEK/Erk signaling cascade. FEBS Lett 531:65–68
34. **Rizzo M, Romero G** 2002 Pharmacological importance of phospholipase D and phosphatidic acid in the regulation of the mitogen-activated protein kinase cascade. Pharmacol Ther 94:35–50
35. **Andresen BT, Jackson EK, Romero GG** 2001 Angiotensin II signaling to phospholipase D in renal microvascular smooth muscle cells in SHR. Hypertension 37:635–639
36. **Shome K, Rizzo MA, Vasudevan C, Andresen B, Romero G** 2000 The activation of phospholipase D by endothelin-1, angiotensin II, and platelet-derived growth factor in vascular smooth muscle A10 cells is mediated by small G proteins of the ADP-ribosylation factor family. Endocrinology 141:2200–2208
37. **Bhattacharya M, Babwah AV, Godin C, Anborgh PH, Dale LB, Poulter MO, Ferguson SS** 2004 Ral and phospholipase D2-dependent pathway for constitutive metabotropic glutamate receptor endocytosis. J Neurosci 24:8752–8761
38. **Fang Y, Park IH, Wu AL, Du G, Huang P, Frohman MA, Walker SJ, Brown HA, Chen J** 2003 PLD1 regulates mTOR signaling and mediates Cdc42 activation of S6K1. Curr Biol 13:2037–2044
39. **Andresen BT, Romero GG, Jackson EK** 2004 AT2 receptors attenuate AT1 receptor-induced phospholipase D activation in vascular smooth muscle cells. J Pharmacol Exp Ther 309:425–431
40. **Andresen BT, Shome K, Jackson EK, Romero GG** 2005 AT2 receptors cross talk with AT1 receptors through a nitric oxide- and RhoA-dependent mechanism resulting in decreased phospholipase D activity. Am J Physiol Renal Physiol 288:F763–F770
41. **Yang Z, Asico LD, Yu P, Wang Z, Jones JE, Bai RK, Sibley DR, Felder RA, Jose PA** 2005 D5 dopamine receptor regulation of phospholipase D. Am J Physiol Heart Circ Physiol 288:H55–H61
42. **Hammond SM, Jenco JM, Nakashima S, Cadwallader K, Gu Q, Cook S, Nozawa Y, Prestwich GD, Frohman MA, Morris AJ** 1997 Characterization of two alternately spliced forms of phospholipase D1. Activation of the purified enzymes by phosphatidylinositol 4,5-bisphosphate, ADP-ribosylation factor, and Rho family monomeric GTP-binding proteins and protein kinase C-α. J Biol Chem 272:3860–3868
43. **Zeniou-Meyer M, Zabari N, Ashery U, Chasserot-Golaz S, Haeberlé AM, Demais V, Bailly Y, Gottfried I, Nakanishi H, Neiman AM, Du G, Frohman MA, Bader MF, Vitale N** 2007 Phospholipase D1 production of phosphatidic acid at the plasma membrane promotes exocytosis of large dense-core granules at a late stage. J Biol Chem 282:21746–21757
44. **Han L, Stope MB, de Jesús ML, Oude Weernink PA, Urban M, Wieland T, Rosskopf D, Mizuno K, Jakobs KH, Schmidt M** 2007 Direct stimulation of receptor-controlled phospholipase D1 by phospho-cofilin. Embo J 26:4189–4202
45. **Mahon MJ, Segre GV** 2004 Stimulation by parathyroid hormone of a NHERF-1-assembled complex consisting of the parathyroid hormone I receptor, phospholipase Cβ, and actin increases intracellular calcium in opossum kidney cells. J Biol Chem 279:23550–23558
46. **Sneddon WB, Syme CA, Bisello A, Magyar CE, Rochdi MD, Parent JL, Weinman EJ, Abou-Samra AB, Friedman PA** 2003 Activation-independent parathyroid hormone receptor internalization is regulated by NHERF1 (EBP50). J Biol Chem 278:43787–43796
47. **Mahon MJ, Donowitz M, Yun CC, Segre GV** 2002 Na^+/H^+ exchanger regulatory factor 2 directs parathyroid hormone 1 receptor signalling. Nature 417:858–861
48. **Daaka Y, Luttrell LM, Ahn S, Della Rocca GJ, Ferguson SS, Caron MG, Lefkowitz RJ** 1998 Essential role for G protein-coupled receptor endocytosis in the activation of mitogen-activated protein kinase. J Biol Chem 273:685–688
49. **Pierce KL, Maudsley S, Daaka Y, Luttrell LM, Lefkowitz RJ** 2000 Role of endocytosis in the activation of the extracellular signal-regulated kinase cascade by sequestering and nonsequestering G protein-coupled receptors. Proc Natl Acad Sci USA 97:1489–1494
50. **Ahn S, Nelson CD, Garrison TR, Miller WE, Lefkowitz RJ** 2003 Desensitization, internalization, and signaling functions of β-arrestins demonstrated by RNA interference. Proc Natl Acad Sci USA 100:1740–1744
51. **Sneddon WB, Liu F, Gesek FA, Friedman PA** 2000 Obligate mitogen-activated protein kinase activation in parathyroid hormone

stimulation of calcium transport but not calcium signaling. Endocrinology 141:4185–4193
52. **Lefkowitz RJ, Whalen EJ** 2004 β-Arrestins: traffic cops of cell signaling. Curr Opin Cell Biol 16:162–168
53. **Gesbert F, Sauvonnet N, Dautry-Varsat A** 2004 Clathrin-independent endocytosis and signalling of interleukin 2 receptors IL-2R endocytosis and signalling. Curr Top Microbiol Immunol 286: 119–148
54. **Wu C, Lai CF, Mobley WC** 2001 Nerve growth factor activates persistent Rap1 signaling in endosomes. J Neurosci 21:5406–5416
55. **Galperin E, Sorkin A** 2008 Endosomal targeting of MEK2 requires RAF, MEK kinase activity and clathrin-dependent endocytosis. Traffic 9:1776–1790
56. **Xue L, Lucocq J** 1998 ERK2 signalling from internalised epidermal growth factor receptor in broken A431 cells. Cell Signal 10:339–348
57. **Kraft CA, Garrido JL, Fluharty E, Leiva-Vega L, Romero G** 2008 Role of phosphatidic acid in the coupling of the ERK cascade. J Biol Chem 283:36636–36645
58. **Lang P, Gesbert F, Delespine-Carmagnat M, Stancou R, Pouchelet M, Bertoglio J** 1996 Protein kinase A phosphorylation of RhoA mediates the morphological and functional effects of cyclic AMP in cytotoxic lymphocytes. EMBO J 15:510–519
59. **Kwak JY, Uhlinger DJ** 2000 Downregulation of phospholipase D by protein kinase A in a cell-free system of human neutrophils. Biochem Biophys Res Commun 267:305–310
60. **Egan JJ, Gronowicz G, Rodan GA** 1991 Parathyroid hormone promotes the disassembly of cytoskeletal actin and myosin in cultured osteoblastic cells: mediation by cyclic AMP. J Cell Biochem 45:101–111
61. **Mitchell R, Robertson DN, Holland PJ, Collins D, Lutz EM, Johnson MS** 2003 ADP-ribosylation factor-dependent phospholipase D activation by the M3 muscarinic receptor. J Biol Chem 278:33818–33830

THE JOURNAL OF BIOLOGICAL CHEMISTRY VOL. 285, NO. 19, pp. 14756–14763, May 7, 2010

Parathyroid Hormone Receptor Directly Interacts with Dishevelled to Regulate β-Catenin Signaling and Osteoclastogenesis*[S]

Received for publication, January 11, 2010, and in revised form, February 26, 2010 Published, JBC Papers in Press, March 8, 2010, DOI 10.1074/jbc.M110.102970

Guillermo Romero[‡], W. Bruce Sneddon[‡], Yanmei Yang[‡], David Wheeler[‡], Harry C. Blair[§], and Peter A. Friedman[‡1]

From the [‡]Laboratory for G Protein-coupled Receptor Biology, Department of Pharmacology and Chemical Biology, and the [§]Department of Pathology, University of Pittsburgh School of Medicine, Pittsburgh, Pennsylvania 15261

Bone growth and remodeling depend upon the opposing rates of bone formation and resorption. These functions are regulated by intrinsic seven transmembrane-spanning receptors, the parathyroid hormone receptor (PTH1R) and frizzled (FZD), through their respective ligands, parathyroid hormone (PTH) and Wnt. FZD activation of canonical β-catenin signaling requires the adapter protein Dishevelled (Dvl). We identified a Dvl-binding motif in the PTH1R. Here, we report that the PTH1R activates the β-catenin pathway by directly recruiting Dvl, independent of Wnt or LRP5/6. PTH1R coimmunoprecipitated with Dvl. Deleting the carboxyl-terminal PTH1R PDZ-recognition domain did not abrogate PTH1R-Dvl interactions; nor did truncating the receptor at position 480. However, further deletion eliminating the putative Dvl recognition domain abolished PTH1R interactions with Dvl. PTH activated β-catenin in a time- and concentration-dependent manner and translocated β-catenin to the nucleus. β-Catenin activation was inhibited by Dvl2 dominant negatives and by short hairpin RNA sequences targeted against Dvl2. PTH-induced osteoclastogenesis was also inhibited by Dvl2 dominant negative mutants. These findings demonstrate that G protein-coupled receptors other than FZD directly activate β-catenin signaling, thereby mimicking many of the functions of the canonical Wnt-FZD pathway. The distinct modes whereby FZD and PTH1R activate β-catenin control convergent or divergent effects on osteoblast differentiation, and osteoclastogenesis may arise from PTH1R-induced second messenger phosphorylation.

Wnts are secreted lipid-modified glycoproteins that act as ligands to stimulate signal transduction pathways through FZD (frizzled) receptors and LRP5/6 (lipoprotein receptor-related protein 5/6) co-receptors. Canonical and non-canonical Wnt signaling pathways have been described (1). In the canonical pathway, in the absence of Wnt ligands, β-catenin is targeted to a destruction complex with APC (adenomatous polyposis coli), CK1 (casein kinase 1), GSK3β (glycogen synthase kinase 3β), and axin. Amino-terminal phosphorylation by CK1 and GSK3β followed by subsequent ubiquitination targets β-catenin for proteasomal degradation (2). Wnt binding to cognate FZD receptors and LRP5/6 causes recruitment of the PDZ (PSD-95, Discs-large, and ZO-1) protein Dvl (Dishevelled) to the plasma membrane by direct interaction with FZD receptors. The recruitment of Dvl to the plasma membrane results in the formation of Dvl oligomers, which interact with axin. Parallel phosphorylation of the co-receptors LRP5 and LRP6 induces binding to axin, resulting in disruption of the destruction complex. As a consequence, β-catenin escapes proteasomal degradation and translocates to the nucleus, where it regulates the activity of the transcription factors TCF (T cell factor) and Lef (lymphocyte enhancer-binding factor).

Ten FZD receptors constitute a distinct family of seven transmembrane-spanning receptors (3). Whether or not they couple to G proteins remains controversial (4). Notably, they bear the closest phylogenetic relation to Family B1 GPCRs including the type 1 parathyroid hormone receptor (PTH1R) (5). Four of the 10 frizzled receptors (FZD1, -2, -4, and -7) contain a canonical carboxyl-terminal PDZ recognition domain, (D/E)(S/T)$X\Phi$, where Φ represents a hydrophobic residue, generally L/I/V but sometimes M, as in the PTH1R (6, 7). This motif mediates interactions with PDZ proteins, such as NHERF1 (Na/H exchange regulatory factor-1) (8).

Bone growth and remodeling are regulated by parallel signaling pathways involving the PTH1R and FZD (9). Considerable evidence now strongly implicates Wnt/FZD signaling in regulating bone formation (9–11). β-Catenin signaling is required for suppression of chondrocyte differentiation and induction of osteoblastogenesis. Multiple lines of genetic evidence establish the critical participation of canonical β-catenin activity for early osteoblast differentiation (12). Acting on mature osteoblasts, stimulation of the PTH1R produces RANKL (receptor activator of NFκB ligand), which binds the RANK (receptor activator of NFκB) receptor on osteoclast precursors and induces formation of osteoclasts by signaling through NFκB[2] and JNK. Homologous recombination of PTH1R, RANKL, or RANK results in mice with profound bone phenotypes (13–15). Gene knock-out of elements of FZD and the canonical β-cate-

* This work was supported, in whole or in part, by National Institutes of Health Grants DK54171 (to P. A. F.) and GM08208 (to D. W.).

[S] The on-line version of this article (available at http://www.jbc.org) contains supplemental Video 1 and Figs. 1–3.

[1] To whom correspondence should be addressed: Dept. of Pharmacology and Chemical Biology, University of Pittsburgh School of Medicine, W1340 Biomedical Science Tower, 200 Lothrop St., Pittsburgh, PA 15261. E-mail: paf10@pitt.edu.

[2] The abbreviations used are: NFκB, nuclear factor-κB; JNK, Jun kinase; PTH, parathyroid hormone; CHO, Chinese hamster ovary; TIRF, total internal reflection fluorescence; TRITC, tetramethylrhodamine isothiocyanate; EGFP, enhanced green fluorescent protein; GPCR, G protein-coupled receptor; CREB, cAMP-response element-binding protein; shRNA, short hairpin RNA; HA, hemagglutinin.

nin signaling pathway likewise produce profound disruption of normal bone formation or turnover (9–11). Recent work shows that PTH promotes β-catenin activation (16–18). The interaction between PTH1R and FZD signaling pathways is largely unexplored. Nissenson and co-workers (19) observed that PTH increased FZD1/2 mRNA levels in UMR cells. Other findings establish that PTH increases β-catenin levels in UMR, MC3T3-E1, and SAOS cells (16, 17, 20) and that ablation of the Wnt antagonist, secreted frizzled-related protein, blunts the anabolic action of PTH (21). More recently, Cao and co-workers (18) showed that PTH1R signals through LRP6. Further evidence for the interaction of PTH and β-catenin pathways in regulating bone turnover comes from studies showing that overexpression of sFRP1 attenuates PTH-dependent bone anabolism (22). Together, these and other studies imply that the actions of PTH may be partially mediated through β-catenin signaling. The mechanisms underlying PTH1R and FZD cross-talk are unknown. We now describe multiple lines of cross-talk between the two pathways and show that PTH activates β-catenin in an LRP- and Wnt-independent manner.

EXPERIMENTAL PROCEDURES

Cell Culture—CHO cells (Invitrogen) were cultured in Ham's F-12 medium supplemented with 10% fetal bovine serum, 100 units/ml penicillin, 100 μg/ml streptomycin, and 10 μg/ml blasticidin. UMR-106 and UAMS-32P cells were cultured in Dulbecco's modified Eagle's medium/F-12 medium supplemented with 10% fetal bovine serum, 100 units/ml penicillin, and 100 μg/ml streptomycin. MC4 cells were obtained from Dr. G. Xiao (University of Pittsburgh) and cultured in α-modified minimum essential medium with 10% fetal bovine serum, 100 units/ml penicillin, and 100 μg/ml streptomycin. Cells were maintained at 37 °C in a humidified atmosphere of 5% CO_2, 95% air.

Short Hairpin RNA Treatments—The expression of Dvl1, Dvl2, and Dvl3 in UMR cells was determined by quantitative RT-PCR. Dvl2 mRNA accounted for over 90% of the Disheveled mRNA expressed in these cells (not shown). Constructs coding for specific shRNA targeted against rat Dvl2 were purchased from SA Biosciences (Frederick, MD). Four different constructs were screened for their ability to knock down Dvl2 expression in UMR cells. The two most efficient constructs were selected for further use. The sequences targeted by these constructs (shDvl2-1 and shDvl2-2, respectively) are GCCTACCTTCTCCTACCAATACC and TTCAACTTGGTGCTCTTCTTAGT. UMR-106 cells were co-transfected with 1 μg of TOP-Flash luciferase reporter and 2 μg of either a scrambled shRNA or shDvl2 plasmids. Two days following transfection, the cells were treated with either vehicle, 100 ng/ml recombinant Wnt3a, 100 nM PTH(1–34), or 5 mM LiCl for 24 h. Cell lysates were assayed for luciferase expression using a commercial luciferase assay system (Promega, Madison, WI) as per the manufacturer's instructions.

Coimmunoprecipitation and Immunoblot Analysis—Interactions of PTH1R or FZD with Dvl were analyzed as described (23). Briefly, 6-well plates of the indicated cells were transiently transfected with HA-PTH1R, HA-PTH1R(ETVA), HA-PTH1R(480-stop), HA-PTH1R(470-stop), HA-FZD, Myc-Dvl, or the respective empty vector. 48 h later, the cells were lysed with Nonidet P-40 (50 mM Tris, 150 mM NaCl, 5 mM EDTA, 0.5% Nonidet P-40) supplemented with protease inhibitor mixture I and incubated for 15 min on ice. Solubilized materials were incubated overnight at 4 °C with HA.11 monoclonal affinity matrix. Total lysates and immunoprecipitated protein, eluted by the addition of SDS sample buffer, were analyzed by SDS-polyacrylamide gels and transferred to Immobilon-P membranes (Millipore) using the semidry method (Bio-Rad). Membranes were blocked overnight at 4 °C with 5% nonfat dried milk in Tris-buffered saline plus Tween 20 (TBST) and incubated with the indicated antibodies (HA (Covance, catalog no. MMS-101R), Myc (Santa Cruz Biotechnology, Inc. (Santa Cruz, CA), catalog no. SC-40), active β-catenin (Millipore, catalog no. 05-665), or β-catenin (Millipore, catalog no. 06-734)) for 2 h at room temperature. The membranes were then washed and incubated with goat anti-rabbit IgG or sheep anti-mouse IgG conjugated to horseradish peroxidase at a 1:5000 dilution for 1 h at room temperature. Protein bands were visualized with a luminol-based enhanced chemiluminescence substrate.

β-Catenin—MC4 cells were passaged onto 6-well plates and 24 h later were transfected with 1 μg/well TopFlash (Super 8× TopFlash, Addgene) and 1 μg/well Xdd1, a mutant of *Xenopus* Xdsh1 harboring a PDZ domain deletion (24), or empty vector, as indicated, using FuGENE 6 (Roche Applied Science). 48 h after transfection, cells were treated with 100 nM PTH(1–34) for 6 h. Lysates were prepared using Reporter Lysis Buffer (Promega, catalog no. E-3971). Luciferase activity was assayed using the BrightGlo luciferase assay system (Promega, catalog no. E-2620). 10 μl of lysate was added to a single tube. An equal volume of BrightGlo substrate was then added, and luminescence was measured for 10 s in a Turner BioSystems luminometer (model TD-20/20).

Imaging—Myc- and mRFP1-tagged Dvl2 constructs were obtained from T. Kirchhausen (Harvard Medical School). Live cell imaging of the translocation of mRFP1-Dvl2 to the plasma membrane was done by confocal microscopy using a Zeiss LSM5 equipped with a Harvard Biosystems incubation chamber maintained at 37 °C. Images were collected every 20 s.

To measure β-catenin translocation to the nucleus, ROS 17/2.8 cells were treated with 100 nM PTH(1–34) for 8 h, fixed, permeabilized, blocked with 5% goat serum, and incubated with a commercial anti-β-catenin antibody (Millipore). β-Catenin was detected using a TRITC-labeled secondary antibody. The cells were then examined using an Olympus Fluoview 1000 confocal microscope equipped with 405- and 561-nm lasers.

To measure PTH1R internalization, cells were co-transfected with a human EGFP-tagged PTH1R and mRFP-Dvl2. Receptor internalization was measured using total internal reflection fluorescence (TIRF) microscopy as described (25). Briefly, cells expressing both PTH1R-EGFP and mRFP-Dvl2 were identified by epifluorescence. The cells were then challenged with 100 nM PTH(1–34), and the disappearance of the surface-delimited PTH1R-EGFP was determined by TIRF. Data were collected at 20-s intervals for up to 20 min. The rate of internalization was determined from the fit of the collected data to a single exponential (25).

Osteoclastogenesis—Nonadherent bone marrow cells were prepared by removing femurs from 30–90-day-old C57BL/6J mice and flushing the marrow cavity with minimum essential medium (Invitrogen) containing 15% fetal bovine serum (Hyclone). Marrow cells were seeded at a density of 2.5×10^5 cells/cm^2 in the same medium and cultured for 48 h. Nonadherent cells were collected and seeded at a density of 2×104 cells/cm^2 on a cushion of UAMS-32 osteoblastic cells in minimum essential medium containing 10% fetal bovine serum. PTH(1–34) was added at the indicated concentrations, and the co-cultures were maintained at 37 °C in 5% CO_2. On day 3, one-half of the medium was replaced with fresh medium. After 6–8 days, cells were fixed and stained for tartrate-resistant acid phosphatase. The plate was scanned, and staining density was determined with Image J (National Institutes of Health, Bethesda, MD).

Statistics—Data are presented as the mean ± S.E., where n indicates the number of independent experiments. Curve fitting and data analysis were performed using GraphPad Prism (GraphPad Software, Inc., San Diego, CA). Multiple comparisons were evaluated by analysis of variance with post-test repeated measures analyzed by the Bonferroni procedure. Differences greater than $p \leq 0.05$ were assumed to be significant.

RESULTS

Direct Interactions between PTH1R and Dvl—Recruitment of Dvl to the plasma membrane is mediated by direct interactions between FZD and the PDZ domain of Dvl proteins. These interactions occur primarily through the binding of a critical region (KT*XXX*W) within the proximal portion of the carboxyl terminus of all 10 FZD receptors (26). Analysis of the PTH1R sequence revealed the presence of a similar motif (KSWSRW; see Fig. 1*A*). The putative Dvl-binding domain of the PTH1R starts at position 472 in a portion of the intracellular tail topologically comparable with that of FZD. We hypothesized that the PTH1R controls the β-catenin pathway by binding to this domain of Dvl.

To determine if the PTH1R interacts with Dvl proteins, we performed co-immunoprecipitation experiments using HA-tagged PTH1R and Myc-tagged Dvl2. As shown in Fig. 1, *B* and *C*, the PTH1R co-immunoprecipitates with Dvl2. To identify the structural determinants required for PTH1R interactions with Dvl2, we co-transfected the Myc-Dvl2 construct with various HA-tagged PTH1R mutants and performed additional coimmunoprecipitation studies. The results are shown in Fig. 1*D*. Wild-type PTH1R (ETVM) co-immunoprecipitated with Dvl2 (*lane 1*). It should be noted that the PTH1R sequence contains a canonical carboxyl-terminal PDZ ligand (^{590}ETVM). This motif is not responsible for Dvl binding because a PTH1R harboring a mutated carboxyl-terminal PDZ recognition domain (ETVA) bound Dvl2 comparably with the wild type receptor (*lane 2*). Mutation of ETVM to ETVA is sufficient to abolish PTH1R interaction with the PDZ protein NHERF1 (27). Likewise, a truncated PTH1R lacking the PDZ-binding domain but bearing the putative Dvl recognition domain (480-stop) also co-immunoprecipitated with Dvl2 (*lane 3*). This finding demonstrates that PTH1R interactions with Dvl are not mediated by the carboxyl-terminal canonical PDZ-binding motif of the PTH1R. Importantly, a PTH1R lacking the putative Dvl-binding domain (470-stop) failed to co-immunoprecipitate with Dvl (*lane 4*), although it was well expressed (*bottom*). These findings show that the PTH1R interacts with Dvl through a specific recognition sequence located between residues 470 and 480. This result supports the hypothesis that the ^{472}KSWSRW sequence in PTH1R (Fig. 1*A*) constitutes the Dvl-binding motif.

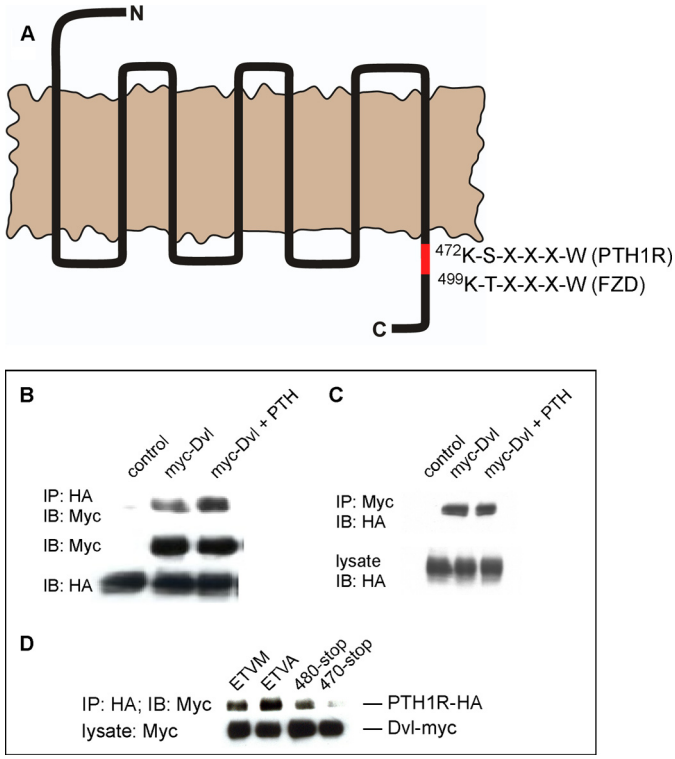

FIGURE 1. **Dvl interactions with the PTH1R.** *A*, seven-transmembrane receptor model showing sequence and common location of the Dvl-binding domain in PTH1R and FZD. A PDZ recognition motif is present at the carboxyl terminus of the PTH1R and of FZD1, -2, -4, and -7. *B*, interactions between PTH1R and Dvl. Coimmunoprecipitation experiments were conducted on CHO-N10 cells stably expressing a human HA-tagged PTH1R construct (23) that were transfected with Myc-Dvl2. Where indicated, cells were treated with 100 nM PTH(1–34) (15 min). The HA-PTH1R construct was immunoprecipitated (*IP*), and the presence of Myc-Dvl2 in the immunoprecipitate was determined by immunoblotting (*IB*). *C*, interactions between PTH1R and Dvl. CHO-N10 cells stably expressing HA-PTH1R were transfected with Myc-Dvl2. Cell lysates were immunoprecipitated with specific anti-Myc antibody, and the presence of the PTH1R in the immunoprecipitate was determined using anti-HA antibodies. *D*, the interactions of the PTH1R with Dvl2 are mediated by an amino acid sequence contained between residues 470 and 480 of the PTH1R. CHO-N10 cells were transfected with wild-type PTH1R (ETVM), a receptor harboring a carboxyl-terminal mutation that abolishes classical PDZ-PDZ domain interactions (ETVA), or receptor forms truncated at position 480 or 470. Immunoprecipitation and detection were performed as described (23, 51).

PTH Activation and Stabilization of β-Catenin—A defining characteristic of Wnt signaling pathways is ligand-induced redistribution and subsequent oligomerization of Dvl proteins (28). Fig. 2*A* shows that PTH promotes translocation of Dvl to the cell membrane. CHO cells expressing PTH1R-EGFP (*green*) were transiently transfected with red fluorescent mRFP1-Dvl2. Images were collected at 20-s intervals. Before the addition of PTH(1–34), the PTH1R was membrane-delimited, and Dvl2

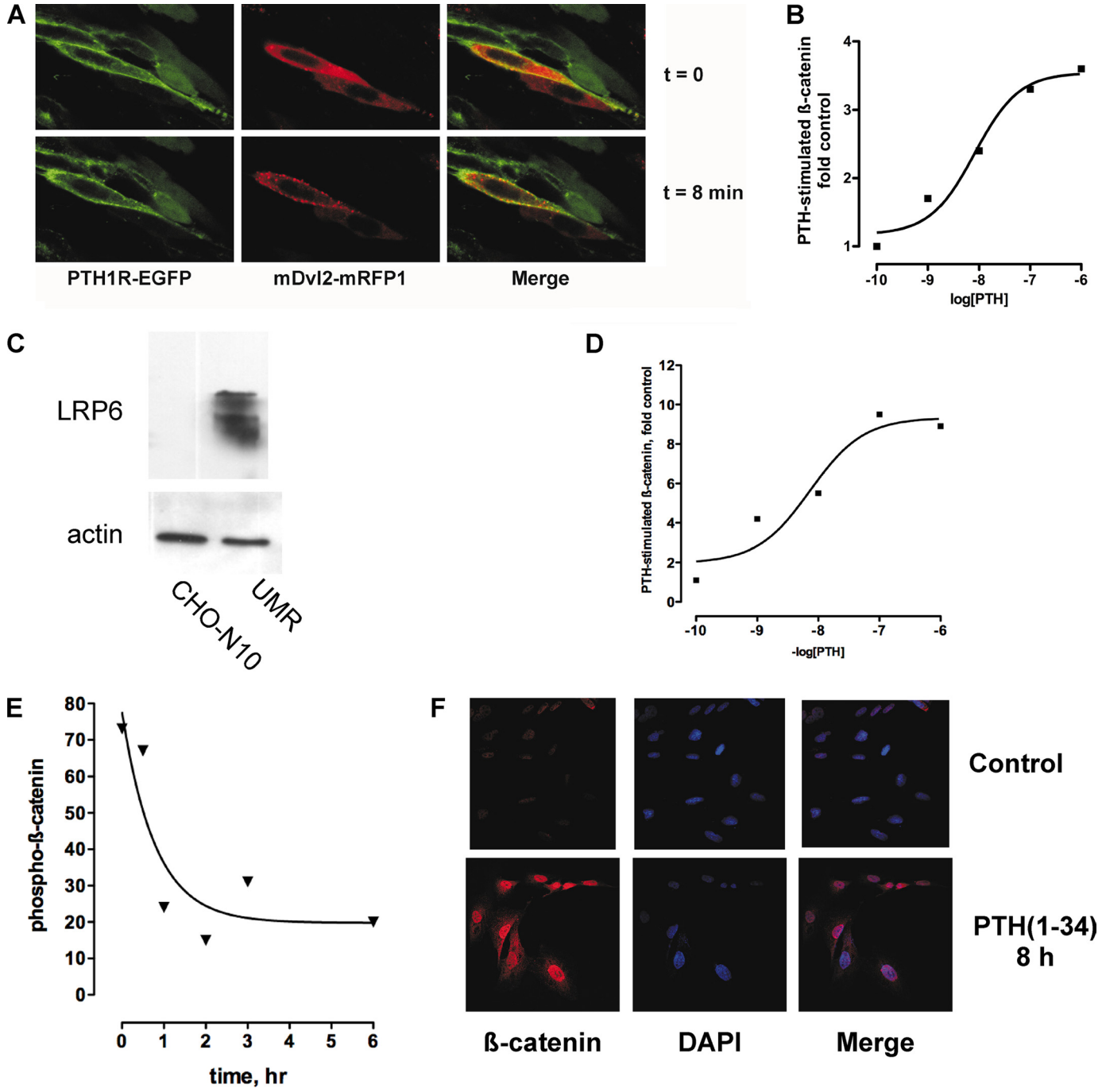

FIGURE 2. **Recruitment of Dvl and β-catenin activation, stabilization, and nuclear translocation following activation of PTH1R.** *A*, PTH treatment induces translocation of Dvl2 to the plasma membrane. CHO cells expressing EGFP-PTH1R (*green*) were transiently transfected with mRFP-Dvl2. Confocal images were collected at 20-s intervals after the addition of 100 nM PTH(1–34). The *images* shown correspond to $t = 0$ and 8 min. Note the accumulation of red Dvl2 in discrete puncta (*arrows*, *center panels*). See supplemental Video 1. *B*, PTH-dependent β-catenin activation in CHO cells. CHO cells were transfected with HA-tagged human PTH1R and reporter TOP/FOP plasmids as described under "Experimental Procedures." *C*, CHO cells do not express LRP6. The expression of LRP6 in UMR-106 cells is shown for comparative purposes. *D*, concentration-dependent stimulation of β-catenin activation by PTH. MC4 cells were transiently transfected with TOPFlash and 48 h later were studied as described under "Experimental Procedures." *E*, stabilized β-catenin (*i.e.* dephosphorylated β-catenin) in MC4 bone cells after stimulation with PTH(1–34). *F*, translocation of activated β-catenin to the nucleus. ROS 17/2.8 cells were challenged with 100 nM PTH(1–34) for 8 h and then fixed and stained for dephosphorylated β-catenin and 4′,6-diamidino-2-phenylindole (*DAPI*), to stain nuclei.

was diffusely expressed throughout the cytoplasm (Fig. 2*A* and supplemental Video 1). Following the addition of PTH, Dvl was recruited to the cell membrane, where it concentrated in discrete puncta a few min after treatment (Fig. 2*A*, *arrows*), whereas the PTH1R internalized. Unlike FZD4, which significantly co-localizes with Dvl2 even in the absence of ligand (29), the PTH1R and Dvl2 co-localize only transiently after receptor activation. This result suggests somewhat weaker interactions between PTH1R and Dvl or the presence of additional regulatory proteins. Importantly, Fig. 2*A* and supplemental Video 1 also show cells expressing only one of the fluorescent constructs. In this situation, PTH treatment failed to induce Dvl2

translocation in cells that did not express the PTH1R. Thus, activation of the PTH1R causes translocation of the Dvl2 to the cell surface.

To determine if recruitment of Dvl2 to the cell surface correlates with downstream functions of the PTH1R, we measured β-catenin activation using a TCF/Lef reporter (30). The results shown in Fig. 2*B* demonstrate that PTH stimulates β-catenin activity in CHO cells transfected with the human PTH1R. Notably, LRP5/6 expression in CHO cells determined by quantitative RT-PCR is negligibly low. mRNA for LRP5 were undetectable, and LRP6 was at background levels (data not shown). Immunoblots with specific antibodies confirm the low expression of LRP6 (Fig. 2*C*), strengthening the conclusion that β-catenin activation by the PTH1R is independent of LRP5/6 in CHO cells.

The above results demonstrate activation of β-catenin by PTH in heterologous expression systems. These findings were validated in bone cells expressing endogenous levels of the PTH1R. Fig. 2*D* shows that in MC4 cells, PTH activated β-catenin in a concentration-dependent manner. Activation of β-catenin occurs upon dissociation of the axin-APC-GSK3β complex, which results in reduced phosphorylation and stabilization of non-phosphorylated β-catenin. β-Catenin then accumulates in the cytoplasm before being translocated to the nucleus, where it exerts its transcriptional effects. The results in Fig. 2, *E* and *F*, illustrate the time course of β-catenin accumulation and nuclear translocation after challenge with PTH(1–34), respectively. Therefore, stimulation of the PTH1R results in the translocation and oligomerization of Dvl2 at the plasma membrane and the inhibition of β-catenin phosphorylation, which in turn leads to the activation and nuclear translocation of β-catenin. These phenomena are benchmarks of the activation of the canonical Wnt signaling pathway.

Dvl Mediates PTH1R Actions—To analyze the role of Dvl proteins in mediating the effects of PTH, we used two different Dvl mutants. Xdd1 is a well characterized dominant negative mutant of *Xenopus* Dishevelled (Xdsh) lacking amino acids 301–381, which include the core of the Xdsh PDZ domain (31). AHEA-Dvl2 is a double point mutant that blocks FZD4 internalization and planar cell polarity signaling (29). As shown in Fig. 3*A*, the stimulation of β-catenin signaling by PTH was blocked by expression of either Dvl mutant compared with the empty vector control. These results support the conclusion that the activation of β-catenin by PTH is mediated by the interactions of the PTH1R with Dvl proteins. To confirm the role of Dvl in PTH1R-mediated activation of β-catenin, the endogenous levels of Dvl proteins were manipulated using short hairpin RNA constructs. The expression of the isoforms Dvl1, Dvl2, and Dvl3 in UMR cells was examined using quantitative reverse transcription-PCR, which demonstrated that Dvl2 accounted for >90% of the Dvl message present (supplemental Fig. 1). Therefore, we transfected UMR cells with shRNA constructs that specifically targeted Dvl2. This treatment reduced Dvl2 protein levels by over 50% (supplemental Fig. 2). This number is an underestimate of the actual silencing effects of the shRNA constructs because the data shown were not corrected to account for transfection efficiency. β-Catenin activation was measured in cells co-transfected with Dvl2-targeted shRNA or scrambled control vectors (Fig. 3*B*). As shown, PTH-dependent β-catenin activity was severely impaired by expression of Dvl2-specific shRNA.

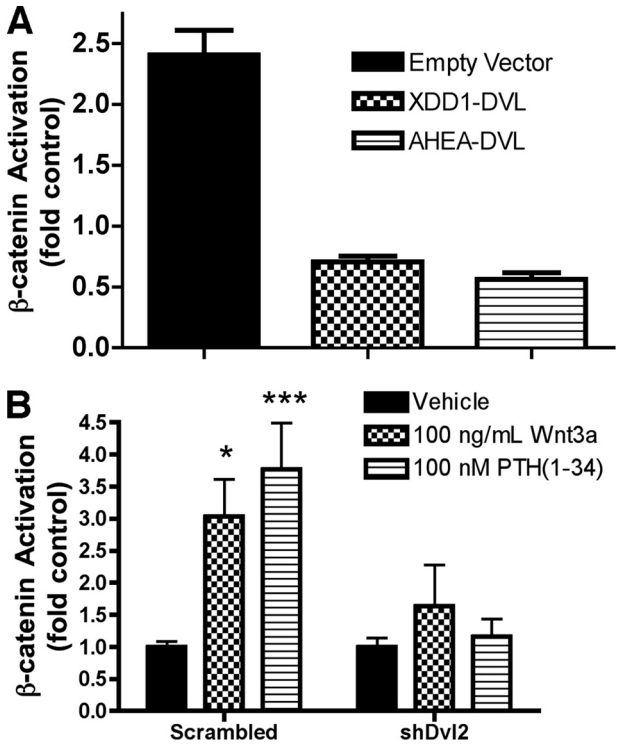

FIGURE 3. **Dvl requirement for PTH1R activation of β-catenin.** *A*, inhibition of β-catenin activation by the expression of dominant negative Dvl constructs, XDD1 and AHEA-Dvl2. UMR-106 cells were co-transfected with TOPFlash reporter (or the control plasmid, FOPFlash) and either empty vector or the specified Dvl mutant (XDD1 or AHEA-Dvl2). β-Catenin activation was determined from chemiluminescence data as described under "Experimental Procedures." *B*, Dvl2-specific shRNA inhibits PTH- and Wnt3A-dependent β-catenin activation in UMR-109 cells. In these experiments, Dvl2 expression was inhibited by co-transfecting two plasmids coding for Dvl2-specific shRNA together with the TOPFlash or FOPFlash reporters.

We further examined the effects of Dvl2 mutants on the function of the PTH1R. Neither Xdd1 nor AHEA-Dvl2 interfered with PTH-induced activation of adenylyl cyclase (supplemental Fig. 3). However, overexpression of AHEA-Dvl2 interfered with PTH1R endocytosis (Fig. 4, *A* and *B*). Notably, both mutants blocked PTH-induced osteoclastogenesis as determined by tartrate-resistant acid phosphatase (*TRAP*) staining (Fig. 4, *C* and *D*). These results strongly support the hypothesis that some crucial effects of PTH are mediated by direct binding of Dvl proteins by the PTH1R.

The present results strongly support the hypothesis that some crucial effects of PTH are mediated by direct binding of Dvl proteins by the PTH1R. We excluded the possibility that the inhibitory actions of the Dvl mutants arose from interfering with PTH1R signaling through adenylyl cyclase by measuring the effects of XDD1 and AHEA-Dvl2 constructs on PTH-stimulated cAMP. Neither Xdd1 nor AHEA-Dvl2 interfered with PTH-induced activation of adenylyl cyclase (supplemental Fig. 3).

DISCUSSION

The findings described here identify Dvl as a molecular router, integrating signals derived from FZD and PTH1R to

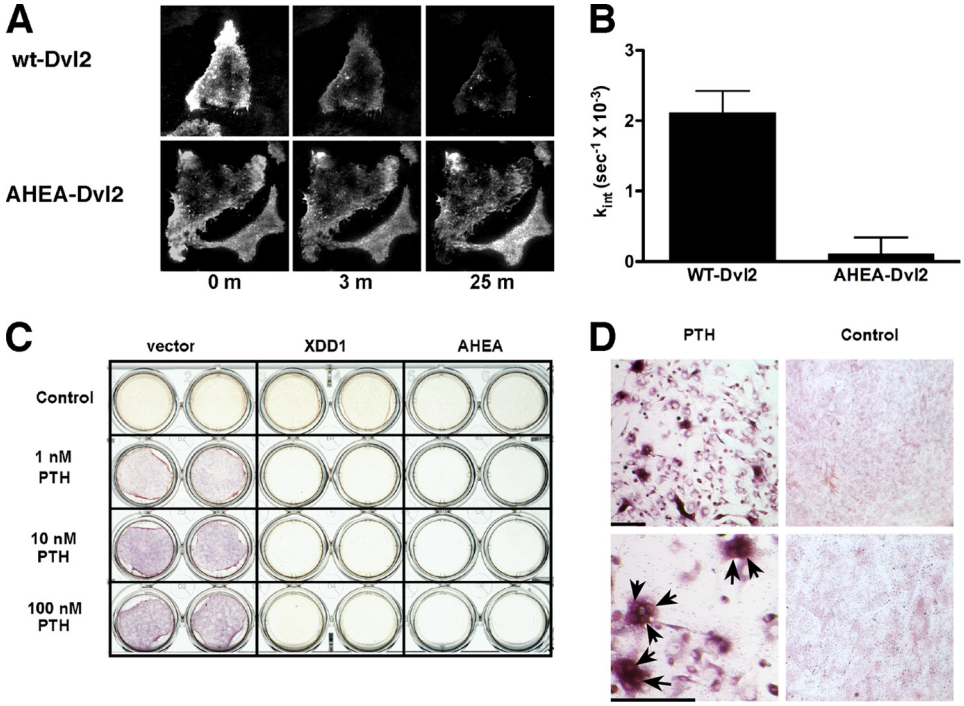

FIGURE 4. **Dvl is required for PTH-dependent PTH1R internalization and osteoclastogenesis.** *A*, AHEA-Dvl2 blocks ligand-induced PTH1R internalization. Rat osteosarcoma cells transfected with PTH1R-EGFP and mRFP1-Dvl2 were imaged at 20-s intervals after the addition of 100 nM PTH(1–34) using TIRF. The data obtained with cells that express wild-type Dvl2 are shown in the *top panel*. The *bottom panel* shows the results of the expression of AHEA-Dvl2. *B*, summary of the PTH1R internalization results obtained. The rate constant of internalization of the PTH1R was calculated from TIRF microscopy data. Only cells that expressed both proteins (as determined from green and red fluorescence measurements) were used in these calculations. The data show the average of five different cell plates examined in three independent experiments. *C*, PTH promotes osteoclastogenesis through a β-catenin-mediated pathway. UAMS-32P cells were co-cultured with non-adherent bone marrow cells (52). PTH(1–34) at increasing concentrations was added in the presence of empty vector, XDD1 dominant negative Dvl, or AHEA dominant negative Dvl. After 6 days, tartrate-resistant acid phosphatase activity was determined using naphthol phosphate as a substrate and fast garnet to label the product as a *red-purple* precipitate. *D*, low and high magnification views of the cells shown in *C*. Tartrate-resistant acid phosphatase staining was primarily localized to multinucleated osteoclasts (*arrowheads*). *Bar*, 100 μm.

control osteoclast formation. Regulation of Wnt signaling by GPCRs other than FZD has been described (32–34). However, we demonstrate here for the first time that Dvl proteins play an important role in the activation of β-catenin by classical GPCRs. In all previous studies, the activation of β-catenin has been linked to the activation of classical G-protein mediated pathways. For instance, stimulation of α-adrenergic and endothelin-1 receptors in cardiomyocytes leads to the activation of β-catenin by a mechanism that involves the recruitment of Akt to the β-catenin degradation complex and the subsequent phosphorylation and inactivation of GSK3β (32). Likewise, the lysophosphatidic acid receptors LPA_2 and LPA_3 activate β-catenin-dependent pathways by a mechanism downstream of the activation of PKC (33). Finally, PGE_2 receptors, acting through protein kinase A, stabilize β-catenin in colon cancer cells (34). Importantly, β-arrestins interact with phosphorylated Dvl, and transient co-expression of β-arrestin-1 with either Dvl1 or Dvl2 stimulates a β-catenin reporter even in the absence of Wnt (35). More recently, it has been suggested that β-arrestin is required for the Dvl-mediated disruption of the β-catenin destruction complex (36). The work presented here demonstrates that the PTH1R activates β-catenin signaling by direct interactions with Dvl.

Dvl contains three functional domains: an amino-terminal Dix domain, a centrally located type 1 PDZ domain, and a carboxyl-terminal Dep domain (37). The structural basis for the interaction of FZD with Dvl is somewhat unconventional. Thus, despite the presence of a carboxyl-terminal PDZ binding motif, it has been argued that Dvl interacts with FZD through a non-canonical, internal sequence (38, 39). Interestingly, Dvl binds to the PTH1R through the comparable K(S/T)*XXX*W sequence despite the presence of a carboxyl-terminal PDZ recognition motif. Thus, Dvl interacted robustly with the PTH1R even following mutation of the PDZ-binding motif or truncation of the PTH1R distal to the putative Dvl-binding sequence.

The mechanism by which the PTH1R promotes the redistribution of Dvl involves direct interactions of the receptor with Dvl. Arrestin-mediated Dvl2 binding can be ruled out because the PTH1R(480-stop) binds Dvl2 with an efficiency comparable with that of the wild type receptor (see Fig. 1*D*). This truncated receptor is devoid of the core of serines that are phosphorylated by G-protein receptor kinases and mediate the binding of arrestin, located between residues 489 and 501 (40, 41). The direct involvement of Dvl in the signaling pathways leading to β-catenin activation is further supported by the finding that two different Dvl mutants block TCF/β-catenin-dependent transcription and PTH-induced osteoclastogenesis. Were the PTH1R modulating these downstream effects through the activation of protein kinase A or Akt and the phosphorylation of GSK3β, the actions of PTH would be expected to be insensitive to the expression of dominant negative Dvl mutants, and this was not the case.

Recent studies show that PTH can activate Wnt signaling despite overexpression of Dkk1 (42). The results described here are consistent with these findings and may explain the results with Dkk1. Upon stimulation by PTH, the PTH1R recruits Dvl and does so independent of FZD and LRP5/6 (and therefore of Dkk1).

The present work demonstrates for the first time that GPCRs other than the members of the FZD subfamily may interact with and activate Dvl proteins. The possibility that additional receptors may also use this mechanism to activate β-catenin-dependent protein expression remains to be explored.

The dominant negative effects of the AHEA-Dvl2 mutant require additional comment. AHEA-Dvl2 interacts normally with FZD4 but cannot bind AP-2 and, as a consequence, acts as

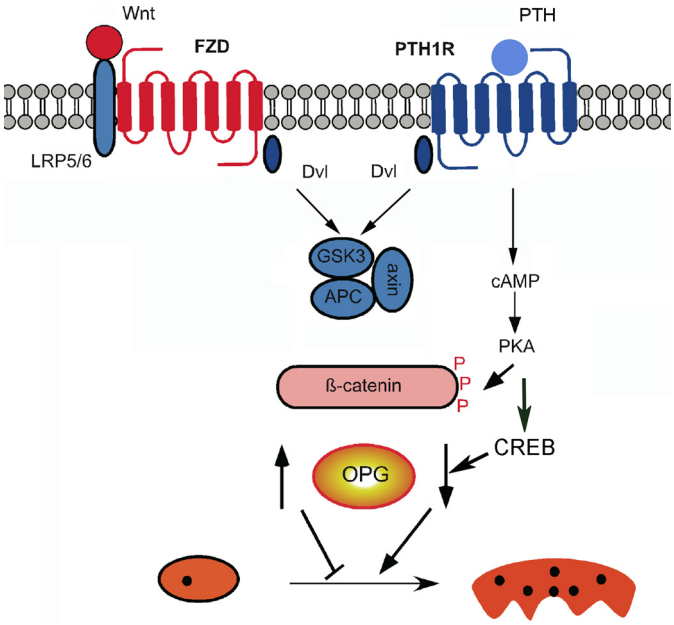

FIGURE 5. **Working model for divergent effects of PTH1R and FZD signaling and action on osteoclastogenesis.** Activation of FZD and of PTH1R stimulates β-catenin. In the case of FZD, this leads to inhibition of osteoclastogenesis, whereas activation of the PTH1R increases osteoclastogenesis. We propose that the divergent actions of FZD or PTH1R effects are due to protein kinase A-dependent phosphorylation of β-catenin and GSK3β and the activation of CREB. *PKA*, protein kinase A.

a dominant negative for Wnt5a-induced FZD4 internalization (29). This effect was recapitulated with the PTH1R (Fig. 4, *A* and *B*). However, although AHEA-Dvl2 interferes with Wnt5a-dependent JNK phosphorylation, it does not block Wnt5a-induced β-catenin activation in HEK-293 (human embryonic kidney) cells (29). AHEA-Dvl2 clearly disrupted PTH-induced PTH1R osteoclastogenesis and β-catenin-dependent gene transcription in the bone-derived cell models used here. Because AHEA-Dvl2 blocked PTH1R endocytosis, this phenomenon can be explained by a requirement for PTH1R internalization in the activation of the β-catenin pathway. This is consistent with recent reports showing that β-arrestin plays an important role in the coupling of Wnt signaling to β-catenin activation (36).

The results described here regarding the effects of PTH *versus* Wnt activation of β-catenin present an apparent paradox. Although both ligands lead to activation of β-catenin, they have opposite actions on osteoclastogenesis. Although β-catenin mediates convergent actions of PTH1R and FZD upon mineralization, it promotes divergent actions on osteoclastogenesis as we propose here. A model incorporating this scheme is shown in Fig. 5.

PTH promotes osteoclastogenesis, whereas Wnt stimulation of β-catenin blocks osteoclastogenesis. One crucial difference in the signaling cascades downstream of Wnt ligands and PTH is the activation of cAMP production by the latter. We propose that the modulation of β-catenin signaling by cAMP and protein kinase A during stimulation with PTH contributes significantly to the differences observed between Wnt- and PTH-driven responses. These effects may be due to differential phosphorylation of β-catenin (43, 44) or of GSK3 (45) by protein kinase A. Alternatively, the generation of cAMP activates the cAMP-response element-binding protein (CREB), which in turn interacts with β-catenin and regulates its function (46, 47). Phosphorylation, whether of β-catenin or GSK3, may occur at different sites or may be of different duration (*i.e.* transient *versus* sustained). A clear distinction between Wnt- and PTH-dependent β-catenin activation is that the latter proceeds in an environment with elevated cAMP and protein kinase A activity and, perhaps, CREB. We propose that phosphorylation by protein kinase A of β-catenin (43, 44) or of GSK3 (45) modifies the β-catenin response, leading to divergent patterns of gene expression (Fig. 5). Consistent with this theory, independent studies established that even in the same cell type, protein kinase A can promote or prevent β-catenin-dependent effects, depending on the particular agonist (48). Thus, we envision that Wnt or PTH-stimulated β-catenin activation may evoke opposite actions on osteoclastogenesis by eliciting similar β-catenin responses in a different intracellular background.

PTH promotes bone accretion when administered intermittently but promotes bone resorption when continuously applied. Intermittent PTH administration of PTH causes phosphorylation of LRP6 and stabilization of β-catenin in mouse osteoblasts (18). By contrast, continuous PTH treatment failed to stimulate β-catenin. Thus, the anabolic action of PTH may arise in part from the participation of the canonical β-catenin pathway but independent of Wnt.

Other explanations can be advanced for the different effects of β-catenin activation by Wnt and PTH. For instance, divergent effects of PTH and Wnt on β-catenin may arise from the expression patterns of PTH1R and FZD, respectively, during osteoblast maturation (49, 50). Additionally or alternatively, differences in β-catenin actions upon osteoclastogenesis could be due to distinct actions of PTH or Wnt upon apoptosis. Irrespective of the mechanism, it is likely to have important implications for understanding and treating skeletal disorders.

Acknowledgment—We appreciate the assistance of Dr. M. Feili-Hariri in isolating marrow stromal cells.

REFERENCES

1. Malbon, C. C., and Wang, H. Y. (2006) *Curr. Top. Dev. Biol.* **72,** 153–166
2. Gordon, M. D., and Nusse, R. (2006) *J. Biol. Chem.* **281,** 22429–22433
3. Schulte, G., and Bryja, V. (2007) *Trends Pharmacol. Sci.* **28,** 518–525
4. Malbon, C. C. (2004) *Front. Biosci.* **9,** 1048–1058
5. Barnes, M. R., Duckworth, D. M., and Beeley, L. J. (1998) *Trends Pharmacol. Sci.* **19,** 399–400
6. Songyang, Z., Fanning, A. S., Fu, C., Xu, J., Marfatia, S. M., Chishti, A. H., Crompton, A., Chan, A. C., Anderson, J. M., and Cantley, L. C. (1997) *Science* **275,** 73–77
7. Wang, S., Raab, R. W., Schatz, P. J., Guggino, W. B., and Li, M. (1998) *FEBS Lett.* **427,** 103–108
8. Weinman, E. J., Hall, R. A., Friedman, P. A., Liu-Chen, L. Y., and Shenolikar, S. (2006) *Annu. Rev. Physiol.* **68,** 491–505
9. Baron, R., and Rawadi, G. (2007) *Endocrinology* **148,** 2635–2643
10. Krishnan, V., Bryant, H. U., and Macdougald, O. A. (2006) *J. Clin. Invest.* **116,** 1202–1209
11. Hartmann, C. (2006) *Trends Cell Biol.* **16,** 151–158
12. Bodine, P. V., and Komm, B. S. (2006) *Rev. Endocr. Metab. Disord.* **7,** 33–39
13. Lanske, B., Karaplis, A. C., Lee, K., Luz, A., Vortkamp, A., Pirro, A., Karperien, M., Defize, L. H., Ho, C., Mulligan, R. C., Abou-Samra, A. B., Jüp-

pner, H., Segre, G. V., and Kronenberg, H. M. (1996) *Science* **273,** 663–666
14. Kong, Y. Y., Yoshida, H., Sarosi, I., Tan, H. L., Timms, E., Capparelli, C., Morony, S., Oliveira-dos-Santos, A. J., Van, G., Itie, A., Khoo, W., Wakeham, A., Dunstan, C. R., Lacey, D. L., Mak, T. W., Boyle, W. J., and Penninger, J. M. (1999) *Nature* **397,** 315–323
15. Li, J., Sarosi, I., Yan, X. Q., Morony, S., Capparelli, C., Tan, H. L., McCabe, S., Elliott, R., Scully, S., Van, G., Kaufman, S., Juan, S. C., Sun, Y., Tarpley, J., Martin, L., Christensen, K., McCabe, J., Kostenuik, P., Hsu, H., Fletcher, F., Dunstan, C. R., Lacey, D. L., and Boyle, W. J. (2000) *Proc. Natl. Acad. Sci. U.S.A.* **97,** 1566–1571
16. Kulkarni, N. H., Halladay, D. L., Miles, R. R., Gilbert, L. M., Frolik, C. A., Galvin, R. J., Martin, T. J., Gillespie, M. T., and Onyia, J. E. (2005) *J. Cell. Biochem.* **95,** 1178–1190
17. Tobimatsu, T., Kaji, H., Sowa, H., Naito, J., Canaff, L., Hendy, G. N., Sugimoto, T., and Chihara, K. (2006) *Endocrinology* **147,** 2583–2590
18. Wan, M., Yang, C., Li, J., Wu, X., Yuan, H., Ma, H., He, X., Nie, S., Chang, C., and Cao, X. (2008) *Genes Dev.* **22,** 2968–2979
19. Chan, S. D., Karpf, D. B., Fowlkes, M. E., Hooks, M., Bradley, M. S., Vuong, V., Bambino, T., Liu, M. Y., Arnaud, C. D., Strewler, G. J., and Nissenson, R. A. (1992) *J. Biol. Chem.* **267,** 25202–25207
20. Suzuki, A., Ozono, K., Kubota, T., Kondou, H., Tachikawa, K., and Michigami, T. (2008) *J. Cell. Biochem.* **104,** 304–317
21. Bodine, P. V., Seestaller-Wehr, L., Kharode, Y. P., Bex, F. J., and Komm, B. S. (2007) *J. Cell. Physiol.* **210,** 352–357
22. Yao, W., Cheng, Z., Shahnazari, M., Dai, W., Johnson, M. L., and Lane, N. E. (2010) *J Bone Miner. Res.* **25,** 190–199
23. Wang, B., Bisello, A., Yang, Y., Romero, G. G., and Friedman, P. A. (2007) *J. Biol. Chem.* **282,** 36214–36222
24. Hay, E., Faucheu, C., Suc-Royer, I., Touitou, R., Stiot, V., Vayssière, B., Baron, R., Roman-Roman, S., and Rawadi, G. (2005) *J. Biol. Chem.* **280,** 13616–13623
25. Wheeler, D., Sneddon, W. B., Wang, B., Friedman, P. A., and Romero, G. (2007) *J. Biol. Chem.* **282,** 25076–25087
26. Umbhauer, M., Djiane, A., Goisset, C., Penzo-Méndez, A., Riou, J. F., Boucaut, J. C., and Shi, D. L. (2000) *EMBO J.* **19,** 4944–4954
27. Sneddon, W. B., Syme, C. A., Bisello, A., Magyar, C. E., Rochdi, M. D., Parent, J. L., Weinman, E. J., Abou-Samra, A. B., and Friedman, P. A. (2003) *J. Biol. Chem.* **278,** 43787–43796
28. Gao, C., and Chen, Y. G. (2010) *Cell. Signal.* **22,** 717–727
29. Yu, A., Rual, J. F., Tamai, K., Harada, Y., Vidal, M., He, X., and Kirchhausen, T. (2007) *Dev. Cell* **12,** 129–141
30. Korinek, V., Barker, N., Morin, P. J., van Wichen, D., de Weger, R., Kinzler, K. W., Vogelstein, B., and Clevers, H. (1997) *Science* **275,** 1784–1787
31. Sokol, S. Y. (1996) *Curr. Biol.* **6,** 1456–1467
32. Haq, S., Michael, A., Andreucci, M., Bhattacharya, K., Dotto, P., Walters, B., Woodgett, J., Kilter, H., and Force, T. (2003) *Proc. Natl. Acad. Sci. U.S.A.* **100,** 4610–4615
33. Yang, M., Zhong, W. W., Srivastava, N., Slavin, A., Yang, J., Hoey, T., and An, S. (2005) *Proc. Natl. Acad. Sci. U.S.A.* **102,** 6027–6032
34. Castellone, M. D., Teramoto, H., Williams, B. O., Druey, K. M., and Gutkind, J. S. (2005) *Science* **310,** 1504–1510
35. Chen, W., Hu, L. A., Semenov, M. V., Yanagawa, S., Kikuchi, A., Lefkowitz, R. J., and Miller, W. E. (2001) *Proc. Natl. Acad. Sci. U.S.A.* **98,** 14889–14894
36. Bryja, V., Gradl, D., Schambony, A., Arenas, E., and Schulte, G. (2007) *Proc. Natl. Acad. Sci. U.S.A.* **104,** 6690–6695
37. Schwarz-Romond, T., Metcalfe, C., and Bienz, M. (2007) *J. Cell Sci.* **120,** 2402–2412
38. Wong, H. C., Bourdelas, A., Krauss, A., Lee, H. J., Shao, Y., Wu, D., Mlodzik, M., Shi, D. L., and Zheng, J. (2003) *Mol. Cell* **12,** 1251–1260
39. London, T. B., Lee, H. J., Shao, Y., and Zheng, J. (2004) *Biochem. Biophys. Res. Commun.* **322,** 326–332
40. Malecz, N., Bambino, T., Bencsik, M., and Nissenson, R. A. (1998) *Mol. Endocrinol.* **12,** 1846–1856
41. Tawfeek, H. A., Qian, F., and Abou-Samra, A. B. (2002) *Mol. Endocrinol.* **16,** 1–13
42. Guo, J., Liu, M., Yang, D., Bouxsein, M. L., Saito, H., Galvin, R. J., Kuhstoss, S. A., Thomas, C. C., Schipani, E., Baron, R., Bringhurst, F. R., and Kronenberg, H. M. (2010) *Cell Metab.* **11,** 161–171
43. Hino, S., Tanji, C., Nakayama, K. I., and Kikuchi, A. (2005) *Mol. Cell. Biol.* **25,** 9063–9072
44. Taurin, S., Sandbo, N., Qin, Y., Browning, D., and Dulin, N. O. (2006) *J. Biol. Chem.* **281,** 9971–9976
45. Fang, X., Yu, S. X., Lu, Y., Bast, R. C., Jr., Woodgett, J. R., and Mills, G. B. (2000) *Proc. Natl. Acad. Sci. U.S.A.* **97,** 11960–11965
46. Takemaru, K. I., and Moon, R. T. (2000) *J. Cell Biol.* **149,** 249–254
47. Hecht, A., Vleminckx, K., Stemmler, M. P., van Roy, F., and Kemler, R. (2000) *EMBO J.* **19,** 1839–1850
48. Hogarth, D. K., Sandbo, N., Taurin, S., Kolenko, V., Miano, J. M., and Dulin, N. O. (2004) *Am. J. Physiol. Cell Physiol* **287,** C449–C456
49. Ek, E. T., Dass, C. R., and Choong, P. F. (2006) *Crit. Rev. Oncol. Hematol.* **60,** 1–8
50. Westendorf, J. J., Kahler, R. A., and Schroeder, T. M. (2004) *Gene* **341,** 19–39
51. Wang, B., Yang, Y., and Friedman, P. A. (2008) *Mol. Biol. Cell* **19,** 1637–1645
52. Fu, Q., Jilka, R. L., Manolagas, S. C., and O'Brien, C. A. (2002) *J. Biol. Chem.* **277,** 48868–48875

Oncogene (2010), 1–11

www.nature.com/onc

ORIGINAL ARTICLE

Direct interaction between NHERF1 and Frizzled regulates β-catenin signaling

DS Wheeler[1,2], SR Barrick[1], MJ Grubisha[1,2], AM Brufsky[3,4], PA Friedman[1,3] and G Romero[1,4]

[1]*Laboratory for GPCR Biology, Department of Pharmacology and Chemical Biology, University of Pittsburgh School of Medicine, Pittsburgh, PA, USA;* [2]*Medical Scientist Training Program, University of Pittsburgh School of Medicine, Pittsburgh, PA, USA;* [3]*Department of Medicine, University of Pittsburgh School of Medicine, Pittsburgh, PA, USA and* [4]*University of Pittsburgh Cancer Institute, University of Pittsburgh School of Medicine, Pittsburgh, PA, USA*

Although Wnt-Frizzled (Fzd) signaling is critical in the pathophysiology of carcinomas, its role in human breast cancer has been difficult to establish. We show here that the adaptor protein Na^+/H^+ exchange regulatory factor1 (NHERF1), a protein abundantly expressed in normal mammary epithelium, regulates Wnt signaling, maintaining low levels of β-catenin activation. NHERF1's effects are mediated by direct interactions between one of its PSD-95/drosophila discs large/ZO-1 (PDZ) domains and the C-terminus of a subset of Fzd receptors. Loss of NHERF1 in breast cancer cell lines enhances canonical Wnt signaling and Wnt-dependent cell proliferation. Furthermore, the mammary glands of NHERF1-knockout mice exhibit increased mammary duct density accompanied by increased proliferation and β-catenin activity. Finally, we demonstrate a negative correlation between NHERF1 expression and nuclear β-catenin in human breast carcinomas. Taken together, these results provide a novel insight into the regulation of Wnt signaling in normal and neoplastic breast tissues, and identify NHERF1 as an important regulator of the pathogenesis of breast tumors.
Oncogene advance online publication, 30 August 2010; doi:10.1038/onc.2010.389

Keywords: NHERF1; EBP50; breast cancer; Wnt; Frizzled; beta-catenin

Introduction

Aberrant Wnt signaling causes breast neoplasia in animal models (reviewed in Fantozzi and Christofori, 2006). In humans, however, the involvement of Wnt signaling in breast cancer pathogenesis remains unclear. Stable, ectopic expression of specific Wnts can transform primary human mammary epithelium, which can form invasive tumors in mouse xenograft models (Ayyanan *et al.*, 2006). About 60% of the breast cancers show evidence of increased β-catenin activity but the mechanism and significance of these observations have not been elucidated (Lin *et al.*, 2000; Ryo *et al.*, 2001).

Correspondence: Dr G Romero, Laboratory of GPCR Biology, Department of Pharmacology and Chemical Biology, University of Pittsburgh, School of Medicine, E1355 BST, Pittsburgh, PA 15261, USA. E-mail: ggr@pitt.edu
Received 26 March 2010; revised and accepted 21 July 2010

The Na^+/H^+ exchange regulatory factor 1 (NHERF1, also known as the Ezrin-binding phosphoprotein of 50 kDa, EBP50) is a cytosolic PSD-95/*Drosophila* discs large/ZO-1 (PDZ) adaptor protein abundantly expressed in human mammary epithelium. NHERF1 was initially identified as a regulator of the localization, signaling and traffic of G protein-coupled receptors, ion channels and transporters (reviewed in Weinman *et al.*, 2006). Recently, NHERF1 has been proposed to function as a tumor suppressor (Dai *et al.*, 2004; Pan *et al.*, 2006; Kreimann *et al.*, 2007). Knockdown of NHERF1 increases cellular proliferation and migration of various breast cancer cell lines (Pan *et al.*, 2006, 2008). Furthermore, when introduced in a mouse xenograft model, NHERF1-knockout cells were more aggressive and produced greater numbers of metastases (Pan *et al.*, 2006). NHERF1 mutations occur in 3% of the human breast tumors, whereas loss of heterozygosity at the NHERF1 locus (17q25.1) occur in over 50% of primary beast tumors (Dai *et al.*, 2004). Both are correlated with poor prognosis and early death (Dai *et al.*, 2004).

The mechanism by which NHERF1 regulates tumor growth and migration is unclear. The search for potential NHERF1 targets revealed that 8 out of 10 human Frizzled (Fzd) receptors terminate in a canonical PDZ ligand (x-S/T-x-V/L; see Figure 1a) (Songyang *et al.*, 1997). In this study, we investigated the hypothesis that NHERF1 directly interacts with Fzd receptors and regulates Wnt signaling. We show that NHERF1 interacts directly with a subset of Fzd receptors, and that ablation of NHERF1 increases Wnt signaling and Wnt-dependent proliferation. Furthermore, NHERF1-knockout mice exhibit enhanced β-catenin activation and increased mammary duct density. Finally, NHERF1 expression and β-catenin activation are negatively correlated in human breast tumors. Therefore, we conclude that NHERF1's function as a tumor suppressor is a consequence of its role in the regulation of canonical Wnt signaling.

Results

NHERF1 binds Fzd receptors

We developed a Chinese hamster ovary cell model system (CHO-N10), in which NHERF1 expression is

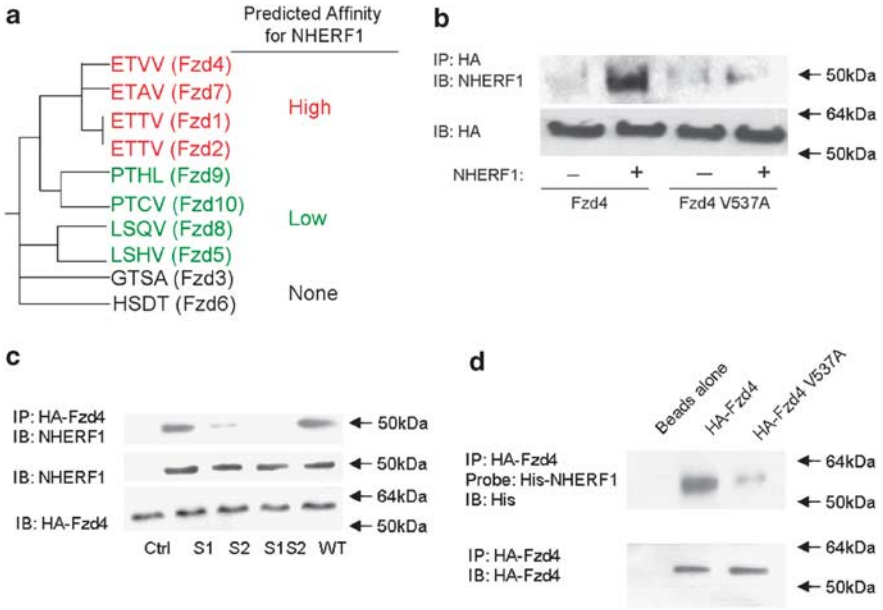

Figure 1 NHERF1 interacts with the C-terminal PDZ ligand of Fzd receptors. (**a**) Human Fzd receptors cluster into three groups based on their alignment of their C-termini. Fzd1, 2, 4 and 7 terminate in the consensus sequence E-T-x-V which is predicted to have high affinity for the PDZ domains of NHERF1 (Karthikeyan *et al*., 2001). The C-terminal sequences of Fzd5, 8, 9 and 10 are also expected to bind PDZ domains but are predicted to have lower affinity for NHERF1. Fzd3 and 6 do not terminate in a consensus PDZ ligand and thus are not expected to interact with NHERF1. (**b**) NHERF1 coimmunoprecipitates with HA-Fzd4 in CHO-N10 cells. Mutation of the C-terminal valine to alanine (V537A) abrogates this interaction. (**c**) Fzd4 interacts primarily with the second PDZ domain of NHERF1 (PDZ2). CHO cells were transfected with NHERF1 mutants (S1: mutated PDZ1, S2: mutated PDZ2; S1S2: mutated in both PDZ domains; WT: wild type). (**d**) The binding of NHERF1 to Fzd4 is caused by direct interactions. HA-tagged Fzd4 was expressed in CHO cells, extracted and incubated with specific agarose beads linked to anti-HA antibody or with beads in the absence of anti-HA antibody. The material bound to the beads was resolved by SDS-PAGE and blotted onto nitrocellulose. The blot was developed with recombinant His-tagged NHERF1 isolated from *Escherichia coli* followed by horseradish peroxidase-tagged anti-His antibody. The only NHERF1-positive bands present in the gel corresponded to the molecular weight of the immunoprecipitated HA-Fzd4. ctrl, control.

undetectable under basal conditions and induced by the addition of tetracycline (Wheeler *et al*., 2007). These cells express low levels of endogenous Fzd receptors (Supplementary Table 1). To investigate the interaction between NHERF1 and Fzd, CHO-N10 cells were transfected with hemagglutinin (HA)-tagged human Fzd4 and induced by tetracycline to express NHERF1. As seen in Figure 1b, NHERF1 coimmunoprecipitated with Fzd4. To demonstrate that the interaction between Fzd4 and NHERF1 is governed by PDZ domain–PDZ ligand interactions, the C-terminal valine of Fzd4 was mutated to alanine (Fzd4 V537A). We previously showed that the equivalent mutation abrogates the interactions of NHERF1 with the parathyroid hormone receptor type 1 (Wheeler *et al*., 2007). The interaction between the Fzd4 V537A and NHERF1 was reduced by 95% when compared with the wild type (Figure 1b, lanes 2 and 4). Therefore, NHERF1 binds Fzd4 via the receptor's terminal PDZ ligand.

To determine which of the two PDZ domains of NHERF1 was responsible for these interactions, we transfected CHO cells with NHERF1 variants in which the cores of PDZ1, PDZ2 and both PDZ1 + PDZ2 had been mutated: S1 (defective PDZ1), S2 (defective PDZ2) and S1S2 (defective PDZ1 and PDZ2) (Wheeler *et al*., 2007). The data shown in Figure 1c demonstrate that the S1 mutant binds Fzd4 as effectively as wild-type NHERF1, whereas Fzd4 binding to the S2 and S1S2 variants is very significantly reduced. We conclude, therefore, that Fzd4 interacts preferentially with PDZ2.

Finally, to demonstrate that the interactions of Fzd4 and NHERF1 are direct, we performed an overlay assay using recombinant His-tagged NHERF1 purified from *E. coli*. The results, shown in Figure 1d, demonstrate that recombinant NHERF1 binds Fzd4, supporting the hypothesis that the interactions between NHERF1 and Fzd receptors are direct. Further, support to the conclusion that these interactions are direct is the demonstration that the interaction of recombinant NHERF1 with V537A-Fzd4 is very significantly reduced when compared with the wild-type receptor (Figure 1d).

Previous work demonstrated that NHERF1 tethers membrane proteins to the actin cytoskeleton localizing them to distinct stress fiber domains and decreasing their lateral mobility (Bates *et al*., 2006; Wheeler *et al*., 2007). NHERF1 expression caused Fzd4 to aggregate along phalloidin-positive fibers in stark contrast to the uniform distribution observed in control cells (Figures 2a and b). The distribution of Fzd4 V537A was diffuse independently of NHERF1 expression (Figures 2c and d). Expression of S1-NHERF1 caused induced redistribution of Fzd4 into bundle-like structures indistinguishable from those formed by the expression of

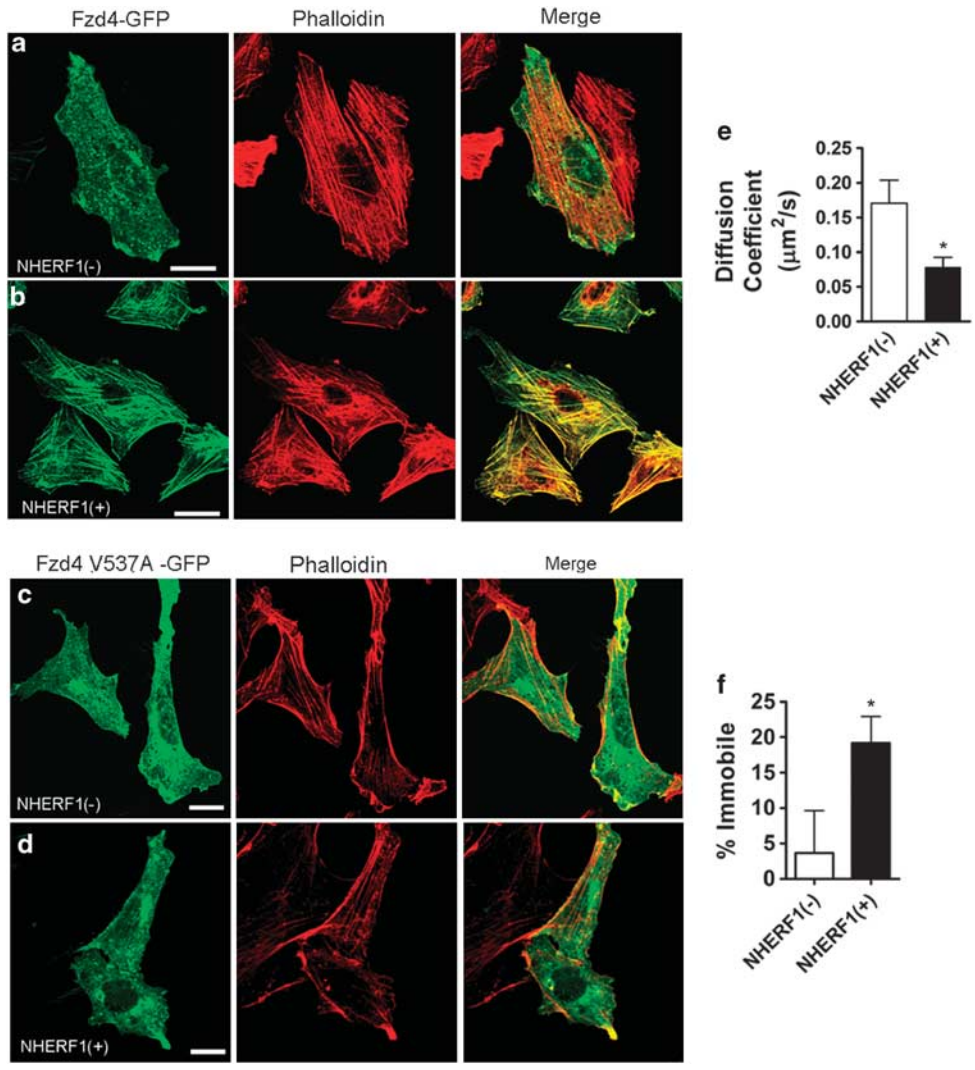

Figure 2 NHERF1 modulates the distribution and dynamics of Fzd4. (**a**) CHO-N10 cells were transiently transfected with Fzd4-eGFP and stained with Texas Red isothiocyanate conjugated phalloidin. Fzd4-eGFP has a uniform membrane distribution and does not colocalize with phalloidin-stained actin fibers. (**b**) Expression of NHERF1 causes Fzd4-eGFP to aggregate along phalloidin-positive actin fibers. (**c**, **d**) Expression of NHERF1 does not alter membrane distribution of Fzd4 V537A-eGFP consistently with the inability of this mutant to bind PDZ domains. Scale bar represents 5 μm. (**e**, **f**) The lateral mobility of Fzd-eGFP in control and NHERF1 expressing CHO-N10 cells was measured by fluorescence recovery after photobleaching. NHERF1 expression decreased the diffusion coefficient of Fzd4-eGFP from 0.17 to 0.07 $\mu m^2/s$. NHERF1 expression also caused a concomitant fivefold increase in the immobile fraction (*$P<0.05$, Students' *t*-test).

wild-type NHERF1 (Supplementary Figure 1a). As expected, this redistribution was not observed upon expression of the S2 or S1S2 NHERF1 constructs (Supplementary Figure 1b, c). When the lateral mobility of Fzd4-eGFP was measured using fluorescence recover after photobleaching, NHERF1 expression decreased the diffusion coefficient of Fzd4-eGFP by 54% and increased the immobile fraction by over fivefold (Figures 2e and f). These results demonstrate that the interaction of PDZ2 of NHERF1 with the terminal PDZ ligand of Fzd4 tether the receptor to the actin cytoskeleton.

Direct interaction with NHERF1 regulates Wnt signaling

To determine the effects of NHERF1 on Fzd signaling, Fzd2, 3, 4 and 7 were transfected into CHO-N10 cells and β-catenin activation was measured using the TOP/FOP luciferase reporter assay. On the basis of their terminal amino acid sequence, Fzd2, 4 and 7 are predicted to interact with NHERF1, whereas Fzd3 is not (Figure 1a). Wnt3a-conditioned medium induced β-catenin activation in cells expressing Fzd2, 3 and 7, whereas Wnt5a-conditioned medium stimulated β-catenin activity in Fzd4-transfected cells. Fzd2, 4 and 7 showed impaired Wnt-induced β-catenin activation in the presence of NHERF1 (76, 86 and 74% decrease, respectively) (Figure 3a). In contrast, Wnt signaling via Fzd3 was unaffected by NHERF1 expression (Figure 3a). Likewise, the Fzd4 V537A was significantly less sensitive to NHERF1-induced inhibition, consistent with its inability to bind NHERF1 (Figure 3b).

We next examined the effects of the S1, S2 and S1S2 NHERF1 mutants on Wnt-induced β-catenin activation.

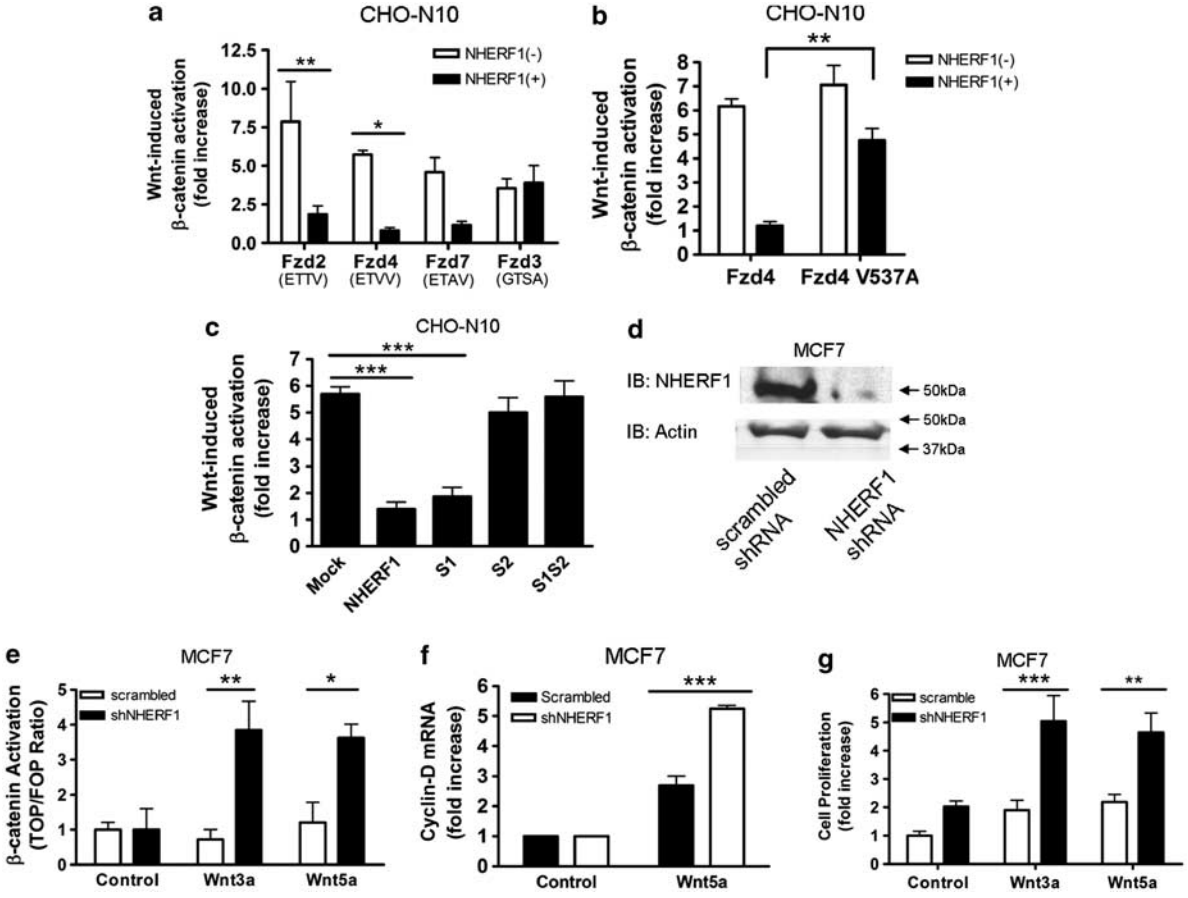

Figure 3 Enhanced Wnt signaling occurs in the absence of NHERF1. (**a**) CHO-N10 cells were cotransfected with the indicated Fzd receptors and either TOP or FOP luciferase reporter plasmid. NHERF1 expression blunted Wnt-induced luciferase expression via Fzd2, 4 and 7 but had no effect on Wnt signaling through Fzd3 (**$P<0.01$, *$P<0.05$, Two-way analysis of variance (ANOVA) with Bonferroni *post-hoc* tests). (**b**) Mutational ablation of the Fzd4 PDZ ligand (Fzd4 V573A) rescues Wnt signaling from NHERF1 inhibition. This mutation has no effect on Wnt singaling in the absence of NHERF1. (**c**) Wnt-induced β-catenin activation was blocked by wild-type NHERF1 and NHERF1 containing a mutated PDZ1 domain (S1). This inhibition was not caused by expression of NHERF1 containing a mutated PDZ2 domain (S2) or with both PDZ domains mutated (S1S2) (***$P<0.001$, One-way ANOVA with Tukey *post-hoc* tests). (**d**) Transfection of MCF7 cells with NHERF1 targeted short hairpin shRNA reduced expression by 95%. (**e**) NHERF1 knockdown enhanced Wnt-induced β-catenin activation in MCF7 cells (*$P<0.05$, **$P<0.01$, Two-way ANOVA with Bonferroni *post-hoc* tests). (**f**) Following 8 h of treatmnent with Wnt, NHERF1-knockdown cells shown increased levels of cyclin-D1. (***$P<0.001$, Two-way ANOVA with Bonferroni *post-hoc* tests). (**g**) Wnt-induced proliferation was measured using a 24 h radiolabeled-thymidine incorporation assay. MCF7 cells lacking NHERF1 showed marked proliferative responses to both Wnt3a and Wnt5a compared with scrambled controls (**$P<0.01$, ***$P<0.001$, Two-way ANOVA with Bonferroni *post-hoc* tests).

S1-NHERF1 functioned identically to wild type, whereas NHERF1 containing mutations in the second PDZ domain (S2 and S1S2) showed no inhibition of Wnt signaling (Figure 3c). Thus, interaction between the second PDZ domain of NHERF1 and Fzd govern NHERF1-mediated regulation of Wnt signaling. Importantly, two of the three mutations detected in the human breast cancer (K172N and R180W) are located within the second PDZ domain of NHERF1 (Dai *et al*., 2004).

Loss of NHERF1 expression in breast cancer cells enhances Wnt-induced β-catenin activation and cell proliferation

As NHERF1 regulates Wnt signaling in CHO-N10 cells, we hypothesized that the tumor suppressor activity of NHERF1 in breast cancer may result from the modulation of Wnt signaling. To investigate this, MCF7 and MDA MB-231 human breast cancer cell lines were selected because they have similar Fzd repertoires (Supplementary Table 1), while representing two extremes of NHERF1 expression. MCF7 cells express high levels of NHERF1, whereas MDA MB-231 cells express trace amounts (Figure 3d, Supplementary Figure 2a and Supplementary Table 1). Transient transfection with short hairpin RNA targeted against NHERF1 decreased protein expression by 95% in MCF7 cells (Figure 3d). Transfection of MDA MB-231 cells with NHERF1 was able to reconstitute NHERF1 expression to levels comparable with those observed in MCF7 cells (Supplementary Figure 2a).

At baseline, both MCF7 and MDA MB-231 cells showed little β-catenin activation, suggesting that Wnt secretion and autocrine stimulation are not active. MCF7 cells showed no significant increase in β-catenin activation when stimulated with either Wnt3a- or

Wnt5a-conditioned medium. In contrast, NHERF1-knockdown MCF7 cells responded to both Wnt3a and Wnt5a stimulation with approximately fourfold increases in β-catenin activity (Figure 3e).

Cyclin-D1 is a well established target gene of β-catenin known to influence cellular proliferation and breast cancer prognosis (Gillett *et al*., 1996; Tetsu and McCormick, 1999; Umekita *et al*., 2002). Cyclin-D1 levels were evaluated by quantitative PCR in control and NHERF1-knockdown MCF7 cells after the treatment with Wnt5a. As expected, NHERF1-knockdown cells expressed significantly greater amounts of cyclin-D1 in response to Wnt (Figure 3f). Furthermore, both Wnt3a and Wnt5a significantly increased the rate of proliferation NHERF1-knockdown MCF7 cells compared with control cells (Figure 3g).

This trend was recapitulated in the MDA MB-231 cells. Stimulation of control MDA MB-231 cells (lacking NHERF1) resulted in a significant activation of β-catenin. These effects were blocked by transfection with NHERF1 (Supplementary Figure 2).

Increased duct density and β-catenin levels in the mammary glands of NHERF1-knockout mice

Our *in vitro* data predict that the loss of NHERF1 in mammary tissue should result in increased Wnt signaling and a hyperproliferative phenotype. We examined the fourth and fifth mammary glands from 10–week-old virgin NHERF1−/− mice and compared them with those of wild-type littermates. Breast tissue from the NHERF1−/− mice exhibited greater density of mammary ducts (Figures 4a and b). A subset of the knockout mice (30–40%) manifested a more severe phenotype consisting of adipose atrophy accompanied by capillary and ductal dilation (Figure 4c). Overall, the loss of NHERF1 expression resulted in a three- to fourfold increase in duct density (Figure 4d). Because the total body weight and fat contents of NHERF1−/− mice were comparable with those of wild-type animals, the observed increase in duct density is most likely the result of increased breast proliferation. This was confirmed by using an *in vivo* 5-bromo 2′-deoxy-uridine (BrdU) staining protocol to identify proliferating cells in the mammary ducts. The results show increased incorporation of BrdU in the knockout mammary ducts (Figure 4e; $P<0.03$, $n=4$).

Mammary ducts from wild-type animals showed strong NHERF1 staining along the apical membrane of epithelial cells and faint β-catenin staining along all epithelial membranes (Figure 4f). Ducts from NHERF1−/− animals had increased levels of β-catenin staining and a greater percentage of β-catenin localized within the nucleus (Figures 4f and g). Taken together, these results suggest that the loss of NHERF1 leads to the increased ductal proliferation and density, which correlate with enhanced β-catenin activation.

Correlation between NHERF1 expression and β-catenin activation in human breast cancer tissues

β-Catenin activation is a negative predictor of prognosis and survival in human breast cancer (Lin *et al*., 2000; Dolled-Filhart *et al*., 2006). Because our data link loss of NHERF1 expression to increased Wnt signal transduction, we predicted a negative correlation between NHERF1 expression and β-catenin activity in human tumor samples. To test this hypothesis, breast cancer biopsies of varying stages and estrogen receptor/progesterone receptor status were stained for NHERF1 and β-catenin (see Supplementary Table 2 for detailed characteristics of the clinical samples). Antibody staining demonstrated low levels of β-catenin in tumors expressing high levels of NHERF1, independently of their estrogen receptor/progesterone receptor status. Furthermore, β-catenin staining was weak and membrane delimited in high-NHERF1 tumors, resembling the pattern observed in mammary tissues from wild-type mice (Figure 5a). In contrast, β-catenin expression was greater in tumors that expressed little or no NHERF1 (Figure 5b). This increased expression was accompanied by an increase in the percent of β-catenin observed within the nucleus. Furthermore, the aggregated data demonstrated a strong negative correlation between NHERF1 expression and the fraction of β-catenin within the nucleus ($r=0.69$, $F=8.729$, $P=0.0105$) (Figure 5c). Further analysis demonstrated this negative correlation to be independent of estrogen receptor/progesterone receptor status and tumor stage. In normal control tissues, nuclear β-catenin staining was uniformly low and unrelated to NHERF1 staining ($r=0.03$, $F=0.046$, $P=0.8386$; Figure 5d).

NHERF1 interferes with Fzd-Dvl binding

Because of the short C-terminal tail of Fzd receptors, the Dvl and NHERF1 binding sites are separated by as few as 13 amino acids. Therefore, we hypothesized that the interaction between NHERF1 and Fzd may alter the recruitment and the activation of Dvl. To investigate this, we coimmunoprecipitated HA-Fzd4 and myc-Dvl2 in the presence or absence of NHERF1. In the absence of NHERF1, Fzd4 coimmunoprecipitated notably greater amounts of Dvl2 (Figure 6a, compare lane 1 and 2). After stimulation with Wnt, identical amounts of Dvl were coimmunoprecipitated suggesting that Wnt binding induces dissociation of NHERF1 and binding to Dvl (Figure 6a, lanes 3 and 4). To confirm that this was the case, the effects of Wnt-conditioned medium on the coimmunoprecipitation of HA-Fzd4 and NHERF1 was examined using CHO-N10 cells. The results demonstrate that Wnt induces dissociation of NHERF1 and Fzd4 (Supplementary Figure 3).

Total internal reflection fluorescence (TIRF) microscopy was used to investigate the effects of NHERF1 on Fzd-Dvl interactions with greater temporal resolution. TIRF allows imaging of a very thin optical section containing the plasma membrane, such that changes in the fluorescence intensity detected by TIRF reflect traffic of the fluorescent protein to and from the plasma membrane. mRed-Dvl2 was found to be uniformly distributed in the cytoplasm of CHO-N10 cells expressing NHERF1 (Figure 6b). On stimulation with Wnt5a, Dvl2 was recruited to the membrane (Figure 6d).

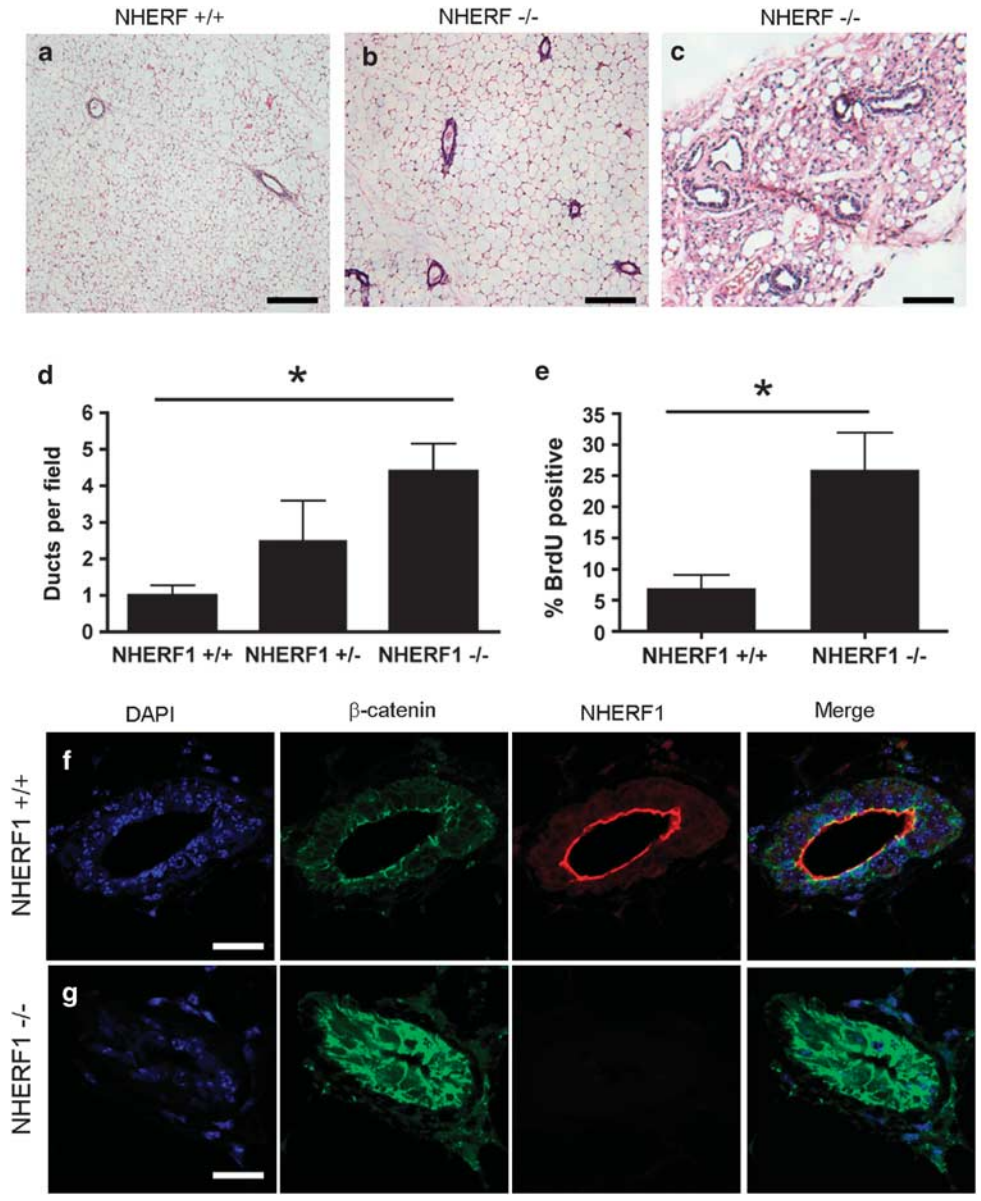

Figure 4 Mammary glands of NHERF1 knockout mice exhibit increased β-catenin signaling, elevated ductal density, and increased cell proliferation. The fourth and fifth breasts from virgin NHERF1+/+ and NHERF1−/− littermates were removed and histologically prepared. (**a**) Representative images from 10-week-old NHERF1+/+ mouse. (**b**) Representative images from a 10-week-old NHERF1−/− mouse. (**c**) A subset of NHERF1−/− mice presented a more severe phenotype characterized by a loss of adipose tissue, capillary dilation and ductal dilation. Scale bar represents 200 μm. (**d**) Quantification of ductal density in NHERF1+/+ and NHERF1−/− mice (*$P<0.05$, Students' *t*-test). (**e**) Increased mammary duct proliferation in NHERF1−/− females. (**f**) Individual duct from NHERF1+/+ mouse stained with 4′,6-diamidino-2-phenylindole (DAPI; blue), anti-β-catenin (green) and anti-NHERF1 (red). NHERF1 decorates the apical surface, whereas β-catenin staining is observed along all membranes of the epithelial cells. Scale bar represents 20 μm. (**g**) Individual duct from NHERF1−/− mouse. β-catenin staining is augmented and is no longer restricted to the membrane. Scale bar represents 20 μm.

In control cells, Dvl2 was localized to the plasma membrane under basal conditions (Figure 6c). The addition of Wnt had no effect on the amount of Dvl2 at the plasma membrane (Figure 6d). These data suggest that Wnt binding causes a slow dissociation of NHERF1 resulting in a retardation of the coupling of Fzd and Dvl. These observations imply, therefore, that the effects of NHERF1 on Wnt signaling are a consequence of the inhibition of Fzd-Dvl precoupling, which results in slower, significantly attenuated responses.

Coupling between Fzd receptors and Dvl has been shown to be critical for proper Fzd internalization and signaling (Chen *et al*., 2003; Yu *et al*., 2007). Thus, the binding of NHERF1 to Fzd should reduce Fzd-Dvl precoupling and result in impaired Wnt-induced Fzd internalization. Consistent with this hypothesis, CHO-N10 cells lacking NHERF1 internalized a remarkable

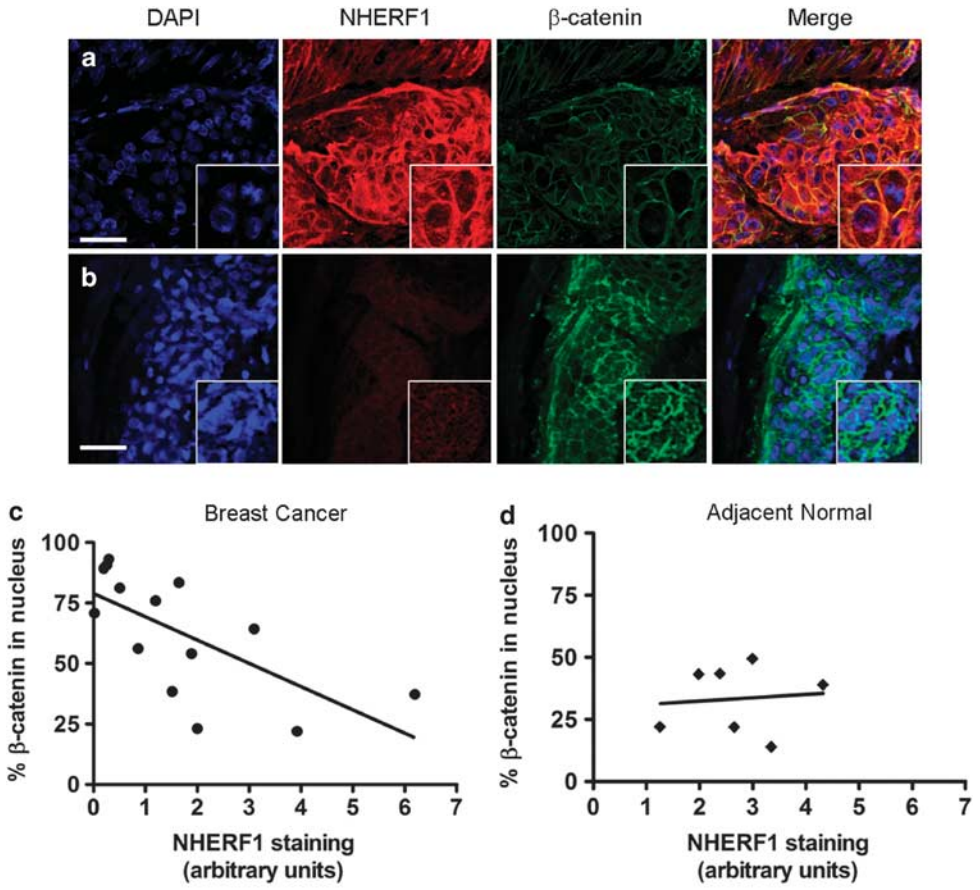

Figure 5 β-catenin activation and NHERF1 expression are negatively correlated in human breast cancer samples. Human breast cancer biopsies were stained with 4′,6-diamidino-2-phenylindole (DAPI; blue), anti-β-catenin (green) and anti-NHERF1 (red). (**a**) Samples which robustly expressed NHERF1 had a faint, membranous β-catenin staining pattern. There was minimal colocalization between β-catenin staining and nuclear DAPI staining (insert). (**b**) Samples with nominal NHERF1 staining exhibited a large percentage of β-catenin staining within the nucleus. Scale bar represents 20 μm in the main panel and 10 μm in insert. (**c**) NHERF1 expression is negatively correlated with the percentage of β-catenin staining occurring within the nucleus. (**d**) No correlation between NHERF1 expression and nuclear β-catenin is observed in adjacent normal tissue.

70% of their Fzd4 receptors in response to Wnt5a, whereas <20% of the surface Fzd4 is internalized in cells expressing NHERF1 (Figure 6e). In contrast, the endocytosis of the V537A-Fzd4 mutant is insensitive to the expression of NHERF1, internalizing readily whether NHERF1 is expressed or not (Figure 6e).

On the basis of results presented here, we propose the following model for the regulatory role of NHERF1 in breast cancer (Figure 6f). Normal breast tissues and low-grade ductal carcinomas express NHERF1, which attenuates Wnt signaling by impairing Fzd-Dvl precoupling. Under these conditions, the growth of breast epithelia is mainly controlled by estrogen-regulated signals. As the tumor progresses NHERF1 expression diminishes due to genetic changes or as a consequence of treatment with anti-estrogens. Reduced levels of NHERF1 facilitate coupling of Fzd receptors to Dvl and, subsequently, enhanced Wnt signaling. Wnt then becomes a driving force in the proliferation of the tumor, inducing epithelial-to-mesenchymal transition and resulting in increasing malignancy and tumor metastasis.

Discussion

Our findings show that NHERF1 regulates canonical Wnt signaling. We demonstrate that NHERF1 modulates Dvl recruitment and Wnt-induced β-catenin activation through a direct interactions between the second PDZ domain of NHERF1 and the C-terminal PDZ ligand of a selected subset of Fzd receptors. In the absence of NHERF1, Fzd precouples with Dvl, resulting in augmented canonical Wnt signaling. This conclusion is further supported by the finding that NHERF1-knockout mice show increased mammary duct proliferation and density correlated with increased β-catenin activation. Likewise, human breast tumors show a significant negative correlation between NHERF1 expression and β-catenin activation. We conclude, therefore, that NHERF1 expression is required for proper Wnt signaling in normal mammary epithelium. Loss of NHERF1 results in dysregulation of Wnt function that leads to increased proliferation and possibly dysplastic changes of the mammary epithelium. Whether this is NHERF1's main role in the regulation

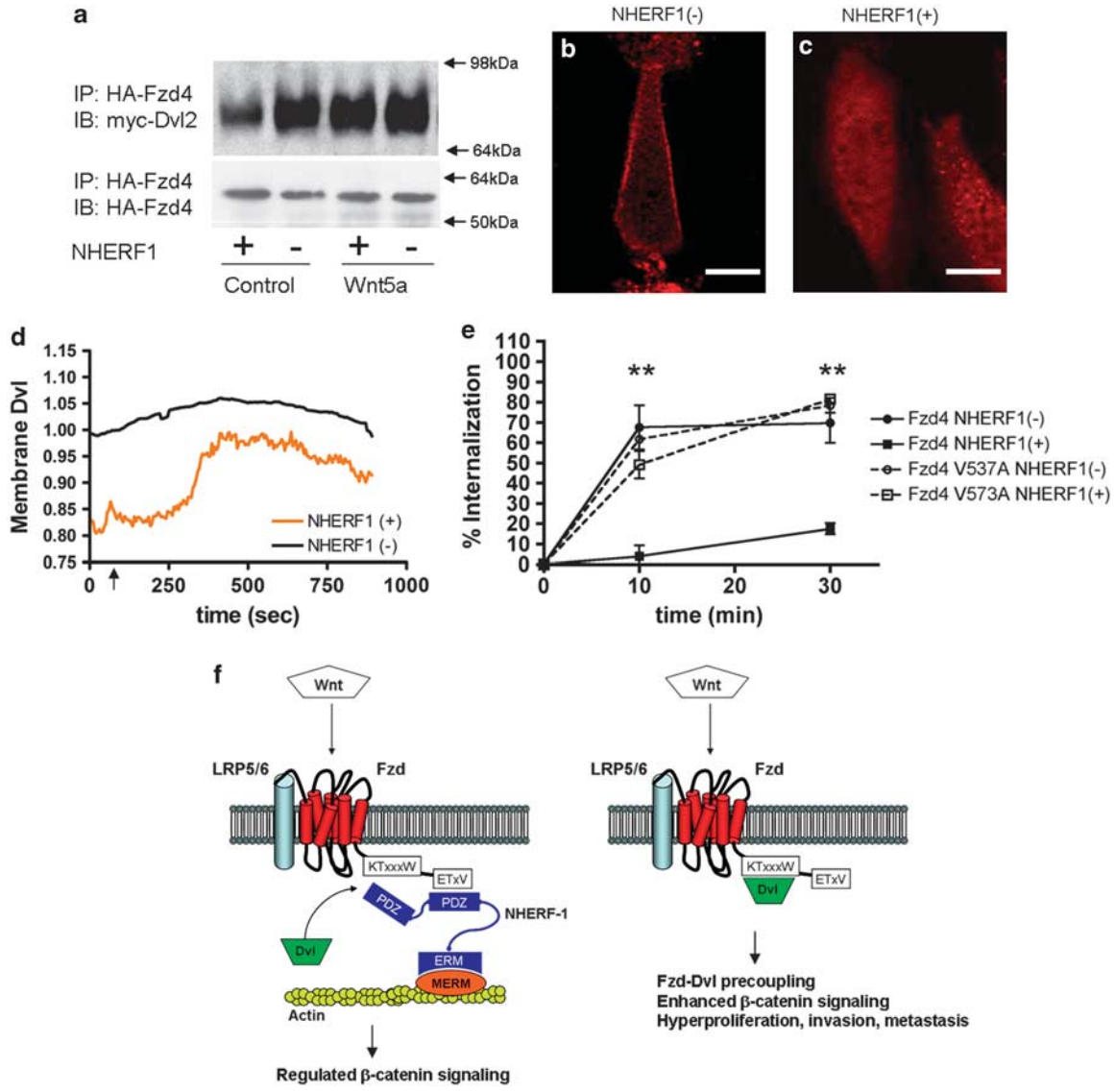

Figure 6 Fzd-Dvl precoupling is disrupted by NHERF1. (**a**) Coimmunoprecipitation between myc-Dvl2 with HA-Fzd4 was assessed in CHO-N10 cells before and 10 min after Wnt5a treatment. Interaction between Dvl2 and Fzd was clearly enhanced in the absence of NHERF1 before Wnt5a addition. The amount of Dvl2-Fzd complex after treatment with Wnt5a was independent of NHERF1 expression. (**b**) mRed-Dvl2 has a uniform cytoplasmic distribution in CHO-N10 cells expressing Fzd4 and NHERF1. (**c**) In the absence of NHERF1, mRed-Dvl2 localizes predominantly to the membrane. Scale bar represents 5 μm. (**d**) CHO-N10 cells expressing mRed-Dvl2 and Fzd4-GFP were rapidly imaged using TIRF microscopy. All intensity measurements are normalized to Fzd4-GFP to account for receptor internalization. Addition of Wnt5a is indicated by an arrow. In NHERF1 expressing cells, the addition of Wnt5a induced a translocation of Dvl2 to the plasma membrane. The amount of membrane associated Dvl2 did not change with addition of Wnt5a in control cells. (**e**) Fzd4 internalization was inferred from decreases in surface staining as measured by flow cytometry. In the absence of NHERF1, Wnt5a trigger extensive Fzd4 internalization (**$P = 0.002$, Student's *t*-test). As expected, the internalization of the V537A-Fzd4 mutant is insensitive to NHERF1 expression. (**f**) In normal mammary epithelium, NHERF1 occupies the C-terminus of Fzd receptors tethering it to the actin cytoskeleton. Loss of NHERF1 allows abnormal Fzd-Dvl precoupling, which results in pathologically enhanced Wnt-induced β-catenin activation and hyper-proliferation.

of mammary tissues remains to be determined. A recent report has linked NHERF1 to the regulation of the tumor suppressor PTEN and the subsequent attenuation of platelet-derived growth factor signaling in breast cancer (Pan *et al*., 2008). Thus, in mammary epithelium, NHERF1 seems to have multiple functions that converge in the regulation of normal cell proliferation.

Our findings show that NHERF1 inhibits Fzd2, 4 and7 but not Fzd3-dependent β-catenin activation. Thus, Wnt signaling is expected to be insensitive to NHERF1 expression in cells harboring high levels of Fzd3. Likewise, because Fzd6 does not contain a canonical PDZ ligand sequence in its C-terminus, we predict that Fzd6 signaling will be insensitive to NHERF1 expression. Thus, as only a subset of Fzd receptors are targets for NHERF1 regulation, the expression profile of the Fzd receptors in breast tumors is of primary interest. Importantly, the Fzd expression profile of breast cancer cells shows a predominance of Fzd5,2 and 1, which account for well over 90% of the

Fzd mRNA produced by MCF7 cells (Supplementary Table 1) and contain canonical PDZ ligand sequences. A similar expression profile was found in MDA MB-231 cells, suggesting that this pattern of expression may be typical for breast epithelium. Furthermore, our data demonstrate that Wnt signaling is attenuated by NHERF1 expression in both MCF7 and MDA-MB231 cells, confirming the hypothesis that NHERF1 regulates Wnt signaling in breast cancer.

Normal and malignant breast tissues express several other PDZ proteins that reportedly interact with Fzd receptors. For instance, syntenin, an adaptor protein that, like NHERF1, contains two PDZ domains in tandem, reportedly interacts with a subset of Fzd receptors and modulates non-canonical Wnt signaling during the embryonic development of *Xenopus* (Luyten *et al*., 2008). Furthermore, syntenin is highly expressed in breast cancer tissues, also mediating non-canonical Wnt signaling and inducing cell migration and invasion (Koo *et al*., 2002). However, there is no evidence that syntenin regulates canonical Wnt signaling in any way. In fact, neither the knockdown nor the overexpression of syntenin have any effects on the activation of the β-catenin pathway during the development of *Xenopus* (Luyten *et al*., 2008).

A second PDZ protein expressed in epithelial tissues is the membrane-associated guanylate kinase family member MAGI-3 (Laura *et al*., 2002). MAGI-3 contains six PDZ domains in tandem, and reportedly interacts with Fzd4 via its second PDZ domain (Yao *et al*., 2004). This interaction modulates the activation of Jnk and the non-canonical Wnt signaling pathway. However, as in the case of syntenin, the interactions of MAGI-3 and Fzd receptors do not affect β-catenin signaling in any measurable way (Yao *et al*., 2004). Associations between Fzd receptors and several other PDZ proteins have been reported in mammalian systems (Wawrzak *et al*., 2009). However, most reported interactions have been linked exclusively to the positive modulation of non-canonical Wnt signaling. In general, no evidence of the regulation of Wnt-dependent β-catenin activation by PDZ proteins has been reported to date in mammalian systems. NHERF1 is, therefore, unique among PDZ proteins in its role as a negative regulator of Wnt-dependent β-catenin signaling in breast epithelium.

Some recent reports have suggested that NHERF1 is overexpressed in breast cancer cells as compared with normal mammary tissues (Cardone *et al*., 2007; Song *et al*., 2007; Mangia *et al*., 2009). Although this is not surprising because NHERF1 expression is positively regulated by the estrogen receptor (Ediger *et al*., 1999), it implies that loss of NHERF1 is unlikely to be the primary cause of the transformed phenotype. However, NHERF1 expression is greatly reduced in the more invasive ER-negative tumors (Stemmer-Rachamimov *et al*., 2001; Song *et al*., 2007). These findings suggest a unique role for NHERF1 in the evolution of estrogen-driven ER-positive tumors into more aggressive Wnt-driven tumors. In ER-positive ductal carcinomas, which express NHERF1, proliferation is driven by classical ER-dependent pathways with relatively little contribution from Wnt signaling. We propose that the loss of NHERF1 via genetic or epigenetic changes increases the contribution of Wnt signaling in tumor growth, thus allowing the loss of the ER, promoting epithelial-to-mesenchymal transition and increasing tumor aggressiveness.

If true, this hypothesis may have significant implications for the treatment of ER-positive breast cancer. The majority of ER-positive carcinomas are successfully treated with antiestrogens, such as tamoxifen, which inhibit ER-dependent growth. However, tamoxifen treatment reduces NHERF1 expression by approximately 70% in cell culture systems (Ediger *et al*., 1999). Chronic treatment with antiestrogens will likely decrease NHERF1 expression in the tumor, which would increase its sensitivity to Wnt ligands, thus switching the proliferative drive from estrogen dependent to Wnt dependent. This model explains the paradoxical observation that ER-positive tumors recurring after prolonged antiestrogen treatment are inhibited by the administration of estrogens (Ellis *et al*., 2009). We propose that this inhibition is mediated by estrogen-induced expression of NHERF1, which then inhibits Wnt-dependent proliferation. This model highlights the importance of NHERF1 as a marker for Wnt sensitivity and the importance of targeting the Wnt signaling pathways for the treatment of breast carcinomas.

Materials and methods

Breast biopsies

All biopsy samples were obtained in accordance with the University of Pittsburgh Internal Review Board. Sample characteristics are summarized in Supplementary Table 2.

Materials and constructs

Anti-NHERF1, anti-β-catenin, anti-myc and anti-HA (HA.11) antibodies were purchased from Upstate Biotechnology (Lake Placid, NY, USA), Millipore (Billerica, MA, USA), Sigma (St Louis, MO, USA) and Covance (Princeton, NJ, USA). Secondary antibodies were from Jackson ImmunoResearch (West Grove, PA, USA). Texas Red isothiocyanate conjugated phalloidin was purchased from Invitrogen (Carlsbad, CA, USA). All other materials were purchased from Sigma unless otherwise indicated. Human Fzd2, 3 and 7 were purchased from OpenBiosystems Inc (Huntsville, AL, USA) and subcloned into pcDNA3.1(+) using EcoRI and XhoI. NHERF1-targeted short hairpin RNA plasmids have been previously described (Wang *et al*., 2007). TOP and FOP plasmids were supplied by Dr Paul Monga. Fzd4-HA, Fzd4-eGFP, myc-Dvl2 and mRed-Dvl2 plasmids were kindly provided by Dr T Kirchhausen (Yu *et al*., 2007).

Cell culture

CHO-N10 cells were grown as described (Wheeler *et al*., 2007). MCF7 and MDA MB-231 cells were grown in DMEM/F12 medium (Mediatech Inc, Manassas, VA, USA) supplemented with 10% fetal bovine serum (Invitrogen) and 1% penicillin/streptomycin. Wnt3a, Wnt5a and control L-cells were purchased from American Type Culture Collection and grown in Dulbecco's modied Eagle's medium supplemented with 10%

fetal bovine serum and 1% penicillin/streptomycin. Conditioned media was removed from cells after 4 days in culture and returned to a pH of 7.4 by addition of 4-(2-hydroxyethyl)-1-piperazineethanesulfonic acid buffer. FuGENE 6 (Roche Applied Sciences, Indianapolis, IN, USA) was used for all transfections.

Fluorescence recovery after photobleaching
Fluorescence recovery after photobleaching was conducted as described previously (Wheeler *et al*., 2007). Briefly, cells seeded onto Mattek dishes were transfected with the indicated plasmids. Small circular regions of the plasma membrane were bleached with a 405 nm laser line and images were collected every second for 1–2 min. The images were exported to ImageJ (National Institute of Health) and the average fluorescent intensity of the bleached region was measured. The diffusion coefficient was calculated using the Stokes–Einstein equation for two-dimensional diffusion. The bar graph represents aggregate data from ~20 cells imaged over three sessions.

TIRF microscopy
TIRF studies were carried out as previously described (Wheeler *et al*., 2007). Red and green TIRF images were collected sequentially every 5 s for 15 min. A baseline was established with 2 min of imaging before the addition of Wnt5a. The average Dvl2 intensity was normalized to the average Fzd intensity and graphed using GraphPad Prism.

Receptor internalization
Internalization of membrane proteins was measured using flow cytomerty as described (Garrido *et al*., 2009). CHO-N10 cells stably transfected with HA-Fzd4 containing an extracellular HA epitope were treated with Wnt5a, washed twice with ice-cold phosphate-buffered saline and fixed with 0.5% paraformaldehyde for 5 min. This protocol left the cell membrane intact and impermeant to antibodies. Cells were scraped and incubated in 3% bovine serum albumin for 30 min to block nonspecific binding. The cells were stained with anti-HA (Covance) followed by anti-rabbit-Alexa-680. The fluorescence of each cell was measured using a flow cytometer and reflected the amount of Fzd4 on the surface. Percentage Fzd internalization was calculated as: $100 \times (1 - \text{geometric mean fluorescence } (t)/\text{geometric mean fluorescence } (t=0))$.

Quantitative breast histology
The fourth and fifth breasts of 10-week-old NHERF1 +/+ and NHERF1−/− mice were removed and fixed in buffered formalin. After fixation, they were embedded in paraffin and sectioned. Slides from different depth in the breast tissue were stained with haematoxylin and eosin. Each slide was imaged 10 times at ×20 magnification. Coordinates were randomly generated; if breast tissue did not occupy 90% of the visual field, new coordinates were generated. The average number of ducts per field was calculated for each slide. The bar chart represent average ducts per field measured from three NHERF1 +/+ animals and five NHERF1−/− animals (two having the more severe phenotype). For BrdU staining the animals were injected with 50 μg/g of body weight 6 h before harvesting the breast tissues. BrdU incorporation was determined with anti-BrdU antibody (GE Healthcare, Piscataway, NJ, USA).

TOP/FOP Luciferase assay
Cells were stimulated with control, Wnt3a-, or Wnt5a-enriched medium for 8 h. Cells were lysed with Reporter Lysis Buffer (Promega, Madison, WI, USA) and transferred to a 96-well plate. The luminescence of each well was recorded for 5 s after addition of BioGlo Luciferase substrate (Promega). The ratio of TOP/FOP signal was calculated and normalized to control conditions. Bars represent data from at least three experiments conducted in duplicate.

Quantitative real-time PCR
RNA was extracted using Trizol (Invitrogen) and transcribed into complementary DNA using a Clontech (Mountain View, CA, USA) Advantage RT–for-PCR kit. Quantitative real-time PCR was performed on an Applied BioSystems (Carlsbad, CA, USA) StepONe real-time PCR system using SYBR Green (Qiagen, Valencia, CA, USA) with the primers listed in Supplementary Table 3. All samples were run in duplicate and normalized to glyceraldehyde 3-phosphate dehydrogenase.

Statistical analysis
Each experiment was repeated at least three times. All statistical tests were conducted using GraphPad Prism.

Conflict of interest

The authors declare no conflict of interest.

Acknowledgements

This work was supported by grants DK083211 (DSW), DK079864 (GR) and DK54171 (PAF) from the National Institutes of Health. We also acknowledge support from the Office of the Senior Vice Chancellor for the Health Sciences of the University of Pittsburgh (GR).

Author contributions: DSW and GR conceived the study, designed and executed experiments, analyzed the data and prepared the paper. SRB aided with animal studies and designed experiments. MJG performed biochemical assays. AB selected the human subjects and aided with pathological characterization. PAF and GR supervised the analysis of the data and edited the paper.

References

Ayyanan A, Civenni G, Ciarloni L, Morel C, Mueller N, Lefort K *et al*. (2006). Increased Wnt signaling triggers oncogenic conversion of human breast epithelial cells by a Notch-dependent mechanism. *Proc Natl Acad Sci USA* **103**: 3799–3804.

Bates IR, Hebert B, Luo Y, Liao J, Bachir AI, Kolin DL *et al*. (2006). Membrane lateral diffusion and capture of CFTR within transient confinement zones. *Biophys J* **91**: 1046–1058.

Cardone RA, Bellizzi A, Busco G, Weinman EJ, Dell'Aquila ME, Casavola V *et al*. (2007). The NHERF1 PDZ2 domain regulates PKA-RhoA-p38-mediated NHE1 activation and invasion in breast tumor cells. *Mol Biol Cell* **18**: 1768–1780.

Chen W, ten Berge D, Brown J, Ahn S, Hu LA, Miller WE *et al*. (2003). Dishevelled 2 recruits beta-arrestin 2 to mediate Wnt5A-stimulated endocytosis of Frizzled 4. *Science* **301**: 1391–1394.

Dai JL, Wang L, Sahin AA, Broemeling LD, Schutte M, Pan Y. (2004). NHERF (Na + /H + exchanger regulatory factor) gene mutations in human breast cancer. *Oncogene* **23**: 8681–8687.

Dolled-Filhart M, McCabe A, Giltnane J, Cregger M, Camp RL, Rimm DL. (2006). Quantitative in situ analysis of beta-catenin expression in breast cancer shows decreased expression is associated with poor outcome. *Cancer Res* **66**: 5487–5494.

Ediger TR, Kraus WL, Weinman EJ, Katzenellenbogen BS. (1999). Estrogen receptor regulation of the Na + /H + exchange regulatory factor. *Endocrinology* **140**: 2976–2982.

Ellis MJ, Gao F, Dehdashti F, Jeffe DB, Marcom PK, Carey LA *et al*. (2009). Lower-dose vs high-dose oral estradiol therapy of hormone receptor-positive, aromatase inhibitor-resistant advanced breast cancer: a phase 2 randomized study. *JAMA* **302**: 774–780.

Fantozzi A, Christofori G. (2006). Mouse models of breast cancer metastasis. *Breast Cancer Res* **8**: 212.

Garrido JL, Wheeler D, Vega LL, Friedman PA, Romero G. (2009). Role of phospholipase D in parathyroid hormone type 1 receptor signaling and trafficking. *Mol Endocrinol* **23**: 2048–2059.

Gillett C, Smith P, Gregory W, Richards M, Millis R, Peters G *et al*. (1996). Cyclin D1 and prognosis in human breast cancer. *Int J Cancer* **69**: 92–99.

Karthikeyan S, Leung T, Birrane G, Webster G, Ladias JA. (2001). Crystal structure of the PDZ1 domain of human Na(+)/H(+) exchanger regulatory factor provides insights into the mechanism of carboxyl-terminal leucine recognition by class I PDZ domains. *J Mol Biol* **308**: 963–973.

Koo TH, Lee JJ, Kim EM, Kim KW, Kim HD, Lee JH. (2002). Syntenin is overexpressed and promotes cell migration in metastatic human breast and gastric cancer cell lines. *Oncogene* **21**: 4080–4088.

Kreimann EL, Morales FC, de Orbeta-Cruz J, Takahashi Y, Adams H, Liu TJ *et al*. (2007). Cortical stabilization of beta-catenin contributes to NHERF1/EBP50 tumor suppressor function. *Oncogene* **26**: 5290–5299.

Laura RP, Ross S, Koeppen H, Lasky LA. (2002). MAGI-1: a widely expressed, alternatively spliced tight junction protein. *Exp Cell Res* **275**: 155–170.

Lin SY, Xia W, Wang JC, Kwong KY, Spohn B, Wen Y *et al*. (2000). Beta-catenin, a novel prognostic marker for breast cancer: its roles in cyclin D1 expression and cancer progression. *Proc Natl Acad Sci USA* **97**: 4262–4266.

Luyten A, Mortier E, Van Campenhout C, Taelman V, Degeest G, Wuytens G *et al*. (2008). The postsynaptic density 95/disc-large/zona occludens protein syntenin directly interacts with frizzled 7 and supports noncanonical Wnt signaling. *Mol Biol Cell* **19**: 1594–1604.

Mangia A, Chiriatti A, Bellizzi A, Malfettone A, Stea B, Zito FA *et al*. (2009). Biological role of NHERF1 protein expression in breast cancer. *Histopathology* **55**: 600–608.

Pan Y, Wang L, Dai JL. (2006). Suppression of breast cancer cell growth by Na + /H + exchanger regulatory factor 1 (NHERF1). *Breast Cancer Res* **8**: R63.

Pan Y, Weinman EJ, Dai JL. (2008). Na + /H + exchanger regulatory factor 1 inhibits platelet-derived growth factor signaling in breast cancer cells. *Breast Cancer Res* **10**: R5.

Ryo A, Nakamura M, Wulf G, Liou YC, Lu KP. (2001). Pin1 regulates turnover and subcellular localization of beta-catenin by inhibiting its interaction with APC. *Nat Cell Biol* **3**: 793–801.

Song J, Bai J, Yang W, Gabrielson EW, Chan DW, Zhang Z. (2007). Expression and clinicopathological significance of oestrogen-responsive ezrin-radixin-moesin-binding phosphoprotein 50 in breast cancer. *Histopathology* **51**: 40–53.

Songyang Z, Fanning AS, Fu C, Xu J, Marfatia SM, Chishti AH *et al*. (1997). Recognition of unique carboxyl-terminal motifs by distinct PDZ domains. *Science* **275**: 73–77.

Stemmer-Rachamimov AO, Wiederhold T, Nielsen GP, James M, Pinney-Michalowski D, Roy JE *et al*. (2001). NHE-RF, a merlin-interacting protein, is primarily expressed in luminal epithelia, proliferative endometrium, and estrogen receptor-positive breast carcinomas. *Am J Pathol* **158**: 57–62.

Tetsu O, McCormick F. (1999). Beta-catenin regulates expression of cyclin D1 in colon carcinoma cells. *Nature* **398**: 422–426.

Umekita Y, Ohi Y, Sagara Y, Yoshida H. (2002). Overexpression of cyclinD1 predicts for poor prognosis in estrogen receptor-negative breast cancer patients. *Int J Cancer* **98**: 415–418.

Wang B, Bisello A, Yang Y, Romero GG, Friedman PA. (2007). NHERF1 regulates parathyroid hormone receptor membrane retention without affecting recycling. *J Biol Chem* **282**: 36214–36222.

Wawrzak D, Luyten A, Lambaerts K, Zimmermann P. (2009). Frizzled-PDZ scaffold interactions in the control of Wnt signaling. *Adv Enzyme Regul* **49**: 98–106.

Weinman EJ, Hall RA, Friedman PA, Liu-Chen LY, Shenolikar S. (2006). The association. *Annu Rev Physiol* **68**: 491–505.

Wheeler D, Sneddon WB, Wang B, Friedman PA, Romero G. (2007). NHERF-1 and the cytoskeleton regulate the traffic and membrane dynamics of G protein-coupled receptors. *J Biol Chem* **282**: 25076–25087.

Yao R, Natsume Y, Noda T. (2004). MAGI-3 is involved in the regulation of the JNK signaling pathway as a scaffold protein for frizzled and Ltap. *Oncogene* **23**: 6023–6030.

Yu A, Rual JF, Tamai K, Harada Y, Vidal M, He X *et al*. (2007). Association of Dishevelled with the clathrin AP-2 adaptor is required for Frizzled endocytosis and planar cell polarity signaling. *Dev Cell* **12**: 129–141.

Supplementary Information accompanies the paper on the Oncogene website (http://www.nature.com/onc)